DESIGN, DEVELOPMENT AND PERFORMANCE OF THERMOPLASTIC COMPOSITE LEAF SPRINGS

A thesis
submitted in partial fulfillment of the
requirements for the degree of

DOCTOR OF PHILOSOPHY

by

C.SUBRAMANIAN

(06610302)

DEPARTMENT OF MECHANICAL ENGINEERING
INDIAN INSTITUTE OF TECHNOLOGY GUWAHATI
GUWAHATI 781 039
NOVEMBER 2010

CERTIFICATE

It is certified that the work contained in the thesis entitled **Design, Development and Performance of Thermoplastic Composite Leaf Springs** by **C.Subramanian, a** student in the Department of Mechanical Engineering, Indian Institute of Technology Guwahati, India, for the award of the degree of **Doctor of Philosophy** has been carried out under my supervision and this work has not been submitted elsewhere for the degree.

Dr. S. Senthilvelan
Associate Professor
Department of Mechanical Engineering
Indian Institute of Technology Guwahati
Guwahati – 781039, Assam, India.

Dedicated to my parents,

wife and daughter

TABLE OF CONTENTS

Acknowledgements

I am deeply indebted to my thesis supervisor, **Dr. S. Senthilvelan,** for his valuable guidance and steady encouragement throughout my Ph.D program. His constant encouragement, enormous goodwill and unruffled patience made me work at ease and kept me highly motivated throughout my stay with him. Starting from formulating the problems to the final experimental results and their physical interpretations, he remained profoundly involved in my thesis work. He provided me with innovative ideas, helpful books and journals that were very helpful in successfully completing the present thesis. I have immensely benefited from each and every moment of my association with him.

I would like to thank **Prof. Debabrata Chakraborty**, **Prof. Sashindra K. Kakoty** and **Dr**. **G. Pugazhenthi** members of my Doctoral Committee who had steered me into the right path by providing comments, ideas and sharing their expertise throughout my tenure.

I thank the **Head**, Department of Mechanical Engineering, IIT Guwahati for providing me all the necessary facilities and funding to carry out this research work.

I would like to express my sincere thanks to **Prof. P. S. Robi** and **Dr. S. Kanagaraj** for their valuable discussions and suggestions during my experimental work.

I am also deeply indebted to **Prof. Eng. R. Gnanamoorthy**, **Director,** IIITDM, Chennai for permitting me to avail the facilities in his laboratory. I thank **Prof. R. M. Guedes** Department of Mechanical Engineering, University of Porto for helping in the characterization of materials. I thank **CIPET Guwahati** for permitting me to avail the facilities for my research work.

I would like to thank **Dr. Deba Kr. Sarma** and his teammates for helping me a lot during the fabrication process in the workshop. I express my wholehearted gratitude to the technical staff of Mechanical Engineering Department, **Mr. Rituraj Saikia, Mr. Sanjib Sarma, Mr. Jiten Basumatary, Mr. Pranjol Paul and Mr. Dhruba Jyoti Bordoloi** for their contribution and tireless help rendered throughout my research work.

I am sincerely thankful to **Mr. Monash** and **Mr. Anto Pradeep** for their kind help during the course of experiments. **Mr. V. Satheeshkumar** needs a special mention for providing valuable and timely help rendered during the research work. My heart felt thanks to my research colleagues and friends **Dr. Santhosh Kumar, Dr. S.P. Laxmanan, M. Eswaran, D.A. Perumal, A. Satheesh, S. Anbarasu, Ratnakar Das, P. Adaleesan** and **A. Ashok Kumar** for their remarkable moral support without which it would have been difficult for me to stay 3000 km far away from home.

I would like to express my gratitude to my parents **Mr. S. Chithambaram Pillai** and **Mrs. C. Maheswari** for their patience, wishes and the enormous trust they repose in my abilities at all times. I extend my heart full thanks to my wife **Mrs. S. M. Janisha** for her patience and understanding during my tough times of research work.

I appreciate the warmth and motivation extended by my sister **Mrs. C. Ambujam** and sister-in-law **Mr. Dinesh**. I thank my father-in-law **Mr. S. Mathevan** and mother-in- law **Mrs. J. Saraswathi** for encouraging me to join the Ph.D program.

Above all I thank the **Almighty** who bestowed me this opportunity for acquiring a research qualification.

C SUBRAMANIAN

ABSTRACT

KEYWORDS: Leaf Springs; Long fiber reinforced thermoplastics; Wear; Damping; Creep; Fatigue.

In recent years, thermoplastic composites are widening their applications due to their mass production ability, superior strength to weight ratio and mechanical strength. However, utilization of thermoplastic composite material in load bearing engineering applications is limited due to the inadequate understanding of heterogeneous material behavior under service condition. In this work, an attempt was made to investigate the potential of discontinuous fiber reinforced thermoplastic material for suspension leaf spring application. Prior to the product development, relevant mechanical properties for leaf spring applications; adhesive wear, abrasive wear and damping characteristics were investigated. Unreinforced polypropylene, 20% short glass fiber reinforced polypropylene and 20% long glass fiber reinforced polypropylene materials were considered for leaf spring materials and injection molding was chosen as manufacturing technique. Developed leaf springs were evaluated for static, fatigue as well as short term creep performance, besides joint strength performance were evaluated under static and fatigue condition.

Adhesive and abrasive wear characteristics of leaf spring materials were investigated with the help of pin on disc configuration. Fiber length, plastic deformation energy and material crystallinity were identified as the major contributing factors to the wear performance. Various damping sources of the chosen leaf spring materials were investigated with the aid of free, forced vibration and dynamic mechanical analysis. Fiber end density was found to influence the damping behavior of composites significantly.

Design of leaf spring and injection molding die were carried out with commercial finite element analysis and injection molding simulation tools. In-house molded leaf springs were evaluated for its performance with the aid of developed fixture integrated with the servo hydraulic fatigue testing machine (Instron 8801). Static performance tests were evaluated for determining energy storage capability and strain rate sensitiveness of molded leaf spring. Fatigue leaf spring performance was evaluated at fixed frequency, with various loads till 2×10^5 cycles or failure (fracture or 10 % drop in spring rate) whichever was earlier. During fatigue testing, cyclic load-deflection of test leaf spring of each and every cycle was measured; energy dissipation ratio and spring rate of the test leaf springs were reported as an index for the accumulated damage at various stages of life. Short glass fiber reinforced and unreinforced polypropylene leaf springs exhibited drop in spring rate; whereas long glass fiber reinforced polypropylene exhibited fracture as leaf spring failure. Short-term flexural creep tests were performed on molded leaf springs at various stress levels. Experimental creep performance of molded leaf springs for 2 h was utilized to predict the creep performance with the aid of four parameter HRZ model and compared with 24 h experimental creep data. Test results confirmed the suitability of long fiber reinforced thermoplastic material for creep application over other considered materials.

Joint for the developed leaf spring was designed and compared with its static performance. Test joints were subjected to completely reversed fatigue loads, long fiber reinforced leaf spring joint exhibited superior performance at high cycle fatigue conditions and poor performance at low cycle among chosen material, due to its high notch sensitivity characteristics. Load-deflection hysteresis plot of the joints were used to monitor the bearing damage. Failure morphology of joint exhibited net-tension and shear out failures besides bearing damages.

LIST OF TABLES

LIST OF FIGURES

ABBREVIATIONS

ASTM	American Society for Testing and Materials
B	Bearing
C	Cleavage
FFT	Fast Fourier Transform
FLD	Fiber Length Distribution
HMWPE	High Molecular Weight Polyethylene
ISO	International Organization for Standardization
LFLS	Long Fiber Reinforced Leaf Spring
LFPP	Long Glass Reinforced Polypropylene
LFRT	Long Fiber Reinforced Thermoplastics
NT	Net-Tension
PA	Polyamide
PC	Polycarbonate
PE	Polyethylene
PEEK	Polyether ether ketone
PMMA	Polymethylmethacrylate
POM	Polyoxymethylene
PP	Polypropylene
PPE	Propylene-*co*-Ethylene
PPS	Polypropylene Sulfide
PTFE	Polytetrafluoroethylene

RH	Relative Humidity
SAE	Society of Automotive Engineering
SFLS	Short Fiber Reinforced Leaf Spring
SFPP	Short Glass Reinforced Polypropylene
STL	Stereolithographic
UFLS	Unreinforced Leaf Spring
UFPP	Unreinforced Polypropylene
UHMWPE	Ultrahigh Molecular Weight Polyethylene

NOTATIONS

English Symbols

A	Amplitude ratio
a, b, c, e	Curve fitting parameters
b_c	Width at the center
b_w	Full width at half maximum
d	Hole diameter
d_p	Pin diameter
E	Modulus of elasticity
E_{def}	Deformation energy
F_i	Number of fiber count
H	Hardness of the material
H_c	Energy dissipation ratio
h_o	Change in pin length
$J(t)$	Creep Compliance
K	Spring rate
K_c	Unit cell geometry dependent constant
K_d	Wear volume dimension loss
K_m	Wear volume mass loss
K_w	Specific wear rate
K_o	Initial spring rate

K_s	Strength reduction factor
K_t	Theoretical/elastic stress concentration factor
L	Length of the spring
L_c	Crystallite size
L_e	Effective length of the spring
L_n	Number average length of fiber
L_w	Weight average length of fiber
m	Fatigue sensitivity parameter
m_1	Specimen mass before testing
m_2	Specimen mass before after testing
n	Power law exponent
N_f	Total number of cycles prior to failure.
P	Normal load
Q	Notch sensitivity factor
R	stress ratio
R^2	Correlation index
R_a	Average surface roughness
S	Sliding distance
S_b	Leaf spring bending stress
S_e	Specific elastic strain energy
S_o	Static strength
t	Thickness of leaf spring
T	Time period for one cycle

$tan\ \delta$	Loss factor
t_l	Time lag between exciting forcing and response
t_p	Thickness of the composite plate
V	Wear rate
W_b	Weight of the beam
X_1	Vibration amplitude of the first cycle
X_n	Vibration amplitude after n^{th} cycle is
Y	Deflection

Greek Symbols

ξ_e	Elongation to break
ω	Forced exciting frequency
ω_n	Natural frequency
ξ	Damping factor
$\varepsilon(t)$	Time dependent strain
$\varepsilon_t^{'}$	Power law coefficient
ϕ	Phase lag
ρ	Density of the material
δ	Logarithmic decrement
$\delta\ (t)$	Deflection at instantaneous time
δ_i	Fastener translation at initial cycle
δ_N	Fastener translation after N_f fatigue cycle

Δ_N	Hole elongation
δ_p	Fastener/pin displacement
θ	Incident angle
λ	Wavelength of X-ray beam
μ	Coefficient of friction
ξ_b	Bearing strain
ρ	Density of the material
ρ_g	Specific gravity of the specimen
σ	Applied stress level
σ_b	Bearing stress
σ_t	Tensile stress at break
σ_u	Ultimate strength

CHAPTER 1

INTRODUCTION

1.1 OVERVIEW ON COMPOSITE LEAF SPRINGS

Leaf springs are used in automobiles as suspension system to isolate shocks and vibrations transmitted due to the undulation in road conditions to the vehicle in service. Due to the superior performance of specific strain energy, damping and corrosion resistance of composite materials over steel, composite leaf springs are being widely used in light weight vehicles, passenger cars, heavy tank trailer suspension systems and in vibrating machineries (Beardmore, 1986; Morris, 1986; Sancaktar and Gratton, 1999; Qureshi, 2001; Rajendran and Vijayarangan, 2001; Hou *et al.*, 2005). Composite leaf springs are manufactured by any of the following techniques; filament winding, compression molding, pultrusion and hand lay-up vacuum bag process. Filament winding process provides excellent mechanical properties due to utilization of continuous fibers. However, leaf springs with varying thickness and varying contours constrained the higher degree of design flexibility (Qureshi, 2001). Leaf springs of various shapes and sizes can be produced by compression molding; however, manufacturing time involved in compression molding limits the mass production capability (Mallick, 1997). Hand lay-up vacuum bag process involves high level of skills for mixing and control of resin contents which also limit the mass production features of composite leaf springs (Crawford, 1997). Epoxy, polyester and polyimide resins were used for the fabrication of composite leaf spring in the past. Unidirectional E-glass, S-glass and carbon fibers were being used as the reinforcement for leaf springs. The optimal combination of

cost and performance for E-glass fibers provides better potential for commercial leaf spring applications over S-glass and carbon fibers. In the matrix resins, polyester dominates over epoxy resins on the basis of cost and ease of processability (Beardmore and Johnson, 1986). In short, the major limitations of thermoset composite leaf springs are limited production capability.

Hence there is a need to identify new material and manufacturing technique for the composite leaf spring. In the recent years, thermoplastic composite materials are replacing steel and thermoset composite materials due to its low manufacturing cost combined with mass production capability (Deaver and Mcllvaine, 2005; Bartus *et al.*, 2006; Noh *et al.*, 2006; Ning *et al.*, 2007). Due to the mass production requirement in the automotive industries, discontinuous long fiber reinforced thermoplastics (LFRT) have shown significant role in replacing metals, short fiber reinforced thermoplastics, thermoset sheet molding and bulk molding composites (Markarian, 2005). The major difference between short fiber reinforced thermoplastics and LFRT lies in the manufacturing technique. Short fiber reinforced thermoplastic pellets are manufactured by extrusion technique where fibers within pellets are randomly oriented. However due to the pultrusion technique, fibers are well aligned within the pellets of long fiber reinforced thermoplastics (LFRT). Increased length and fiber orientation within pellets help to increase the modulus and strength of the material as high as 90% of that obtained when using continuous fibers (Thomason *et al.*, 2002). The matrices commonly used in engineering application include polypropylene (PP), polyethylene (PE), polyamide (PA) polyether ether ketone (PEEK) etc. (Thomason and Vlug, 1995) due to their superior structural properties. Polypropylene matrix is generally used with E-glass fibers for structural applications due to its cost/performance ratio and ease of processing (Bartus *et. al.*,

2006). The potential for high volume processing combined with high levels of end use and its associated lower manufacturing costs have spurred the current expansion of research activities with polypropylene composites (Thomason, 2002).

1.2 MOTIVATION

In the recent years, long fiber reinforced thermoplastic material are being used extensively in mass transit industrial components which includes; dashboard carriers, front ends, seat shells, battery trays, spare wheel dwells, running boards (Krause *et. al*., 2003; Bartus *et. al*., 2006; Thattaiparthasarathy *et. al*., 2008). In this direction, due to its mass production capability and good endurance strength, the present investigation attempted to recognize and evaluate injection mouldable discontinuous fiber reinforced thermoplastic material for suspension leaf spring application.

Utilization of new materials and manufacturing processes for the functionally critical machine elements necessitates complete systematic understanding of required relevant mechanical properties of the new materials under the service condition. Due to the inadequate available data of the discontinuous fiber reinforced thermoplastics for load bearing application, critical properties for the leaf spring application were investigated for the chosen materials.

In the automobile suspension system, spring ends are bent to form eye through which leaf spring is fixed to the automobile body by the bolts. Since leaf springs experience contact load while in service condition, understanding friction and wear behavior of the leaf spring material under adhesive and abrasive mode with steel material becomes important. Predominant wear occurs through adhesive and abrasive modes (ASM Handbook, 1988; Karger-Kocsis *et al*., 2010). In adhesive wear mode, the surface energy and shear strength significantly influences the wear mechanism,

while in an abrasive wear mode, the toughness and hardness plays a major role (Bayer, 1994).

The inherent damping characteristic of thermoplastic materials aids to be an excellent alternative material over steel and thermoset material for leaf spring application. However, incorporation of discontinuous fibers in the thermoplastic material may significantly influence the damping characteristics of material. Increase in fiber volume fraction increases the storage and loss modulus and reduces the damping behavior of thermoplastic composites (Crema *et al.*, 1989; Wray *et. al.*, 1990; Rezaei *et al.*, 2009). As the main function of leaf spring in the automobile is to absorb shock and vibration, damping performance of the chosen leaf spring materials was investigated in detail. Due to the viscoelastic nature of the chosen thermoplastic leaf spring material, comprehensive understanding of time and temperature dependent mechanical properties is of practical importance.

Some of the major design parameters that decide energy storage capacity of the leaf springs are material and shape (Yu and Kim, 1988). Various forms of leaf springs as suggested by SAE standards were considered and their structural behaviors were predicted using commercial finite element analysis tool. Thermoplastic composite material properties are time dependent due to the viscoelastic behavior (Rosato *et. al.*, 2000). Since suspension leaf springs are subjected to time varying load, performance evaluation of leaf spring at various strain rates becomes crucial. Less hysteresis is generally preferred for leaf springs at service conditions (Yu and Kim, 1988). Presence of discontinuous fibers may alter the material and leaf spring performance, thus static performance of leaf springs *viz.* load carrying capability, strain rate sensitivity and hysteretic behavior need to be investigated in details. Suspension leaf springs are subjected to repetitive cyclic loads while the vehicle is in

operation, thus identifying safe operating regime under fatigue condition is one of the major requirements. Apart from the composite endurance strength, accumulated damage in the form of stiffness loss and energy dissipation should also be addressed (Orth *et al*., 1993). Presence of discontinuous fibers in a matrix contributes to the microscopic stress concentrations at fiber ends and fiber/matrix interface which significantly alters the fatigue behavior (Bureau and Denault, 2004; Bernasconi *et al*., 2007). Hence the failure mechanism and damage progression for the developed product is to be clearly understood.

In the service conditions, suspension leaf springs are subjected to constant stress for long duration as the chassis weight is taken by the suspension system. Besides, leaf springs are also subjected to various stress levels due to the different payload conditions. Thus, creep response investigation of leaf springs made of new material and process is important.

Successful utilization of composite leaf spring lies equally important on the joint performance. Leaf spring should have appropriate joints so that it can be fixed to the axle and the vehicle body to provide a reliable suspension system. The joint strength should have sufficient strength in view of the design load of leaf spring (Yu and Kim, 1988). Bolted joints are preferred for effective end joint over adhesive joint owing to low cost and simplicity in manufacturing (Shokreih and Rezaei, 2003). However, the potential site of stress concentration due to drilling in the joint region determines the strength of a structure. Hence there is a need to identify the joint strength and identify the safe operating regime under fatigue loading conditions.

In a summary an ideal leaf spring should possess the following requirements

- Leaf springs are subjected to contact loads at the ends as well as middle portion, hence wear resistance under adhesive and abrasive condition is one the requirement of leaf spring material.
- Amount of energy storage and release would determine the quality of the suspension system; hence the damping performance of leaf spring material is important.
- Spring rate and static deflection of leaf springs significantly affect the suspension quality; hence load deflection characteristics need to be evaluated.
- Suspension leaf springs are subjected to repetitive fluctuating loads under service conditions hence developed leaf springs must have fatigue resistance.
- Leaf springs are subjected to constant stress for long duration as the chassis weight is taken by the suspension system and hence an ideal leaf spring must have creep resistance.
- Developed leaf springs should be fastened with automobile body, hence joint performance under static and fatigue conditions are important.

1.3 OBJECTIVE

The main objective of the present work is to recognize and evaluate injection moldable discontinuous long fiber reinforced thermoplastic material for leaf spring application.

1.3.1 Major Steps Accomplished to Achieve Objectives

Following major activities were carried out to achieve the above said main objectives

- Friction and wear behavior of leaf spring materials under adhesive and abrasive modes were investigated using standard pin-on disc configuration.

- Damping performance of the leaf spring materials were evaluated with the aid of dynamic mechanical analysis besides free and forced vibration experiments.
- Varying width, constant thickness mono leaf spring geometry was designed with the aid of commercial finite element analysis software, ANSYS®. Die for injection molding was designed and analyzed using commercial plastic part manufacturing software, MOLDFLOW®.
- Injection molding die was fabricated and leaf springs were injection molded using chosen materials in the laboratory.
- Static, fatigue and short term creep performance of the molded test leaf springs were evaluated with the aid of in-house developed fixture integrated with servo hydraulic fatigue testing facility.
- Leaf spring end joint was designed with aid of commercial finite element analysis software, ANSYS®. Designed joints were evaluated experimentally under static and fatigue conditions with the aid of developed fixture integrated with servo hydraulic testing facility.

1.4 ORGANISATION OF THE THESIS

First chapter briefly discusses the motivation of the present work which includes limitation of thermoset composite leaf spring, need for new class of material and manufacturing technique for leaf spring. Methodology adopted to achieve major objectives of the present work is outlined in this chapter.

Literature review on wear, damping, fatigue and creep performance of chosen class of leaf spring materials and thermoplastic composites were discussed in the second

chapter. Prior works related to design; manufacturing and evaluation of thermoset composite leaf springs are also discussed in this chapter.

Third chapter discussed the materials used for developing thermoplastic leaf springs and test specimens. Efforts carried out to determine the fiber length distribution is also highlighted in this chapter.

Experimental friction and wear performance of discontinuous fiber reinforced leaf spring materials under adhesive and abrasive modes is discussed in chapter four.

Fifth chapter reported various damping sources of leaf spring material with various experimental techniques; free vibration, forced vibration, dynamic mechanical analysis. Correlation of hysteretic heating with material damping is also reported in this chapter.

Design of leaf spring as per society of Automotive Engineering (SAE) standards and finite element analysis are discussed in chapter six. Computer aided simulation results of leaf spring manufacturing and manufacturing details of die and leaf spring are included in this chapter. Preliminary static performance of developed leaf spring with the aid of developed fixture is also reported in this chapter.

Fatigue performance along with the failure morphology of test leaf spring is presented in chapter seven. Damage progression during service with the aid of cyclic load-deflection plot is also discussed. Chapter seven also presented short term flexural creep performance of test leaf springs.

Chapter eight presented static and fatigue performance of leaf spring end joint. Influence of clearance and notch on joint performance is also reported along with the failure mechanisms.

Major conclusions drawn from the present work and scope for the future work are outlined in the last chapter.

CHAPTER 2

LITERATURE SURVEY

2.1 INTRODUCTION

Research and development of thermoset composite leaf springs progressed significantly for the past three decades. Present work attempted to identify the scope of using thermoplastic composite material for leaf spring application. Since there is a need to review the prior work to understand the relevant mechanical behaviors of thermoplastic composite for leaf spring applications; adhesive wear, abrasive wear, damping, static, fatigue and creep behavior of thermoplastic materials were presented in this chapter. In the present work, long fiber reinforced thermoplastic material is considered for leaf spring, hence its various engineering application was also dealt in the chapter. This chapter also presented prior work on metallic and thermoset composite leaf spring to understand the methodology followed in design, manufacturing and performance evaluation. Joint performance is one of the crucial issues in the composite part performance evaluation of leaf springs for the structural application; hence prior work on joint design and performance evaluation of polymer composites is also presented in this chapter.

2.2 CHARACTERIZATION OF THERMOPLASTIC COMPOSITES

2.2.1 Adhesive Wear Characteristics

Relative motion between the mating surface and fracture of adhesive bonded junction contributes to the adhesive wear (Clerico and Patierno, 1979).

In contact applications, low friction coefficient, self lubrication, good chemical resistance of polymers provides a greater scope over metals (Throp, 1982). The major parameters that affect the sliding wear characteristics of polymers are normal load, sliding velocity, counter face roughness, surface energy, temperature, molecular orientation of the polymers and viscoelastic nature of polymer (Stachowiak and Batchelor, 2001).

Formation of transfer film on the metal counter face influences the coefficient of friction to a greater extent (Owei and Schipper, 1991). Higher sliding speed and normal load resulted in higher wear rate due to the formation of thicker molten film in ultrahigh molecular weight polyethylene (UHMWPE) (Barrett *et al*., 1992). Bahadur (2000) visualized that the formation of transfer layer in polytetrafluoroethylene (PTFE) on the counter face reduced the friction and wear characteristics of the polymer and reported that wear performance depends on the stability of transfer film. Mergler *et al.* (2004) investigated the adhesive wear of polyoxymethylene (POM) and reported that the formation of transfer layer is due to mechanical interlocking of polymer material and metal asperities.

Addition of glass and carbon fibers significantly enhances the wear resistance of polymers (Clerico and Patierno, 1979; Palabiyik and Bahadur, 2002; Unal *et al*., 2004). Bahadur and Polineni (1996) visualised the fluctuations of friction coefficient with respect to sliding distance for glass fabric-reinforced polyamide composites and reported the influence of changing conditions at the interface caused by periodic ploughing and rolling action of debris. The wear behaviour of short fiber-reinforced composites is dominated by the process of fiber peeling-off (Voss and Friedrich, 1987). Zhang *et al*. (2000) studied the influence of fiber length on glass fiber-epoxy composites and reported the enhanced ability of longer fibers to avoid fiber peeling.

Zhang *et al.* (2006) investigated the effect of fiber length on tribological properties of short carbon fiber reinforced epoxy composites and confirmed that longer fiber composite possessed better resistance than shorter fiber thermoset composites. Mathew *et al*. (2007) conducted wear tests on a reciprocating sliding test rig with ball-on-plate configuration for four types of directionally oriented warp knit glass performs with polyester, vinylester and epoxy resin and reported the enhanced wear resistance of epoxy resin compared to counterparts. Mathew *et al*. (2009) have studied the effect of sliding frequency on the reciprocating sliding wear behavior of 3D-plywoven interlocked structures with varying interlacement for nylon fiber/polyester resin composites and identified the best composite based on the arrangement of interlacement

2.2.2 Abrasive Wear Characteristics

Abrasive wear is the material loss due to the passage of hard material over the soft surface. Abrasive wear process in polymers involves dissipation of frictional work and its resultant damage is relatively larger volume than adhesive wear (Briscoe, 1981). Mechanical properties; hardness and material crystallinity found to improve the abrasive wear resistance (Briscoe and Evans, 1989). Arnold *et al*. (1991) investigated the importance of interfacial adhesion to improve the wear resistance of glass filled rubber. Helen *et al*. (1996) investigated the influence of crystallinity over wear resistance of nylon matrix. Experimental observations revealed that higher percentage of crystallinity in the polyamide matrix due to optimized cooling history provided higher wear resistance and higher scratch coefficient. Due to repeated passage of pin over the same wear track, the wear debris formed accumulates between the spaces between the abrasive grits (Rabinowicz, 1995).

Abrasive wear of reinforced polymers is influenced by the matrix, reinforcement and the operating parameters; load, velocity and abrasive grit size (Harsha and Tiwari, 2002). Harsha and Tewari (2003) found that the specific wear rate of polyaryletherketone composites under multi pass condition was less than that of single pass condition and identified the influence of counter face modification under multi pass abrasive condition. Clogging of abrasive grits depends upon the wear debris size and also the abrasive grit size for nylon clay composites (Srinath and Gnanamoorthy, 2006).

2.2.2.1 Influence of Fiber Reinforcement on Abrasive Wear

The abrasive wear behavior of PEEK/polypropylene sulfide (PPS) blended thermoplastic polymer reinforced with short carbon and glass fiber was investigated by Lhymn *et al*. (1985) and reported that the wear rate was sensitive to the orientation of the fiber axis with respect to the sliding direction. Cirino *et al.* (1987) studied the abrasive wear behavior of unidirectional continuous glass fiber and focused the effect of operating variables on the polymer matrices. Sole and Ball (1996) reported that the addition of mineral fillers to the polypropylene matrix decreased the wear resistance during the single pass abrasive wear test. It was also found that the shape and size of the reinforcing filler influences the wear performance under abrasive wear condition. McGee *et al.* (1997) investigated the importance of fiber matrix adhesion in reducing the abrasive wear resistance in the graphite filled nylon matrix configuration.

Bijwe *et al*. (2001) reported that the addition of glass, aramid and carbon fibers in polyetherimide composites improved the abrasive wear characteristics and reported the influence of operating parameters on abrasive wear resistance. Barkoula and Karger (2002) investigated the erosive wear of polypropylene reinforced with

glass fibers with length of 2 and 10 mm and reported fiber length did not affect the erosive wear at high impact angle. Tong *et al*. (2006) reported the influence of aspect ratio on wear resistance; with the addition of wollastonite fibers with a large aspect ratio, the abrasive wear resistance was improved by hindering the easy removal of fibers from high molecular weight polyethylene (HMWPE) matrix. Suresha *et al.* (2007) investigated the worn out surface of carbon epoxy and glass epoxy composites using scanning electron microscope and visualized the breakage of more glass fibers compared to carbon fiber due to improved interfacial adhesion between epoxy and carbon fiber. Kanagaraj *et al*. (2010) observed the decrease in wear coefficient and wear volume with the addition of carbon nano tubes in ultrahigh molecular weight polyethylene (UHMWPE) polymer and reported that wear volume increases with the sliding distance.

2.2.3 Damping Characteristics of Thermoplastic Composites

Discontinuous fibers in the composite material alter damping characteristics owing to the presence of fiber-matrix interfacial bond, voids and stress concentrations around fiber ends (Nelson and Hancock, 1978; Kenny and Marchetti, 1995; Chandra *et al*., 1999). Damping behavior of short glass and boron fiber epoxy composite material was high compared to continuous fiber material for the same volume fraction of fibers due to high stress concentration near the fiber tips and friction loss due to fiber matrix interface (Hashin,1970). Damping characteristics of short steel fiber reinforced silicon rubber was carried out with both bonded and unbonded fiber/matrix interfaces by Nelson (1976). It was observed that the influence of interfacial slip in unbonded material was more pronounced in affecting the damping and stiffness of the composite. Gupta *et al*. (1990) identified various sources of energy absorbing

mechanisms in short glass fiber reinforced polypropylene from tensile test due to plastic deformation of the matrix, de bonding and fiber pull-out. Interfacial strength in fiber reinforced thermoplastics alters the damping values to a greater extent (Carwalho and Bretas, 1990; Kubat *et al.*, 1990). High shear stress at the end of the fiber with a bonded interface found to be most viable mechanism for increased damping (Chandra *et al.*, 1999). Gassan and Bledzki (2000) investigated jute fiber reinforced polypropylene and reported that the influence of fiber matrix adhesion plays a vital role on dynamic modulus and specific damping capacity. Adams and Maheri (2003) proposed a model to understand the basic damping mechanisms of laminated composite plates, in which the damping capacity for various fiber orientations was estimated and compared with experimental results. Understanding the interaction between fatigue damage and damping is necessary to improve the composite microstructure (Kultural and Eryurek, 2007).

2.2.3.1 Damping Evaluation through Free and Forced Vibrations

Free vibrations characteristic of visco-elastic materials were evaluated through Fourier analysis (Ruland, 1984). Saurez *et al*. (1986) reported the influence of fiber length on the damping characteristics of discontinuous aramid and boron fiber reinforced epoxy laminates and observed that composite with low fiber aspect ratios exhibited good damping behavior. Hadi and Ashton (1986) investigated the influence of fiber orientation on the damping properties of glass epoxy material through flexural resonance method at various frequencies and reported the increase in loss factor with the decrease in fiber volume fraction. Crema *et al.* (1989) evaluated damping coefficient by exciting a cantilever specimen made of short glass fiber reinforced thermoplastics with different fiber orientations and experimental results were

compared with classical models. Wray *et al.* (1990) investigated the influence of fiber orientations and volume fractions towards logarithmic decrement for short glass fiber reinforced polypropylene. A reduction of logarithmic decrement with increased storage and loss modulus with increase in fiber volume fraction was observed. Lee *et al.* (1994) investigated the dynamic characteristics of carbon fiber reinforced polyether-ether-ketone through flexural and torsional vibration tests; measured natural frequency and specific damping capacity were compared with finite element analysis results. Gu *et al.* (2000) used vibration damping technique for evaluating the properties in the interfacial region and observed an inverse relationship between damping and interface for glass-fiber-reinforced epoxy resin composites. Material damping reduces structural vibrations and thereby moderate propagation of fatigue damage (Croce *et al*., 2001; Zhang and Hartwig, 2001). Chandradass *et al*. (2007) investigated the damping characteristics of hybrid nanocomposite laminates by reinforcing short fiber chopped strand mat and organically modified montmorillonite clay by conducting free vibration tests. Improvement in damping factor was observed up to 3% by weight of organically modified clay.

2.2.3.2 Damping Evaluation through Dynamic Mechanical Analysis

Dynamic mechanical analysis permits to understand the viscoelastic behavior of polymers over a wide range of temperatures and frequencies. Thomason and Groenewoud (1996) highlighted the importance of fiber length in the retention of stiffness between the glass transition and melting temperatures of polypropylene matrix. Addition of short sisal fibers in the polypropylene matrix increases the storage and loss modulus but lowers the damping factor due to reduced molecular mobility (Joseph *et al*., 2003). Sefrani and Berthelot (2005) investigated the temperature effect

on the stiffness and damping of glass fiber epoxy material manufactured through hand layup process. Near the glass transition temperature of the matrix, the material rapidly becomes very soft and dampened over a short temperature range. The glass transition temperature of carbon fiber polypropylene composite increased with the increase in fiber length (Rezaei *et al*., 2009).

2.2.4 Fatigue Performance of Thermoplastic Composites

Utilization of glass fiber thermoplastic composites in structural applications demands the understanding of fatigue behavior in service conditions. Due to the viscoelastic characteristics of the matrix material, fatigue behavior of thermoplastic composites is significantly influenced by alternating stress, frequency, mean stress, temperature, surface condition and environment (Manson *et al*., 1975; Sauer and Richardson, 1976; Martin and Gerberich, 1976).

Polymer structure, molecular weight, fillers and reinforcement also influences the fatigue strength considerably (Dally and Carrillo, 1969; Warty *et al*., 1979; Karger-Kocsis and Friedrich, 1988). Mandell (1983) observed accumulating creep strain and decreasing modulus until failure for nylon 66 glass fiber composites during fatigue testing. Mandell and Chevaillier (1985) observed that failure of pure polyvinyl chloride involves craze, crack initiation growth and coalescence during fatigue and reported the formation of crazes in stabilizing the crack growth. It was also reported that the major mechanism of cumulative damage for reinforced thermoplastics are the creep-rupture of the matrix combined with debonding of the fibers. Fatigue damage in discontinuous fiber reinforced engineering thermoplastics under alternating loading is induced by the initiation and crack propagation in the matrix and destruction of bonding at the polymer/matrix interface (Karger-Kocsis and Friedrich, 1988).

Apart from composite endurance strength of the composites evaluated from fatigue tests, accumulated damage in the form of stiffness loss, energy dissipation and rise in temperature were also addressed by Orth *et al*. (1993). Lin *et al.* (1996) investigated the stiffness loss of long glass reinforced polyamide composites and observed the crack formation along with stiffness deterioration. Ferreira *et al*. (1999) observed the temperature rise during fatigue testing of glass fiber reinforced polypropylene and correlated with the deteriorating stiffness of the composite. Long glass fiber thermoplastics exhibited high fatigue crack propagation resistance than short glass fiber due to the less stress concentration sites (fiber ends) for a given fiber volume fraction (Karger-Kocsis and Friedrich, 1988). Czigany and Karger-Kocsis (1993) investigated the failure mode of short and long glass fiber polypropylene and reported an increase in fracture toughness of the long glass fibers composite due to the improved fiber/matrix coupling and stress transfer capability. Khanh and Denault (1994) used post yield fracture mechanics theory to investigate the fracture performance in long glass fiber reinforced polypropylene and reported that the crack growth resistance was improved with the fiber volume fraction and an performance plateau was reached when the glass fiber volume fraction reached 35%. Wyzgoski and Novak (1995) reported that the presence of long glass fibers imparted improved fatigue resistance than short fiber reinforced nylon 66 due to the presence of higher modulus long glass fibers.

Interfacial strength of a composite plays a significant role in the fatigue behavior. Gamstedt *et al.* (1998) observed no significant improvement of static strength but significant improvement of fatigue performance for the maleic-anhydride grafted polypropylene matrix. Bureau and Denault (2004) studied the dependence of temperature on flexural fatigue of continuous glass fiber polypropylene and observed

the major role of fiber–matrix interface on mechanical properties. Rajeesh et al. (2010) studied the influence of relative humidity on indentation hardness and flexural fatigue of polyamide 6 nanocomposites and reported a reduction in hardness and modulus of the composite with the increase in humidity. Hysteresis heating and molecular orientations were spotted as the main reason for drop in modulus during fatigue.

2.2.4.1 Hysteretic Heating of Thermoplastic Composites

Viscoelastic nature of thermoplastic composites dissipates energy in the form of hysteretic heating during fatigue and cause thermal softening (Sauer and Richardson, 1979). Presence of fibers in the matrix reduces thermal softening (Rosato *et al*., 2001). Rittel *et al*. (2003) examined the hysteretic thermal response of modified polymethylmethacrylate (PMMA) at high stress level and chain mobility was identified as contributing parameter under cyclic loading. Moisa *et al*. (2005) reported the heat generation of polymethylmethacrylate (PMMA) and polycarbonate (PC) material under cyclic compressive loading and observed the significant influence of frequency and applied stress on heat generation.

Bellenger *et al*. (2006) investigated the bending fatigue performance of glass fiber reinforced polyamide 66 and measured specimen temperature using infra red camcorder. Experimental observations revealed that damage was initiated at fiber ends close to sample edges where the stress concentration was high and the damage propagates from sample edges to sample core during fatigue. Kultural and Eryurek (2007) observed an increase in fatigue life with the addition of calcium carbonate in polypropylene matrix under high frequency loading conditions. In this work, influence of loading frequency and percentage of calcium carbonate over material

temperature rise was also investigated. Addition of long glass fibers in the polypropylene matrix reduced the temperature rise during dynamic loading conditions due to the hysteretic phenomenon and provides higher fatigue life (Goel *et al*., 2008).

2.2.5 Creep Performance of Thermoplastic Composites

Common problem associated with the unreinforced thermoplastics is creep under moderate to severe stress at elevated temperature. Creep resistance of thermoplastic composites is significantly improved by increase in fiber loadings (Gupta and Lahiri, 1980; Silverman, 1987). Silverman (1987) compared and investigated the flexural creep response for long glass and short glass fiber-reinforced polycarbonate and polypropylene polymers at various temperatures. Reduction in creep performance at elevated temperature was visualized for short fiber materials. Dynamic mechanical analysis (DMA) was utilized to investigate the viscoelasticity of injection-molded nylon 6/6 material reinforced with short and long glass fibers by Sepe (1994) and reported an increase in creep resistance for long glass fiber reinforced nylon composites.

Challa and Progelhof (1995) investigated the effect of temperature on the creep characteristics of polycarbonate and developed a relationship based on Arrhenius theory to develop creep master curves. Long-glass-fiber-reinforced thermoplastics offer advantages in components that are subject to creep because of their superior creep resistance and more isotropic performance in comparison with short-fiber counterparts (Kim *et al*., 1997). Pegoretti and Ricco (2001) studied the propagation of crack under creep for varying temperature conditions for polypropylene composites and observed that speed with which the crack progresses was dependent on the test temperature. Krishnaswamy (2005) performed extensive

creep rupture testing on high density polyethylene pipes at various hoop stress levels and temperatures and observed the dependency of density and crystallinity towards failure. Houshyar (2005) reported the improvement in creep properties with the addition of long polypropylene fibers in propylene-*co*-ethylene (PPE) matrix and visualized the improvement in interfacial properties. Trans-crystallization of the polypropylene matrix was observed in the PPE samples due to the thin layer of matrix on the reinforcement, which was attributed to good impregnation and wetting of the fibers. Greco *et al.* (2007) investigated the flexural creep behavior for compression molded glass fiber reinforced polypropylene at various applied stress level. The effect of matrix crystallinity was highlighted for the improvement in creep properties for glass fiber reinforced polypropylene in their work. Acha *et al*. (2007) studied the influence of interfacial adhesion in discontinuous jute fiber reinforced polypropylene. Relation between interfacial properties and creep deformation were investigated. Higher creep resistance was observed for polypropylene composites with good interfacial bonding which was confirmed by the observation of the composite fractured surfaces.

2.2.5.1 Creep Models

Findley and Khosla (1955) conducted creep tests for unreinforced thermoplastics; polyethylene, polyvinyl chloride and polystyrene. Approximation was carried out for the linear viscoelastic region by power law and compared the creep performance by estimating the power law coefficient and power law exponent. Liou and Tseng (1997) used Findley power law to estimate the creep compliance of carbon fiber nylon composites in hygrothermal condition. Power law model was modified by Hadid *et al*. (2002) by incorporating the time and stress dependence during creep loading of

polyamide specimens and estimated four parameters for describing the deformation occurring in the material. Hadid *et al.* (2004) used stress–time superposition principle to predict long-term material creep behavior of injection molded fiber glass reinforced polyamide. Master curves were developed and a perfect superposition of the curves at various stress levels was visualized. Fan and Novak (2006) used strain energy equivalence theory and developed a creep predictive model to predict the creep behavior of talc filled polypropylene.

Experiments were performed at various strain rates and later predicted for creep performance at various stresses. Banik *et al*. (2008) reported the improvement in creep resistance due to unidirectional reinforcement for polypropylene-polypropylene composites. Burger and Findley power law model were used to predict the short term creep behavior and the underlying deformation mechanisms were also investigated. Liu *et al*. (2008) used multi-Kelvin element theory and power law functions to predict creep compliance in polyethylene material and compared with the tensile creep experiments. Chevali *et al*. (2009) studied the flexural creep response of nylon 6/6, polypropylene and high-density polyethylene long fiber thermoplastic composites. Four parameter model proposed by Hadid *et al*. (2002) was used to fit the experimental data and good agreement was visualized. Nylon 6/6 had the least creep compliance than polypropylene and high-density polyethylene.

2.2.6 Engineering Application of Long Fiber Reinforced Thermoplastics

Injection molded long-fiber reinforced thermoplastic products possess mechanical properties that approach to those of a component made by continuous fiber reinforcement (Marshal, 1987). Long fiber reinforced pellets for injection molding enhance fatigue strength, impact, temperature resistance than that of conventional

short-fiber compounds (Thomason, 2002). Deaver and Mcllvaine (2005) replaced steel with long fiber reinforced polypropylene in running boards and reported significant weight reduction, corrosion resistance, scratch resistance and cost reduction due to the replacement. Bartus *et al.* (2006) used long glass fiber thermoplastic polypropylene to develop bus seat by extrusion-compression molding and confirmed 43% weight reduction and 18% cost reduction. Process simulation was carried out to study the extent of filling and fiber orientation.

Noh *et al.* (2006) developed a door module with 40% long glass fiber reinforced polypropylene and reported a weight reduction of 12% for the door module assembly. The developed door module was subjected to various tests; waterproof test, drop-weight test and stiffness test. Weight reduction of 60 % was achieved by Thattaiparthasarathy *et al.* (2008) with the replacement of metallic battery door by long glass fiber polypropylene for mass transit application; fiber orientation in the final molded part was verified experimentally and stiffness measurement was compared with the finite element results. Vaidya *et al*. (2008) used 40% weight of long glass fiber nylon thermoplastic for developing tailcone for military application. Finite element analysis was carried out for the design and evaluation of the composite tailcone considering pressure, gravitational and temperature load during the flight. Field tests were also conducted to verify the design and manufacturing aspects of long fiber composite tailcone.

2.3 METALLIC LEAF SPRING

Rajendran and Vijayarangan (2001) carried out static and modal analysis for graduated seven leaf springs joined by two U-bolts to evaluate the strength and vibration behavior. Leevy and Cao (2004) explored the fundamentals of combining

dissimilar materials and showed the role of combined equivalent modulus on overall stiffness characteristics of multi leaf spring design. Sugiyama *et al*. (2005) demonstrated the use of nonlinear finite element formulations to study the performance of leaf spring under dynamic conditions. Moon (2007) carried out simulation to plot the hysteretic curve of steel leaf springs and validated with the experimental results. Dynamic stress analysis was on the taper steel leaf spring with the developed multi-body dynamic model. Yoo *et al*. (2007) proposed a numerical procedure to estimate the fatigue life of leaf springs and identified crucial design parameters in influencing the fatigue life. Liu (2009) studied the stress, stiffness and inter-leaf slippage of tapered leaf spring using finite element tool and reported the stiffness change due to slippage between individual leafs.

Santika *et al*. (1988) performed durability test on leaf spring with shock absorbers using servo hydraulic test machine at constant amplitude. Leaf spring characteristics; spring rate and damping force were evaluated. In general metallic leaf spring failure diagnosis involves examination of manufacturing and failure histories through macroscopic inspection, chemical analysis, metallographic analysis and hardness measurements (Mukhopadhyay *et al*., 1997; Graham, 2004; Herrera *et al*., 2004). Belogur *et al*. (2004) examined the characteristics of steel and titanium alloy leaf springs towards corrosion resistance, thermo mechanical properties and relaxation capacity. Fuentes *et al.* (2008) investigated the fracture behavior due to mechanical fatigue and observed that crack nucleated at the region of the central hole in secondary leaf of the spring.

Tanaka *et al*. (1985) observed a reduction in fatigue strength due to fretting for high strength spring steel and effectively utilized J-integral theory to predict the crack propagation. Mutoh *et al*. (1986) reported the deterioration of surface quality due to

fretting fatigue between mating leaves of multi leaf steel leaf spring and reported the substantial decrease in the fatigue strength of the component. The modification of leaf spring tensile surface by shot-peening created residual compressive stresses resulted in fatigue life and stress corrosion resistance improvement (Siswosuwarno *et al*., 1985; Todinov, 2000). The effect of shot peening on full scale testing of leaf springs was conducted by Aggarwal *et al*. (2006) and developed a fatigue model based on the surface modification on the leaf spring. The model addressed the influence of various shot peening conditions on the leaf spring performance and reported the influence of fretting fatigue between mating leaves in decreasing the fatigue life.

2.4 COMPOSITE LEAF SPRING DESIGN

Leaf spring accounts for 10-20 % of the unsprung weight and hence reduction of unsprung mass helps to improve ride characteristics and increased fuel efficiency (Tanabe *et al*., 1982). Various design works on thermoset leaf springs have been reported in the past. Morris (1986) developed a program to determine the thickness at the center, maximum stress and maximum shear stress for a single transverse leaf spring made of glass fiber epoxy material. In addition, the developed program was utilized to obtain load deflection values for zero to full bump loads. Lo *et al.* (1987) analyzed the glass fiber epoxy leaf spring as a curved beam with various sections carrying a concentrated load, later expressions were derived along the length of the leaf spring at various sections and design was used for tank trailer suspension system.

Yu and Kim (1988) considered leaf spring as two tapered cantilever beam and estimated the optimal taper ratio as 0.5. Beam dimensions for the glass fiber reinforced epoxy leaf spring were determined by considering the vertical end force and later finite element analysis was carried out. Corvi (1990) utilized Timoshenko

beam theory for developing composite beam for leaf spring application by considering vertical and transverse loading conditions. Effect of fiber volume fraction, fiber lamination angle on leaf spring behavior was also evaluated. Sancaktar and Gratton (1999) used spread sheet solver for optimizing the glass fiber epoxy leaf spring for solar vehicle application and highlighted the importance of providing high moment of inertia at the center of the leaf spring where it is subjected to high moments. Rajendran and Vijayarangan (2001) used genetic algorithm to determine the width and thickness at the axle seat for the designed glass fiber epoxy leaf spring. Qureshi (2001) used Tsai-Hill failure criterion for developing an expression as a function of thickness and position along the spring. Later the developed equation for the glass epoxy leaf spring was utilized to determine the thickness at any section along the leaf spring length. Shokrieh and Rezaei (2003) used finite element tool to optimize fiber glass epoxy resin leaf spring by considering Tsai-Wu failure criterion and reported a higher natural frequency and weight reduction for the proposed thermoset leaf spring compared to that of metallic leaf spring.

Mold part quality is significantly influenced by the gate location as it influences the plastic flow into the mold cavity. Luscher and Houser (2000) investigated the influence of gating position and packing pressure on the transmission error and shrinkage of Polyketone gears and validated the results with mold flow software. Transmission error was found to be dependent on the gating position and shrinkage was found to be maximum on the gated side of the gear. Imihezri *et al*. (2006) analyzed two different types of profile with and I and T cross-sections using mould flow analysis for automotive clutch pedal made from glass fiber reinforced polyamide and reported that I cross-section is superior to T section in terms of load carrying capability. Zainudin *et al*. (2002) reviewed the numerical and experimental

investigations carried out on short glass fiber reinforced injection molded thermoplastics towards fiber orientation distribution (FOD) and reported the influence of injection speed, fiber concentration, cavity thickness and gate location in deciding the FOD. Simoes (2001) developed a prototype vehicle by considering the aesthetics and ergonomic design. Composite sandwich structure made of woven carbon fabric and commercial polyvinyl chloride foam material was utilized for the cockpit and chassis.

2.5 DEVELOPMENT AND PERFORMANCE OF COMPOSITE LEAF SPRINGS

During the past two decades, significant effort has been made by the automotive industries to utilize thermoset material for leaf spring application. Commonly used manufacturing techniques in the past were filament winding, compression molding, combination of both and hand lay-up vacuum bag process. Delphi (1981) used filament winding technique with epoxy resin and unidirectional fiber glass (Liteflex®) for rear suspension of corvette cars. Road test conducted on Liteflex® composite springs confirmed the potential of improved durability, ride and shock isolation. Daughtery (1981) studied the hybrid combination of steel with fiber glass-epoxy leaves and reported cost-effective solution. Beardmore and Johnson (1986) used glass fiber reinforced epoxy resin for composite leaf springs and stressed the importance of enhanced ultimate and fatigue strength compared to metals. Morris (1986) used 50 % volume of glass fibers in epoxy matrix for fabricating leaf spring with the aid of filament-winding as well as compression molding process. The springs were installed in the vehicle and the spring rate was checked statically. Real time tests were carried out under harsh road conditions to simulate the accelerated fatigue tests and observed

local delamination due to fiber damage on the tensile side of leaf spring. Beardmore (1986) demonstrated three types of manufacturing process involved in fabricating leaf springs by compression molding, hand lay-up and pultrusion. The advantage of using pultrusion technique in manufacturing constant cross section spring was highlighted in his methodology.

Lo *et al.* (1987) developed constant width, variable thickness glass fiber reinforced epoxy leaf spring for tank trailer suspensions by compression molding. Spring rate was measured in the laboratory and delamination was observed adjacent to clamping area due to the existence of excessive torque. Yu and Kim (1988) used filament winding technique followed by compression molding process for fabricating glass fiber epoxy leaf spring. Static test was conducted using electro-hydraulic spring testing machine and observed a good agreement between experimental and designed spring rate. Fatigue performance test was carried out and stiffness retention was visualized for the design load. Theren and Lundin (1990) replaced three leaf steel springs with filament wounded glass fiber epoxy leaf spring and conducted static and fatigue test. The static test was carried out by subjecting the leaf springs to vertical loads, lateral loads, braking loads, rolling loads and observed a satisfactory performance. Fatigue tests were conducted using a developed fatigue test rig and observed a satisfactory performance. Sancaktar and Gratton (1999) used hand lay-up technique for fabricating glass epoxy leaf spring and the stiffness was measured using three point bending technique. Qureshi (2001) developed variable thickness leaf spring made of glass fiber epoxy material using vacuum bag lay-up technique and road test was performed and reported the enhanced flexibility and reduced noise and harshness level compared to that of steel leaf springs. Hou *et al.* (2005) developed polyester glass fiber leaf springs using resin transfer molding and performed static

tests and showed that the composite leaf springs satisfactorily carry the maximum design load. A dedicated shaker rig was used to investigate dynamic response of the leaf spring under various loading conditions. Shankar and Vijayarangan (2006) reported the development of glass fiber epoxy leaf spring using hand lay-up technique and static performance was investigated with the aid of developed test rig and observed similar spring rate to that of steel leaf spring. Cherruault *et al*. (2010) developed glass fiber-reinforced polyester leaf suspension for rail way freight vehicles using resin transfer molding. Shaker rig testing methodology was utilized to estimate the rail suspension dynamic properties and reported that viscous damping and low dynamic stiffness of glass fiber-reinforced polyester leaf spring provides as an effective solution for track friendly suspension system.

2.6 BOLTED JOINT PERFORMANCE OF COMPOSITE MATERIALS

Joint strength between leaf spring and eye end must have superior strength than that of the designed leaf spring so that composite leaf springs can be a viable suspension system (Yu and Kim, 1988). Bolted joints were found to be more useful than adhesive bonded joints, due to the superior load transfer and less sensitive to the surface preparation characteristics (Camanho and Matthews, 1997). Shokrieh and Rezai (2003) proposed four different types of end joints for the leaf spring application and highlighted the manufacturing easiness and significance of bolted joints. Bolted joints and adhesively bonded joints are commonly being utilized for joining the composite structures. Common failure observed in mechanical joints of polymer composite parts are tension, shear, bearing, cleavage and pull-through failures (ASTM D5961, 2005). Various aspects of joint performance such as geometric configurations, fastener preload, failure mode under static and fatigue conditions, effects of service conditions

(temperature and moisture) on joint performance and non-destructive evaluation techniques have been carried out in the past (Thoppul *et al*., 2008).

2.6.1 Composite Joint Design

Geometric configuration of joint significantly alters the bearing strength and failure mode. Collings (1977) investigated the influence of geometric parameters *viz.* width, hole diameter, end distance and thickness on the joint strength performance and reported that the bearing strength of carbon fiber reinforced plastics can be improved by increasing the lateral compressive stress around the loaded hole. Godwin *et al.* (1982) used glass fiber reinforced polyester material for multi-bolt joints and reported pitch as an important design parameter in the bolted joint performance. Kretsis and Matthews (1985) observed the change in failure mode from bearing to tension when the specimen width decreases for glass fiber reinforced epoxy laminates.

Chen and Lee (1995) investigated the effect of friction, clamping pressure, clearance and stacking sequence of pin loaded joints using finite element technique on glass fiber epoxy laminates. The maximum load that can be sustained before failure was predicted using the maximum stress theory and later confirmed with the experimental results. It was also observed that the dependency of failure mode was dependent on lay-up characteristics rather than fiber/resin combination. Similar observation was substantiated by Park (2001), Okutan (2002), and Lim *et al.* (2006) for E-glass epoxy laminate. McCarthy *et al*. (2005) developed a three dimensional finite element model for multi-bolt, double-lap composite joints and addressed the progressive damage induced due to the effect of clearance and studied the damage mechanisms of the joint. The influence of traction forces by two parallel rigid pin for two parallel circular holes in woven glass fiber - vinylester was investigated by

Karakuzu *et al.* (2008) and reported the influence of end distance on failure mode. Yavari *et al*. (2009) evaluated the stress distribution around the hole of epoxy laminates and reported that the higher friction and smaller plate width would offer safe joint. Atkas *et al.* (2009) observed good agreement between experimental and numerical predictions during the joint performance for glass-epoxy laminate and observed maximum bearing load for the glass fiber epoxy composite plates in double pinned joints, when the ratio of end distance to the hole center was greater than four.

2.6.2 Influence of Clamping, Clearance and Notch on Composite joint

Clamping torque alters the static and fatigue performance of bolted joints. Stockdale and Matthews (1976) investigated the effect of clamping pressure on bolt bearing loads for glass fiber epoxy polymer parts. Static and fatigue strength of the graphite-epoxy laminate was found to be improved with higher clamping torque (Crews, 1981). Sun *et al*. (2002) observed the effect of clamping area on improving the failure load of the graphite epoxy laminate joint. Khashaba *et al*. (2006) investigated the effect of washer size on the strength of composite bolted joints made of glass fiber reinforced epoxy laminates. For a constant clamping torque, the stiffness and the failure load of the joint decreases with the increase in washer diameter due to the reduction in contact pressure with increasing clamping area. Pakdil *et al.* (2007) reported different failure mode at various clamping torque of glass fiber epoxy laminated plate and highlighted the importance of increasing the preload for obtaining safe bolted joint characteristics.

Clearance plays an important role in altering the stiffness and damage encountered in bolted composites (Naik and Crews, 1986). Clearance fits should be avoided due to reduced contact area between the bolt and the bolt-hole, which causes

higher compressive contact stresses on the bearing surface (Scalea *et al*., 1998). McCarthy *et al.* (2005) investigated the bolt hole clearance effect on single bolted, single lap carbon fiber epoxy joint and reported the reduction in joint stiffness due to the increase in clearance.

Material discontinuities due to hole in bolted composite joints produce areas of high stress concentrations which reduce the load-carrying capability of the composite structure. Composite constituent properties play a significant role in deciding the notched-strength performance. Carlsson *et al*. (1989) confirmed higher notch sensitivity in graphite polyetherketone composite than graphite epoxy composite and highlighted the importance of stress relieving mechanism in reducing the notch sensitivity. Swanson *et al*. (1993) observed superior performance of open hole under fatigue loading for toughened matrix system and also reported the enhancement in retaining the residual strength. Pinnell (1996) observed higher open and filled hole tensile strength in thermoplastic than thermoset composites and reported a greater stress relief at the hole edge in thermoplastic material. It was also reported that higher notch sensitivity of thermoset than thermoplastic material provides lower bearing strength to the composite for the same amount of reinforced graphite fibers. Ferreira *et al*. (1997) confirmed that stress concentration was found be more prominent in static and low cycle fatigue for fiber reinforced polypropylene material.

2.7 SUMMARY

Research work carried out on manufacturing and performance of discontinuous fiber reinforced polymer composite leaf springs indicated many intricate issues unlike metallic leaf springs. Literature review was carried out on various material

characteristics relevant to the leaf spring application; wear, damping, energy absorbing capability, fatigue, creep and joint strength characteristics. Time and temperature dependent behavior of polymer material influences the performance characteristics. Addition of fibers affects the heat generation and dissipation characteristics of composites. Incorporation of discontinuous fibers in the polymer matrix alters the material ductility and homogeneity, which alters the performance characteristics and failure mechanisms.

CHAPTER 3

MATERIALS FOR THERMOPLASTIC LEAF SPRINGS

3.1 INTRODUCTION

Ideal spring materials must have high specific strain energy capacity, excellent fatigue life and corrosion resistance. In the recent years, long fiber reinforced thermoplastic material are being used extensively in mass transit industrial components, due to its mass production capability ,good endurance strength ,creep strength etc. which are the major requirement for leaf springs. Injection molded long-fiber reinforced thermoplastic products possess mechanical properties that approach to component made by continuous fiber reinforcement (Marshal, 1987). Increased length and fiber orientation within pellets help to increase the modulus and strength of the material as high as 90% of that obtained when using continuous fibers (Thomason *et al*., 2002). Long fiber reinforced pellets for injection molding enhance fatigue strength, impact, temperature resistance than that of conventional short-fiber compounds (Thomason, 2002). The performance of any injection molded component depends on the retained fiber length after molding process and hence investigation of fiber degradation by measuring fiber length distribution in the molded samples has been carried out in the past by fiber ash test followed by image processing techniques (Bureau and Denault, 2004; Bartus *et al.*, 2006; Bernasconi *et al*., 2007).

Materials used for developing leaf springs and test specimens are presented in this chapter. Processing conditions used for preparing the test specimens and determination of fiber length is also presented in this chapter.

3.2 MATERIALS AND PROCESSING CONDITIONS

Unreinforced polypropylene (UFPP), 20% short glass reinforced polypropylene (SFPP) and 20% long glass reinforced polypropylene (LFPP) were considered for the development of thermoplastic leaf springs. Prior to the development of leaf spring, leaf spring material characteristics like friction and damping were also evaluated for the above materials. SFPP pellets are made from extrusion process where fibers are randomly oriented as shown in figure 3.1 a. LFPP pellets were made from pultrusion technique where fibers are well oriented along the pellet length as shown in figure 3.1 b. Pellets were obtained from Saint-Gobain India, according to the product data sheet (Saint Gobain/Twintex, 2005), the base resin PP was having same molecular weight and same amount of silane type coupling agent was used for the glass fibers in LFPP and SFPP pellets. Since the amount of void content is considerably small and difficult to quantify with the test facility available, void is assumed to be same for both short and long fiber reinforced composites .Since the investigated reinforced materials have the same type and amount of coupling agent, material behavior discussions were limited only to the fiber length.

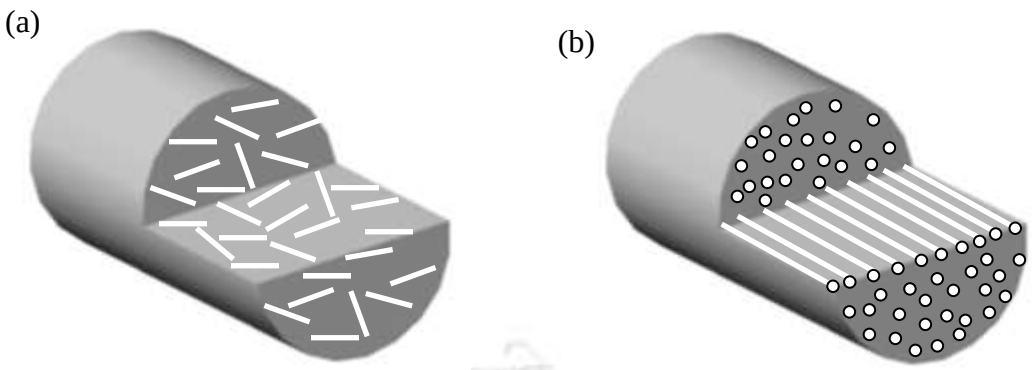

Fig. 3.1 Schematic of fibers in thermoplastic composite pellets (a) extruded short fiber reinforced pellet and (b) pultruded long fiber reinforced pellet

Table 3.1 Injection molding parameters for test specimens

Material	Zone I (°C)	Zone II (°C)	Zone III (°C)	Screw diameter (mm)	Injection speed (mm/s)	Injection pressure (bar)	Mold Temp. (°C)
Unreinforced polypropylene	190	180	175	35	80	100	30
20 % glass fiber reinforced polypropylene	240	235	235	35	65	110	30

Table 3.2 Details of reinforcements and mechanical properties of test materials

(Saint Gobain/ Twintex)

Properties	Unreinforced polypropylene	Short glass fiber reinforced polypropylene	Long glass fiber reinforced polypropylene
Fiber fraction (% by weight) ISO 3451-1	0	20	20
Fiber diameter (mm)	-	0.01	0.01
Tensile Strength (MPa) ISO 527	27	40	75
Flexural Strength (MPa) ISO 178	32	72	125
Flexural Modulus (MPa)	1724	3448	5650
Tensile elongation (%)	>10	4 - 5	3 – 4
Specific gravity ISO 1183A	0.91	1.03	1.04

Pellets were initially maintained at 80°C for 2 h, to remove excess moisture and later injection molded in to rectangular specimens as per ASTM D 638 and ASTM D 6110 standard. Specimens molded as per ASTM D 638 were used for tensile test; fiber ash test to measure the fiber length retained after molding; constant load indentation test to quantify the plastic deformation energy; hysteresis, dynamic mechanical analysis, free and forced vibration test to characterize the damping behaviour; notch sensitivity test to characterize the notch sensitive behavior and tensile fatigue to measure the hysteretic heating and understanding fatigue failure morphology. Specimens molded as per ASTM

D 6110 were used for characterizing the adhesive and abrasive wear behaviour. Molding conditions for preparing the specimen are shown in table 3.1. Mechanical properties of the test materials are listed in table 3.2 (Saint Gobain/Twintex).

3.3 FIBER LENGTH DISTRIBUTION

Rectangular test specimens were heated in a muffle furnace to 600° C for a period of about 6 h to burn out the matrix material and the extracted fibers are shown in figure 3.2. The extracted fibers were dispersed uniformly on a microscopic glass slide. Lengths of at least five hundred fibers were measured using a Zeiss microscope (KS 300) with an image analysis system. Fiber length distribution (FLD) histograms for the test materials are shown in figure 3.3. The number average length (L_n) and weight average length (L_w) were estimated.

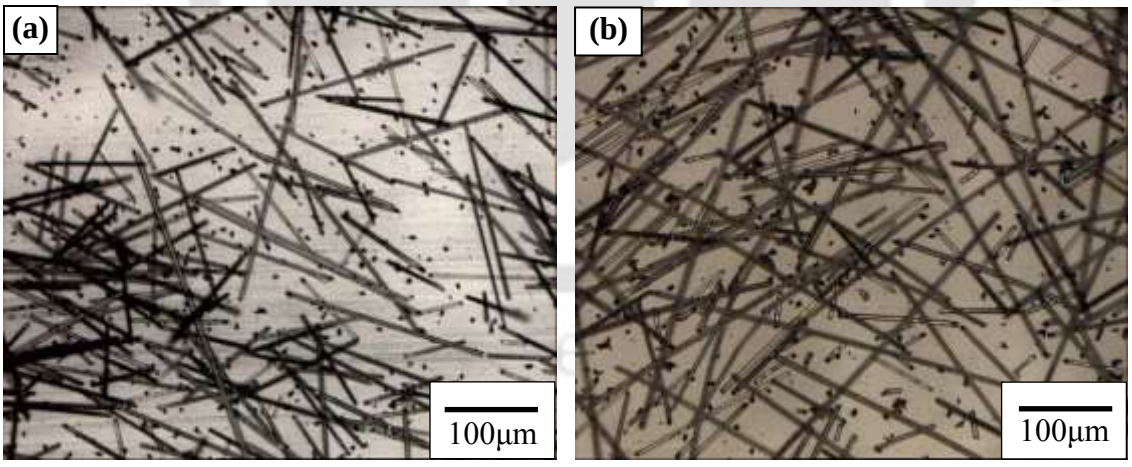

Fig. 3.2 Separated fibers from test materials (a) short fiber reinforced PP and (b) long fiber reinforced PP

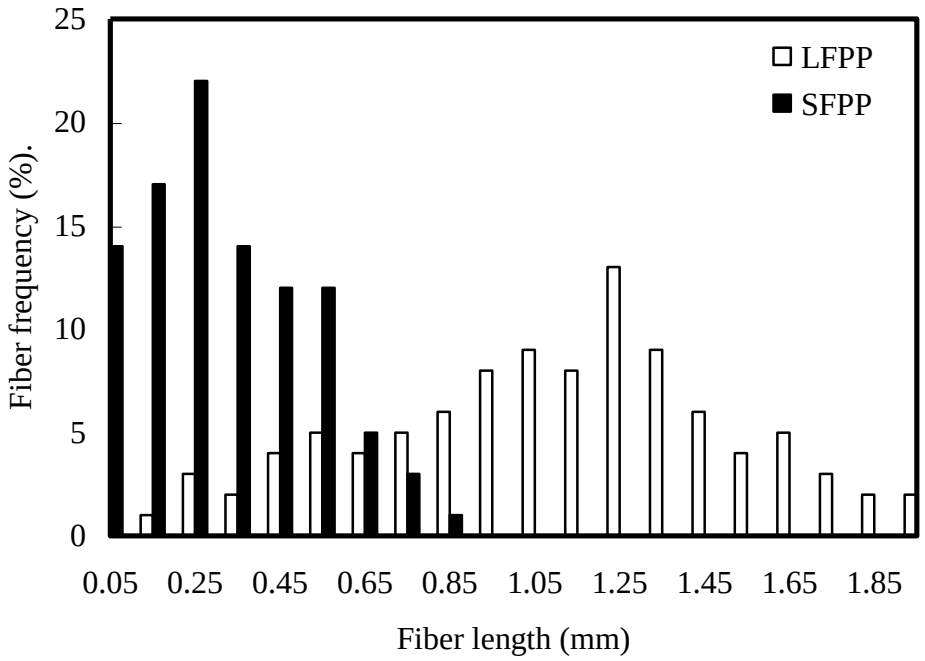

Fig. 3.3 Fiber length distribution of long and short fiber reinforced polypropylene

The number average length was estimated by the following equation

$$L_n = \frac{\sum(F_i\ L_i)}{\sum F_i} \tag{3.1}$$

and the weight average length was estimated using

$$L_w = \frac{\sum(F_i\ L_i^2)}{\sum F_i\ L_i} \tag{3.2}$$

where F_i is the number of fiber count (frequency) of fibers of species i with length L_i. For the SFPP material, number average length $(L_n)_{SFPP}$ and weight average length $(L_w)_{SFPP}$ were 0.32 and 0.44 mm respectively. Similarly for LFPP material, number average length $(L_n)_{LFPP}$ and weight average length $(L_w)_{LFPP}$ were 1.083 and 1.251 mm. Weight average

length (L_w) is commonly used to relate fiber length to mechanical behavior (Bernasconi *et al*., 2007). Hence weight average length was used for further discussions.

3.4 SUMMARY

Materials used for the development of leaf springs and test specimens were highlighted in this chapter. Injection molding processing conditions used for preparing the test specimens was also discussed. Fiber length was measured using fiber ash test followed by image processing. Test results revealed that LFPP possessed approximately three times the retained fiber length than SFPP after injection molding.

CHAPTER 4

FRICTION AND WEAR CHARACTERISTICS OF THERMOPLASTIC LEAF SPRING MATERIAL

4.1 INTRODUCTION

Suspension leaf springs are attached to the axle seat by clamps at the center and the ends are attached to the vehicle chassis through fasteners. During service condition, relative sliding motion between leaf spring with clamps and bolts necessitates to understand the friction and wear performance of the leaf spring material. Leaf spring material must be reasonably wear resistant against the vehicle chassis material, steel under adhesive and abrasive sliding condition (Yamada, 2007). Many attempts (Bahadur and Polineni, 1996; Bijwe *et al*., 2001; Unal *et al*., 2004) have been made in the past to understand the friction and wear performance of thermoplastic composite materials. However, investigations on the influence of fiber length on friction and wear characteristics of discontinuous fiber reinforced composite materials are limited (Bekhet, 1999; Zhang *et al*., 2006). Addition of fibers affect the friction and wear properties of polypropylene and the inclusion of varying fiber length need to be understood for the better utilization.

In this chapter, adhesive and abrasive wear behavior of leaf spring materials was examined with the aid of pin on disc test set up. The effect of fiber reinforcement on plastic energy of deformation, matrix crystallinity and clogging behavior under multi pass abrasive wear condition were investigated. The adhesive and abrasive wear

mechanisms of chosen thermoplastic composites were identified with the aid of wear morphology.

4.2 ADHESIVE FRICTION WEAR

Pin on disc tribometer developed by Srinath and Gnanamoorthy (2005) was utilized to investigate the adhesive friction wear performance for the chosen leaf spring materials and the testing was done as per ASTM G 99 standard. Specimens pertaining to ASTM D 6110 standard were machined to cylindrical pin of 5 mm diameter and 20 mm length. Stainless steel disc (AISI 314) having centre line average surface roughness (R_a) of 0.1433 μm was used as the counter material. Initial hardness (Shore D) of the test materials were measured as per ASTM D 2240 standard. The friction force was measured with the force transducer fixed on the loading lever arm and stored using a personal computer based data acquisition system. Adhesive friction and wear tests were conducted at 19.62 and 29.43 N normal loads with a constant sliding velocity of 0.5 ms^{-1}. Tests were conducted under dry conditions (32 ± 3°C, RH 57 ± 6 %). Data sampling rate for friction force and displacement measurement was kept as 1 Hz. Silica carbide emery paper was used to polish the test specimen to the average surface roughness value of 0.9 R_a (MarSurf M1). Test specimen mass was measured using an electronic balance of 0.1 mg accuracy. Wear tests were conducted up to a sliding distance of 3000 m. At least three tests were conducted at similar test conditions and the average values of frictional force and mass loss were used for further analysis. The specific wear rate (K_w) was calculated using equation 4.1

$$K_w = \frac{(m_1 - m_2)}{\rho_g P S} X\ 1000 \qquad (4.1)$$

where m_1 and m_2 are specimen mass before and after testing in g, ρ_g is the density of the specimen (g/cm^3), P is the normal load in N and S is the sliding distance in m.

Worn surfaces of the pins were observed with scanning electron microscope (Make: LEO) after sputtering with gold coating.

4.2.1 Transient Friction Mechanism

Figures 4.1 (a-b) show the coefficient of friction for UFPP, SFPP and LFPP material under different loading condition.

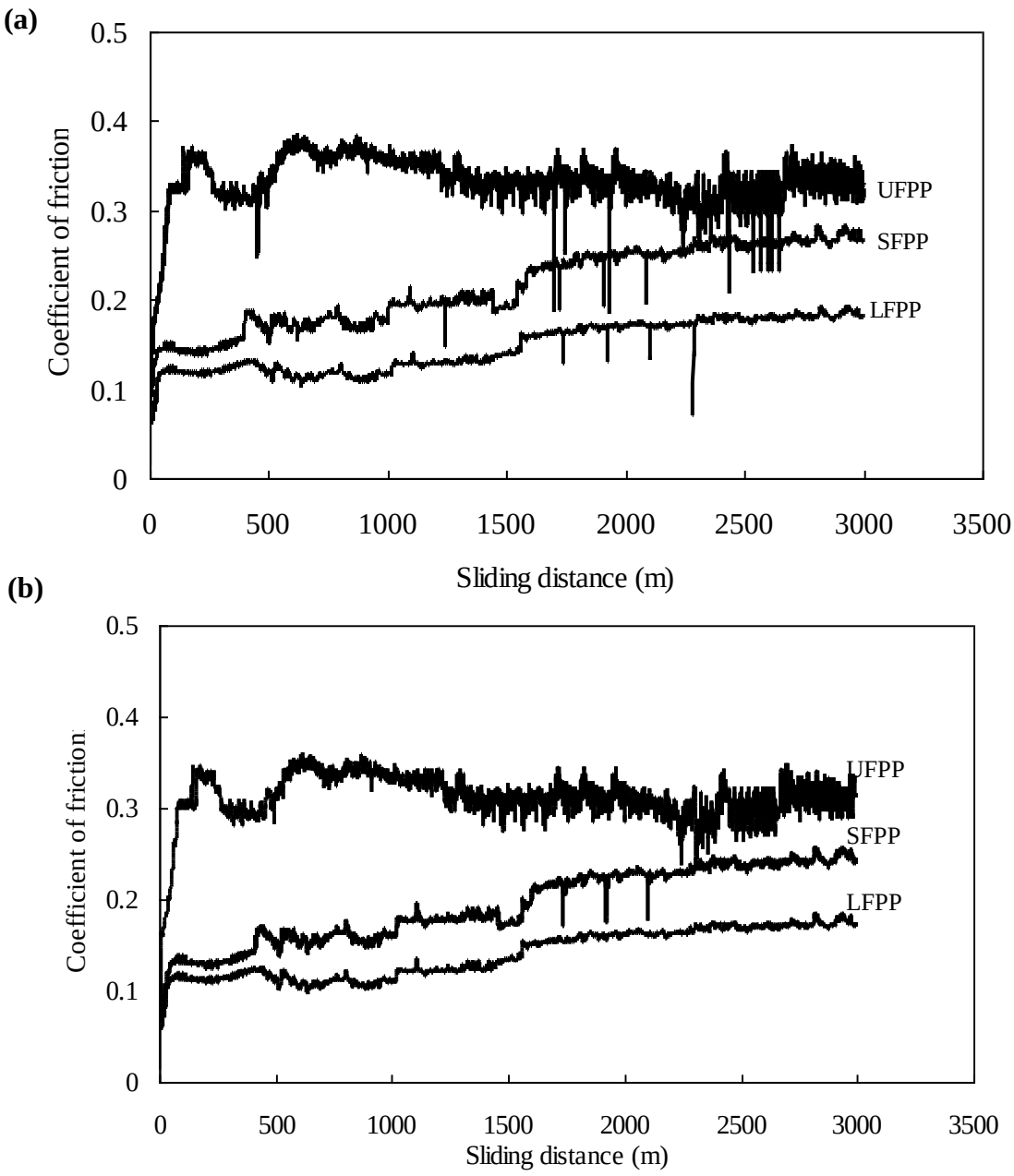

Fig. 4.1 Coefficient of friction at (a) 19.62 N and (b) 29.43 N

From the figure, it was clear that there is a rise in friction coefficient in the initial period (1500 m) after which the friction coefficient reached steady state. In general, formation of transfer film on the counter material plays a significant role in influencing wear mechanism (Bahadur and Polineni, 1996). After the formation of transfer film on the counter face material (figures 4.2(a-c)) coefficient of friction reached steady state. As the sliding distance increases, the real area of contact increases as close as to the apparent area of contact due to the asperities deformation. When two surfaces approach each other, initially their opposing asperities with maximum height come into contact. As the time increases, new pairs of asperities with lesser height make contact forming individual spots (Myshkin *et al*., 2005; Yamaguchi, 1990).

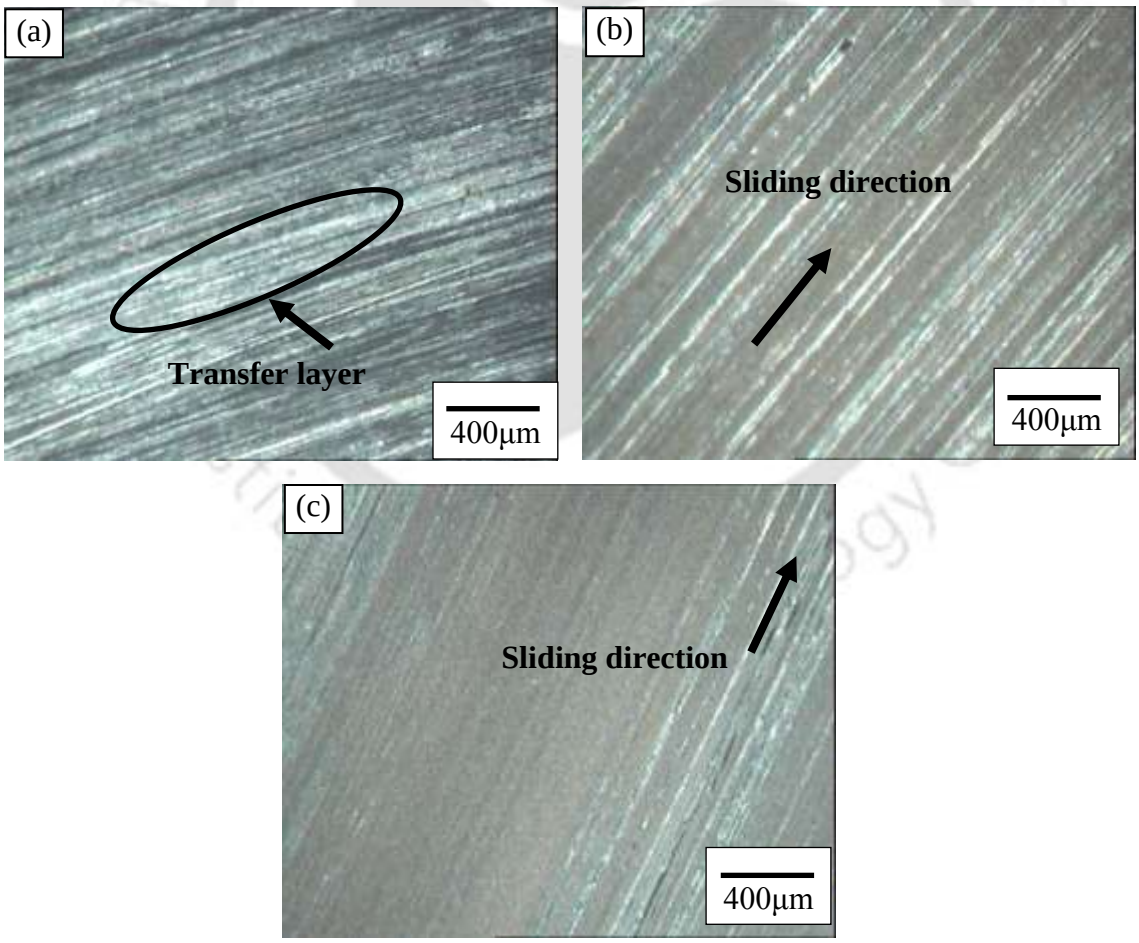

Fig. 4.2 Transfer layer formed on stainless steel at 29.43 N after sliding distance of 3000m *on the counter face due to sliding of (a) UFPP, (b) SFPP and (c) LFPP*

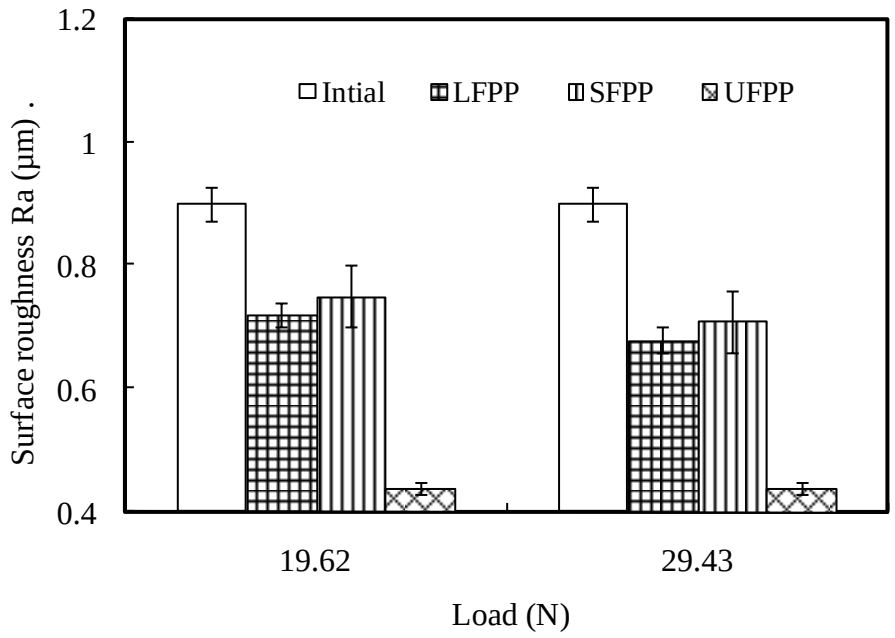

Fig. 4.3 Effect of fiber length on surface roughness

Measurement of surface roughness before and after sliding confirmed this behavior (figure 4.3). The existence of fibers and the breakage of fibers during sliding over the steel counter face obstruct the reduction of surface roughness in fiber reinforced polypropylene when compared to UFPP, hence R_a for soft UFPP was smallest compared to its counterparts. In the initial period of contact, more number of asperities contributes for the dominant abrasive wear. As the sliding distance/time increases, number of asperities was reduced, wherein adhesion wear dominates. Therefore for all the test materials, there was an initial rise in coefficient of friction due to the dominant abrasive friction and later attains stable value due to the dominant adhesive friction.

4.2.2 Influence of Fiber Length on Friction

It was observed from the figures 4.1(a-b), that the fiber length played a significant role in influencing the frictional coefficient of the investigated materials after running

in period (1500 m). The material transfer phenomenon is predominant due to the adhesion between the contacting surfaces. Transfer of material is governed by mechanical interlocking of polymer material to the metal asperities. Generally, particle transfer occurs from weaker to stronger material. From the figures 4.2 (a-c), transfer film thickness was found to be thin in the case of glass fiber reinforced PP than unreinforced PP. Among the reinforcement, LFPP showed thin transfer film than SFPP due to its improved fiber matrix bonding as shown in figures 4.2(b-c). Similar behavior of transfer film was reported by Srivastava and Pathak (1996) for the graphite filled composites, wherein the frictional coefficient initially increased and then dropped to stable value, which confirmed the formation of a graphite transfer film on the counter face. Vaziri *et al*. (1988) reported the increase in polymer specimen weight after sliding with stainless steel disc. In spite of same category of fibers and same amount of coupling agent, LFPP exhibited superior mechanical properties than that of LFPP compared to SFPP. In general the interfacial shear strength is directly proportional to fiber length. For effective composite strengthening, the fiber must have a minimum length through which efficient load transfer is possible. Fibers shorter than this critical length do not serve as load-bearing constituents (Thomason, 2002). Since the fiber length in LFPP is three times more than SFPP, the fiber-matrix bonding was found to be improved which ultimately improved its mechanical properties .To substantiate the above discussions on fiber matrix bonding ,tensile test was carried out on chosen material and fractured surfaces were investigated to understand the fiber- matrix interface. Tests were performed at atmospheric condition (23 °C and 50 % RH). The gauge length of the test material was 50 mm and the crosshead was moved at 1 mm/min speed. Figure 4.4 shows the stress-strain curve of the test materials. Addition of reinforcement increased material

modulus and strength. SEM of SFPP exhibited more fiber pull out failures, whereas SEM of LFPP showed very less/no fiber pull out as indicated in figures 4.5 and 4.6. Thus, increase in fiber length of LFPP material increases surface area of the fiber and provided good interfacial bonding strength with the matrix and thus, fiber pullout was avoided.

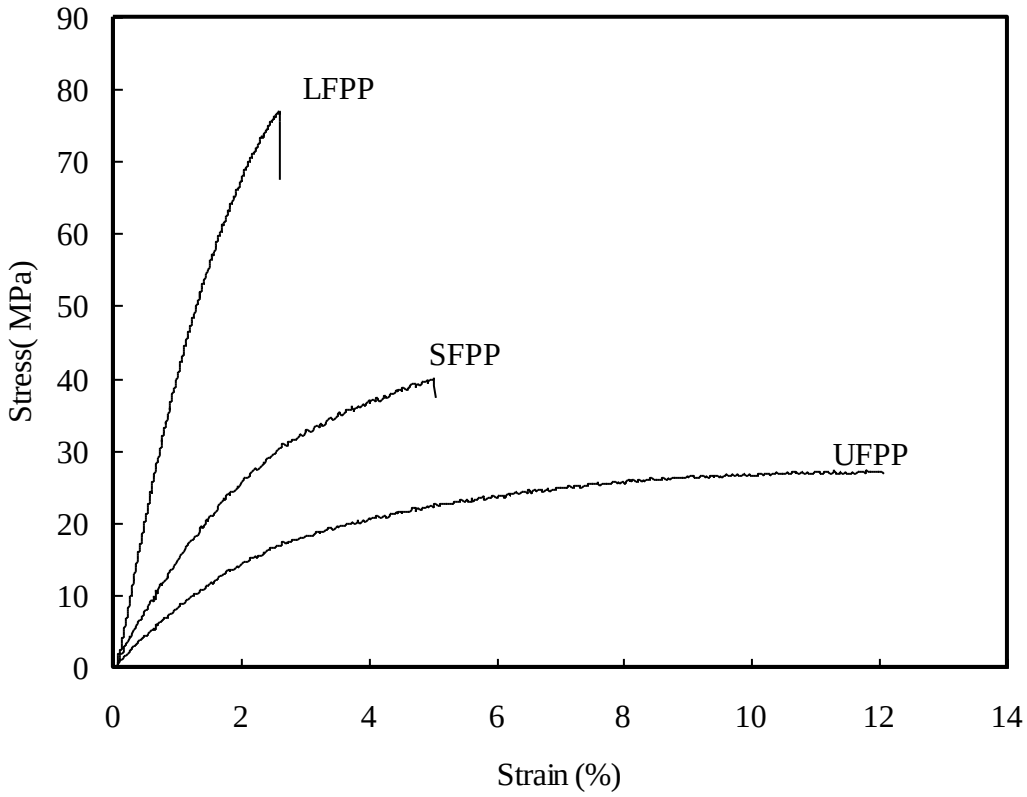

Fig.4.4 Stress-strain curve of unreinforced and reinforced polypropylene

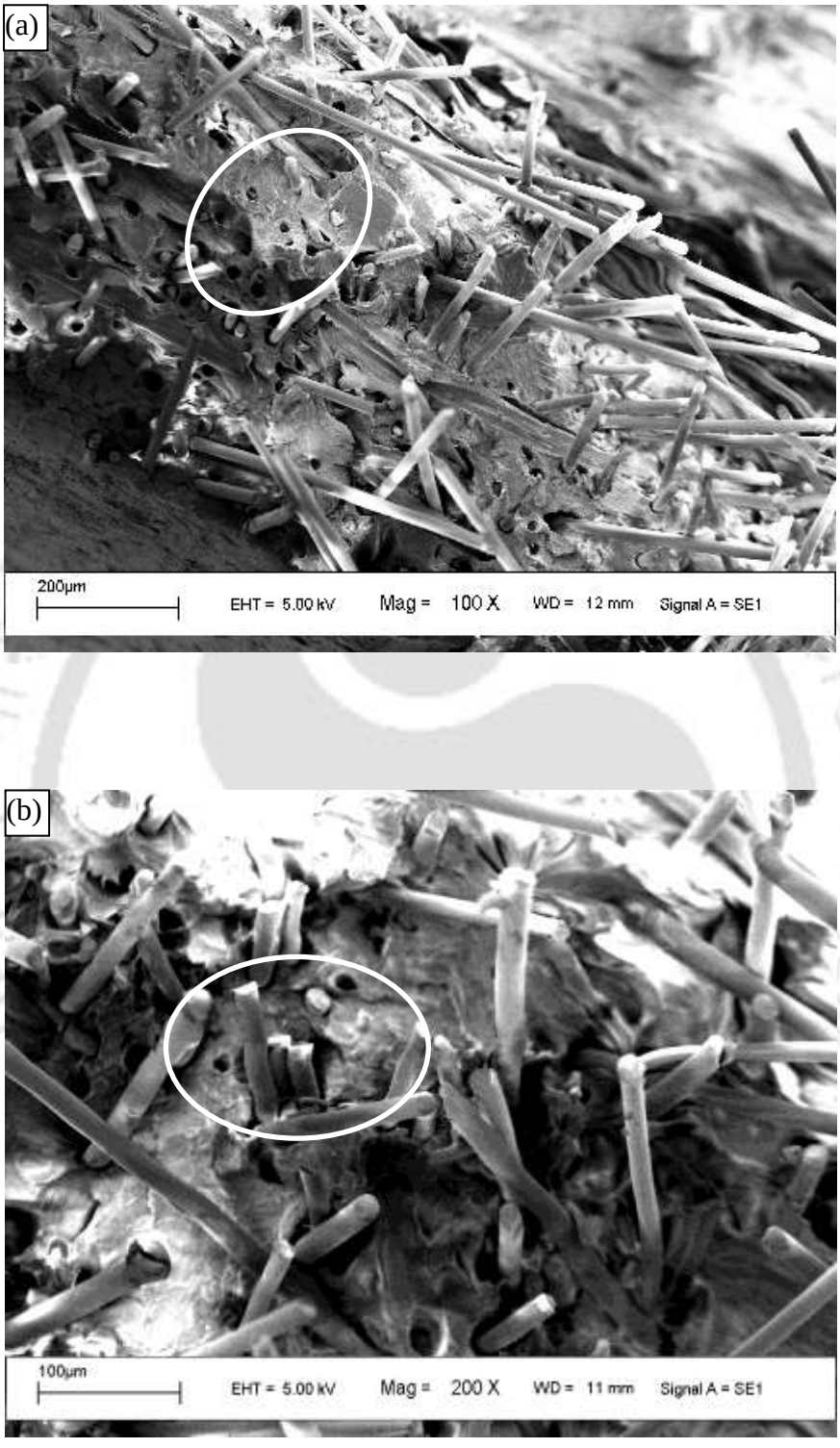

Fig.4.5 SEM of fractured surface of short fiber reinforced polypropylene test specimen showing more fiber pullout failure

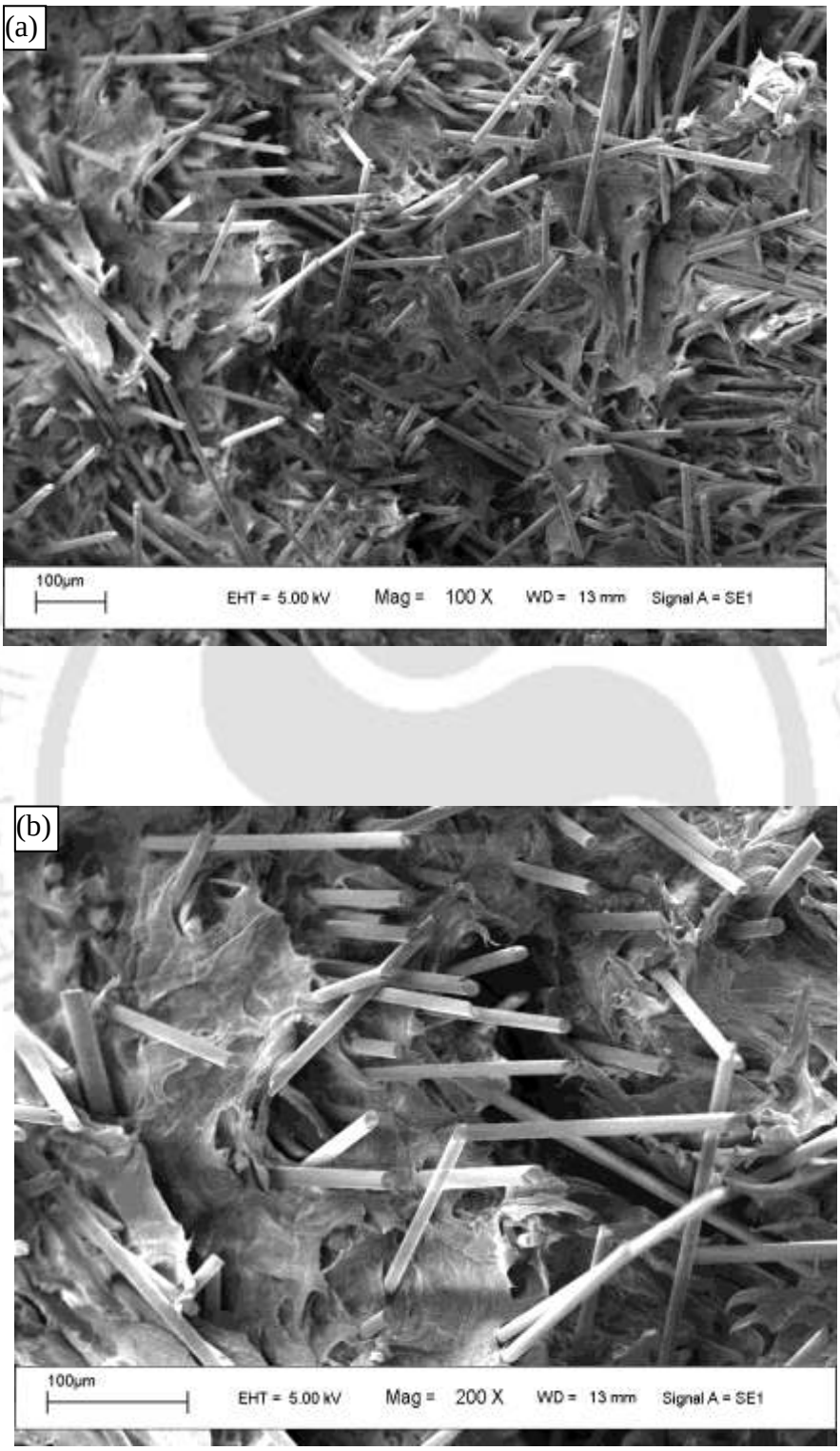

Fig.4.6 SEM of fractured surface of long fiber reinforced polypropylene test specimen showing absence of fiber pullout failure

Presence of long fibers in the LFPP considerably lowered the steady-state frictional coefficient when compared to short fibers in SFPP (figures 4.1 (a-b). This behavior was due to improved strength (Table 3.1, Chapter 3) and hardness of LFPP. Figure 4.7 shows the test material hardness; fiber reinforcement increased material hardness.

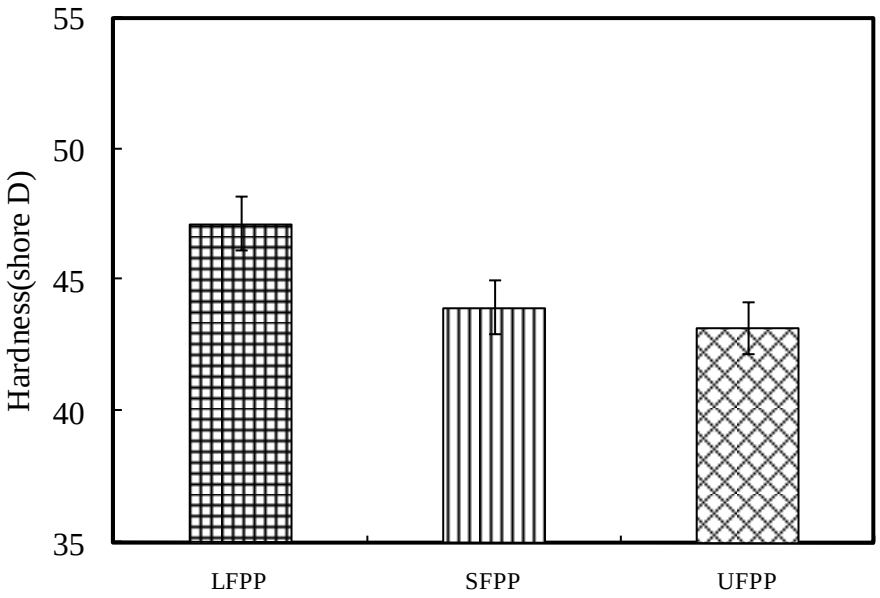

Fig. 4.7 Hardness of reinforced and unreinforced test specimens

4.2.3 Influence of Loading Conditions on Coefficient of Friction and Specific Wear Rate

The influence of load on the coefficient of friction is shown in figure 4.8. The friction coefficient of all the considered test materials decreased marginally with the increase in applied load. This behavior was due to the low sliding resistance offered by the specimen asperities at higher loading condition. In spite of decrease in friction coefficient, specific wear rate of all the test materials increased with the increase in PV as shown in figure 4.9. Increase in specific wear rate was due to the higher normal

load acting on the specimen. For both the load conditions/PV values, reinforced PP exhibited less specific wear rate than unreinforced PP.

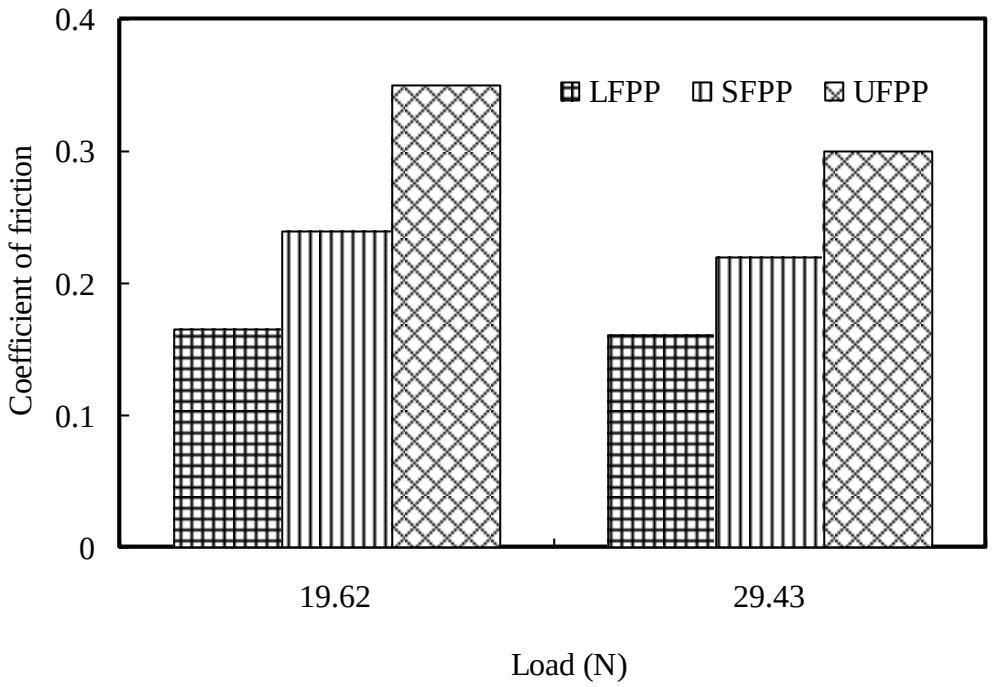

Fig. 4.8 Effect of load on coefficient of friction of test materials

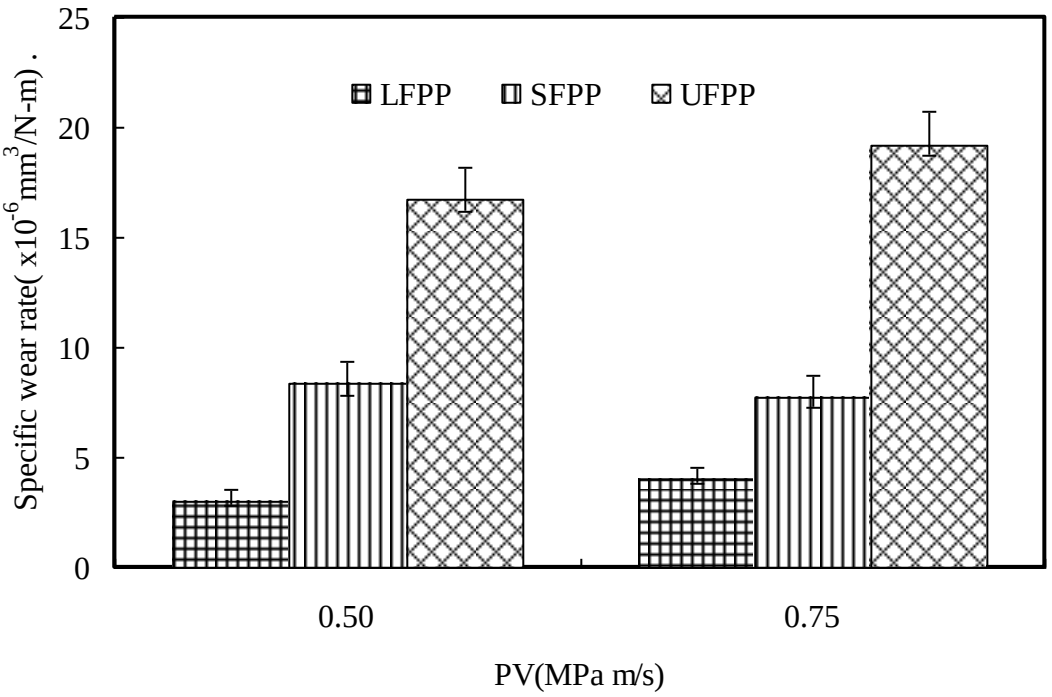

Fig. 4.9 Effect of PV on specific wear rate of test materials

Unal *et al.* (2004) confirmed that addition of glass fiber to polytetrafluoroethylene (PTFE) reduced the wear rate. Among the reinforced PP, LFPP exhibited less specific wear than SFPP and UFPP. This behavior was due to the improved fiber matrix bonding. Khedkar *et al*. (2002) observed enhanced wear resistance in long glass fiber polytetraflouroethylene and reported the importance of higher aspect ratio in improving the adhesion between fiber to the matrix due to more surface area of the fiber in contact. Dwivedi and Chand (2009) visualized the improved wear resistance in sisal fiber reinforced polypropylene with the addition of maleic anhydride and highlighted the enhanced fiber matrix bonding strength between fiber and matrix. Figure 4.10(a) showed the smooth shiny surface embedded with fine worn particles of glass fiber, upon sliding smooth surface was created which considerably reduced the specific wear rate than other two considered materials. Scratch marks in the sliding direction of long fiber reinforced PP (figure 4.10b) depicts the ability of long reinforced glass fibers in withstanding the hard protuberance due to counterface.

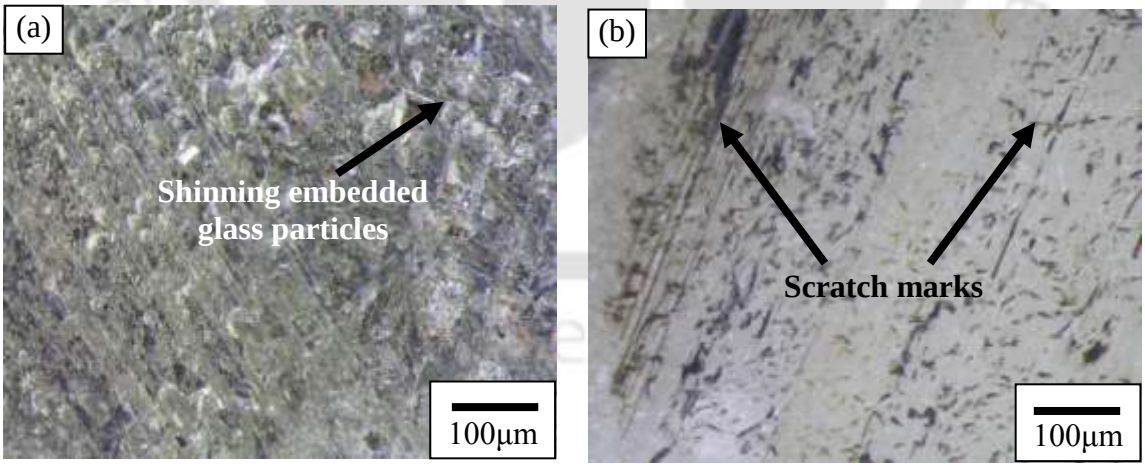

Fig. 4.10 Topography of long fiber reinforced PP at 29.43N

4.2.4 Wear Mechanisms of Test Specimens

Figure 4.11(a) clearly indicated the fiber pullout due to de-bonding in the surface of SFPP, this behavior was due to the presence of more fiber ends as well as poor fiber matrix bonding strength. The debris accumulated at the SFPP specimens (figure 4.11b) acted as a third body abrasive and increases the specific wear rate of SFPP than LFPP. Fibrils formed at the SFPP (figure 4.11c) confirmed the weak bonding between fiber and matrix. Klass *et al.* (2005) also reported the behavior of abrasive reinforced glass fibers that were loosely bounded to PTFE matrix resulted in poor wear resistance. As the fiber length increases, efficiency with which the fiber reinforces the matrix increases.

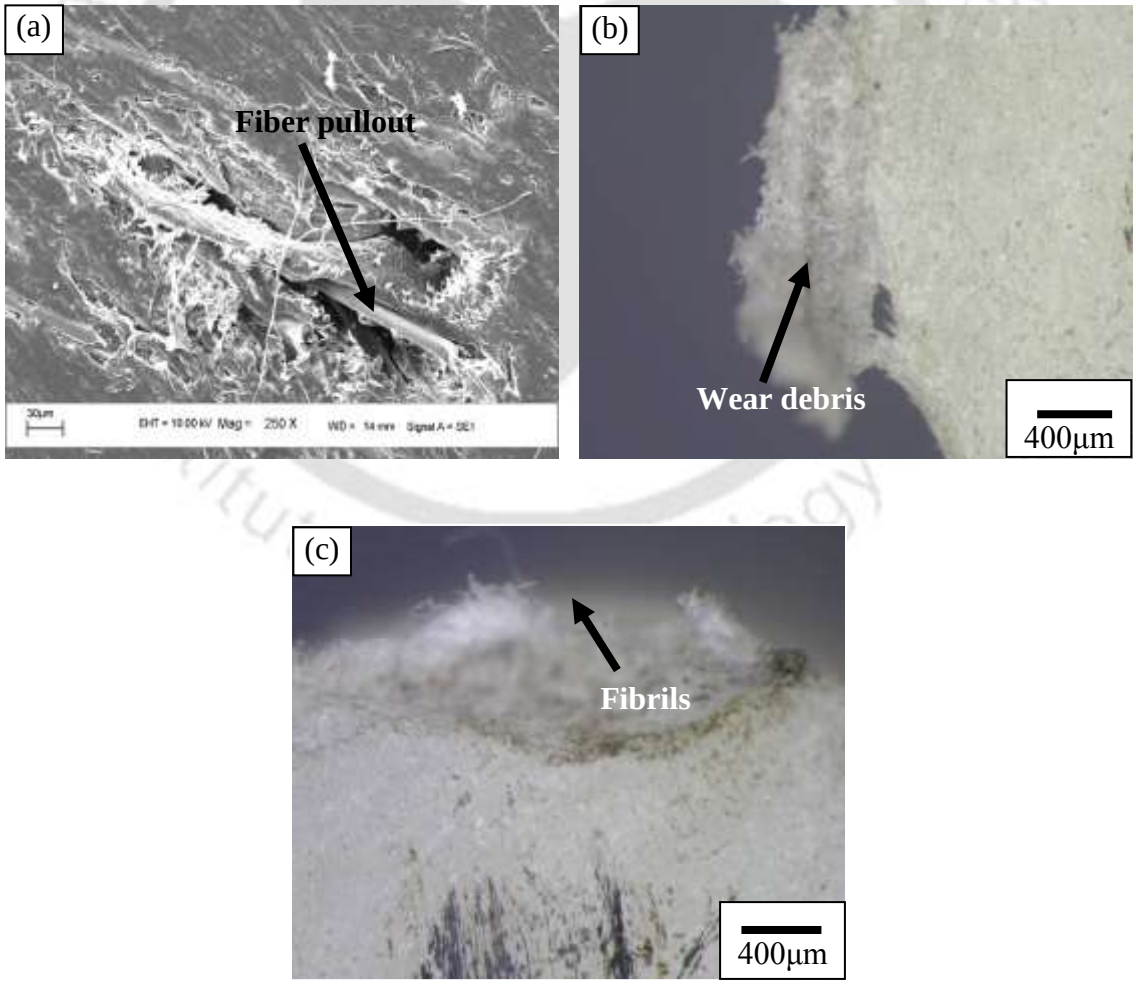

Fig. 4.11 Topography of short fiber reinforced PP at 29.43N

When the load exceeds the maximum allowable fiber strength, fiber breakage failure can be expected. Formation of grooves and some patches of transfer film on the LFPP surface served as a stress concentration region which aided fiber breakage. In the present case, LFPP exhibited broken fibers (figure 4.12a) and fiber entanglement (figure 4.12b) due to the sufficiently larger fiber length and better fiber matrix bond. This type of fiber breakage/entanglement in a surface leaves the surface relatively undisturbed which resulted in good wear resistance. Unreinforced polypropylene exhibited ductile wear as shown in figures 4.13(a-b) and it was dominated by micro ploughing (figure 4.13a) and deep grooves (figure 4.13b) caused due to the asperities of the mating steel disc.

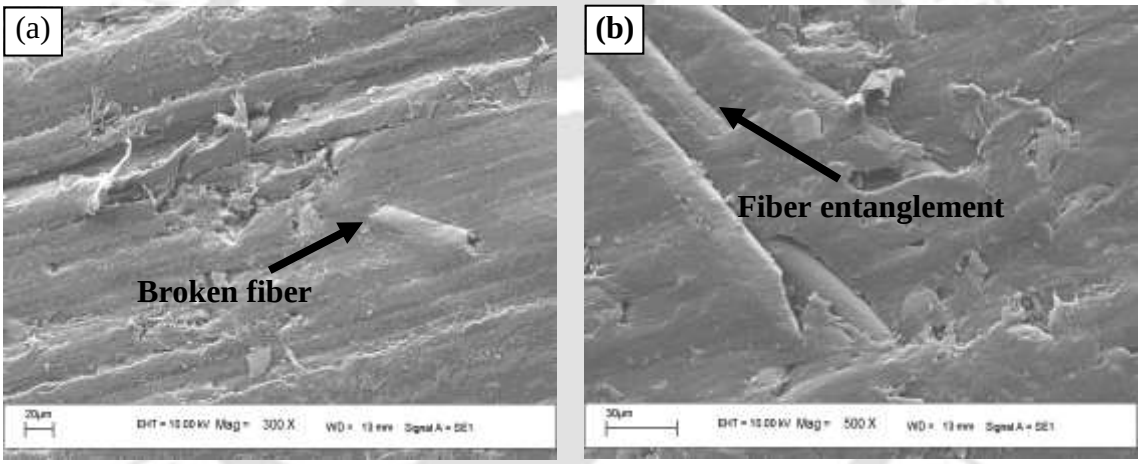

Fig. 4.12 SEM of topography of long fiber reinforced PP at 29.43N

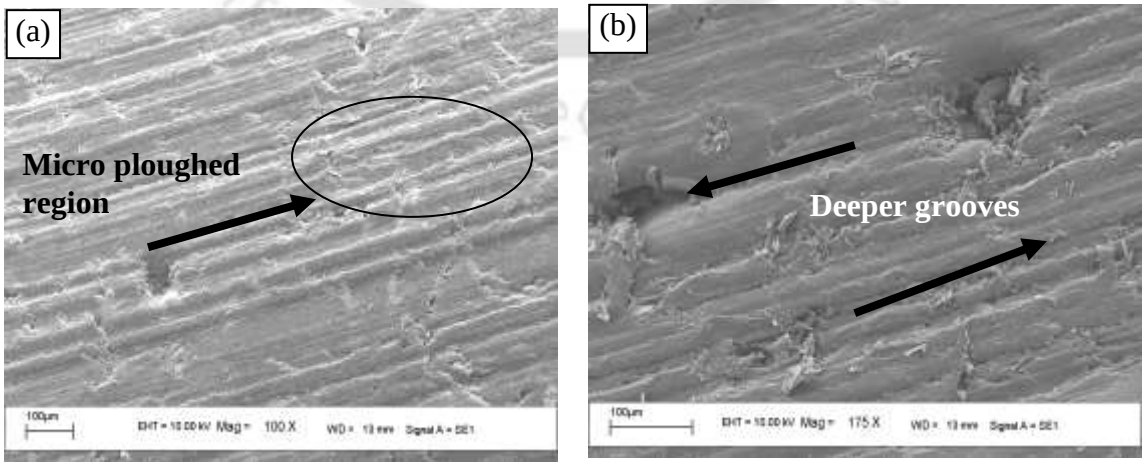

Fig.4.13 SEM of topography of unreinforced PP material at 29.43 N

4.3 ABRASIVE WEAR TEST

Pin on disc test rig used to evaluate adhesive wear was modified to carry out multi pass abrasive wear test. Silicone carbide emery paper (400 and 320 grit size) was firmly attached on the steel disc to alter from adhesive to abrasive counter surface condition. The average particle size of grits 400 and 320 # are 31 and 45 μm respectively (ISO 8486-2:2007). Abrasive wear tests were conducted at 4.91, 9.81 and 14.72 N normal loads at 0.2 m/s sliding velocity. Tests were conducted under laboratory conditions, 32 ± 3°C and RH 57 ± 5 %. Test pins were cleaned before testing and the initial mass was measured using an electronic balance with 0.1 mg accuracy. Abrasive wear tests were conducted up to a sliding distance of 180 m. The sampling rate for the friction force and displacement was kept as 0.5 Hz .The wear loss was quantified by both mass and dimensional loss. The wear volume loss (K_m in mm^3) was calculated using equation 4.2

$$K_m = \frac{(m_1 - m_2) \times 1000}{\rho} \tag{4.2}$$

where m_1 and m_2 are the specimen mass in g before and after testing and ρ is the material density in g/cm^4. Dimensional wear loss was measured using on-line laser displacement transducer of 2 μm accuracy (Keyence). From the change in length, the wear volume (K_d in mm^3) was calculated using equation 4.3

$$K_d = \frac{\pi d_p{}^2 h_o}{4} \tag{4.3}$$

where d_p is the pin diameter in mm and h_o is the change in pin length during test in mm. The worn-out surfaces of the pin and wear debris were observed under microscope to identify the wear mechanism.

4.3.1 Effect of Fiber Length on Abrasive Wear

Influence of fiber length on the abrasive wear performance of leaf spring materials are shown in figure 4.14. LFPP exhibits better resistance than SFPP and UFPP. Increase in fiber length found to improve the abrasive wear resistance of polypropylene. The wear behavior of polymers and composites under abrasive conditions were correlated with the mechanical properties by many models. Ratner *et al*. (1967) developed a correlation where the abrasive wear rate was inversely proportional to the product of tensile stress at break (σ_t) and elongation to break (ξ_e). Thus, the wear rate (V) can be expressed as

$$V = C\frac{\mu P}{H\sigma_t\xi_e} \tag{4.4}$$

where μ, P and H denote the coefficient of friction, load and hardness of the material respectively under study. Cenna *et al*. (2003) modified the Ratner model by replacing the fracture energy ($\sigma_t\xi_e$) with the plastic energy of deformation (E_{def}). It was postulated that the increase in plastic energy of deformation decreased the abrasive wear rate of the material.

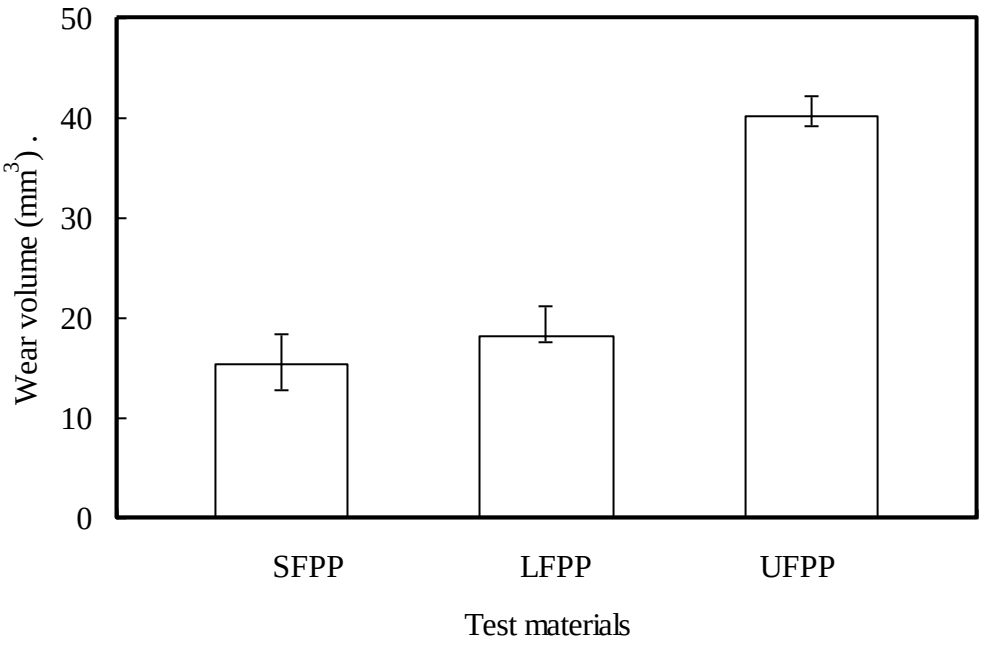

Fig. 4.14 Wear volume at load of 9.81 N for 400# grit size

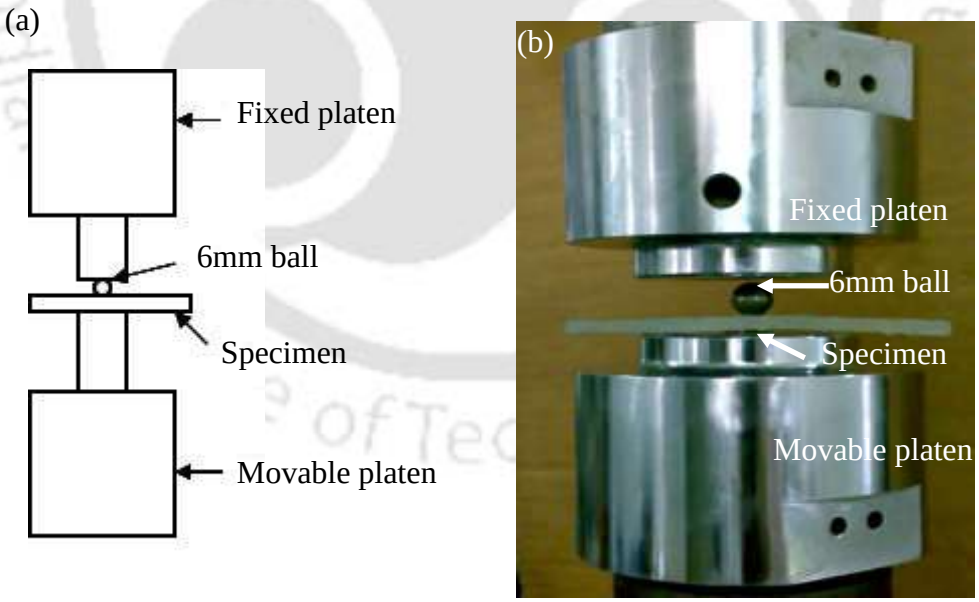

Fig. 4.15 Experimental setup for constant load indentation test (a) schematic diagram (b) photograph

In this work, abrasive wear behavior of chosen leaf spring material was correlated with the plastic deformation energy of material. Servo hydraulic universal fatigue testing machine, Instron 8801 was used to execute the constant load indentation tests. Rectangular flat specimens pertaining to ASTM D 638 were considered and indented with 6 mm diameter hardened steel ball with a constant load of 250 N. The schematic and photographic of the constant load indentation setup is shown in figures 4.15(a-b). Loading and unloading was carried out at 25 N/min and the load-deflection curve is shown in figure 4.16. Results revealed that the plastic deformation energy (area of the curve) was found to be increased with the increase in fiber length (figure 4.17). Deformation energy and wear volume were plotted as a function of reinforcement as shown in (figure 4.18).

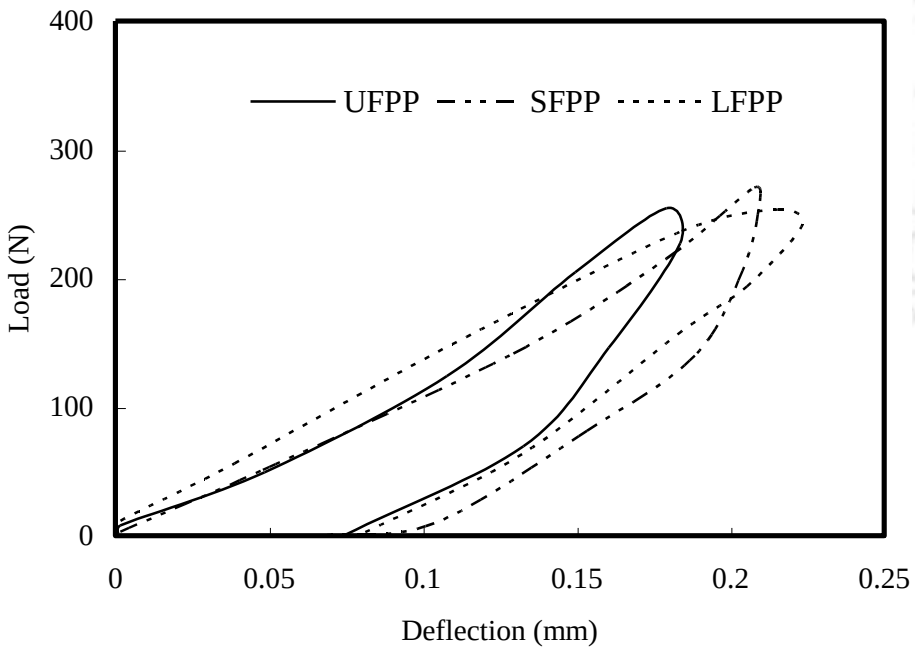

Fig 4.16 Load - deflection curves for test specimens at 250 N indentation load

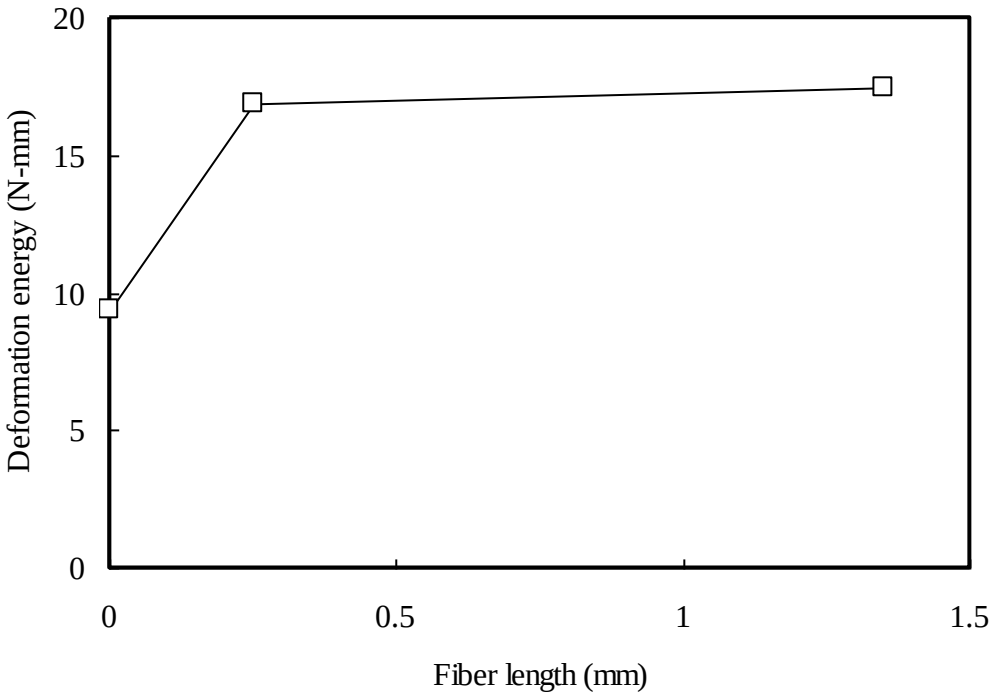

Fig. 4.17 Plastic deformation energy as a function of fiber length

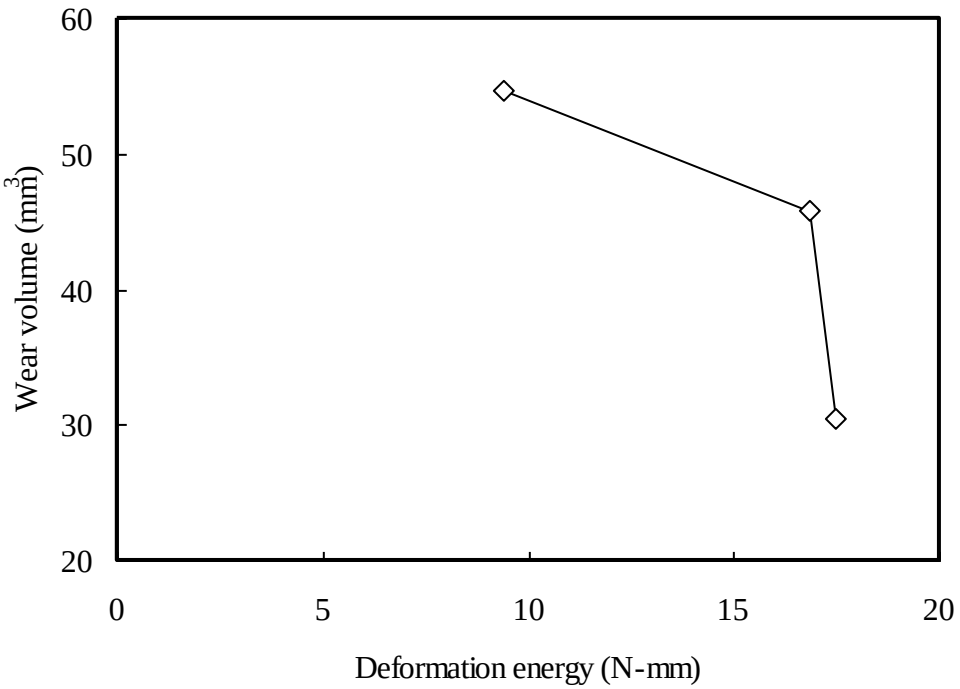

Fig. 4.18 Relation between the wear volume and deformation energy

Three trials were conducted for calculating deformation energy and wear volume; deviations were found to be 3 and 4.5 % respectively. Plastic energy of deformation was found to play a vital role in the wear characteristics. In the multi pass abrasive wear testing, repeated specimen travel over the same wear track accumulates the wear debris (clogging) in the abrasive grit spaces (Rabinowicz,1995). Clogging significantly influences the wear of most polymeric materials.

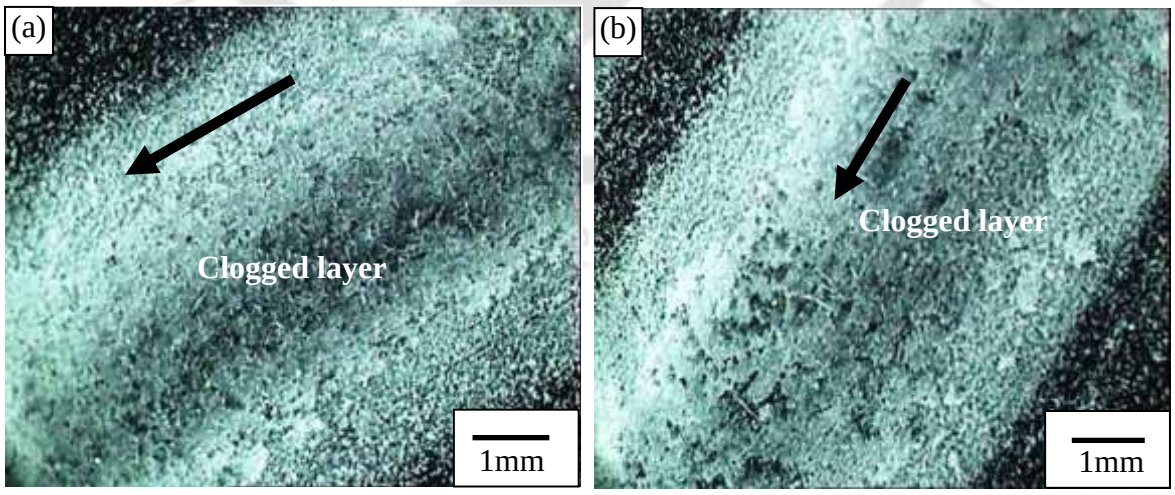

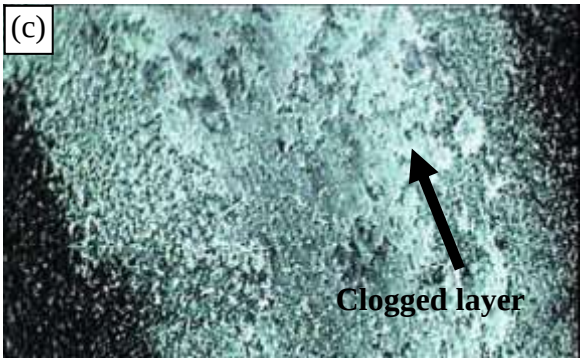

Fig. 4.19 Clogging of abrasive grits for 400# at 9.81 N with (a) LFPP (b) SFPP (c) UFPP

Figures 4.19 and 4.20 showed the clogged abrasive paper and generated wear debris after test. The fine debris formed gets effectively clogged within abrasive grits and resulted in reduction of the grit penetration on the specimen surface. Hence after a certain sliding distance, abrasive wear of the materials decreased and reached stable condition. The amount of clogging was found to be more in unreinforced material than reinforced material and shown in figure 4.19.

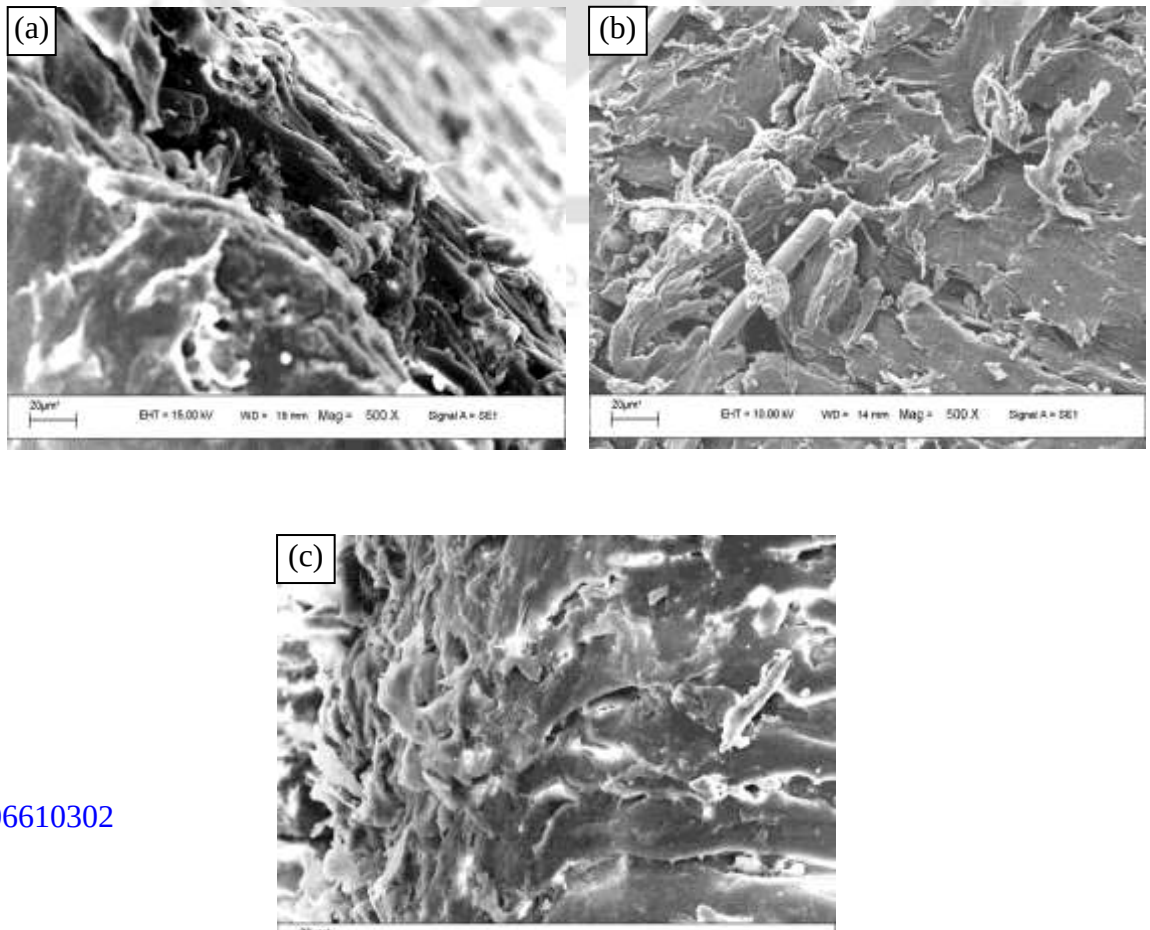

Fig. 4.20 SEM of abrasive wear debris of (a) LFPP (b) SFPP (c) UFPP against abrasive grit size of 400# at 9.81N

Reinforced PP wear debris exhibited less adhesion with abrasive paper as it is the mixture of base resin PP and broken glass fibers which show brittleness. However, the developed clogged layer in UFPP was not sufficiently adhering with the abrasive paper and reinforced PP exhibited stable clogged layer. This was confirmed with the measured dimensional wear loss during testing as shown in figure 4.21. Wear loss in reinforced PP test specimen reached steady state after sliding distance of about 50 m, whereas unreinforced PP kept on increasing. Similar kind of steady state formation was observed for reinforced PP at all the tested grit sizes. Both SFPP and LFPP did not show any appreciable wear loss unlike UFPP beyond sliding distance of about 50 m. In the case of reinforced material, when the abrasive grits were in contact with the matrix, damage rate was initially high. As the sliding distance increases, high modulus glass fibers are exposed to the abrasive surface which prevented the basic material to get abraded rapidly. Clogging did not affect the coefficient of friction as shown in figure 4.22.

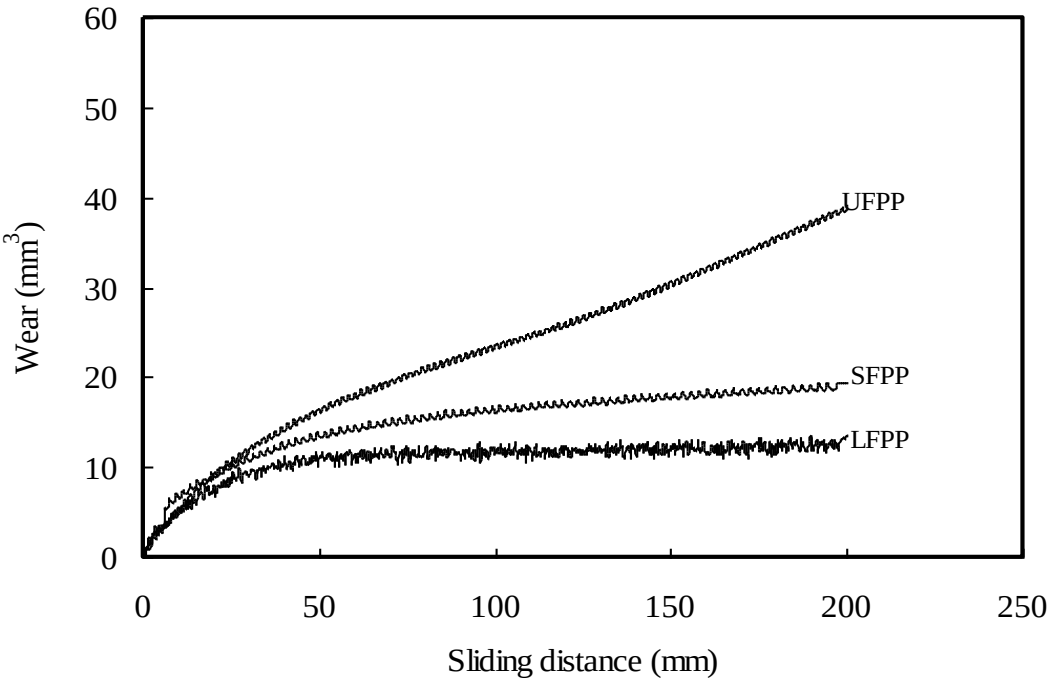

Fig. 4.21 Online abrasive wear volume of test materials at 9.81 N for 400# abrasive grit

(a)

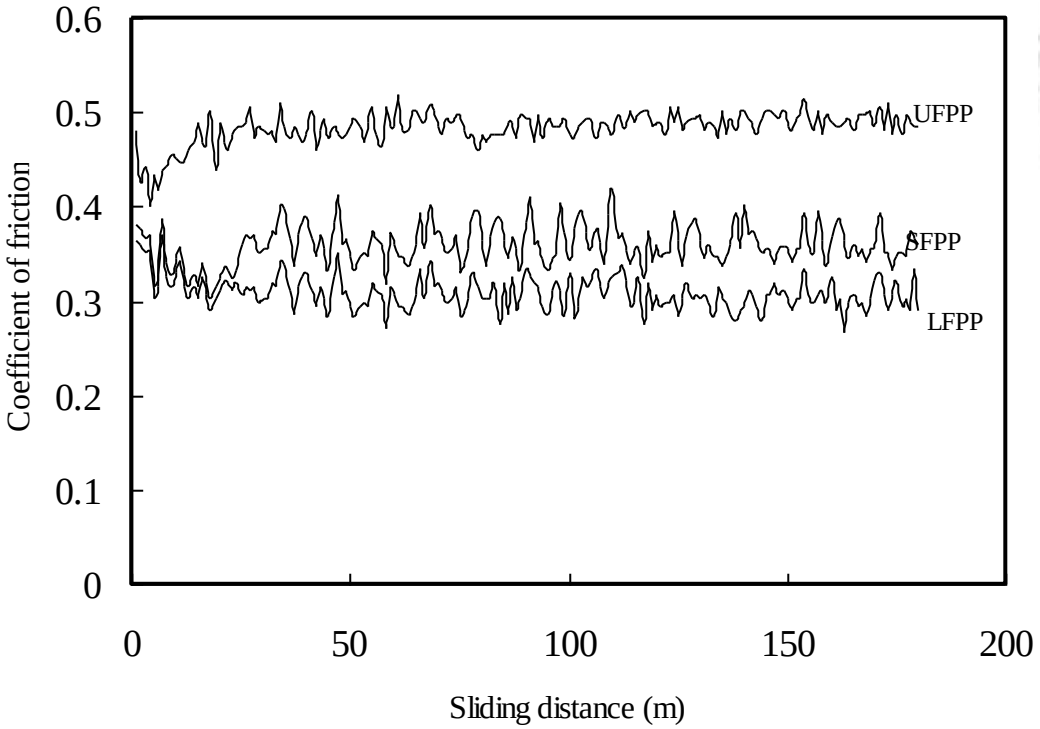

(b)

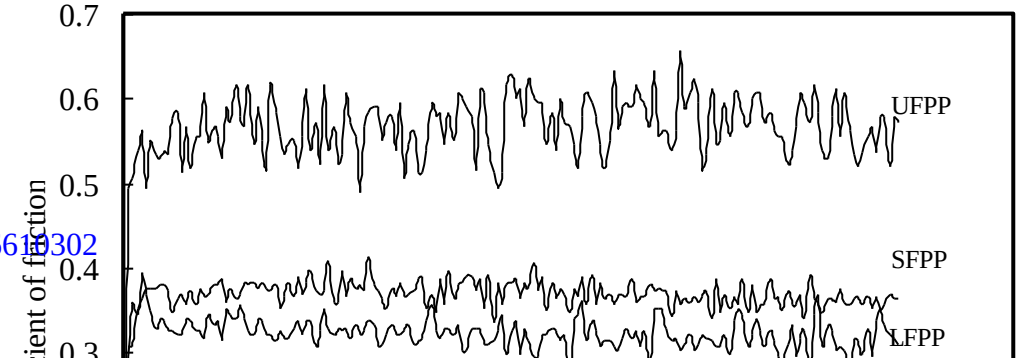

Fig. 4.22 Effect of grit size on friction coefficient of test materials at 14.72 N (a) 400# (b) 320#

For all the considered materials, friction coefficient reached steady state after traversing a few sliding distance. Reinforced PP exhibited less coefficient of friction than unreinforced PP.

4.3.2 Effect of Load and Grit Size on the Abrasive Wear Performance

The abrasive wear of the considered materials was significantly influenced by operating parameters, normal load and abrasive grit size. It was evident from figure 4.23 that the wear volume was dependent on the grit size. Wear volume of all the considered materials was found to be high with 320 # for all the tested loading conditions. When the abrasive wear particle size is large, the real area of contact between the asperity and abrasive surface is less resulting in high contact stress (Srinath and Gnanamoorthy, 2006). These stresses at the contact ease the initiation of cracks and the material was removed easily compared to the abrasive grits of smaller particle size.

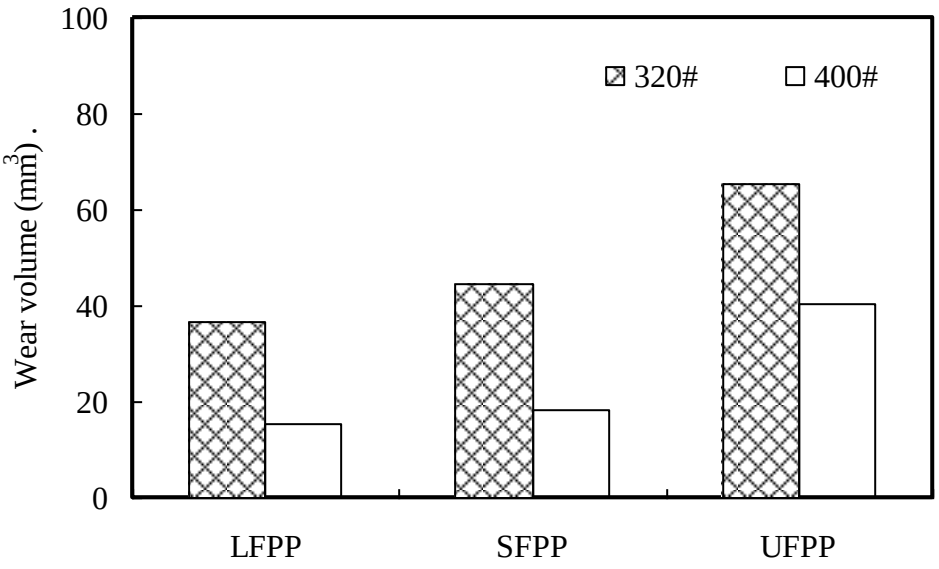

Fig. 4.23 Effect of grit size on abrasive wear volume at 9.81 N

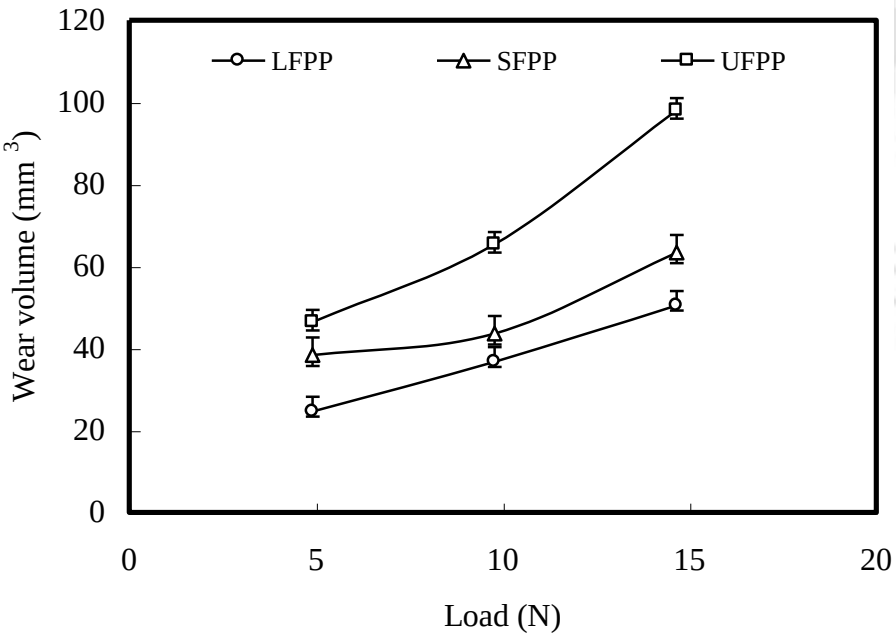

Fig. 4.24 Effect of load on wear volume of test materials at grit size of 320#

Figure 4.24 shows the effect of load on the abrasive wear volume of the tested materials. When the load increases, the contact stress increases between the abrasive

surface and the pin which helps to initiate the cracks and facilitate the material removal. The observed abrasive wear performance at 400# grit was similar at 320# where the wear volume increased with the loading levels.

4.3.3 Wear Topography

In general, condition of abrasive paper is modified when the polymeric materials are subjected to multi pass abrasive testing condition (Lancaster, 1969) where glass fibers tend to fracture or pull out abrasive grits (Harsha and Tewari, 2003). In the present case, abrasive papers were examined to check whether the abrasive grits remain rigidly attached to the paper; no sign of pull out or attrition of abrasive grits was found at test condition. Under multi pass abrasive wear testing, the composite surface undergoes plastic deformation under the action of repeated load. Figure 4.25 delineated that the primary wear mechanism of UFPP as micro ploughing. It also confirmed the presence of wear tracks along the sliding direction. Grooves were formed in series which resulted in debris formation. The wear debris of the pin surface is shown in figure 4.25 (b).

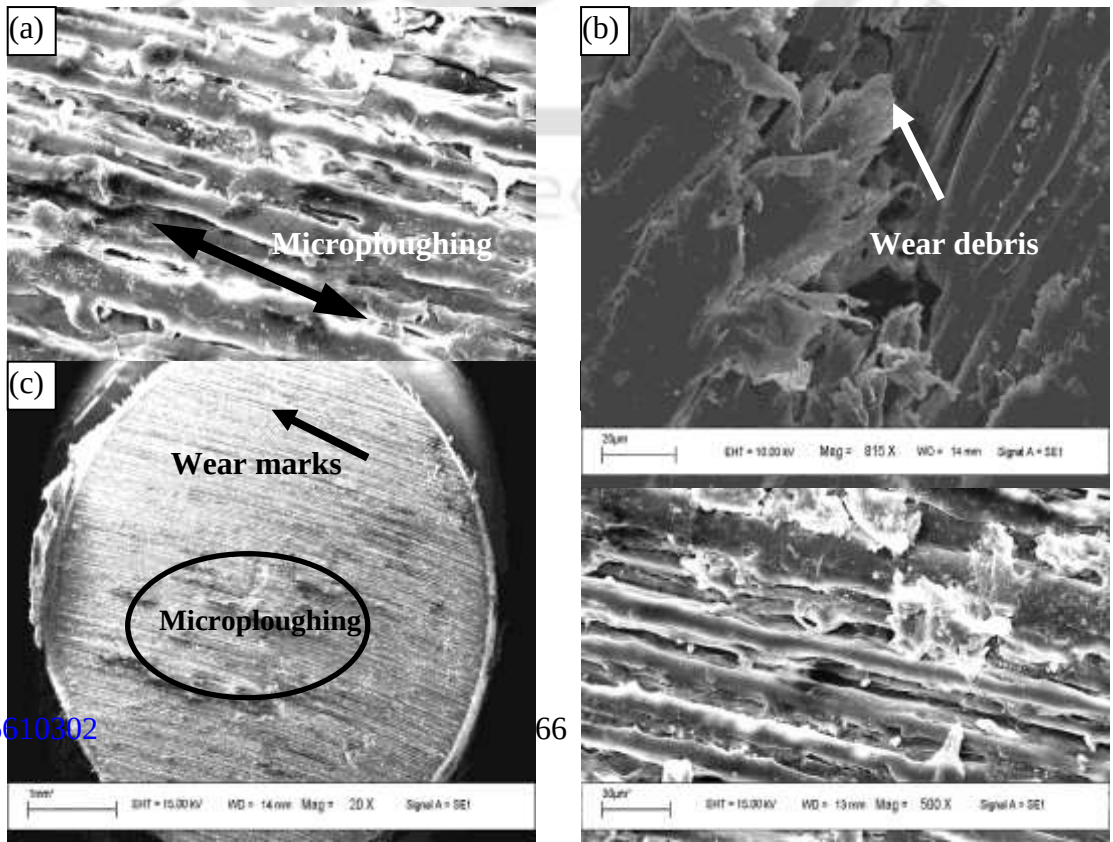

Fig. 4.25 SEM of worn out pin surface of UFPP against abrasive grit size of 400# showing (a) microploughing at 4.91 N (b) abrasive wear debris at 4.91 N (c) microploughing region at 9.81 N and (d) wear particles at 9.81 N

At higher loads, the contact between the test material asperities with the abrasive surface increases which facilitate the ease of material removal. Width of micro ploughing was found to be increased at higher loads (figures 4.25 (a & d)).

In a composite, bonding between fiber and matrix plays a vital role in determining the wear resistance. Helen *et al.* (1996) reported the importance of interfacial bonding on wear resistance. Good interfacial bonding resists the fiber matrix debonding and cohesion is greater in the matrix having high degree of crystallinity. To understand the influence of fiber length over material crystallinity, X-ray diffraction study (Bruker AXS D8) was carried out for the considered materials. Figure 4.26 gives a vivid picture on the crystallinity behavior of fiber reinforced material. The crystallite size (L_c) was computed using the Debye scherrer relation (Klug and Alexander, 1974).

$$L_c = \frac{K_c \lambda}{b_w \cos\theta} \tag{4.5}$$

where K_c is unit cell geometry dependent constant, λ is wavelength of the X-ray beam and b_w is full width at half maximum and θ is incident angle. The computed crystallite size from the equation 4.5 was tabulated in table 4.1 and the crystallite size of LFPP was found to be higher when compared to SFPP and UFPP material. Thus, it was found that increase in fiber length in the composite not only improved interfacial strength but also improved the basic matrix crystallinity which significantly contributed for the better abrasion resistance. Giltrow (1961) postulated a correlation and found that abrasive wear rate was inversely proportional to the square root of

material cohesive energy. Briscoe and Evans (1989) reported that the abrasive wear resistance increased with the improvement in matrix crystallinity. Thus, prior work confirms the role of matrix crystallinity in influencing the wear performance and in the present work; increase in fiber length improves matrix crystallinity besides abrasive wear performance.

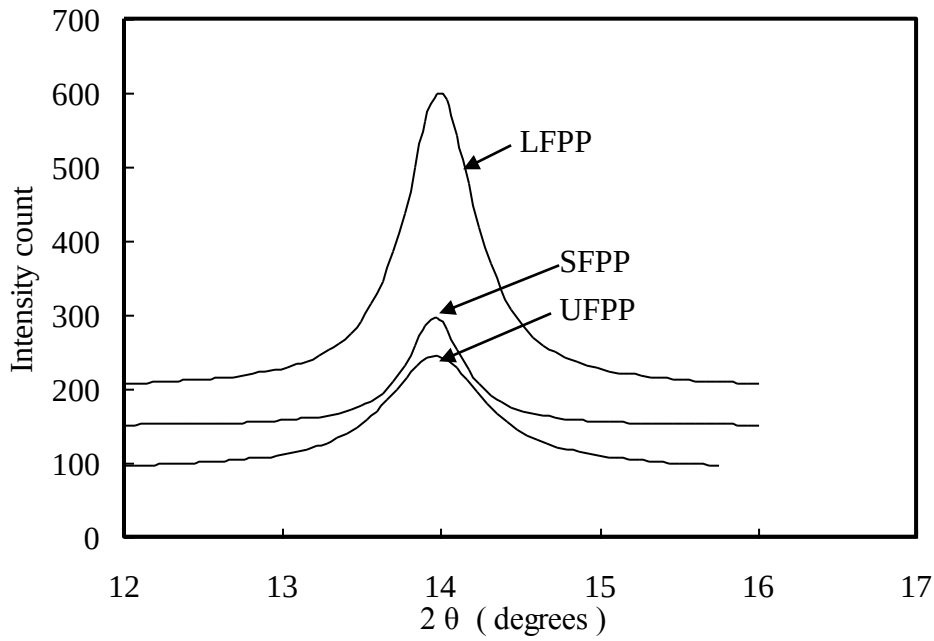

Fig. 4.26 X-ray diffraction pattern for leaf spring materials

Table 4.1 Crystallite size for leaf spring materials

Unreinforced PP			Short glass fiber reinforced PP			Long glass fiber reinforced PP		
2θ (deg)	FWHM b_w (deg)	Crystallite size L_c (Å)	2θ (deg)	FWHM b_w (deg)	Crystallite size L_c (Å)	2θ (deg)	FWHM b_w (deg)	Crystallite size L_c (Å)
14.957	0.88600	100.330	14.964	0.74972	118.615	14.987	0.60586	146.784

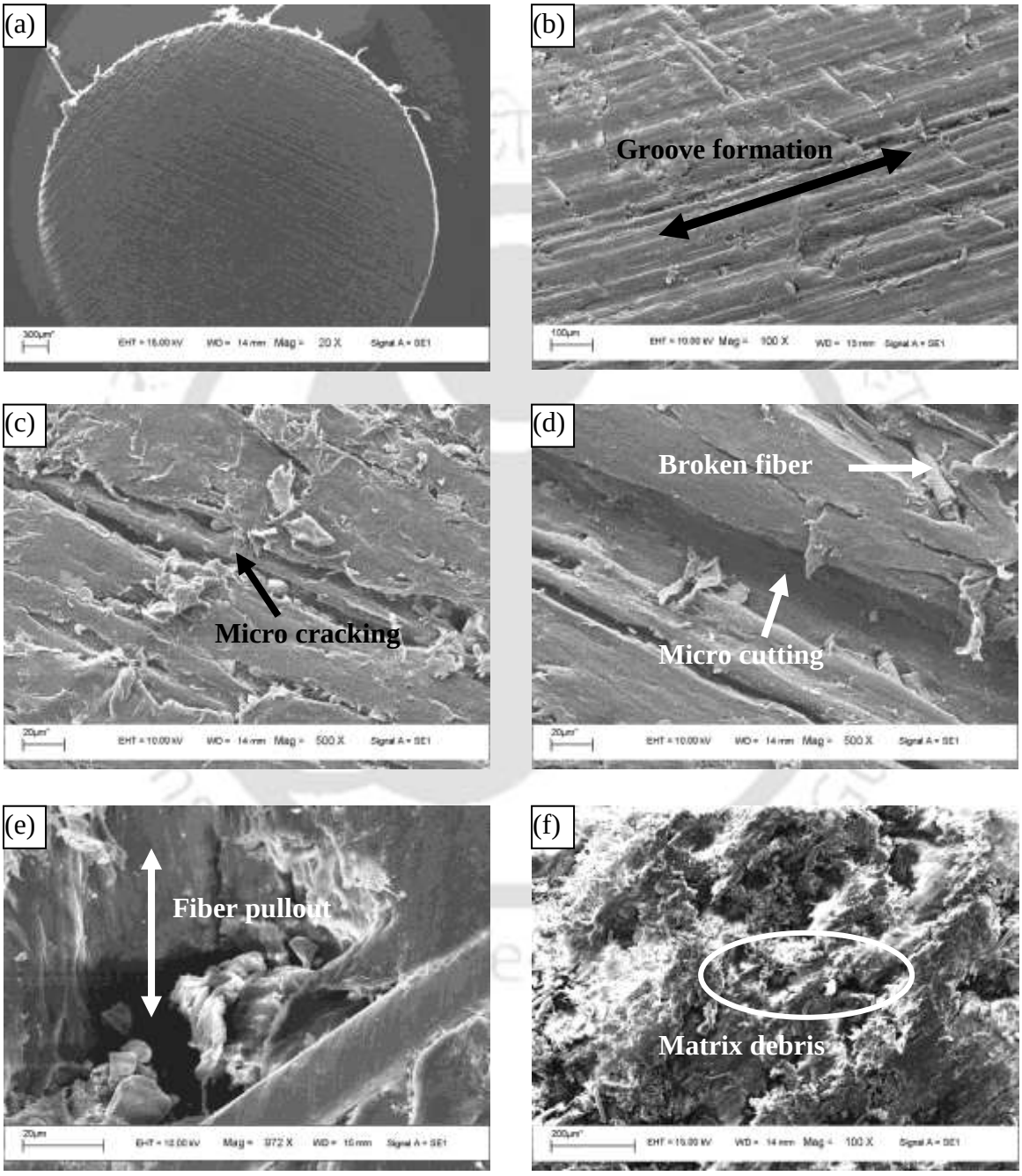

Fig.4.27 SEM of worn out pin surface of SFPP showing (a) smooth worn out surface at 4.91N (b) groove formation at 4.91 N (c) micro cracking at 9.81 N (d) microcutting

at 14.72N (e) fiber pullout at 14.72 N and (f) matrix debris in 320# abrasive sheet at 14.72N.

The surface wear morphology of LFPP and SFPP specimens revealed micro cutting as primary wear mechanism. In the case of SFPP at lower loads, the wear was observed due to micro ploughing in which the matrix was deteriorated and fibers were exposed. This behavior was confirmed with the presence of grooves in sliding direction as shown in figures 4.27(a-b). When the load increases, micro cracking followed by micro cutting was observed and shown in figures 4.27(c-d). Repetitive passage of abrasive particles resulted in micro cracking and fiber pullout as shown in figure 4.27 (e). Figure 4.27 (f) showed the presence of broken glass fibers along with matrix debris in the abrasive sheet.

Increased aspect ratio of fibers in LFPP contribute to have good interfacial adhesive force between fiber and matrix which results in high ploughing force requirement for the matrix rupture. Smooth worn out surface observed in LFPP at loading of 4.91 N shown in figure 4.28 (a) confirmed this behavior. Clogged wear debris observed on the abrasive sheet with less and small size debris (figure 4.28 b) supported the enhanced abrasive wear resistance. High matrix crystallinity and high aspect ratio summarily prevented micro cracking. Micrographs of LFPP (figures 4.28 (c-e)) revealed that, at lower loads the damage towards fiber breakage was found to be less; at higher loads more fibers tend to break. Due to the improved fiber matrix adhesion, de-bonding was not observed in LFPP which contributed to less wear.

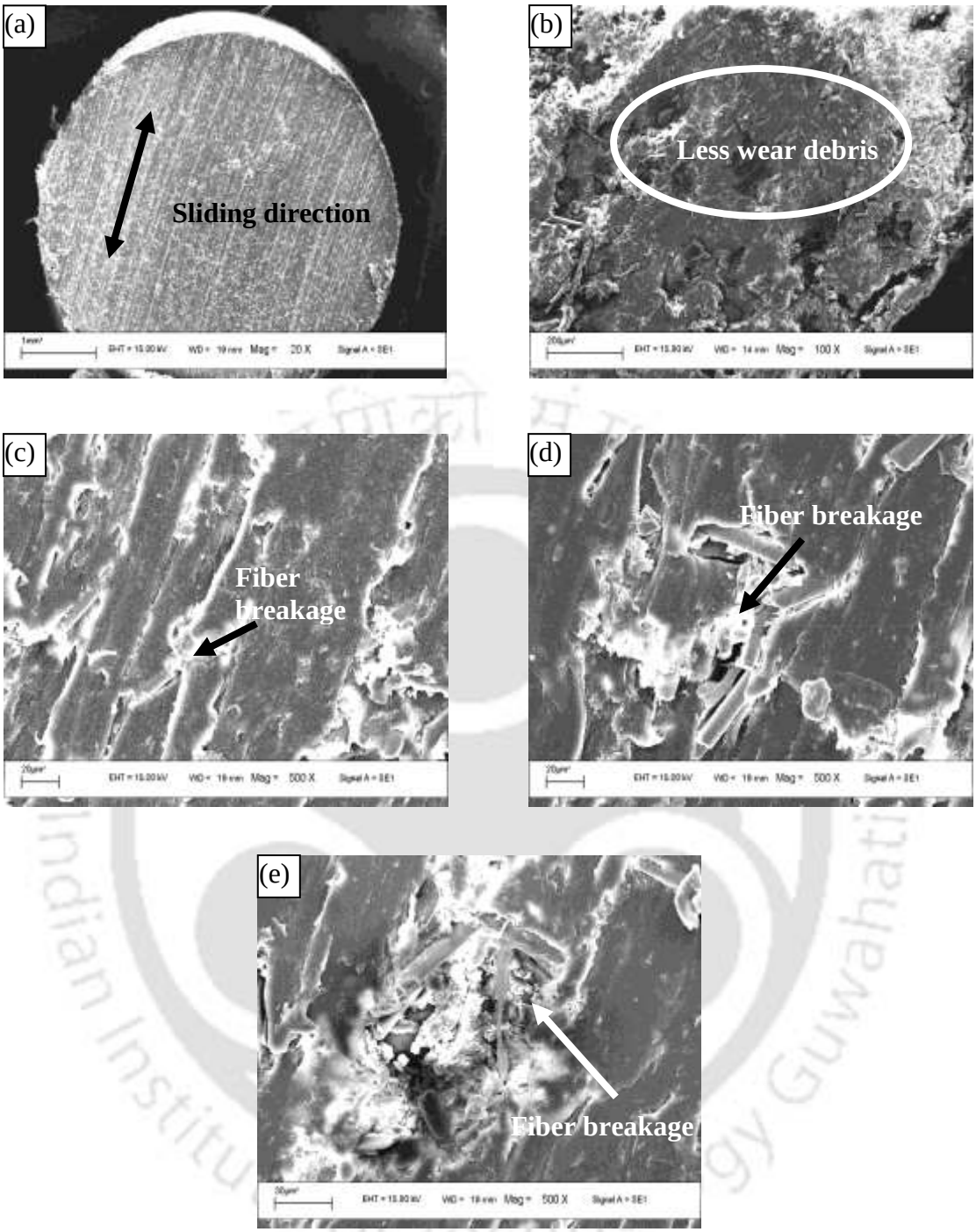

Fig. 4.28 SEM of worn out pin surface of LFPP showing (a) smooth surface at 4.91 N (b) wear debris in 320# abrasive sheet (c) fiber breakage at 4.91 N (d) fiber breakage at 9.81 N and (e) fiber breakage at 14.72 N

4.4 SUMMARY

Friction and wear characteristics were investigated for the leaf spring materials under adhesive and abrasive modes using pin on disc test configuration. Plastic deformation energy and crystallite size of the test materials were correlated with the wear performance.

- Fiber reinforcement improved the hardness and effectively reduced the coefficient of friction than unreinforced material. Among the reinforcement LFPP showed less specific wear rate compared to SFPP in adhesive as well as abrasive modes.
- Improved fiber matrix bonding and presence of less fiber ends in LFPP improved wear resistance compared to that of SFPP and UFPP. Specific wear rate and wear volume of the test materials increased with the increase in load during adhesive and abrasive modes for all the materials.
- Transfer film formation and clogging on the counter face significantly affected the friction-wear behavior during adhesive and abrasive modes respectively. Transfer layer and clogged layer were found to be more pronounced in unreinforced material than reinforced material.
- LFPP exhibited improved plastic deformation energy and matrix crystallinity resulted in superior wear resistance compared to that of SFPP and UFPP.
- Under abrasive mode, UFPP, SFPP and LFPP exhibited microploughing, fiber pullout and fiber breakage respectively as the dominant failure morphology.

CHAPTER 5

DAMPING CHARACTERISTICS OF THERMOPLASTIC LEAF SPRING MATERIAL

5.1 INTRODUCTION

Fatigue resistance with excellent damping is the most desirable material characteristics for leaf spring application (Adams and Maheri, 2003). Inherent material damping characteristics of the composite material aid to replace steel in suspension spring application (Beardmore and Johnson, 1986). Fiber reinforcement in the polymeric material not only enhances strength and stiffness but also alters the damping characteristics of the composite. Enhanced stiffness along with good damping characteristics of discontinuous fiber reinforced thermoplastic material suits many anti-vibration applications. Complete and systematic understanding of all the damping sources of the discontinuous fiber reinforced thermoplastic material is necessary for designing this class of materials for leaf spring application. Discontinuous fibers in the composite alters damping characteristics owing to the presence of fiber-matrix interfacial bond, voids and stress concentrations around fiber ends (Nelson and Hancock, 1978; Kenny and Marchetti, 1995; Chandra *et al*., 1999). Discontinuous fibers in the composite alters damping characteristics owing to the presence of fiber-matrix interfacial bond, voids and stress concentrations around fiber ends (Nelson and Hancock, 1978; Kenny and Marchetti, 1995; Chandra et al., 1999). If the bonding between fiber / matrix is less, then the damping capacity developed by the composite was found to be more. Gupta et al. (1990) performed tensile test in short glass fiber reinforced polypropylene and investigated various types of energy

absorbing mechanisms and reported that debonding and fibre pull-out at the fracture surfaces are the two primary phenomenons influencing the energy absorbing mechanisms. Kultural and Eryurek (2007) evaluated fatigue performance of polypropylene with different percentage of calcium carbonate and confirmed that with the increase in filler content, hysteretic heating and damping capacity was found to be increased. Gassan and Bledzki (2000) investigated the dynamic performance of jute fiber reinforced polypropylene and reported that the strong fiber matrix adhesion enhanced the dynamic modulus of the composite and found to reduce the specific damping capacity. Material damping influences hysteresis heating as well as the ability to absorb vibration during service and hence, a better understanding of the interaction between fatigue damage and damping is essential to design and utilize these materials for better fatigue resistance and damping (Senthilvelan and Gnanamoorthy, 2006).

Many research works have been carried out to understand the influence of fibers on the damping behavior of thermoset and thermoplastic laminate materials (Hadi and Ashton, 1996; Lee *et al.*, 1994; Chandra *et al*., 1999; Adams and Maheri, 2003). Various works were carried out in the past to understand the damping mechanism of discontinuous fiber reinforced thermoplastic materials (Crema *et al.*, 1989; Wray *et al.*, 1990; Kultural and Eryurek 2007), however, the influence of fiber length towards damping performance of the thermoplastic composites was not investigated.

In this chapter, damping performance was evaluated and reported for leaf spring materials; unreinforced, 20 % short and long glass fiber reinforced polypropylene materials by subjecting to elastic and plastic deformation as well as free and forced vibration tests. Logarithmic decrement and phase lag between excited

force and its response were utilized to identify damping sources. Chosen leaf spring materials were subjected to dynamic mechanical analysis to quantify the damping characteristics at various temperature and frequency. The influence of fiber reinforcement and the length of fiber reinforcement on the internal heat generation of discontinuous fiber reinforced thermoplastic material during fatigue was also reported.

5.2 HYSTERESIS DAMPING

Hysteresis energy accumulates within the material when the polymeric materials are subjected to cyclic loading; this energy can be used to quantify material damping (Dominick *et al.*, 2000). In the thermoplastic material, viscous component of the matrix material significantly contributes to the hysteretic energy dissipation which is identified as a major damping source.

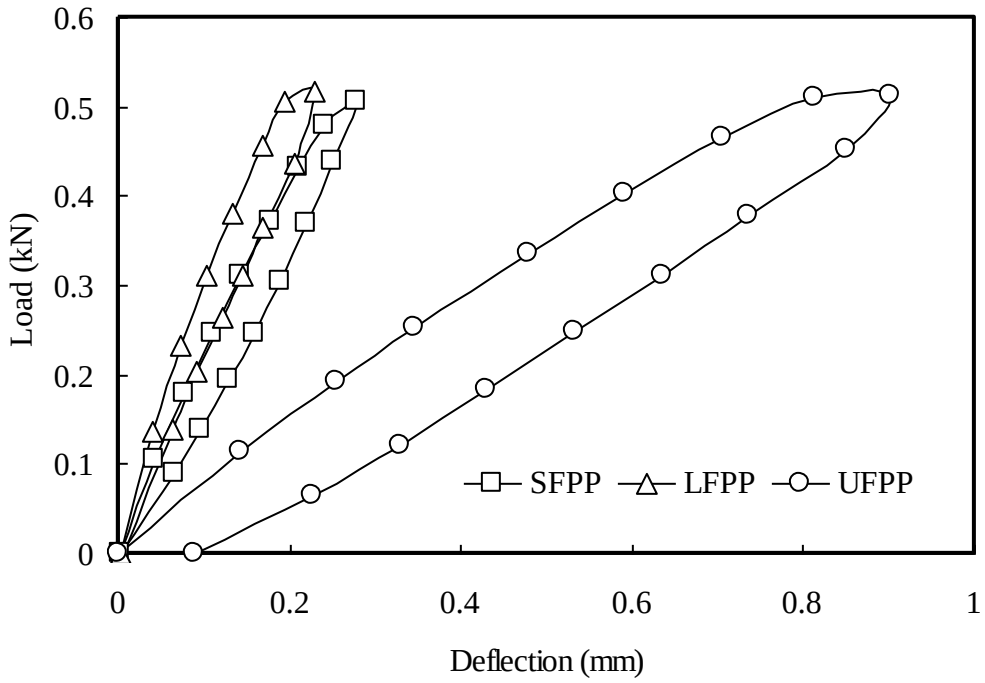

Fig. 5.1 Hysteretic loop of unreinforced and reinforced polypropylene

To quantify damping, chosen leaf spring materials were injection molded into tensile test specimen pertaining to ASTM D 638 standard. Load was applied on the molded tensile test specimens up to 500 N and released back to zero at the rate of 7.5 N/s using servo hydraulic machine (Instron 8801)Mantena *et al*. (1992) used similar methodology for obtaining the hysteresis loop and evaluated the damping performance for pultruded graphite-epoxy beams. Figure 5.1 shows the hysteretic area of chosen leaf spring material formed by the load-deflection curve during loading - unloading of specimen and the dissipated energy within the material per unit cycle was quantified. Hysteretic area of leaf spring materials; UFPP, SFPP and LFPP were found to be 110.85, 30.48 and 25.57 N-mm respectively. Area formed by this loop indicates the hysteresis damping which is partly stored in the microstructure (crazes, shear bands, voids and micro cracks) and partly dissipated as heat. Unreinforced PP exhibited higher area than that of reinforced PP due to the higher viscous content.

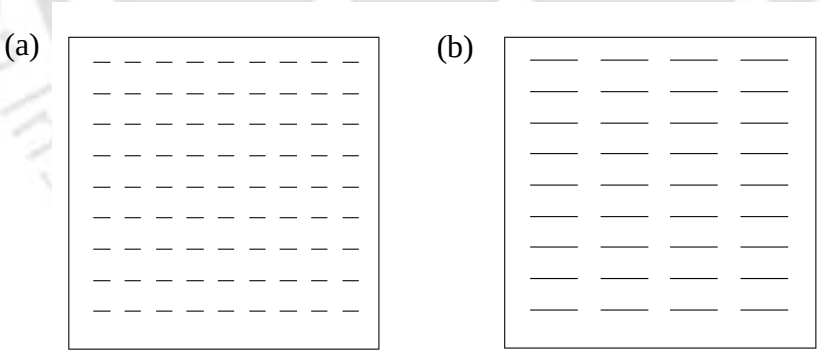

Fig.5.2 Schematic of fibers in a matrix for the same volume fraction (a) short fiber reinforced polymer and (b) long fiber reinforced polymer

Among reinforcement material, SFPP exhibited higher hysteresis area than LFPP due to the presence of more fiber ends/fiber matrix interface area. For the fixed volume fraction of reinforcement, due to the higher fiber ends and fiber matrix interface area (figure 5.2), short fiber reinforced material exhibited superior hysteretic damping characteristics than that of long fiber reinforced material.

5.3 DAMPING DUE TO FIBER-MATRIX INTERFACE

In the composites interface between fiber and the supporting matrix is one of the major damping sources; ideal interface transfers the entire load from matrix to fiber and do not contribute to the damping (Chandra *et al*., 1999). To quantify damping due to the fiber matrix interface, tensile test was carried out on chosen material and fractured surfaces were investigated to understand the fiber- matrix interface as discussed in section 4.2.2 (Figures 4.5 & 4.6)**.** Addition of reinforcement increased material modulus and strength. Increase in fiber length of LFPP material increases surface area of the fiber and provided good interfacial bonding strength with the matrix and thus, fiber pullout was avoided. In the interfacial bonding of fiber and matrix, fiber end is identified as the weakest region and more energy is absorbed in this region and results in improved damping. Due to the more fiber ends (figure 5.2) damping due to fiber matrix interface was higher in SFPP than that of LFPP. Higher strength and modulus of LFPP also confirms less fiber-matrix debonding. Gassan and Bledzki (2000) reported that composite having good fiber-matrix adhesion exhibited less specific damping capacity than composite with poor fiber-matrix adhesion.

5.4 DAMPING UNDER FREE VIBRATION

Damping coefficient was measured by means of the classical method of decay transient in the past (Crema *et al.*, 1989). Energy dissipation through plastic and elastic deformation was neglected when the test specimens were subjected to free vibration. Schematic arrangement for the free transverse vibration testing of specimen is shown in figure 5.3. Specimen (120 × 12 × 3 mm) was clamped at one end and an accelerometer (Bruel and Kjaer, Type 4507) was fixed at the end of the cantilever beam. The initial specimen displacement was provided with an impact hammer. Free end displacement of the specimen was measured and recorded with an accelerometer and finally fed into the data acquisition system.

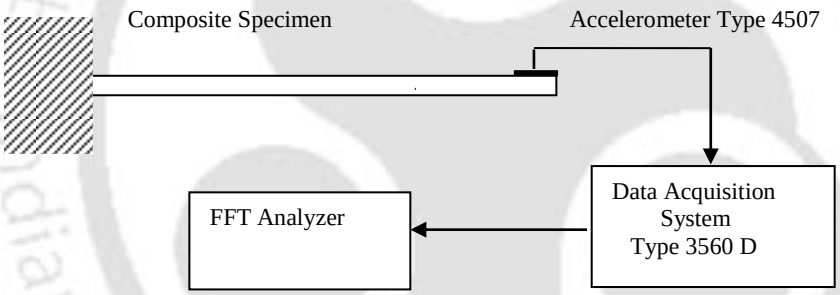

Fig.5.3 Schematic arrangement of experimental setup for free vibration condition

Many works have been reported in the past using similar methodology for the evaluation of damping factor (Saurez *et al*., 1986; Hadi and Ashton, 1996; Valtora *et al*., 2005). From the time domain data, the decay rate of free oscillation was measured by the logarithmic decrement (δ)

$$\delta = \frac{1}{n-1} ln\left(\frac{X_1}{X_n}\right) \tag{5.1}$$

where n is the number of cycles, X_1 is the vibration amplitude of the first cycle and X_n is the vibration amplitude after n^{th} cycle. Damping factor (ξ) was computed from logarithmic decrement (δ) using the following relation

$$\delta = \frac{2\pi\xi}{\sqrt{1-\xi^2}} \tag{5.2}$$

This procedure does not involve any complex signal processing technique, as the amplitude ratio can be obtained directly from the time domain data. Transient time decay curves are shown in figure 5.4. The logarithmic decrement of LFPP, SFPP and UFPP was calculated as 0.2255, 0.3645 and 0.4154 respectively and the corresponding damping factor pertaining to LFPP, SFPP and UFPP materials were found to be 0.0359, 0.0579 and 0.0659 respectively. Wray *et al.* (1990) reported the reduction of logarithmic decrement and damping factor with the increase in fiber volume fraction of glass fibers in the composite. Presence of more fiber ends contributed to improve the damping in SFPP when compared to LFPP as indicated and discussed in the prior section. Damping performance of the chosen leaf spring materials exhibited similar trend as indicted by the hysteresis area.

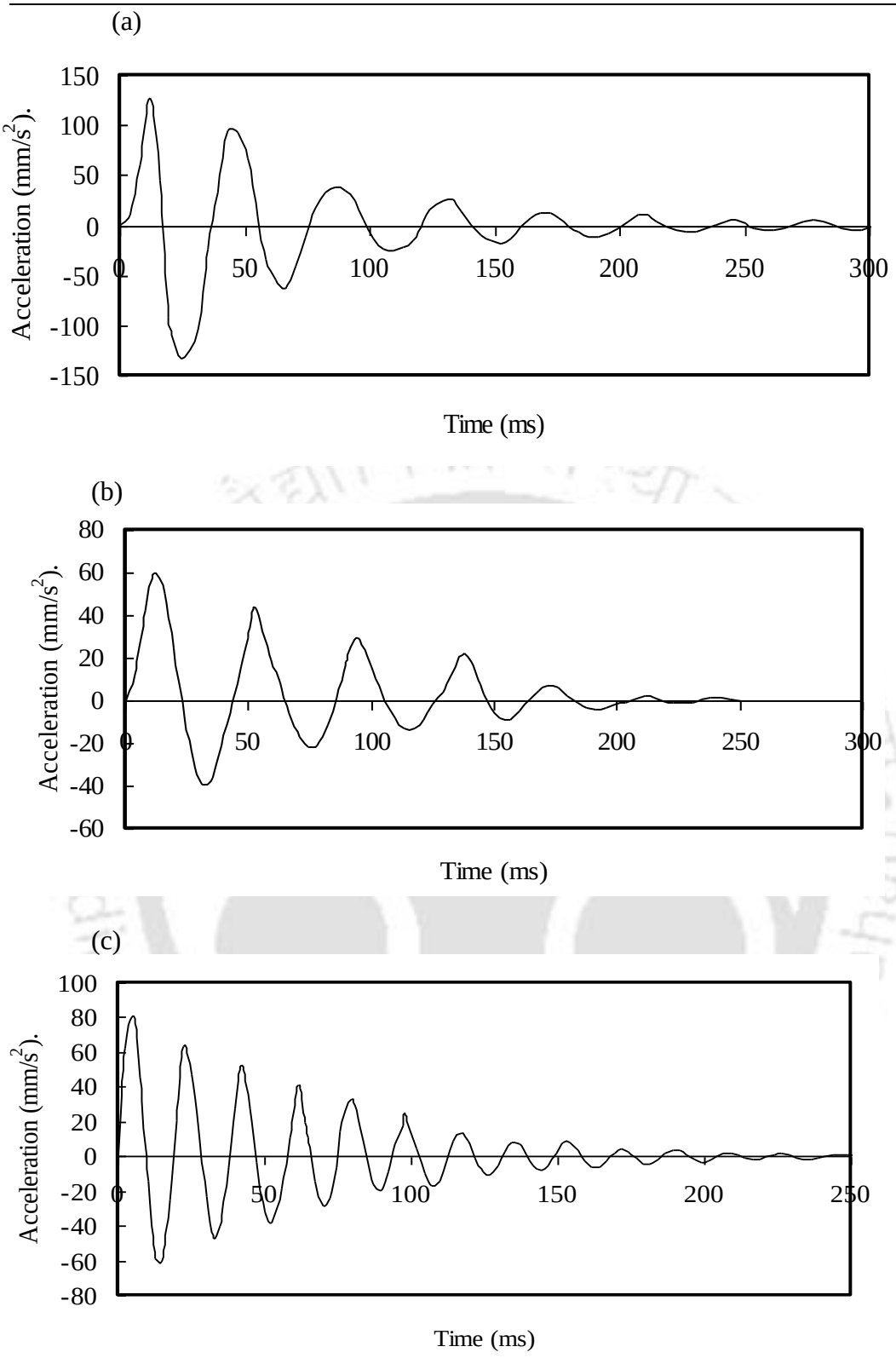

Fig.5.4 Decay curve of (a) unreinforced PP (b) short fiber reinforced PP and (c) long fiber reinforced PP

5.5 DAMPING UNDER FORCED VIBRATION

Energy dissipation through plastic deformation was neglected when the test specimens were subjected to forced vibration. Schematic and experimental arrangements for the forced transverse vibrations of the composite specimen are shown in figures 5.5(a-c). Test specimen was clamped at one end and the force transducer (Bruel and Kjaer, 8230-001) was fixed above the exciter and connected at the other end. An accelerometer was fixed at free end and the signals from the accelerometer (Bruel and Kjaer, Type 4507) and force transducer were measured and stored with respect to time. The schematic of exciting force and its response are shown in figure 5.6 and the phase lag (ϕ) was evaluated using following relation

$$\phi = \frac{t_l}{T} \times 360^0 \tag{5.3}$$

where T is the time period for one cycle and t_l is the time lag in s between exciting forcing and response. Three trials were conducted for all the chosen leaf spring materials**.** Phase lag is the time by which the response lags behind the exciting force and it is a measure of the damping. Valtorta *et al.* (2005) used similar technique by measuring the phase difference between excitation and response for polypropylene fibers and later compared damping measurements from standard dynamic mechanical analysis technique

(a)

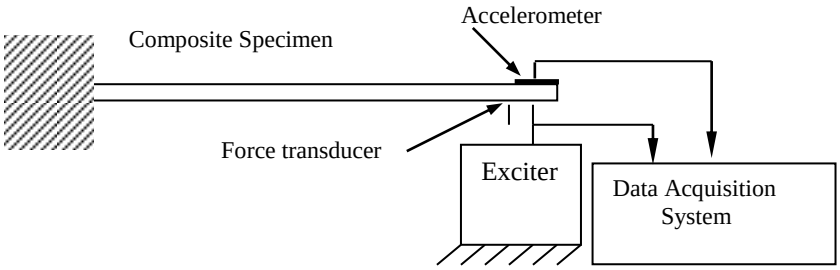

Fig.5.5a Schematic diagram of experimental setup for forced vibration condition

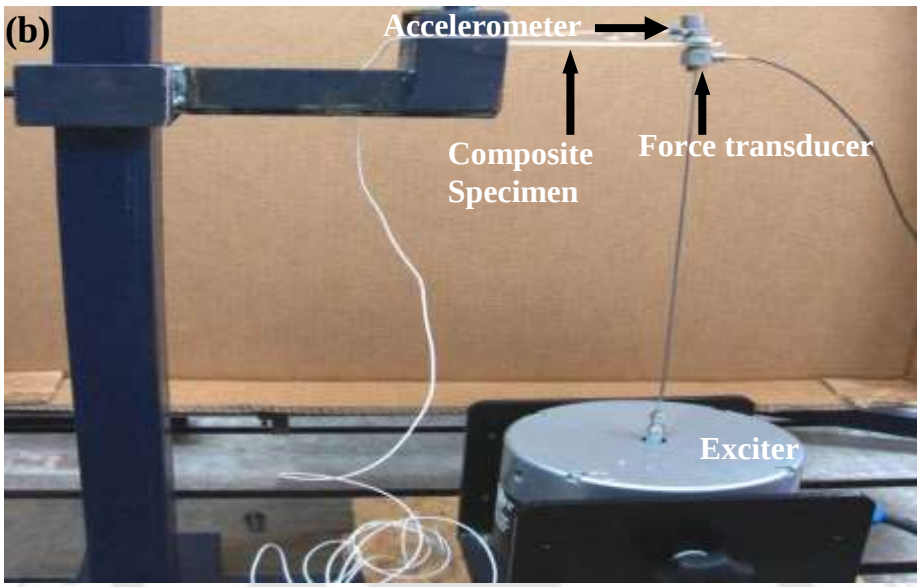

Fig.5.5b Experimental setup for forced vibration condition

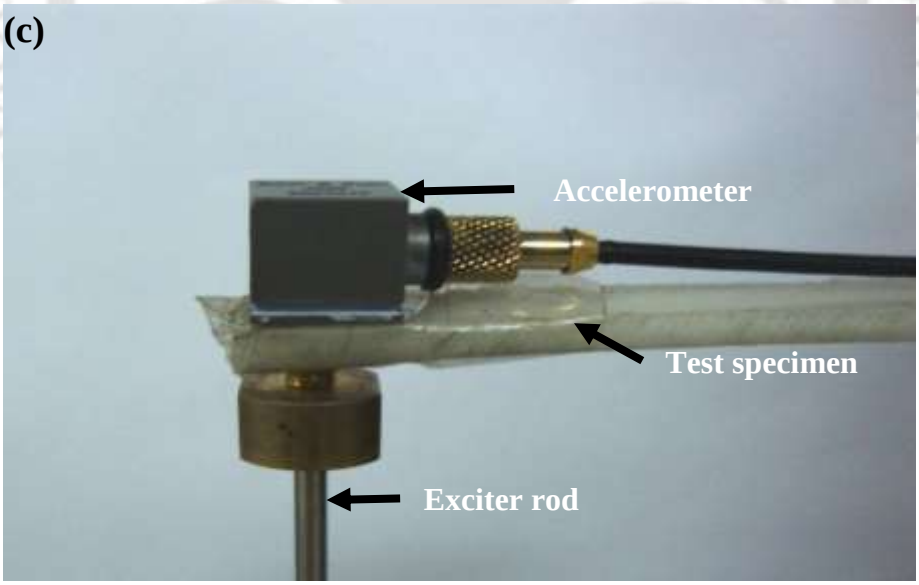

Fig.5.5c Close up view of test setup for forced vibration condition

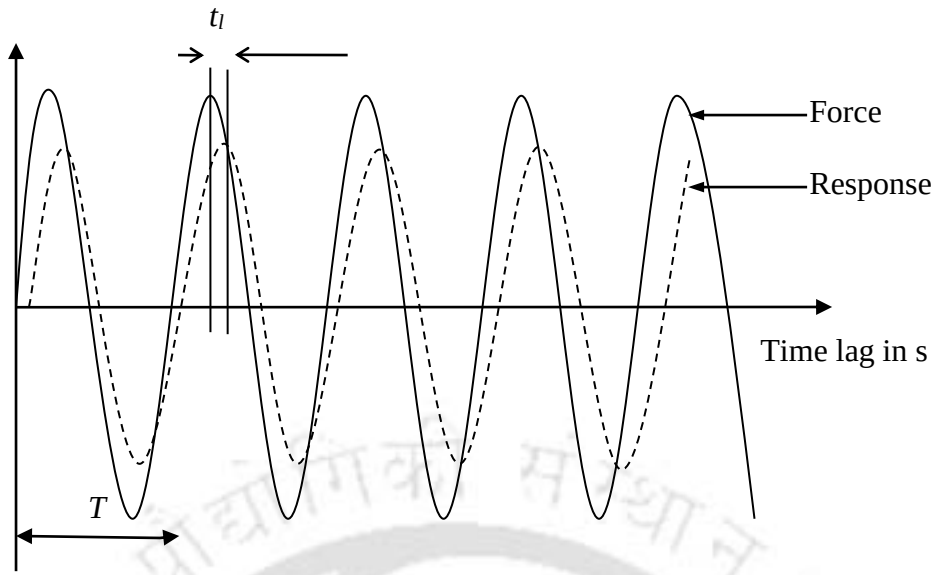

Fig.5.6 Schematic of excitation force and its response

Phase lag is directly proportional to the material damping (Menard, 1999; Aberg and Widell, 2004); higher phase lag angle indicates higher material damping. Damping factor from forced vibration was calculated using the following relation (Genta, 1999)

$$tan\phi = \frac{2\xi\left(\frac{\omega}{\omega_n}\right)}{1-\left(\frac{\omega}{\omega_n}\right)^2} \tag{5.4}$$

where ϕ is the phase lag angle, ω is the forced exciting frequency (20 Hz) and ω_n is the natural frequency. The natural frequency was obtained for the specimen from the Fast Fourier Transform (FFT) analyzer during the free vibration and shown in figures 5.7 (a -c). The phase lag obtained from the forced vibration experiment for all the considered test specimens are shown in figures 5.8 (a-c). Fig. 5.9 shows the mean phase lag of all the considered test specimens and the deviations were found to be well with in 3%. Phase lag of unreinforced, short fiber reinforced and long fiber reinforced PP materials were 31.56°, 28.46° and 27.69° respectively.

(a)

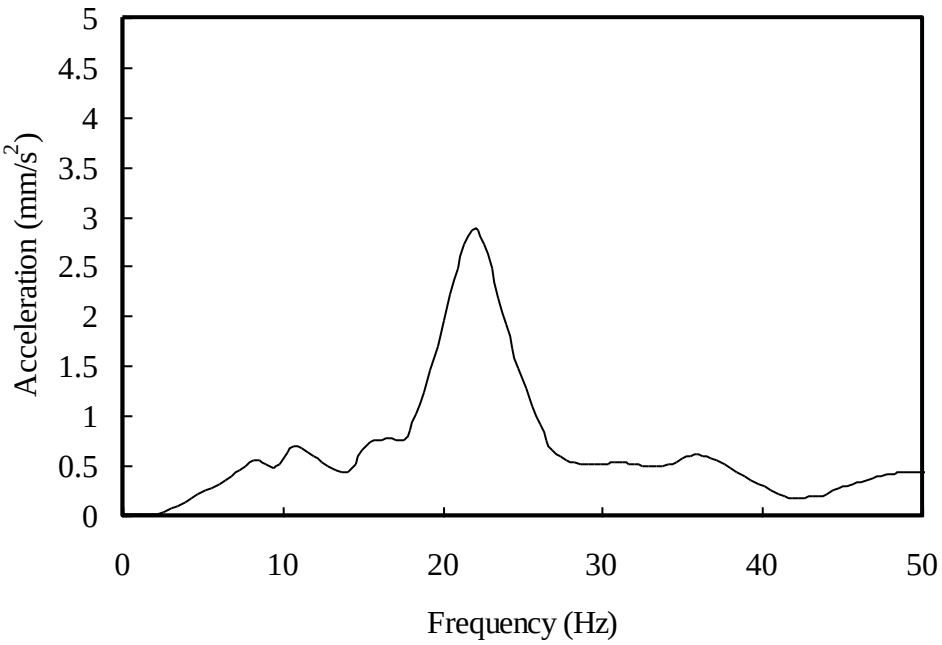
Acceleration (mm/s2)
0
0.5
1
1.5
2
2.5
3
3.5
4
4.5
5
0
10
20
30
40
50
Frequency (Hz)

(b)

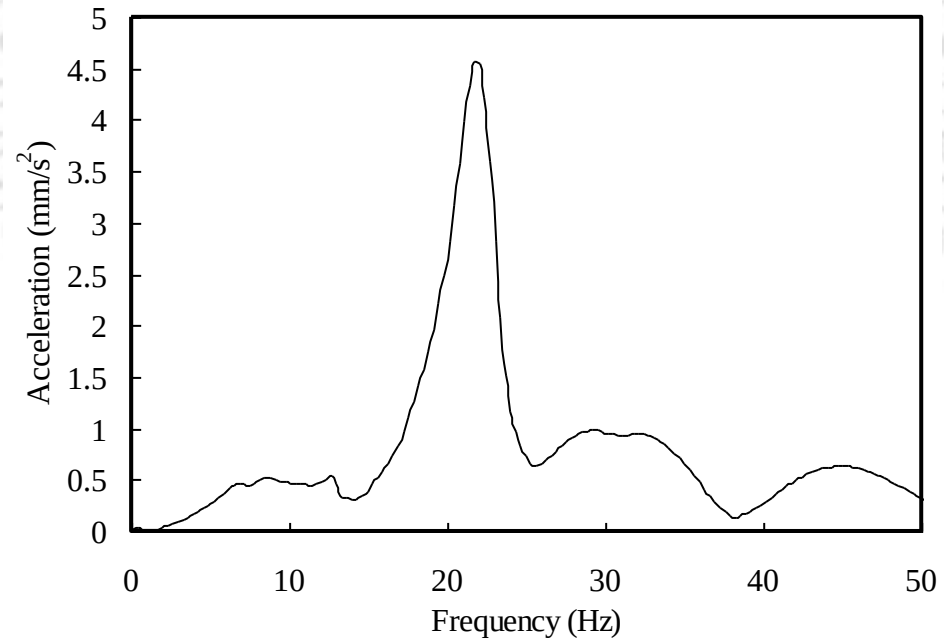
Acceleration (mm/s2)
0
0.5
1
1.5
2
2.5
3
3.5
4
4.5
5
0
10
20
30
40
50
Frequency (Hz)

(c)

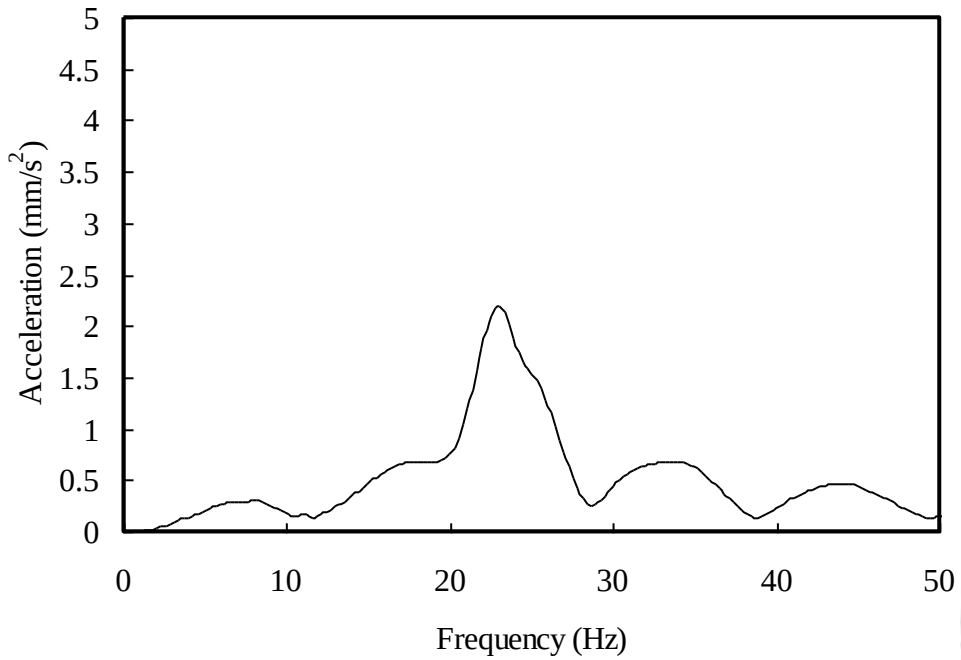

Fig. 5.7 FFT analyzer signal depicting the natural frequency for (a) unreinforced (b) short fiber reinforced PP and (c) long fiber reinforced PP

(a)

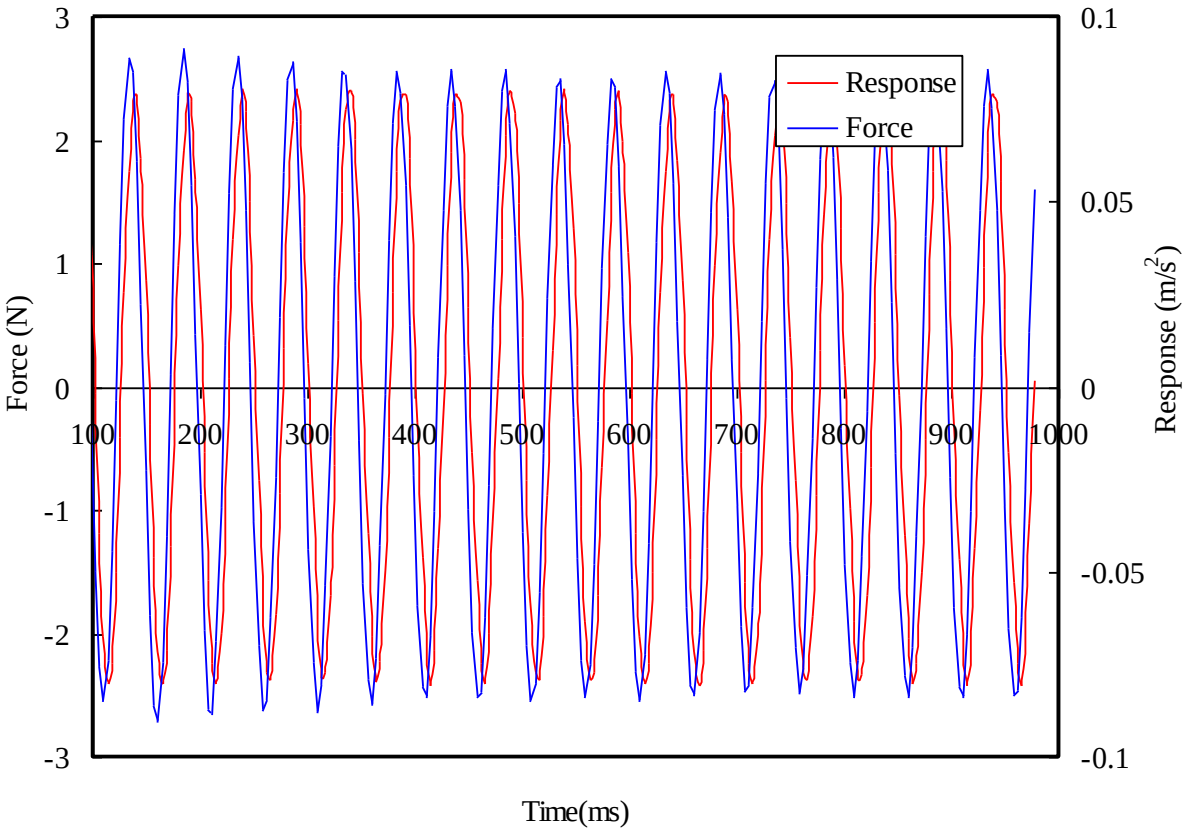

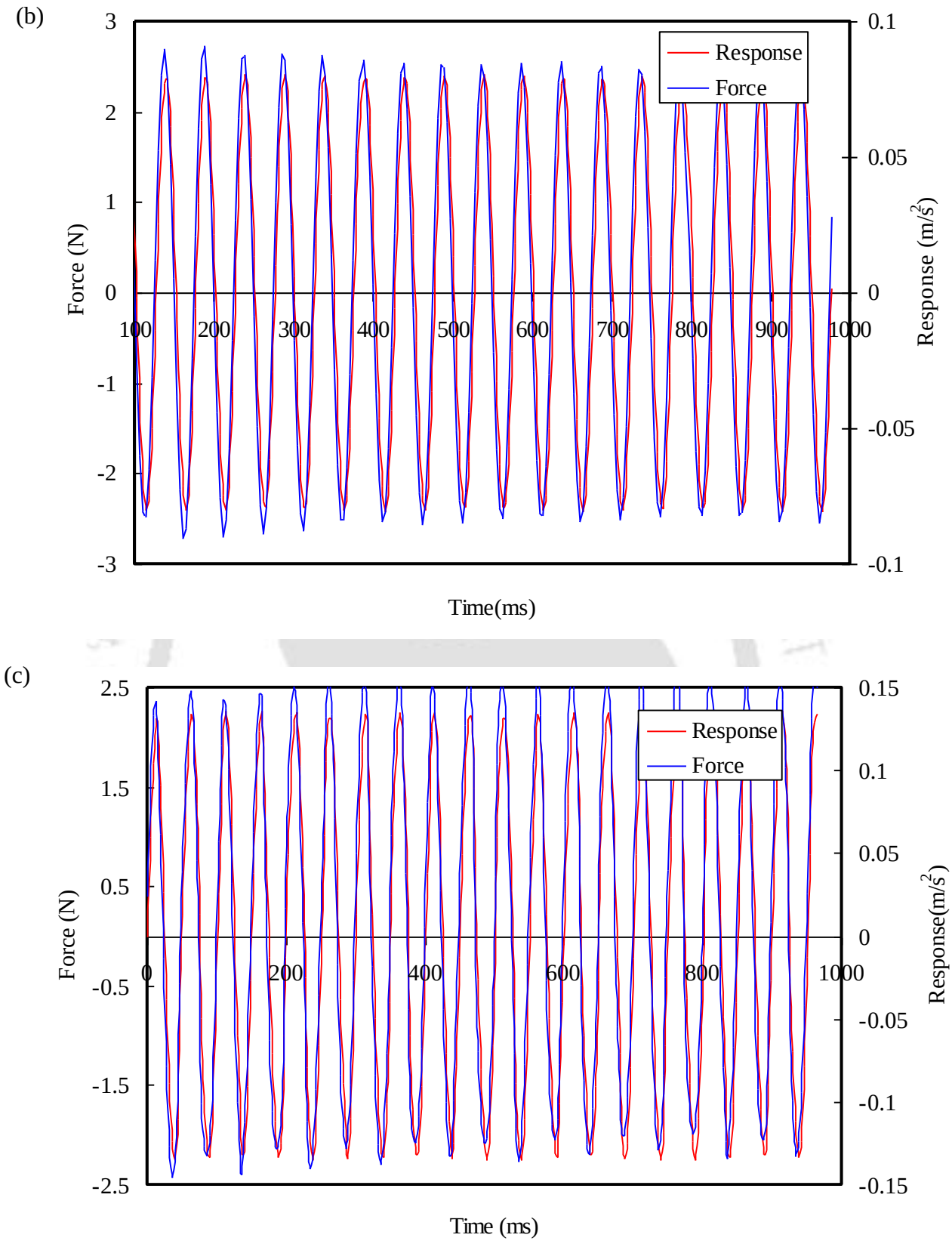

Fig. 5.8 Phase lag plot between excited force and its response for (a) unreinforced PP (b) short fiber reinforced PP and (c) long fiber reinforced PP

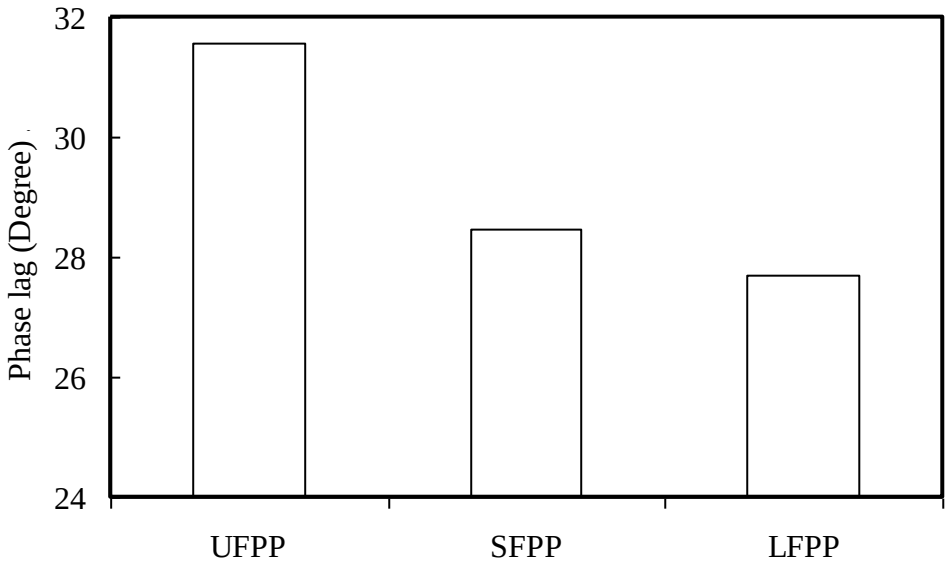

Fig.5.9 Phase lag between excited force and its response of the test specimens

Addition of fibers to the base polypropylene significantly limits the material elastic deformation and decreases the phase lag between the exciting force and the corresponding material response. Among reinforced material, SFPP showed increased phase lag than that of LFPP due to the presence of more fiber matrix interface which ultimately delayed the response to initiate. The calculated damping factor obtained from forced vibration test for LFPP, SFPP and UFPP were 0.0393, 0.0517, and 0.0644 respectively. Since the test specimen geometry and air damping conditions were similar in both free and forced vibration technique, obtained damping factors were almost same. The damping factor and phase lag obtained from forced vibration tests exhibited similar trend to that of hysteretic area and the logarithmic decrement obtained through free vibration tests.

5.6 DYNAMIC MECHANICAL ANALYSIS

In the structural applications, most often materials are subjected to dynamic loads under various temperatures; hence, dynamic performance evaluation at various temperatures helps to design these materials suitably. Dynamic Mechanical Analysis

(DMA) was carried out by applying an oscillating force to a sample and response of material to that force was analyzed.

From DMA, material modulus and loss factor (measure of damping) were found out at various temperatures and frequencies. The modulus measured from DMA is not the same as the Young's modulus of the classic stress-strain curve. In DMA, a complex modulus (E*), elastic/storage modulus (E') and imaginary/loss modulus (E'') were calculated from the material response to the sine wave oscillation. These moduli allow better characterization of the material such as ability of the material to return or store energy (E'), ability to lose energy (E'') and loss factor (the ratio of these effects, tan δ). DMA was carried out on the injection molded test specimens using Perkin-Elmer as per ASTM D6382 standard, DMA/7E. Test specimens were subjected to bending in a cantilever mode with a span length of 70 mm. An oscillatory force of 3 N was applied over a temperature range of 32-92° C and frequency scan was done between 0.1-100 Hz.

Figures 5.10a and 5.10b show the variation of storage modulus and loss modulus of test materials as a function of temperature, tested at 1 Hz frequency. It is vivid that the increase in the fiber length improved the material stiffness at dynamic condition. The storage modulus and loss modulus of LFPP material were found to be higher compared to those of UFPP and SFPP materials. Since the mean fiber length of LFPP (1.251 mm) was larger than that of SFPP (0.4403 mm), the molecular mobility of LFPP polymer matrix was restricted which resulted in superior modulus.

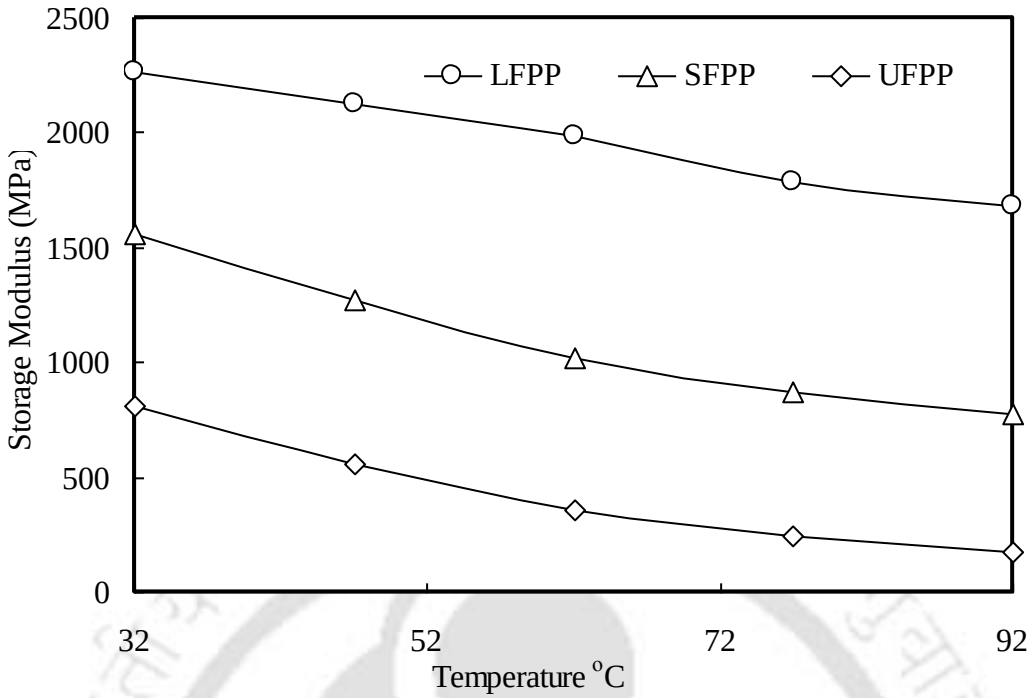

Fig.5.10a Storage modulus of leaf spring materials at various temperature

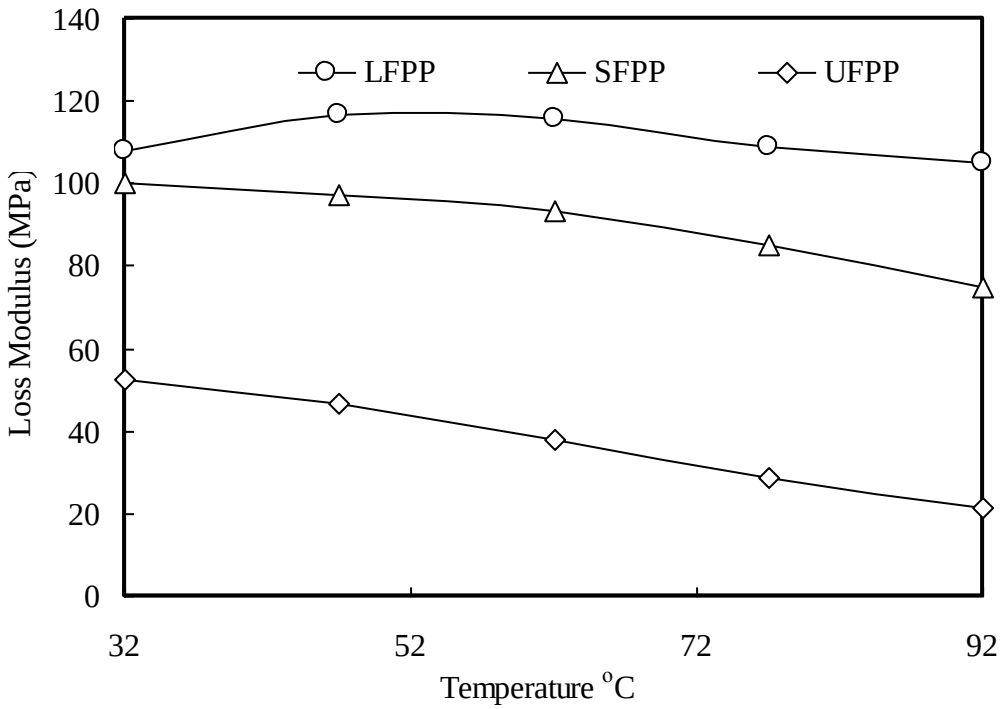

Fig. 5.10b Loss modulus of leaf spring materials at various temperature

When a polymeric material is stressed over long enough time (low frequency), flow occurs; however, when the same material is stressed over very short times (high frequency), the material behaves elastic (Menard,1999). Thus, storage modulus of the test materials was found to increase with the increase in frequency (figure 5.11). It is clear from figures 5.12 (a-b) that the loss factor dropped with the increase in fiber length. The loss factor of chosen materials; LFPP, SFPP and UFPP at room temperature are found to be 0.044, 0.061 and 0.065 respectively. The restraint of polymer molecules due to the existence of high modulus fibers caused the reduction in loss factor in polypropylene composites (Harris *et al.*, 1993). Rezaei *et al.* (2009) observed a reduction in loss factor with the increase in fiber length of carbon fiber reinforced polypropylene composites.

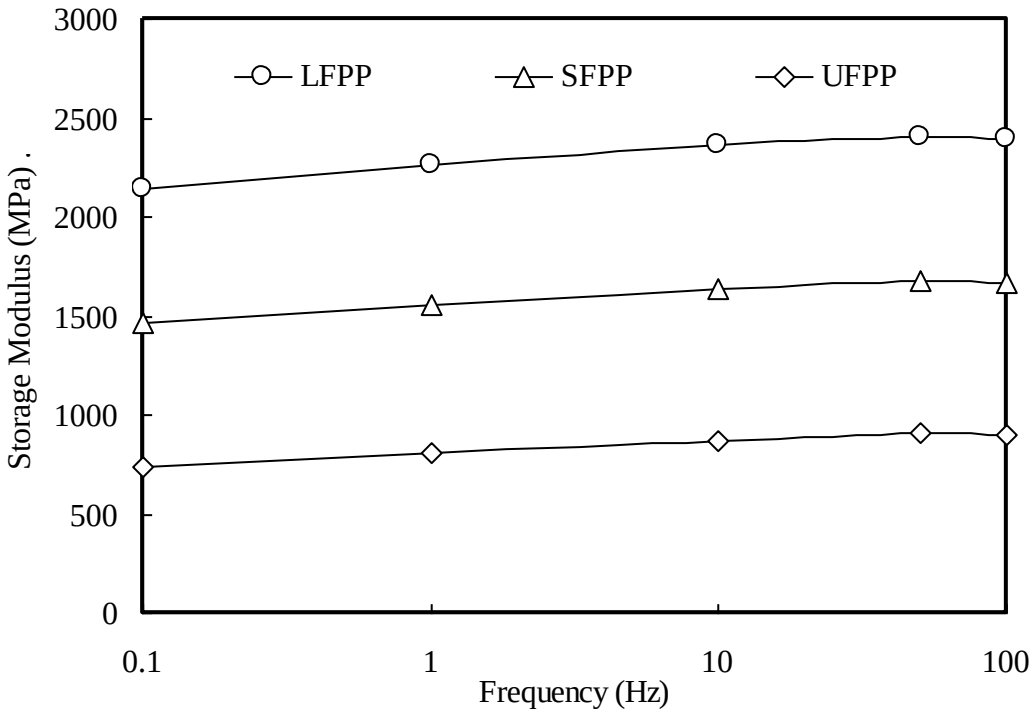

Fig.5.11 Effect of frequency on storage modulus for leaf spring materials

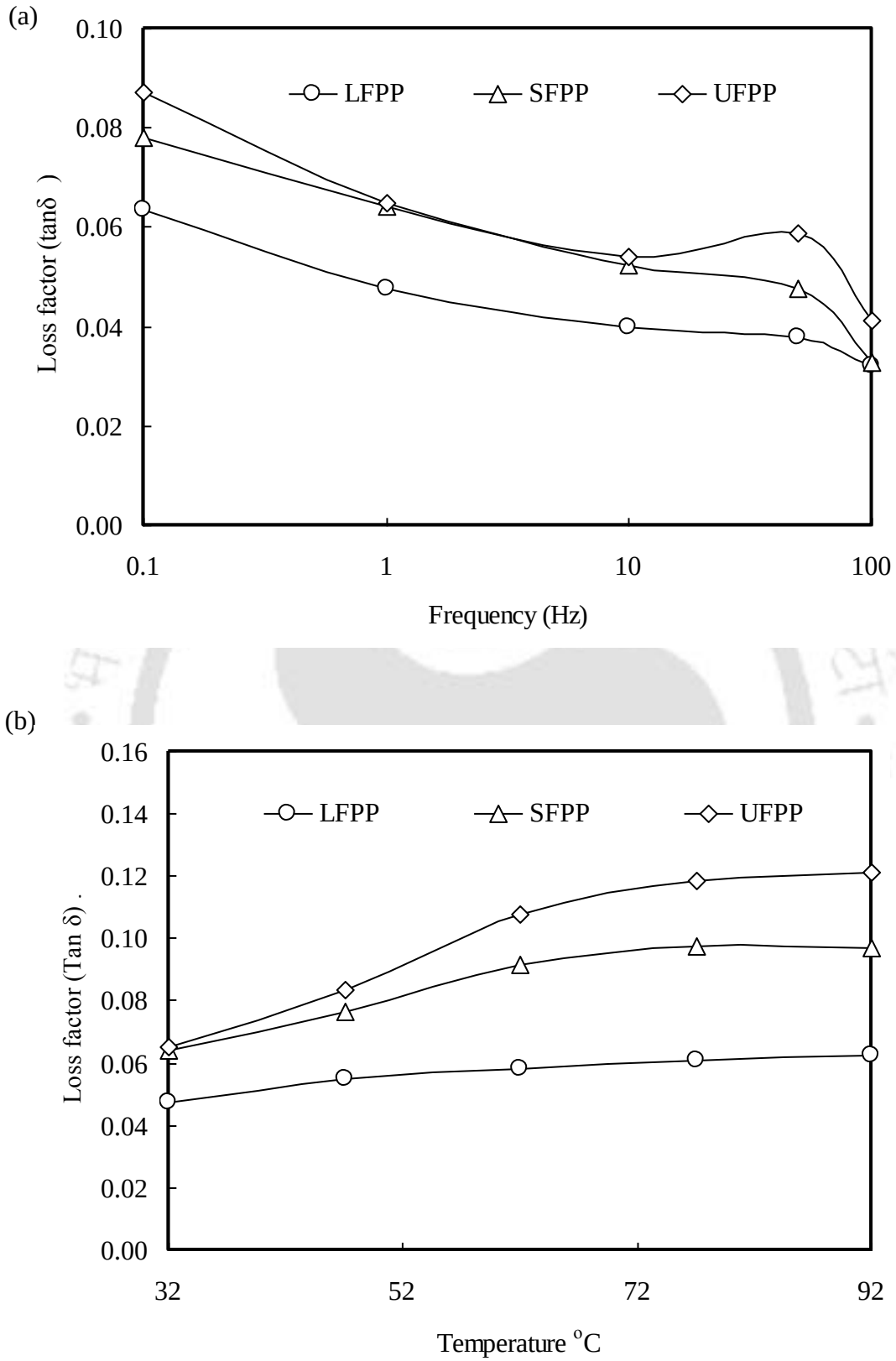

Fig.5.12 Loss factor for leaf spring materials under (a) various frequencies (b) various temperature

Loss factor of chosen material decreased with the increase in frequency (figure 5.12a). Sato *et al*. (1992) also reported similar behavior and this is due to the fact that increased frequency decreases viscoelastic strain decreases and pays the way for increased stiffness (Crawford, 1998; Rosato *et al*., 2000). Loss factor of all the chosen test materials was found to increase with the increase in temperature (figure 5.12b) and this behavior was due to the matrix softening which resulted in increased molecular mobility at elevated temperature. When the test material temperature increases, the free volume, i.e., space for the internal movement of the molecule increases resulted in drop of storage modulus and hence, rise in loss factor was visualized. The increase in damping factor with increase in temperature is less for LFPP due to the reinforcing efficiency of longer glass fiber polypropylene composites. Thomason and Groenewoud (1996) reported the reinforcing efficiency of longer glass fiber polypropylene composites in retaining the modulus at higher temperatures. Damping factor (ξ) was calculated using the relation 5.5 (Landro and Lorenz, 2009)

$$\xi = \frac{tan\delta}{2} \tag{5.5}$$

The damping factor of LFPP, SFPP and UFPP were 0.022, 0.030 and 0.032 respectively. It is to be noted the variation in damping factor obtained through dynamic mechanical analysis and forced vibration was due to the change in geometry of test specimen, type of load, tightening torque (clamping effects) and the effect of air damping (Menard,1999).

5.7 HYSTERETIC HEATING

Viscoelastic characteristics of polymeric materials generate considerable amount of internal friction within the material during mechanical deformation resulting in

hysteresis heat generation. Damping affects the amount of hysteresis heat generation during service (Senthilvelan and Gnanamoorthy, 2006). Rise in temperature due to the material hysteretic heating depends strongly on the damping properties of the material (ASM International, 1988; Kultrural and Eryurek, 2007). Thus, evaluation of internal friction generated in the form of heat for the chosen leaf spring material during cyclic loading is of practical importance.

To investigate the influence of fiber length on the hysteretic heating for leaf spring materials, injection molded tensile test specimens pertaining to ASTM D 638 standard were used. Test specimens were subjected to finite number (7200) of fatigue cycles using servo hydraulic fatigue testing machine(Instron 8801) at 1 Hz and R = 0 (stress ratio) under constant displacement mode. The load required for 1 mm deflection under cyclic sinusoidal loading was measured for the chosen test materials. During testing, specimen temperature was measured using non-contact infra red temperature sensor (Raytek MID, ± 0.1 °C accuracy). Sensor was positioned in such a way to measure the temperature at the middle of the gauge length of tensile specimen. The temperature rise under cyclic load was observed for all the three test materials. The generated heat exceeds the heat transferred to the surroundings because of poor conductivity of the material resulted in specimen heating. During cyclic loading some part of the mechanical work was spent on irreversible molecular processes leading to various microscopic deformations; crazes, shear bands, voids and micro cracks and the other polymeric material, resulting with rise in specimen temperature. In general, fatigue tests are being carried out to evaluate the endurance strength of a material. In this study, the heat generated during cyclic loading was measured and attempted to correlate with the hysteretic heating behavior of the material and hence, material damping.

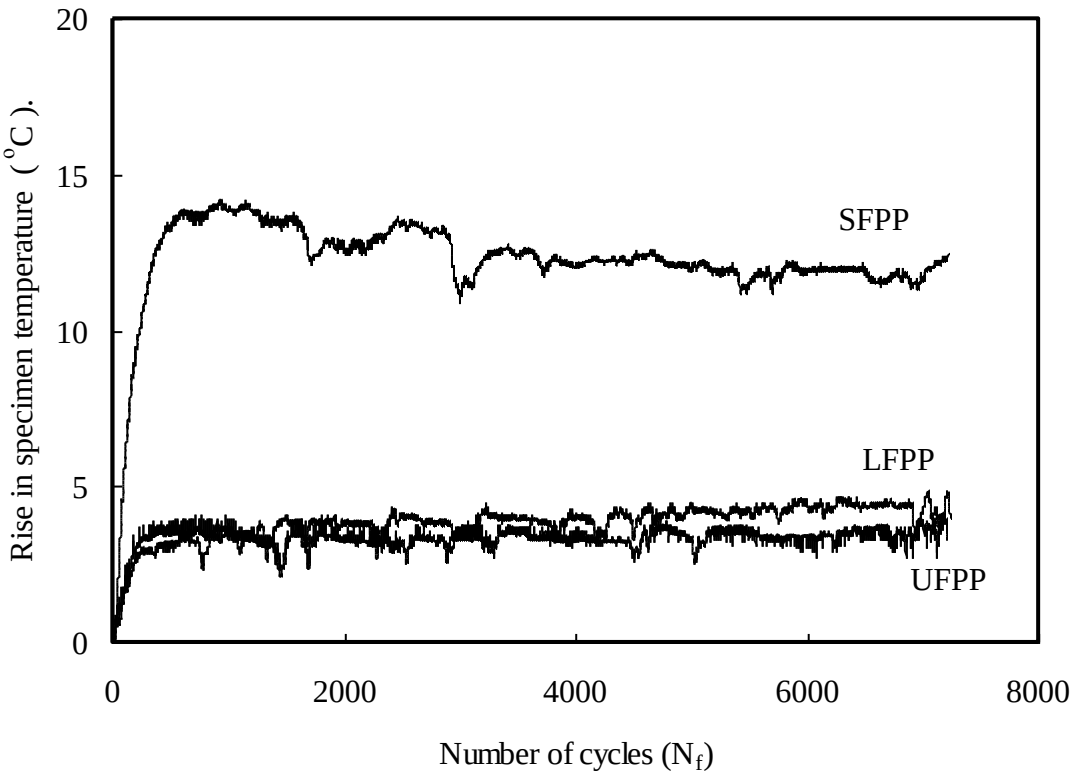

Fig. 5.13 Hysteretic heating of unreinforced and reinforced polypropylene specimens during fatigue

Figure 5.13 shows the measured surface temperature of test materials during fatigue testing. The rise in temperature for unreinforced PP was due to the hysteretic heating behavior of the polypropylene matrix material and the measured surface temperature was less than reinforced PP. In the case of reinforced PP, presence of fibers and fiber matrix interface causes more internal friction resulted in increase of heat generation. Short fiber reinforced PP exhibited higher temperature than that of the long fiber reinforced PP due to the higher internal collision because of its higher fiber ends. For a given volume of material, short fiber reinforced material have more fiber ends than long fiber reinforced material (figure 5.2). Hence, when the short fiber reinforced materials are subjected to cyclic loading, presence of more fiber ends cause more internal friction, resulted in higher heat generation. Kultrural and Eryurek (2007) also

reported similar behavior, wherein higher material temperature was observed when the percentage of calcium carbonate filler in polypropylene was higher under fatigue testing.

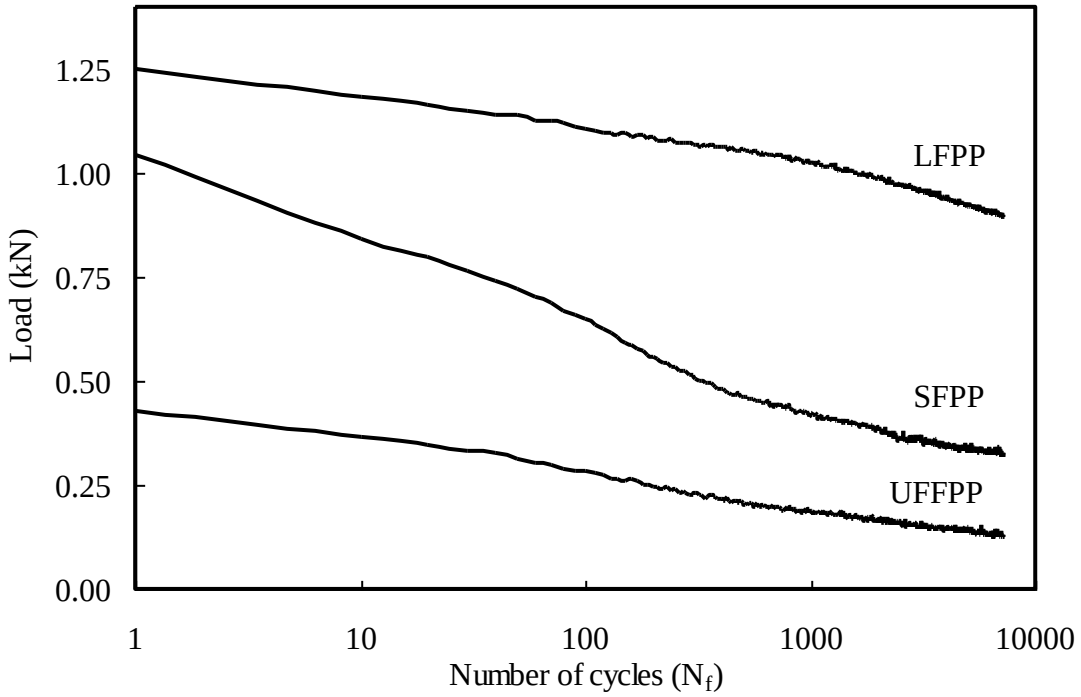

Fig.5.14 Load drop during constant deflection mode for unreinforced and reinforced polypropylene specimens

Figure 5.14 shows the load required for maintaining 1 mm deflection of test materials under fatigue loading. Due to the rise in material temperature and material visco-elastic behavior, load required for the fixed amount of deflection decreased with the progression of cycles. Among reinforced materials, short fiber reinforced material exhibited higher load drop than that of long fiber reinforced material. This behavior was due to the increased rise in material temperature during fatigue as well as weaker fiber matrix bond in the short fiber reinforced material .When the fiber matrix bond is weaker, load drop was observed to be significantly larger due to the slip between fiber and matrix.

5.8 SUMMARY

Damping performance of the chosen leaf spring materials were evaluated through various techniques to identify various individual damping sources. Test materials were subjected to deformation to identify damping sources due to the elastic and plastic deformation. Leaf spring materials were subjected to free and forced vibration, to identify damping sources other than energy dissipation through elastic and plastic deformation. Test materials were also subjected to dynamic mechanical analysis to understand and correlate material damping behavior.

- When the test materials were subjected to elastic as well as plastic deformation, hysteretic area measurement indicated energy dissipation. Unreinforced material exhibited higher energy dissipation than reinforced material. SFPP showed higher energy dissipation than LFPP due to the presence of more fiber ends.
- When the test materials were subjected to free vibration, logarithmic decrement and damping factor were found to decrease with the increase in fiber length. UFPP had the highest damping factor followed by SFPP and LFPP. When the test materials were subjected to forced vibration, UFPP and SFPP exhibited higher phase lag between the excited force and its response than that of LFPP material.
- Dynamic mechanical analysis of test material revealed the improvement of storage modulus with respect to increase in fiber length, LFPP had a higher storage modulus followed by SFPP and UFPP; however, damping factor was found to be reduced with the incorporation of fibers. Damping factor was high for UFPP preceded by SFPP and LFPP.
- Reinforced material showed higher temperature rise than that of unreinforced material under cyclic loading due to the presence of fibers and fiber matrix interfaces. Among reinforced material, SFPP found to exhibit more temperature rise than that of LFPP due to the higher fiber end density and inferior fiber matrix bond.

In a summary unreinforced material exhibited higher energy dissipation than reinforced material. SFPP showed higher energy dissipation than LFPP. Logarithmic decrement and damping factor were found to decrease with the increase in fiber length. UFPP had the highest damping factor followed by SFPP and LFPP. Damping factor was found to be reduced with the incorporation of fibers. Damping factor was high for UFPP preceded by SFPP and LFPP.

CHAPTER 6

DESIGN, MANUFACTURE AND STATIC PERFORMANCE OF THERMOPLASTIC LEAF SPRINGS

6.1 INTRODUCTION

Automobile suspension system isolates passengers and cargos from shocks and vibration due to the road undulations by absorbing, storing and releasing energy. In the suspension system, leaf springs are preferred over air suspension and coil spring due to its simple design. During the past three decades, sufficient amount of research and development work have been carried out on thermoset composite leaf springs (Beardmore, 1986; Rajendran and Vijayarangan, 2001; Qureshi, 2001; Shokrieh and Rezaei, 2003). Design aspects involving shape optimization, reduction of unsprung weight, manufacturing process involved and performance investigation is dealt in many research articles. Applications of leaf spring ranging from solar car (Sancaktar and Gratton, 1999) to railway freight applications (Hou *et al*., 2005) were investigated in the past. Thermoplastic composites are desirable as the leaf spring material due to its high specific strength, ability to manufacture complex shape and corrosion resistance (Yamada, 2007).

In this chapter, design of variable width mono leaf spring with the aid of optimization technique and finite element analysis tool was presented. Designed leaf spring was manufactured by injection molding process. Before development, injection molding simulation software was used to design the appropriate die, gating and processing condition. Manufacturing details of variable width leaf springs with

chosen test materials were also presented in this chapter. Static performance evaluation of leaf springs to understand the load deflection and strain rate sensitiveness is also presented in this chapter.

6.2 LEAF SPRING DESIGN

6.2.1 Material Design

Material and geometry of the leaf springs significantly influence energy storage and leaf spring performance. To identify appropriate material for the leaf spring, specific strain energy of the discontinuous glass fiber thermoplastic polypropylene and conventional leaf spring steel materials were considered. Amount of specific elastic strain energy stored in a system (Yu and Kim, 1988) is given as

$$S_e = \sigma_u^{\,2} / 2\rho E \qquad (6.1)$$

where E is the modulus of elasticity of the material, ρ is the density of the material and σ_u is the ultimate strength of the material. The above equation depicts that most appropriate material for the leaf spring application must have maximum strength and minimum modulus of elasticity. Figure 6.1 shows the specific strain energy of spring steel, unreinforced polypropylene (UFPP), 20 % short glass fiber reinforced polypropylene (SFPP) and 20 % long glass fiber reinforced polypropylene (LFPP) materials and material properties are tabulated in table 6.1. Due to the high specific elastic strain energy, discontinuous long glass fiber reinforced thermoplastic material was identified as a potential material for the leaf spring application.

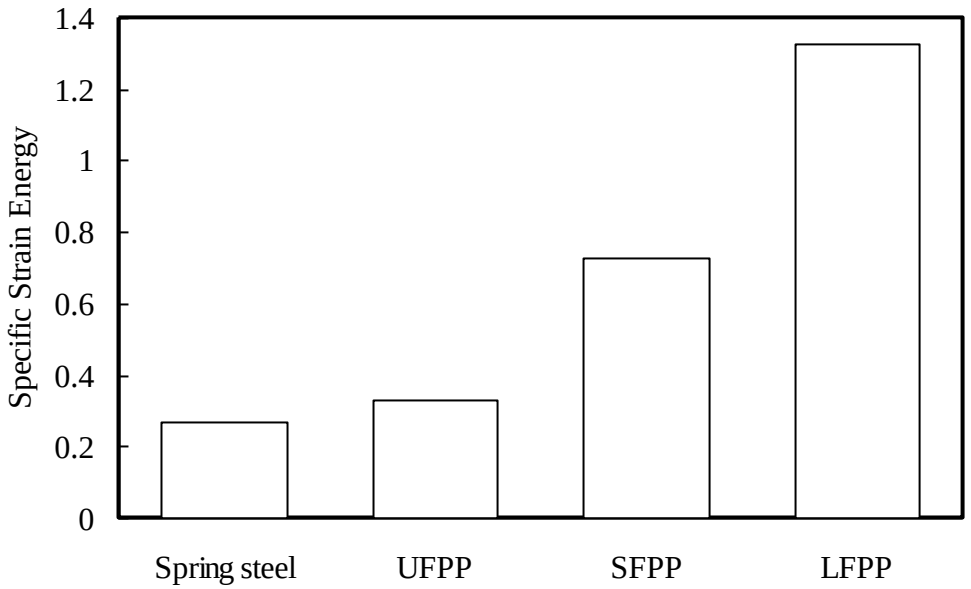

Fig. 6.1 Specific strain energy of the leaf spring materials

Table 6.1 Properties of steel and polypropylene composites

Material	Ultimate strength (N/mm^2)	Modulus of elasticity (N/mm^2)	Density (kg/mm^3)
Spring steel (AISI 5160)	931	205000	7.85
Unreinforced Polypropylene (UFPP)	32	1700	0.908
Short glass fiber Polypropylene (SFPP) (Saint Gobain)	72	3448	1.03
Long glass fiber Polypropylene (LFPP) (Saint Gobain/Twintex)	125	5650	1.04

6.2.2 Leaf Spring Geometry Design

Mono leaf springs are preferred over graduated leaf springs as the damping due to friction between individual leaves is difficult to control. High storage capability of leaf spring can be obtained through uniform stress distribution (Haynes, 1966).

The shape of the leaf spring should provide uniform bending stress along the length of the spring under vertical forces. To fulfill this criteria, different types of design; constant cross section, constant thickness and varying width were considered in the past (Beardmore, 1986; Sancaktar and Gratton, 1999). In the present investigation, width (b_c) and thickness (t) at the axle seat for a specified loading condition were determined by optimizing the volume of spring by considering the geometry as a rectangular spring with constant width and thickness. Later appropriate taper ratio was applied from center to the ends of the leaf spring for varying width.

Leaf spring design was constrained with mechanical properties of chosen leaf spring materials, (unreinforced polypropylene, 20 % short and long glass fiber reinforced polypropylene), shot capacity, processing capability of the injection molding machine and frame size of the fatigue testing machine available at IIT Guwahati.

Leaf spring geometry was constrained to have a maximum weight of 160 g (based on the shot capacity of the injection molding machine). With the above constraint, dimensions at the center of the rectangular beam were determined with the optimization tool box of Matlab®. The function used in the optimization tool box was 'fmincon' and the function uses an inbuilt line search method (Matlab release notes, 2005). The main objective was to minimize the weight of the leaf spring, and it was limited to 160 g with the maximum loading (P) at full deflection as 500 N. Length of the spring (L) is fixed as 300 mm (fixed based on the frame side of the fatigue testing machine).

Detailed optimal problem formulations are as follows:

The objective function can be represented as:

$$F(W_b) = \rho L (b_c .t) \quad (6.2)$$

where W_b is weight of the beam, b_c is width at the center, t is beam thickness at the center and ρ is material density, 1.04g/cc (Twintex, 2005). The upper and lower bound values of design variables, b and t (decided based on the manufacturing limits) are given as

$b_{max} = 60$ mm and $b_{min} = 20$ mm

$t_{max} = 15$ mm and $t_{min} = 5$ mm

Bending stress (S_b) and deflection (Y) are design constraints that are related to design variable and design parameter. Spring rate of thermoset composite leaf springs lies in the range of 20 - 586 N/mm ranging from solar car (Sancaktar and Gratton, 1999) to railway wagon suspension system (Hou *et al*., 2005). In this investigation the upper and lower bound values of spring rate were taken as 30 and 50 N/mm respectively, which give rise to limits of deflection (Y) ranging from 10-16 mm for a maximum load of 500 N.

Design constraints are:

$$S_b = \frac{3PL}{2bt^2} \quad (6.3)$$

$$Y = \frac{PL^3}{4Ebt^3} \quad (6.4)$$

where E is modulus of elasticity. Considering fatigue and static characteristic of the reinforced plastics, a factor of safety 2.5 (Mascarenhas *et al*., 2004) was considered for deciding the value of S_{max} and S_{min}.

The upper and lower bound values of constraints are:

S_{max} = 55 MPa and S_{min} = 35 MPa,

Y_{max} =16 mm and Y_{min} = 10 mm

The bounds related to stress level were considered with reference to the material characteristics of long fiber reinforced polypropylene which is having maximum flexural strength value of 125 N/mm^2. Leaf spring length, design load, density, modulus of elasticity, lower and upper bounds of stress and deflection were given as input to the program, and the design parameters were evaluated. It is vivid from figures 6.2 (a-b) that the design variables and objective function varied initially, then the objective function and design variables converged after 30 iterations. The optimal design values obtained after the analysis is tabulated in table 6. 2

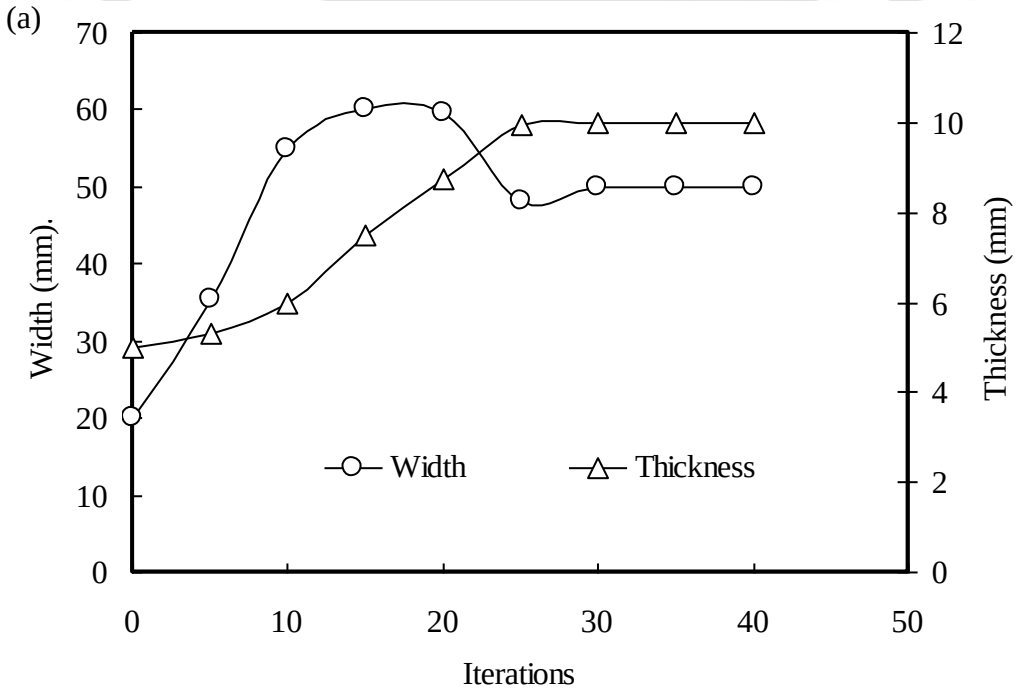

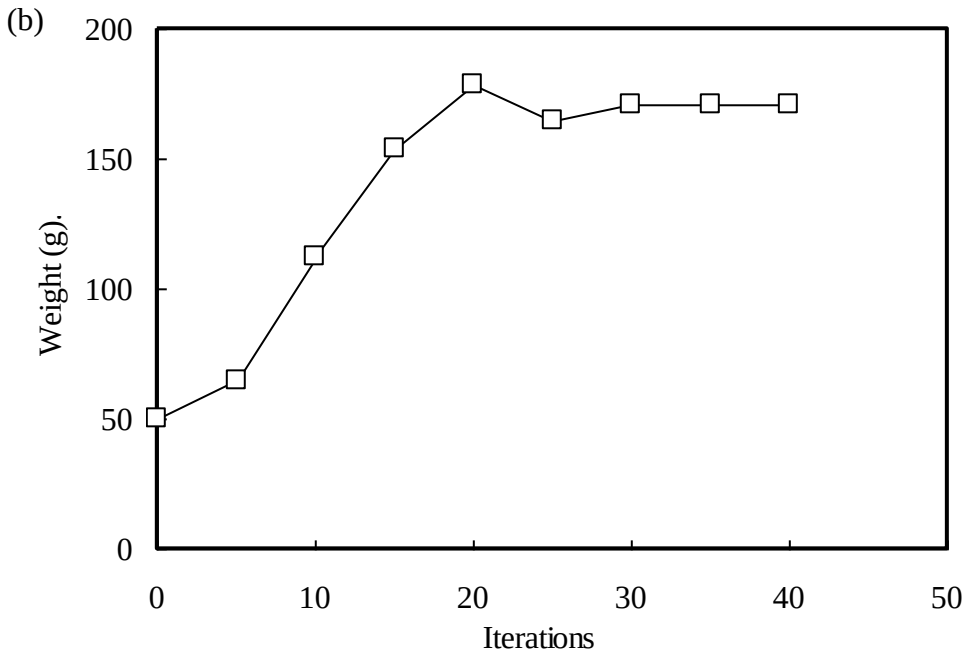

Fig.6.2 Optimization results for (a) leaf spring width and thickness at the center (b) leaf spring weight

Table 6.2 Optimal values of composite leaf spring at the axle seat

Parameters	Composite leaf spring
Width (mm)	50.00
Thickness (mm)	10.00
Maximum stress (MPa)	45.00
Maximum deflection (mm)	11.94

6.2.2.1 Mono Leaf Spring Geometry

After estimating width and thickness of the proposed leaf spring at center, various shapes pertaining to SAE standards (SAE HS-788, 1982) were considered and structural finite element analysis was carried out using commercial tool,

ANSYS® R10. Semi elliptic leaf springs can be considered as the combination of two cantilever springs and half of the leaf spring was considered due to its symmetry. Mono leaf spring shapes were grouped into two types of cantilever beams; Type F (uniform thickness and variable width) and Type T (variable thickness with constant or varying width). Type F was chosen in the present work due to the limited manufacturing facility.

Common configurations such as F-1 (rectangular cantilever), F-2 (trapezoidal cantilever), F-3 (triangular cantilever) and F-4 (modified triangular cantilever) were considered for investigation. For all the chosen configurations, taper ratio of 0.5 was applied from axle seat to end of the spring to minimize the level of bending stress (SAE HS-788, 1996; Yu and Kim, 1988). Loading conditions for all the configurations were provided at the eye end (AB) and displacement is fixed at the axle seat (EFGH) as shown in figure 6.3. Leaf spring was modeled with 3-D, 10 node tetrahedral solid elements; the element is defined by 10 nodes having three degree of freedom at each node. The element has plasticity, hyper elasticity, creep, stress stiffening, large deflection and large strain capabilities (ANSYS® R10, 2006). Arriaga *et al.* (2006) used the same element for polypropylene based composites for simulating the tensile and three point flexural testing and obtained good agreement between predicted and experimental values. The meshed model is shown in figure 6.4. Material properties corresponding to long glass reinforced polypropylene were provided as the input.

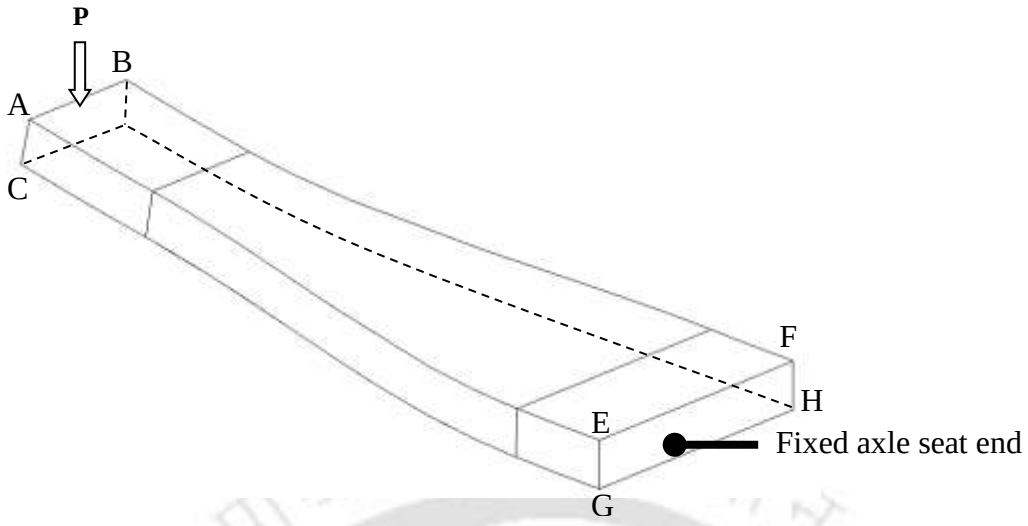

Fig.6.3 Schematic loading condition of a typical symmetric leaf spring

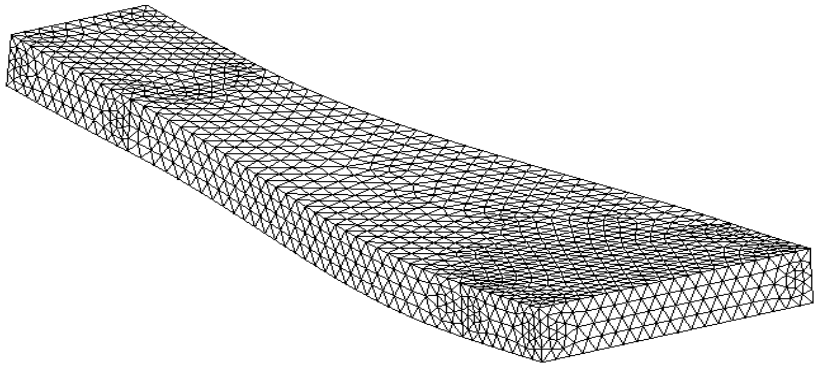

Fig.6.4 Meshed model of typical symmetric leaf spring

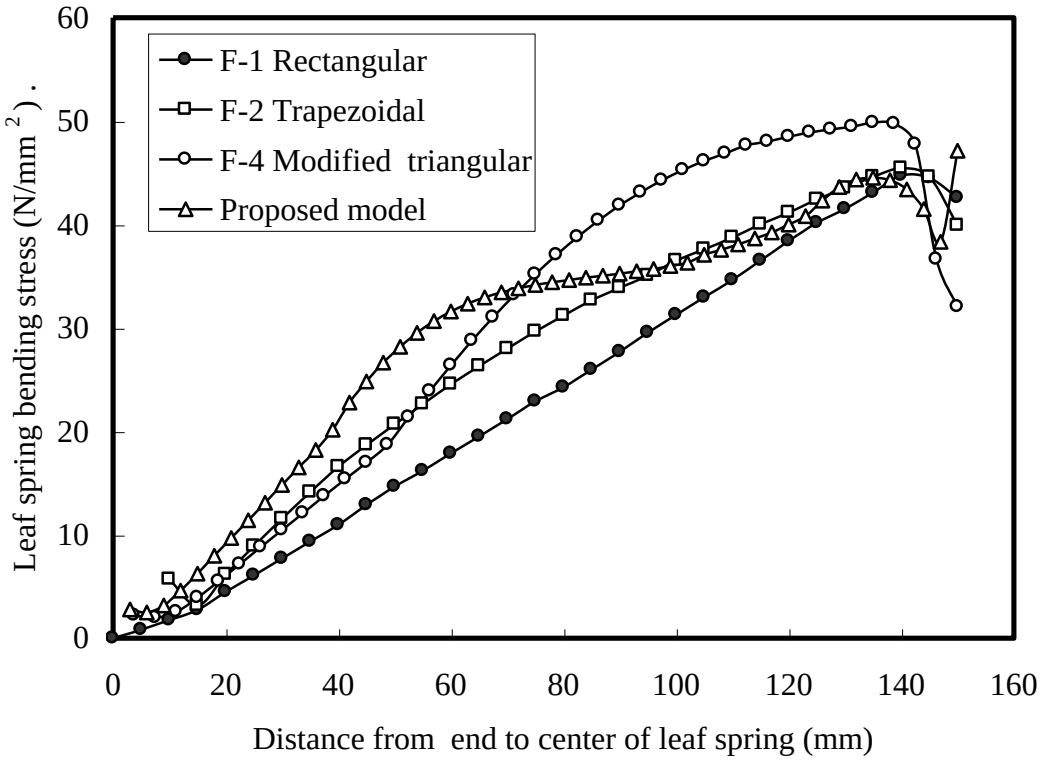

Fig 6.5 Bending stress plot of various leaf spring configurations

Figure 6.5 shows the bending stress plot of considered configurations. Table 6.3 shows few crucial parameters of F-type mono leaf spring configuration. F-1 rectangular cantilever have constant width and thickness, under the application of load maximum stress exist at the axle seat and decrease at a constant rate to zero (figure 6.5). F-2 trapezoidal cantilever have constant thickness, width decreases at a constant rate from the axle seat to a specified dimension at line of load application. F-3 triangular cantilever has constant thickness, width decreases at a constant rate from the axle seat to zero at the point of load application. Stress is constant throughout the length in this configuration; however, this design is not practical as no material is available for load application, and not considered further. The F-4 modified triangular cantilever was found to be slightly less efficient than F-3 model, but facilitates load application.

Table 6.3 Parameters of various F type profile mono leaf springs

No.	*Configuration*	*Max. stress (MPa)*	*Max. deflection (mm)*	*Volume (mm^3)*	*Shape*
1	F-1 Rectangular Cantilever	44.56	11.58	75000	
2	F2 Trapezoidal Cantilever	46.85	12.38	56625	
3	F4 Modified triangular cantilever	49.80	12.97	47778	
4	Proposed model	45.27	12.962	55300	

The proposed model for the current investigation was slightly modified from the F-4 modified triangular cantilever model. In this proposed model, a constant width from a length of 0.85 L from the spring eye towards the axle seat was maintained. This constant width provision was made for a uniform molten flow during injection molding thereby, avoiding incomplete mold filling (Eberle, 2006). Thus, the proposed leaf spring has constant thickness of 10 mm and width at the center and end of the mono leaf spring are 50 and 25 mm respectively.

Convergence study was performed for all the configurations by increasing the number of elements. Smart sizing options were used to increase the number of elements. The number of elements during the convergence study varied from 1429 elements to 77000 elements and the converged values of bending stress and deflection for the proposed model is reported in figure 6.6. Convergence was obtained when the number of elements was 75025. Stress and displacement contour of the proposed model are shown in figures 6.7 (a-b). It is inferred that stress is maximum, at the axle seat and gradually decreases towards the end. It is also noted that the stress distribution is uniform along the taper region unlike the leaf springs with constant width and thickness, where the springs are stressed heavily at one specific location and other parts are stressed lightly. Since this configuration provided constant bending stress along the taper region, the absorbed or stored energy is uniformly distributed along the leaf spring. Detailed leaf spring geometry with dimensions is shown in figure 6.8.

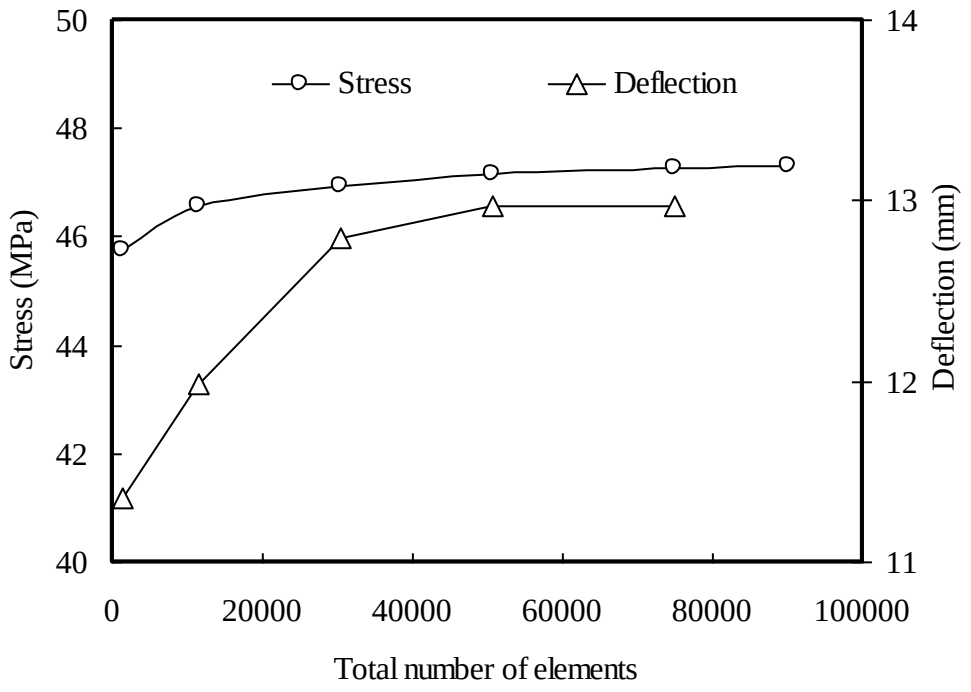

Fig. 6.6 Convergence test results for stress and deflection for the proposed model

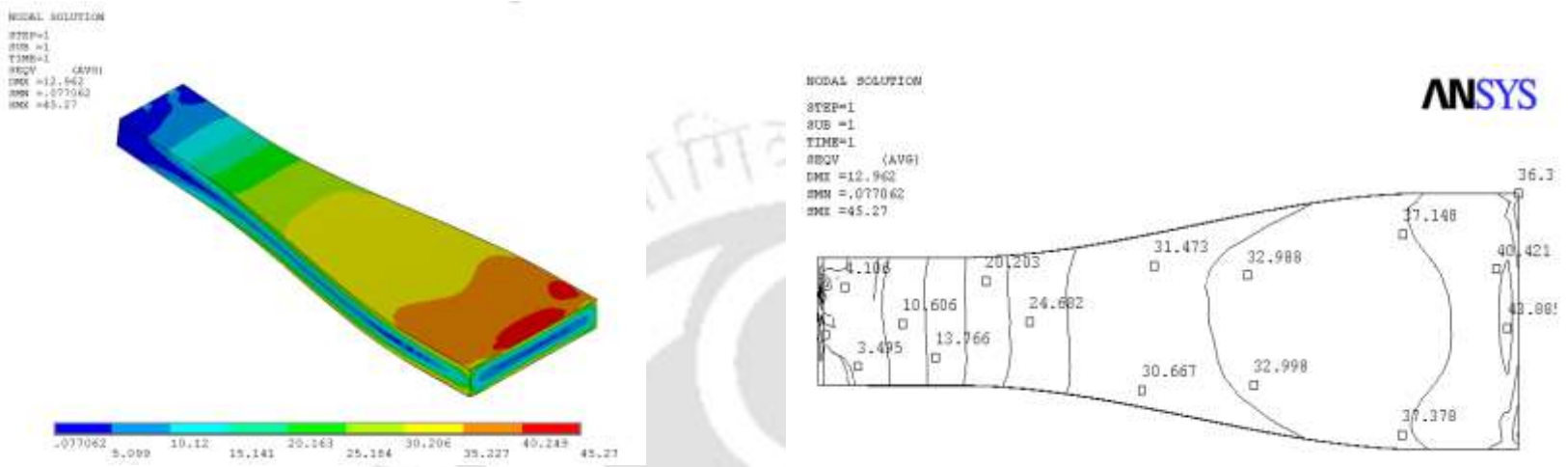

Fig.6.7a Bending stress contour of the proposed model

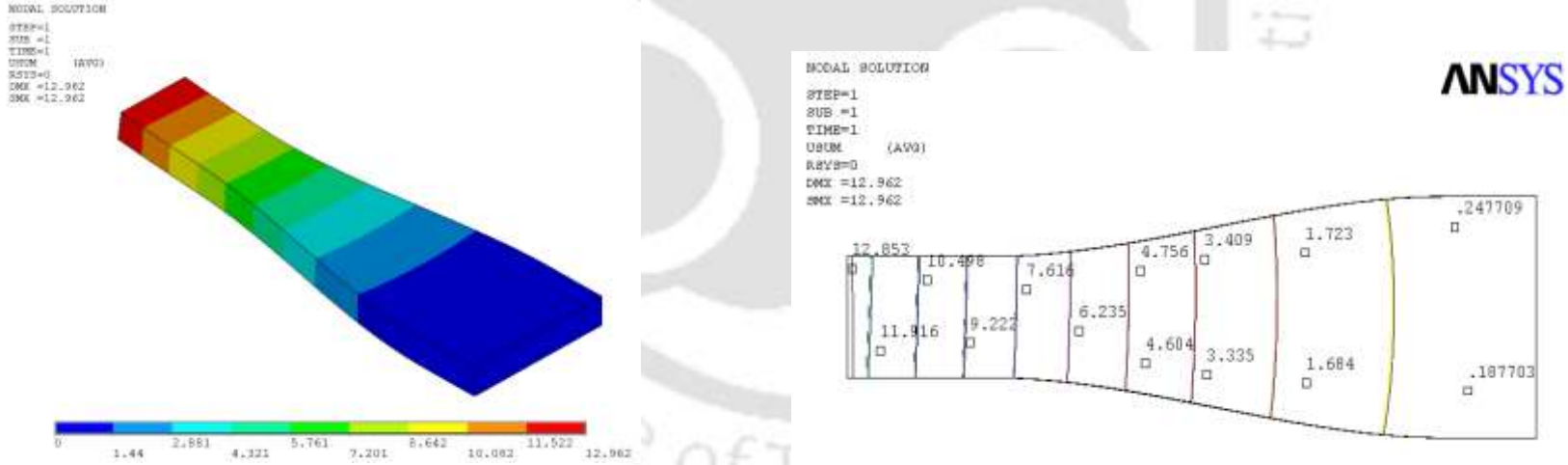

Fig.6.7b Deflection contour of the proposed model

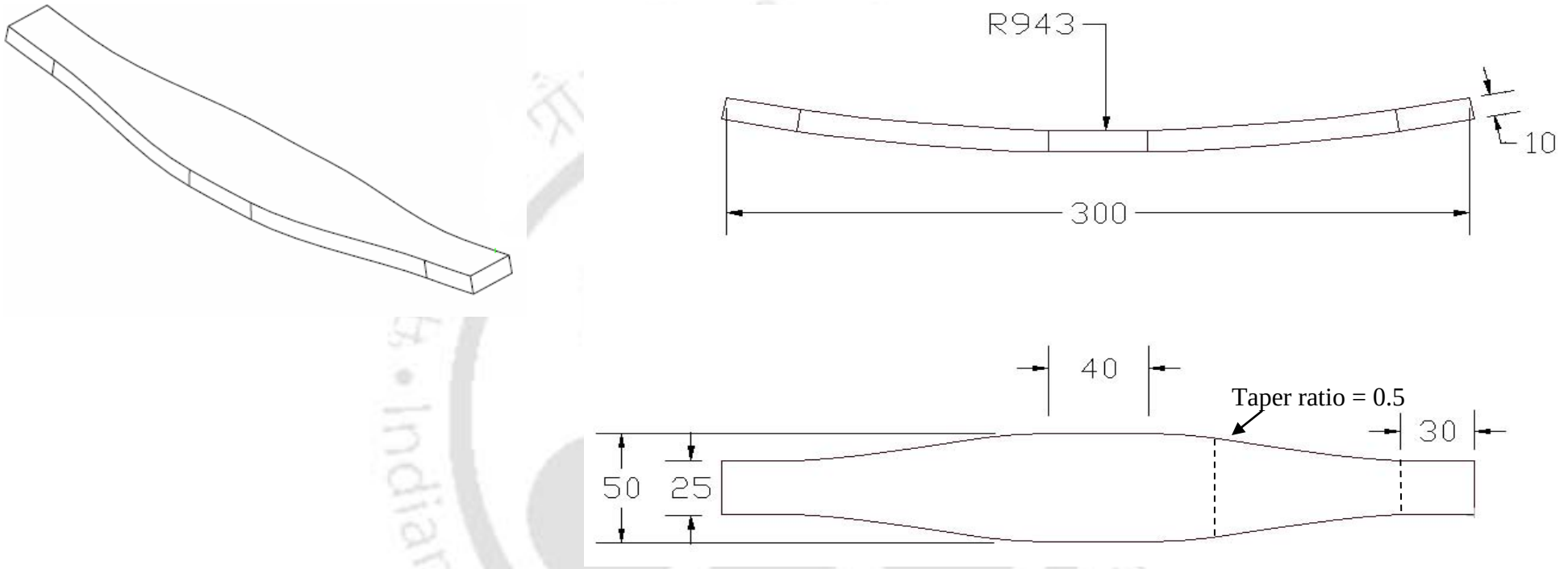

Fig.6.8 Geometry of injection molded leaf spring

6.3 COMPUTER AIDED SIMULATION OF LEAF SPRING MOLDING

Computer aided simulation of injection molding process helps to determine the ideal combination of part geometry, material, mold design and processing conditions that produces quality finished parts. In the present investigation, injection molding simulation of leaf spring was carried out using commercial mold flow software, Mold Flow Plastics Insight®, which helps to confirm the suitability of chosen part geometry, processing conditions and gate design.

6.3.1 Details of Leaf spring Model and Molding Conditions

A three-dimensional model of variable width mono leaf spring was developed using the commercial modeling software, PRO-E 2001® and imported into the mold flow software. The model was meshed with fusion option using triangular elements and the total number of elements was 2290 (figure 6.9). The meshed leaf spring part statistics indicates the match ratio of 93 % and average aspect ratio of 2.4, which were well within the tolerance limit to carry out the filling and shrinkage analysis (Mold Flow, 2000). Since provision for long glass fiber modeling was not present in the used version of mold flow, unreinforced polypropylene, 20% short glass fiber reinforced polypropylene were considered for simulating the leaf spring mold. Molding parameters were initially decided as per data sheet of the raw material supplier (Saint Gobain, 2005). Injection molding machine capacity (Goyani, GM-120), clamping force of 120 ton, injection pressure of 140 MPa and shot capacity of 160 g of polystyrene were specified for simulation. After checking for manufacturability, the molding pressure was fixed as 112 MPa and injection cylinder temperature as 240°C.

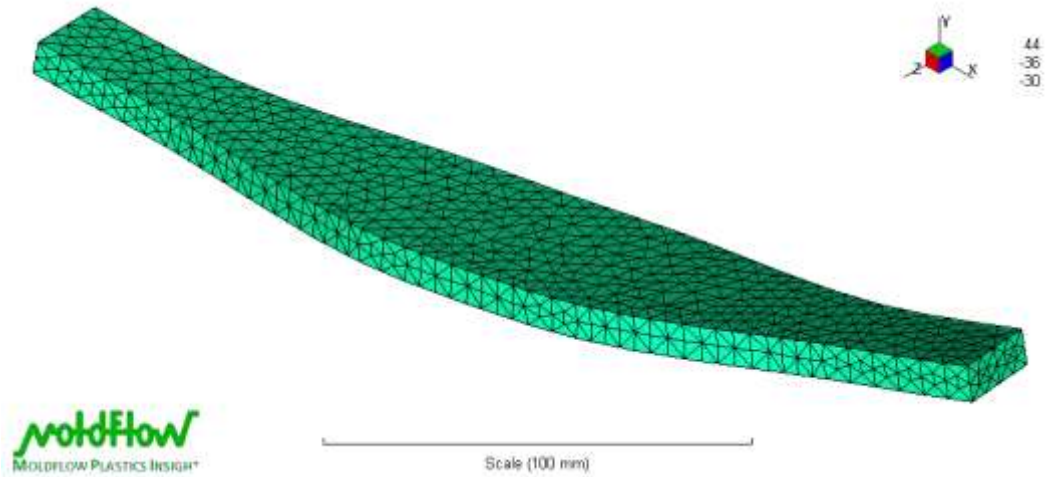

Fig.6.9 Fusion meshed model of leaf spring with triangular elements

6.3.2 Gate Design

Mold part quality is significantly influenced by the gate location as it influences the plastic flow into the mold cavity. Shrinkage and warpage defects can be minimized by choosing appropriate gate location. Meshed leaf spring model and processing conditions were given as input for the gate location analysis. The best gate location was identified (figure 6.10) to eliminate/minimize weld lines, even distribution of pressure in the cavity and maintaining similar melt front temperature. If the gate location is fixed at the center, then two moving melt fronts would form weld lines (Rosato *et al*., 2000). In addition to the leaf spring application, maximum stress is expected at the center and hence it should be free from weld lines. Since the best gate location was identified at the end of the part, standard two-plate mold design was sufficient with pin gates at the end for molding the leaf springs. The fill time result showed the position of the flow front at regular intervals as the cavity fills. Figure 6.11 shows the fill time of unreinforced leaf spring with chosen pin pointed injection gate. The contours were evenly spaced and the contour spacing indicates the speed at

which the polymer was flowing. Widely-spaced contours indicated rapid flow while narrow contours indicated that the part is filling slowly (Mold Flow, 2000). If the part is a short shot (material not filled), the section would show no color.

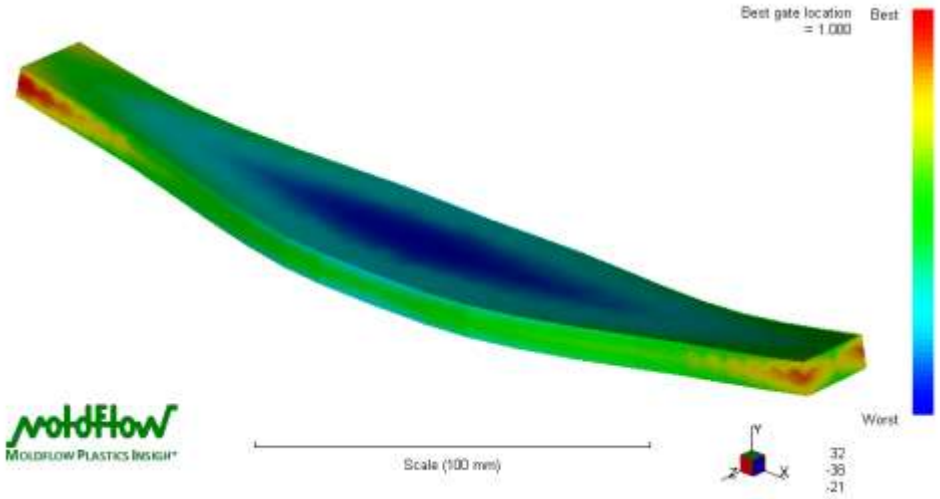

Fig.6.10 Best gate location analysis

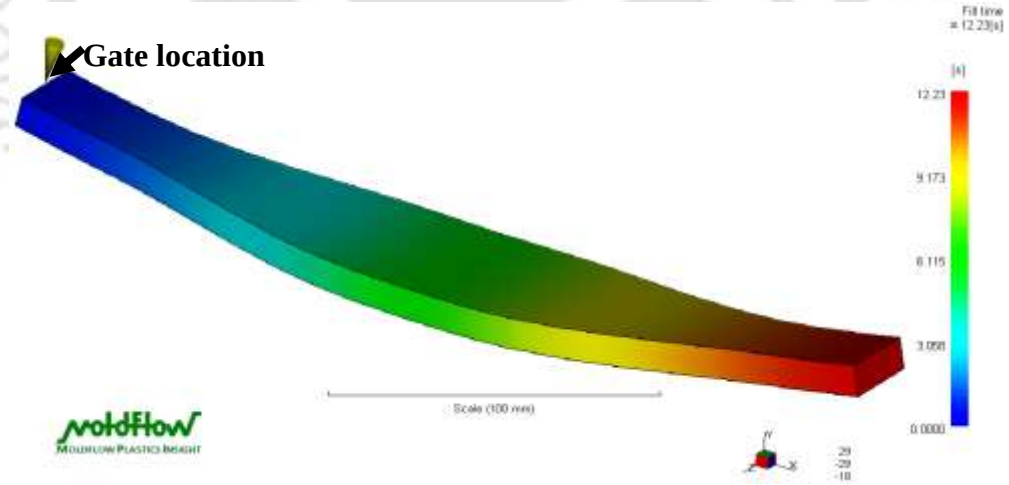

Fig.6.11 Melt flow in unreinforced leaf spring with pointed gate

6.3.3 Mold Shrinkage of Test Leaf Springs

During the filling process, polymer melt was injected into the cavity through sprue, runner and gate. Residual stress was induced due to high pressure, temperature change and relaxation of polymer chains during the process of filling resulted in shrinkage and warpage of the part. Shrinkage values are corresponding to the dimensions parallel and perpendicular to the direction of melt flow in a part. During injection molding of fiber-reinforced polymers, the presence of fibers reduced volumetric shrinkage. Figures 6.12 (a-b) show the volumetric shrinkage of unreinforced and glass-fiber reinforced polypropylene leaf springs respectively. The maximum percentage of volumetric shrinkage for unreinforced and glass fiber reinforced polypropylene leaf springs were 15.97 and 12.47 % respectively.

(a)

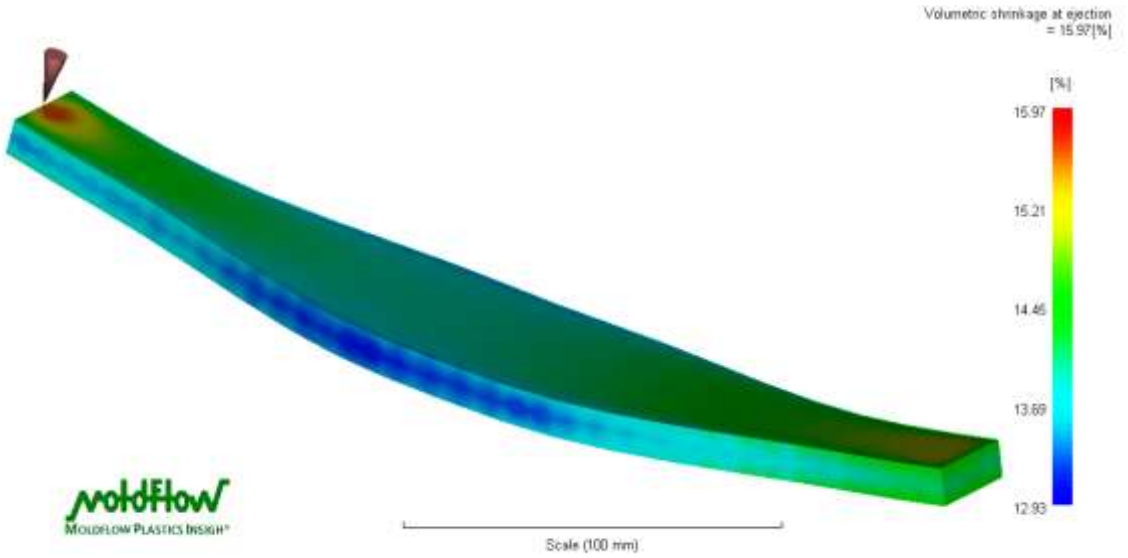

(b)

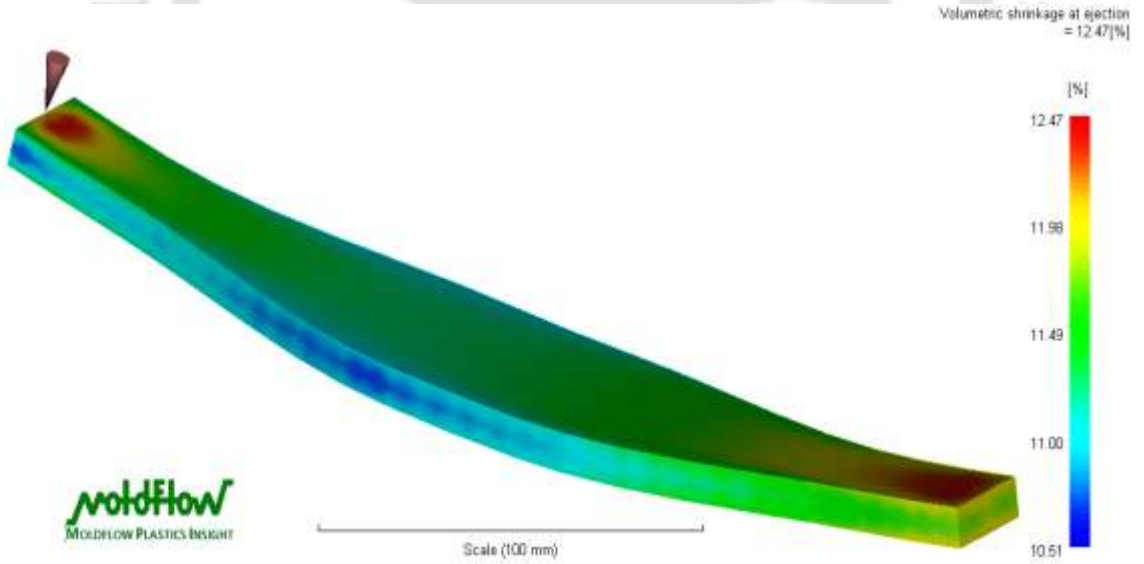

Fig. 6.12 Influence of reinforcement on volumetric shrinkage (a) unreinforced polypropylene leaf spring and (b) 20 % glass fiber reinforced polypropylene leaf spring

6.3.4 Warpage Analysis of Test Leaf Springs

Variation in shrinkage contributes to internal stress which results in part warpage. The shrinkage imbalance in any section of the leaf spring produces a net force, which distorts the leaf spring geometry. Variations in packing pressure, cooling rate and viscous condition of the melt contribute to the deflection of unreinforced leaf springs due to the warpage (figure 6.13a). The amount of maximum warpage deflection in glass reinforced leaf springs is smaller than that of unreinforced leaf springs due to the orientation of glass fibers which causes anisotropic shrinkage (figure 6.13b).

The maximum warpage deflection exhibited in the unreinforced and glass fiber reinforced leaf springs are 3.421 and 0.539 mm respectively. Though reinforced leaf springs exhibited less warpage than unreinforced leaf springs, uniform deflection is not observed along the length as in the unreinforced leaf springs due to the anisotropic shrinkage effects as indicted in figures 6.13a and 6.13b. Hence from the computer aided simulation of leaf spring molding, best gate location was identified and the test results revealed that addition of glass fiber in the matrix reduces the volumetric shrinkage and warpage during injection molding. However, uniform deflection is not observed in glass fiber leaf springs owing to anisotropic shrinkage due to the presence of glass fibers in the matrix.

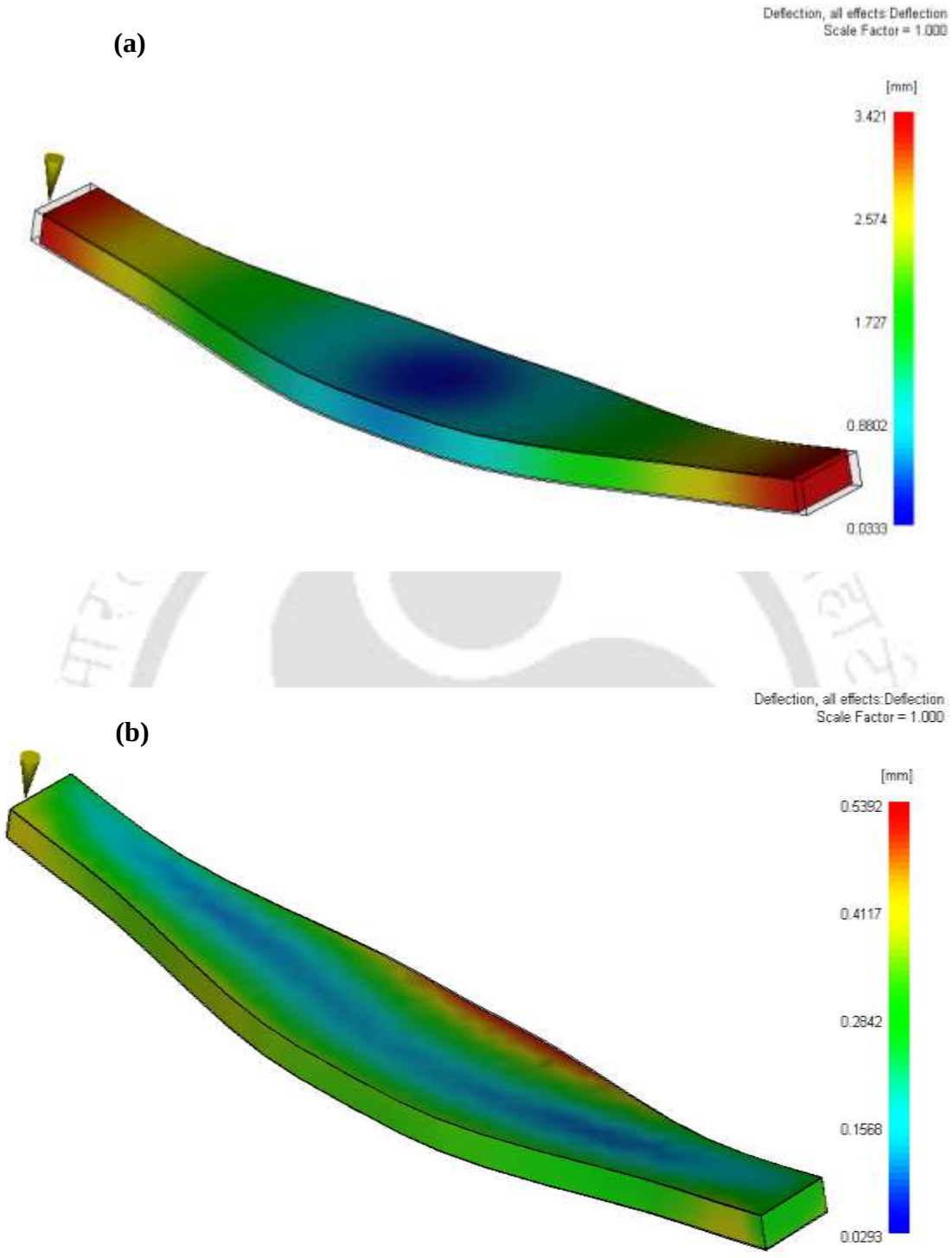

Fig. 6.13 Influence of fiber reinforcement on warpage deflection (a) unreinforced polypropylene leaf spring and (b) 20 % glass fiber reinforced polypropylene leaf spring

6.4 PROCESSING OF THERMOPLASTIC LEAF SPRINGS

Chosen leaf spring materials; unreinforced polypropylene, 20% short glass fiber reinforced polypropylene and 20% long glass fiber reinforced polypropylene were used for injection molding of the leaf spring. Two-plate mold was developed in-house with pin gate at the end of the leaf spring as shown in figure 6.14. Injection molding dies (figure 6.15a) for leaf spring part were machined with a computer numerically controlled machine and the wire cut electric discharge machine, Hitachi (ONA /AX4). Raw materials were initially preheated for two hours at 80°C and during molding, screw speed of 50 rpm and a low back pressure of 0.25 MPa were kept to minimize the damage of residual fiber length. Sufficient cooling time was provided in order to avoid shrinkage. Developed leaf springs are shown in figure 6.15b. Process parameters used for injection molding are listed in table 6.4.

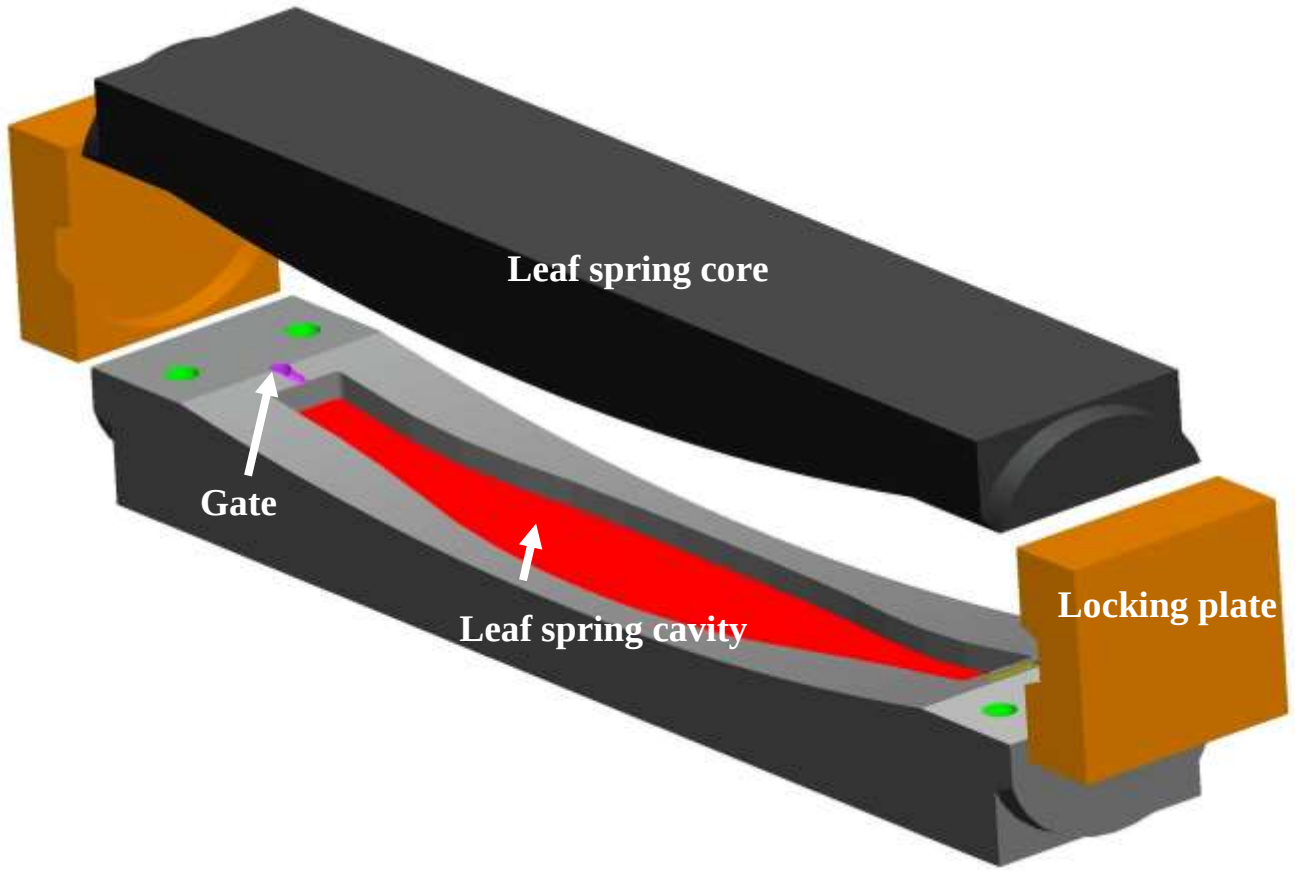

Fig. 6.14 Model showing the details of the die developed

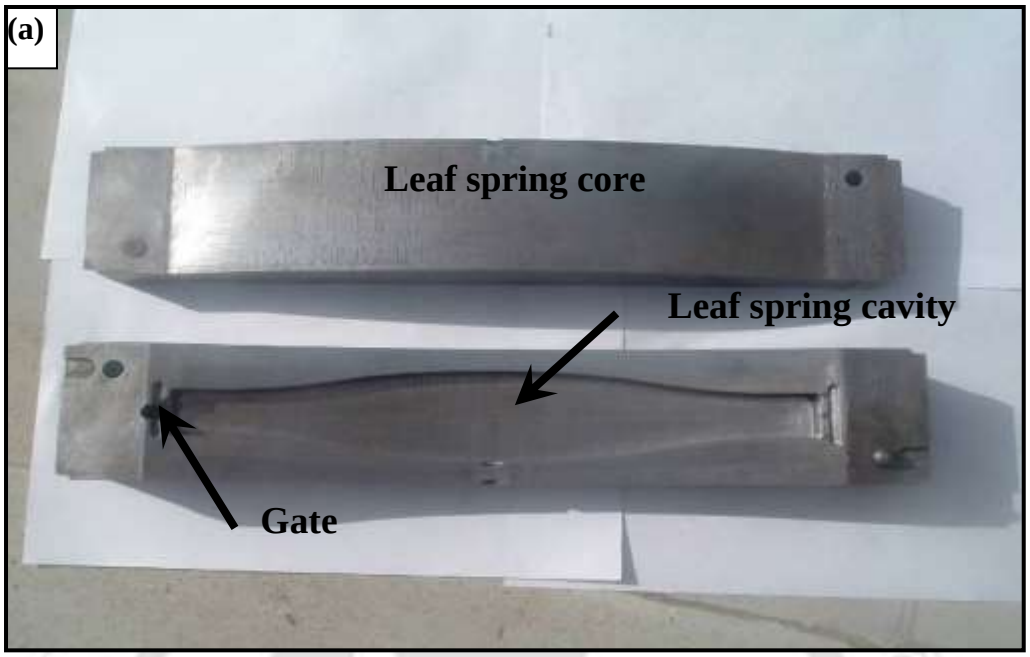

Fig.6.15a Photograph of the developed die

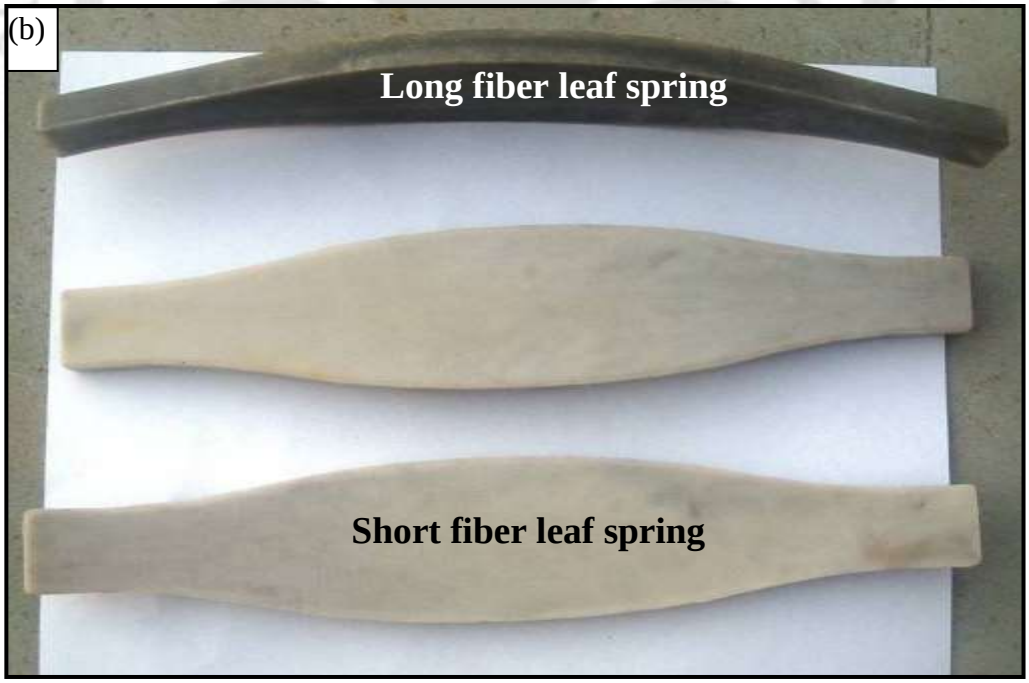

Fig.6.15b Photograph of the developed leaf springs

Table 6.4 Injection molding parameters for the leaf springs

Material	Zone 1 (°C)	Zone 2 (°C)	Zone 3 (°C)	Screw diameter (mm)	Injection speed (mm/s)	Injection pressure (MPa)	Mold Temp. (°C)
Unreinforced polypropylene	190	180	175	35	50	100	40
20 % glass fiber reinforced polypropylene	255	250	240	35	50	100	40

6.5 THERMOPLASTIC LEAF SPRING INSPECTION

Injection molded unreinforced and glass fiber reinforced polypropylene leaf springs were inspected using the 3-D scanner machine (Roland Picza, LPX-250) to estimate the volumetric shrinkage. This machine scans objects using laser light and its wavelength ranged from 600 to 700 nm with a pulse frequency of 2857 Hz. It emits a spot beam onto the scan object and detects reflected light from the object. It performs scanning as it rotates the scan object (0.2- 60°) and moves the laser beam from bottom to top (0.2 to 406.4 mm) (figure 6.16a) and the table was rotated at 15 RPM. The height direction pitch and width direction pitch were kept at 0.2 mm during scanning in order to capture the minute features of the injection molded leaf spring geometry. By this operation, the 3-D scanner machine evaluated the coordinates of molded leaf spring.

Photographic view of the 3-D scanner is shown in figure 6.16b. The file was saved in stereolithographic format (.stl format) using a software Dr.Picza. The solid model captured from the 3-D scanner machine is shown in figure 6.17.

The saved file was imported into the commercial modeling software, PRO-E 2001® and the volume for UFLS, SFLS and LFLS were obtained as 104517, 107503, and 108775 mm^3 respectively. The total volume of the designed spring which was provided in the mold cavity was 110,600 mm^3 (Original volume). Volumetric shrinkage was calculated using the relation 6.5 and reported in table 6.6.

$$\text{Volumetric shrinkage } (\%) = \frac{\text{Change in volume}}{\text{Original volume}} \times 100 \qquad (6.5)$$

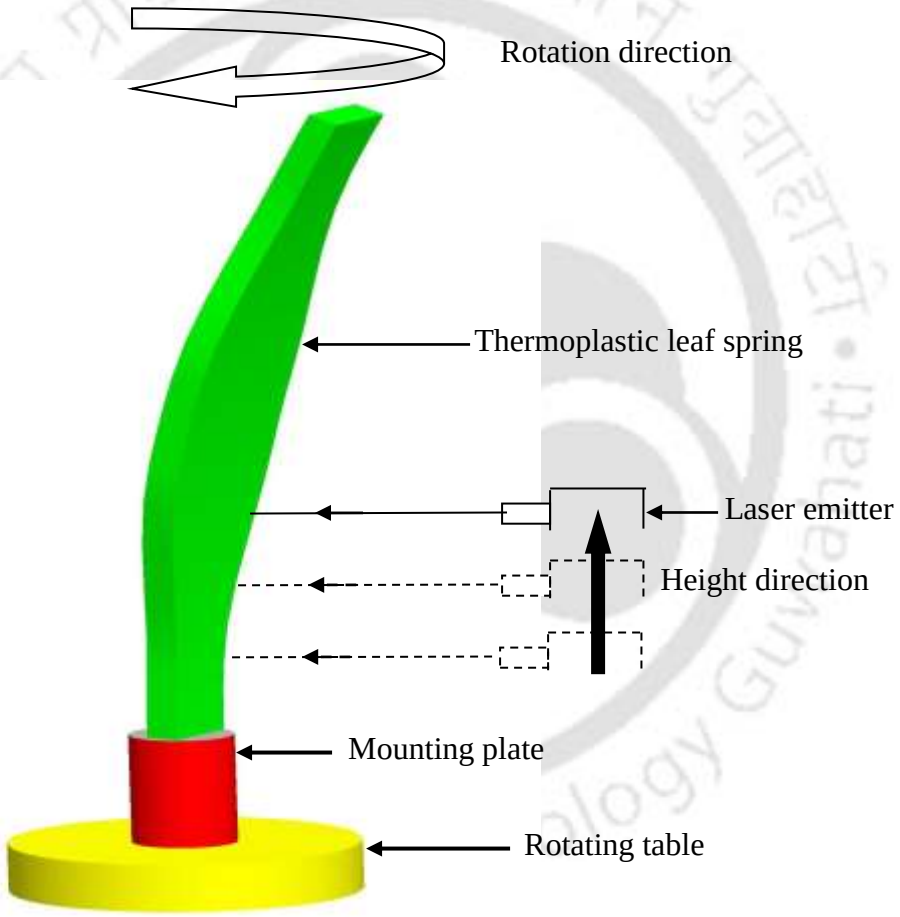

Fig. 6.16a Schematic of the scanning process

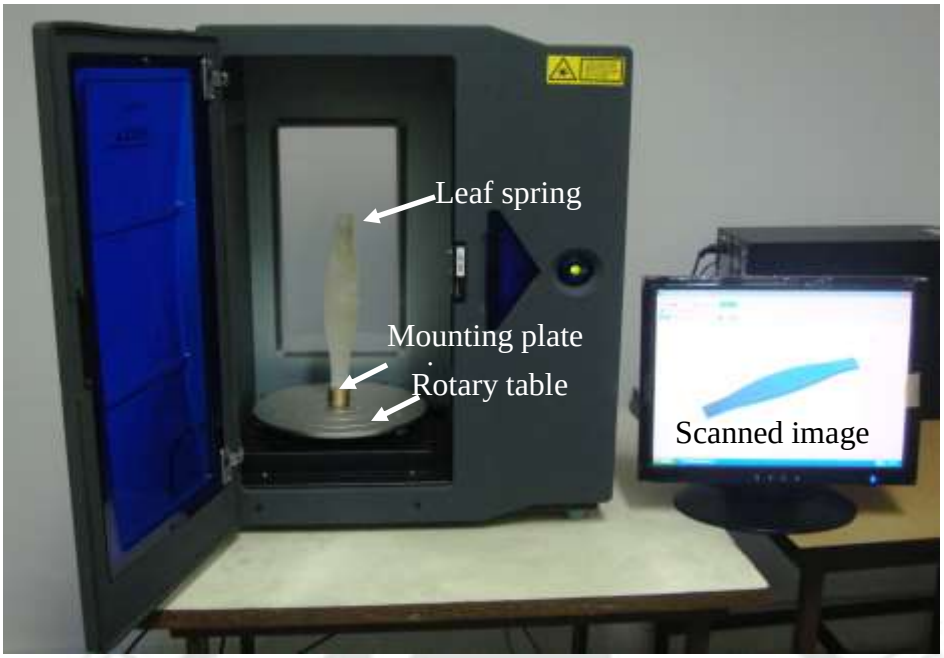

Fig. 6.16b Close-up view of the 3-D scanner with leaf spring

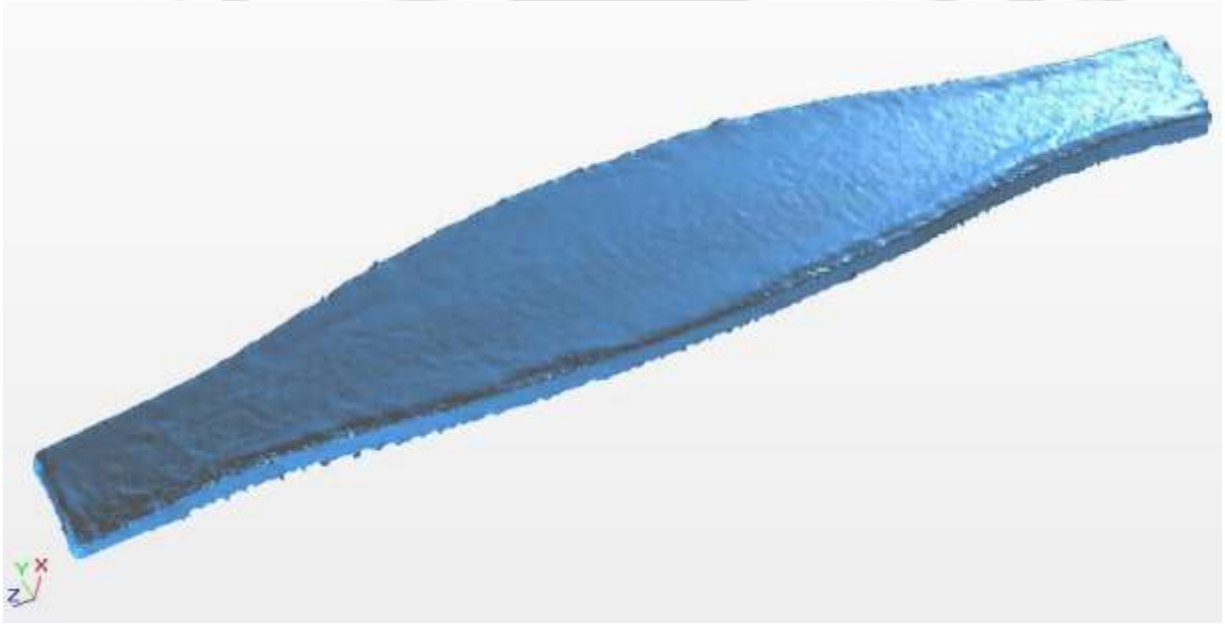

Fig.6.17 Scanned model of leaf spring

Mass of atleast three leaf springs of each material was measured using an electronic balance of 0.1 mg accuracy (Sartorius, Make; BT224S). The mass of UFLS, SFLS and LFLS leaf springs were found to be 93.650 ± 3.5, 109.502 ± 4.2, 112.793 ± 3.9 g respectively. The density of UFPP, SFPP and LFPP were 0.90, 1.03, 1.04 g/cm^3 (Saint Gobain/ Twintex, 2005). The leaf spring volume was calculated by assuming the component is free from voids. The volume of UFLS, SFLS and LFLS were found to be 104055, 106312 and 108454 mm^3 respectively. With the calculated volume, volumetric shrinkage is calculated and reported in table 6.6.

Table 6.5 Volumetric shrinkage by 3-D Scanner and weight measurement

Material	Volumetric shrinkage by inspection in %	Volumetric shrinkage by weight measurement in %
Unreinforced polypropylene	5.50	5.9
20 % short glass fiber reinforced polypropylene	2.80	3.8
20 % long glass fiber reinforced polypropylene	1.65	1.9

6.6 FIXTURE FOR LEAF SPRING PERFORMANCE EVALUATION

In a suspension system, leaf spring ends are attached to the automobile body and center of the leaf spring is supported on the axle through which vertical forces are transmitted. A fixture was designed with a linear guide way (THK E8-0620) and integrated with the existing servo hydraulic fatigue testing machine as shown in figure 6.18a (Instron 8801) to evaluate the performance of molded leaf spring.

With this configuration, cyclic load of sinusoidal, triangular and square wave forms can be applied at the frequency range 0.1 - 10 Hz upto maximum load of 100 kN (load cell capacity) with the maximum stroke length of ± 75 mm. Railway of linear guide was fixed to the lower platen of the fatigue testing machine. Two retaining blocks were fastened over the sliding blocks of guide ways, leaf spring ends were positioned within the retaining blocks. When the load is applied at the centre of the leaf spring through lower platen of the testing machine, leaf spring flattens. To accommodate the increase in length during deflection, leaf spring ends slide over the linear guide way rail.

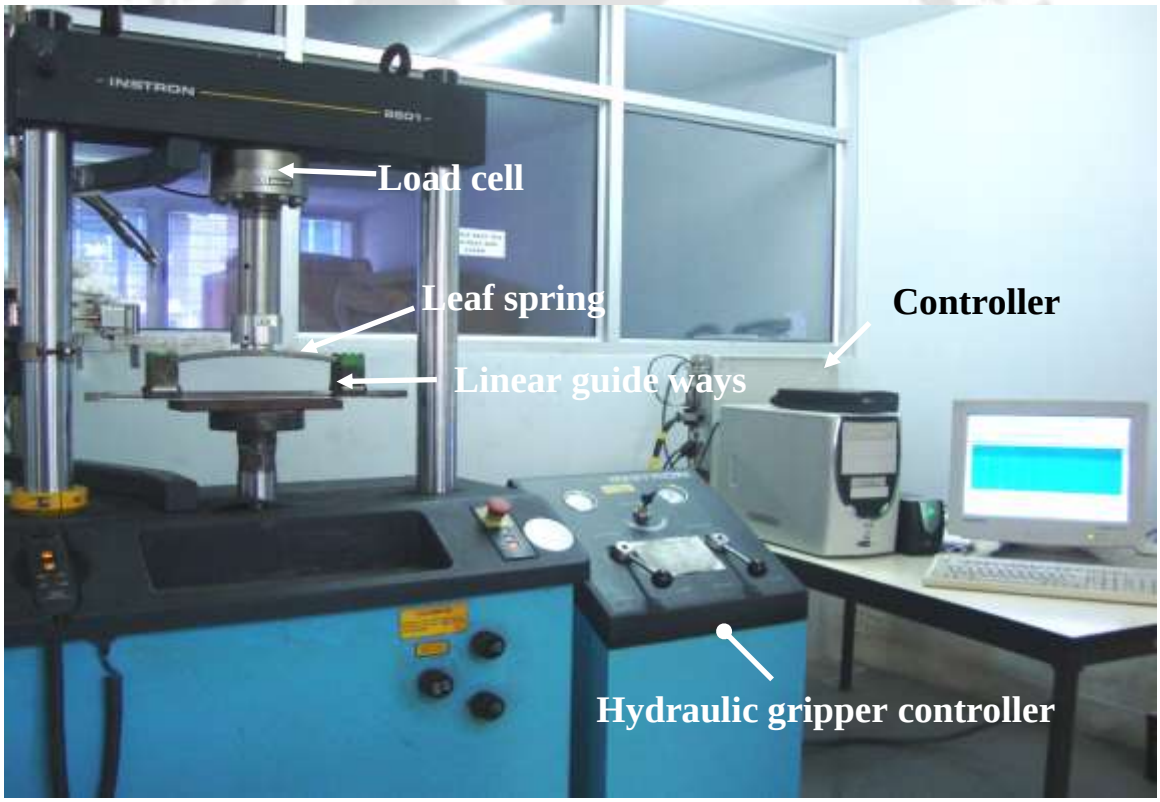

Fig. 6.18a View of servo hydraulic fatigue testing machine

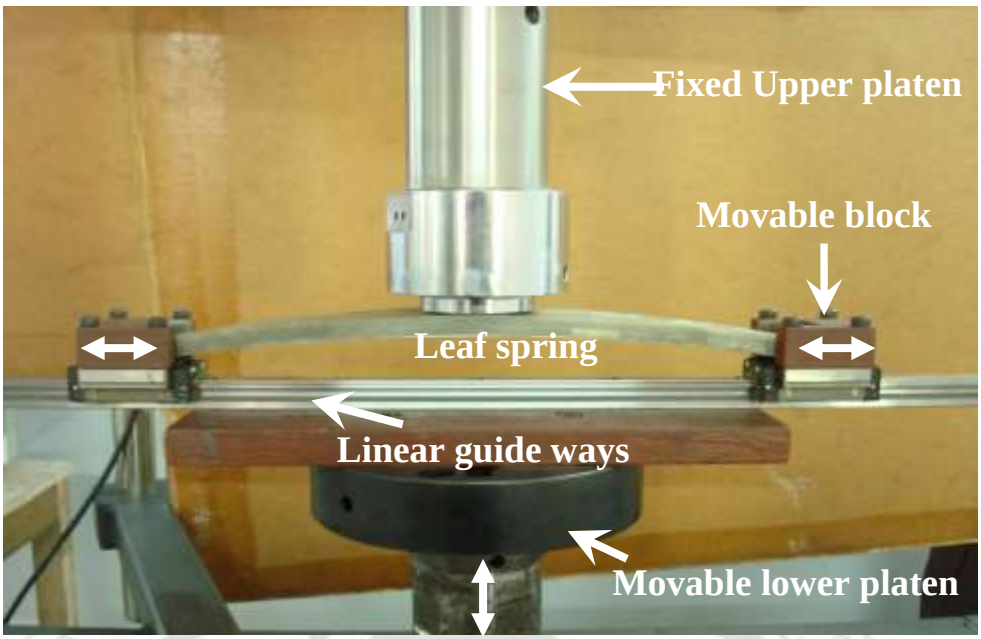

Fig. 6.18b Close up view of fixture with leaf spring

Developed fixture for the performance evaluation of molded leaf spring under loading condition is illustrated in figure 6.18b. The upper platen is fixed and connected to the load cell whereas the lower platen can be moved up and down either through load or displacement controlled servo hydraulic system. During testing, applied load and achieved displacement were measured and recorded using an in-built measurement and data acquisition system.

6.7 STATIC PERFORMANCE EVALUATION OF LEAF SPRINGS

Molded test leaf springs were loaded upto the design deflection of 12 mm and released back as per SAE standard, J1528 (SAE,1996). When a polymeric component is subjected to an external force, part of the work is elastically stored and rest is irreversibly dissipated. Relative magnitude of elastic and viscous components depends on how fast the component is deformed. Composite leaf springs were subjected to strain rates of 1, 5, 10 and 50 mm min^{-1} to characterize the time-dependent

load -deflection behavior. Molded leaf springs were subjected to loading rate of 5, 10 and 20 N/s and the corresponding load deflection curve for loading and unloading were plotted to quantify hysteretic behavior of molded leaf spring. Area enclosed by the loading and unloading curve exhibited the damping behavior of molded composite leaf spring under service condition. Molded leaf springs were also subjected to a maximum deflection of 12 mm and the deflection was maintained constantly for a time period of 15,000 s to investigate the load relaxation characteristics on the molded leaf spring.

6.7.1 Load Deflection Behavior of Leaf Springs

Design of suspension leaf spring is based on strength as well as deflection. Figure 6.19 shows the load-deflection curve of the molded long fiber reinforced leaf spring (LFLS), short fiber reinforced leaf spring (SFLS) and unreinforced leaf spring (UFLS). It is observed from the figure 6.19 that the load required for a deflection of 12 mm for LFLS, SFLS and UFLS are 490, 190 and 110 N respectively. The spring rate of long, short glass fiber reinforced leaf spring and unreinforced leaf spring were computed from the initial portion of the load-deflection curve and found to be 40.1, 15.45 and 9.17 N/mm respectively. Spring rate of LFLS was found to be about three times greater than that of SFLS and five times greater than UFLS. It is to be noted that the above behavior was observed when the tests were carried under constant displacement rate of 5mm/min. Due to the vehicle service condition, suspension leaf springs were subjected to the time varying load, and hence there is a need to understand the load -deflection behavior of molded leaf springs at various strain rates.

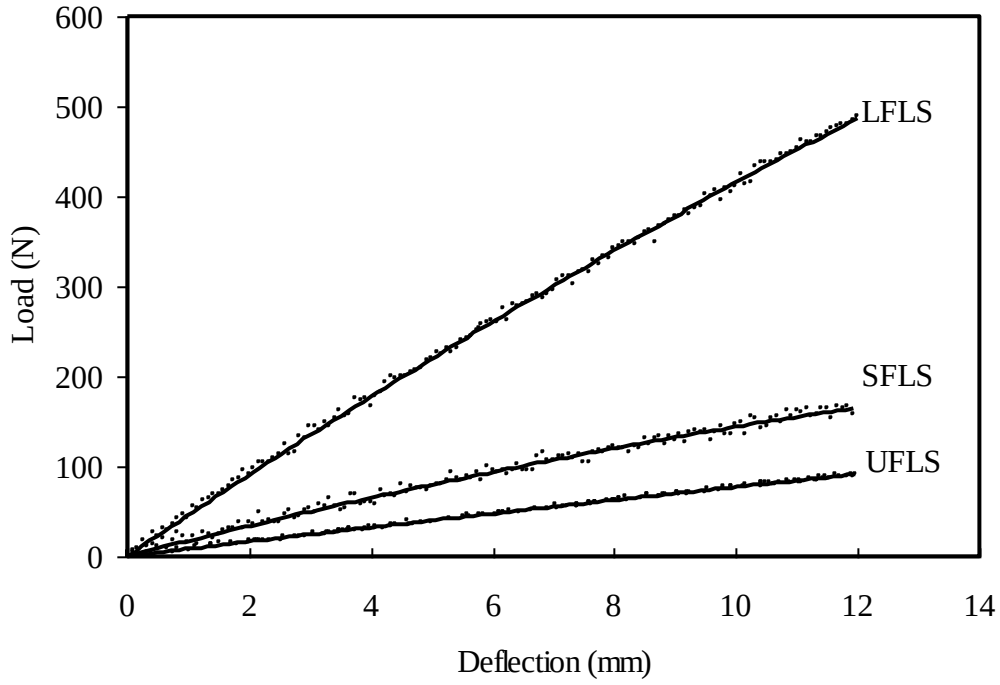

Fig. 6.19 Load - deflection curve for glass fiber reinforced and unreinforced leaf springs

6.7.2 Influence of Strain Rate on Load Deflection Behavior of Leaf Springs

Thermoplastic composite material properties are time dependent due to visco-elastic characteristics of the base polymeric material. Figure 6.20 delineates the strain rate sensitive nature of LFLS, SFLS and UFLS. In the present investigation, displacement rates; 1, 5, 10 and 50 mm/min were considered. For the considered leaf springs, load required for the design deflection of 12 mm increases with the increase in displacement rate. However, strain rate sensitivity of reinforced leaf springs was found to be less than unreinforced leaf springs due to the reduction in matrix ductility because of fiber reinforcement, which is confirmed from the reduction in strain as reported in tensile test (Chapter 5, figure 5.3). Polymeric material's ductility is the measure of viscous component and the strain rate sensitivity is proportional to the viscous component of the material. When the strain rate increases, the viscous component get reduced which accounts for more load carrying capacity.

Since energy is absorbed in the leaf springs, higher the energy absorbed, better is the isolation of a vehicle from vibration. Hence there is a need to understand the energy storage capacity of the molded leaf springs.

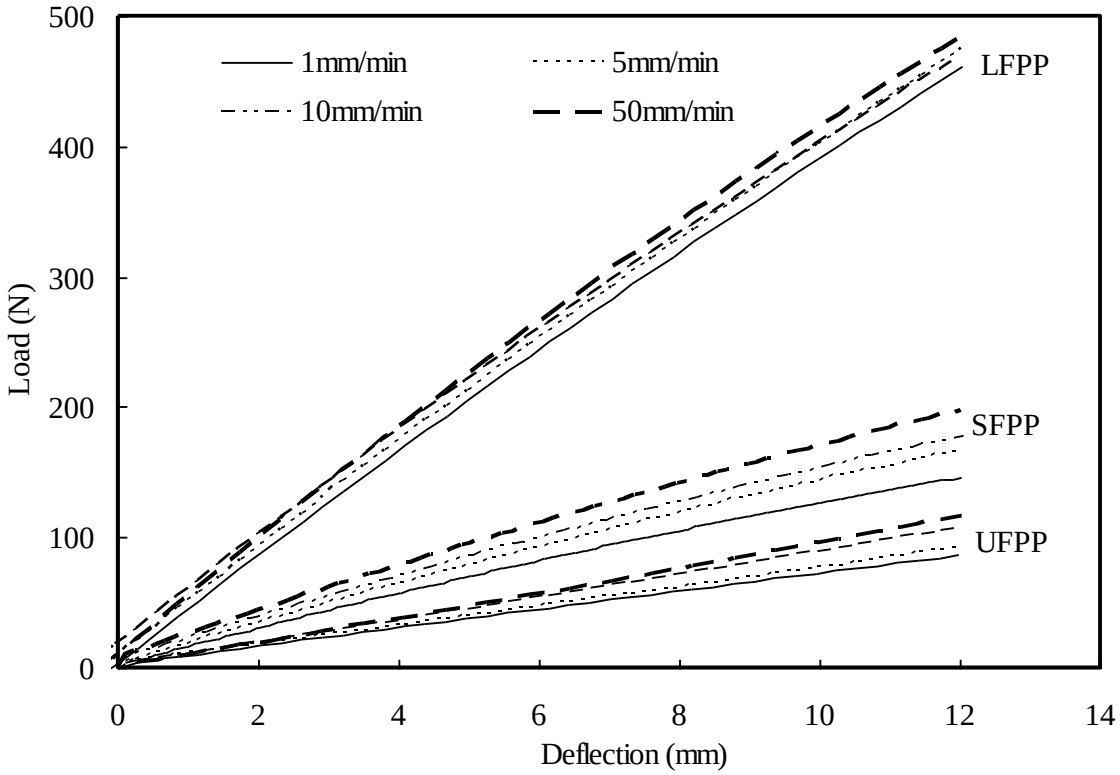

Fig. 6.20 Effect of strain rate on reinforced and unreinforced leaf spring

6.7.3 Energy Storage Capacity of Leaf Springs

In service, spring stress must not exceed allowable stress to avoid permanent set /premature failure. This consideration limits the amount of energy which can be stored in the spring. The absorbed energy for the effective work done was estimated by measuring the area under load-deflection curve for a maximum designed deflection of 12 mm. Energy stored by the chosen UFLS, SFLS and LFLS were 4.55, 9.37 and 24.11 J, LFLS can store more energy than other two chosen leaf springs and this feature enables to provide better vehicle riding comfort.

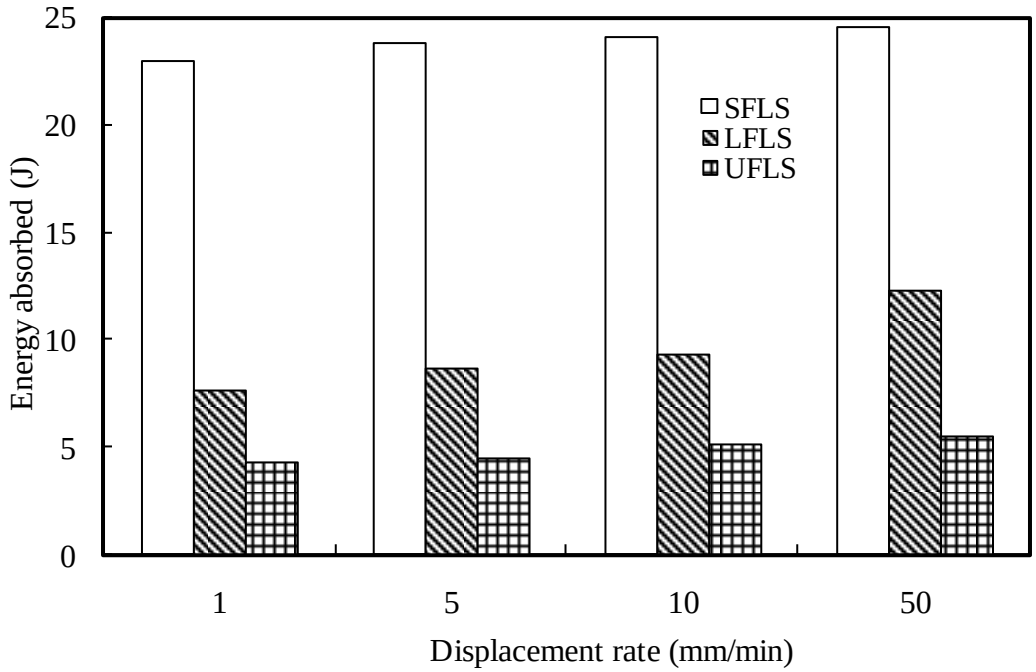

Fig.6.21 Effect of fiber reinforcement on energy absorbed by thermoplastic leaf springs

With the variation in strain rate, the energy storage capacity also varies and it increases with strain rate for the molded leaf spring material. It is also confirmed from figure 6.21 that the energy absorbing behavior of UFLS and SFLS are sensitive to the strain rate than that of LFLS. Damping behavior of leaf spring material significantly influences the performance of leaf spring; hence there is a need to understand the damping behavior of molded leaf springs.

6.7.4 Hysteretic Characteristics of Composite Leaf Springs

High material damping factor of a composite material provide excellent noise and vibration attenuation which is ideal for a good vehicle ride (Hou *et al*., 2005). Visco-elastic characteristics of polymer materials generate significant amount of internal friction within the material during mechanical deformation. In order to quantify the damping characteristics in terms of dissipated energy within the material per unit

cycle, hysteretic performance curve was obtained by loading and unloading the spring. Molded leaf springs were subjected to loading-unloading for a maximum load of 200 N at a loading rate of 5, 10 and 20 N/s. Figure 6.22a shows the hysteretic behavior of LFLS. Figure 6.22b confirmed that UFLS and SFLS dissipated more energy than that of LFLS; in addition, hysteretic losses of LFLS were less sensitive to loading rate due to its enhanced stiffness. Stiffer the material, lesser the plastic deformation, resulted in lowering the hysteretic loss per cycle (Rosato *et al*., 2000).

Less hysteretic effect is preferable under dynamic loading conditions. For a given volume fraction of glass fiber material, short fiber reinforced material have more fiber ends than long fiber reinforced material as reported in section 5.2. Karger-Kocsis and Friedrich (1988) also reported similar observations in the long and short fiber reinforced polyamide 66 composite, where the fracture surface revealed that longer fiber length had a much smaller fiber density per unit area than that of short fiber polyamide composite. Energy is dissipated through the fiber-matrix interface (Gassan and Bledzki, 2007). Therefore, with the presence of more fiber ends in SFPP material, energy dissipation is more than that of LFPP materials. In addition, with the increased fiber length in LFPP material, viscous response is dominated by elastic response. This reduction of viscous response in LFPP material contributes to the less sensitivity towards hysteretic energy dissipation than SFPP material with respect to loading rate.

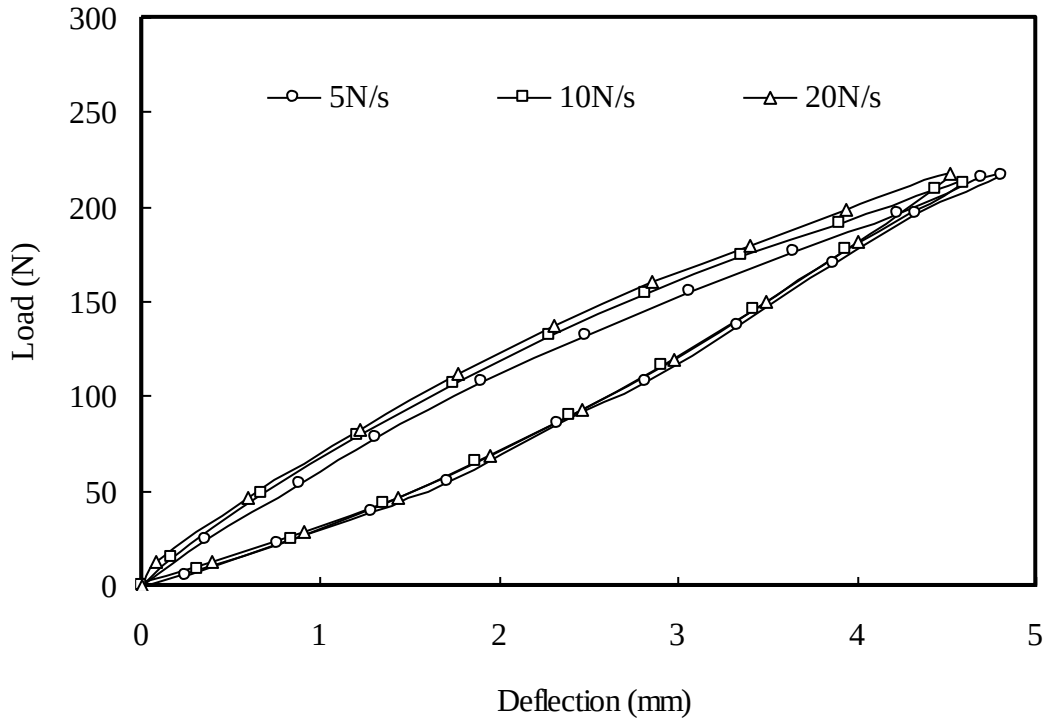

Fig. 6.22 a Loading-unloading curve for molded long fiber reinforced leaf springs

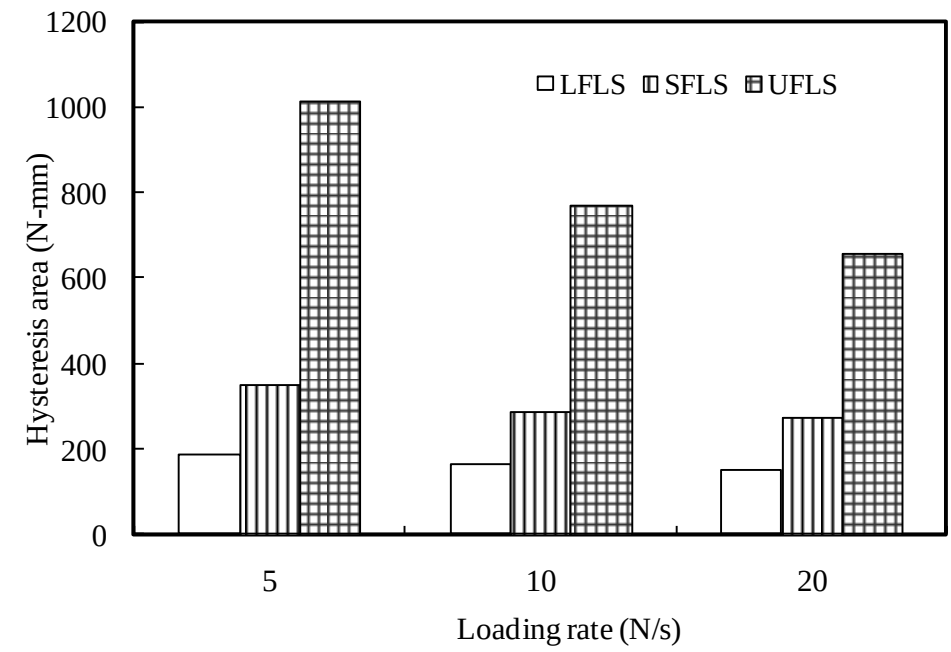

Fig. 6.22b Hysteretic component of molded leaf springs

6.7.5 Load Relaxation Characteristics of Composite Leaf Springs

Load relaxation data exhibit the time dependent response of the structure subjected to constant strain. The load drop for maintaining the required displacement exhibited load relaxation characteristics of the molded leaf springs. Stress relaxation takes place due to non-elastic deformation of material. Figure 6.23 delineates the effect of fiber length on the short term load relaxation behavior of composite leaf spring. Results depict that the rate of load relaxation was found to be higher for short fiber and unreinforced leaf springs. LFLS showed superior creep performance than that of UFLS and SFLS due to increased restriction of the resin deformation rendered by the long fibers (Kim et al., 1997).

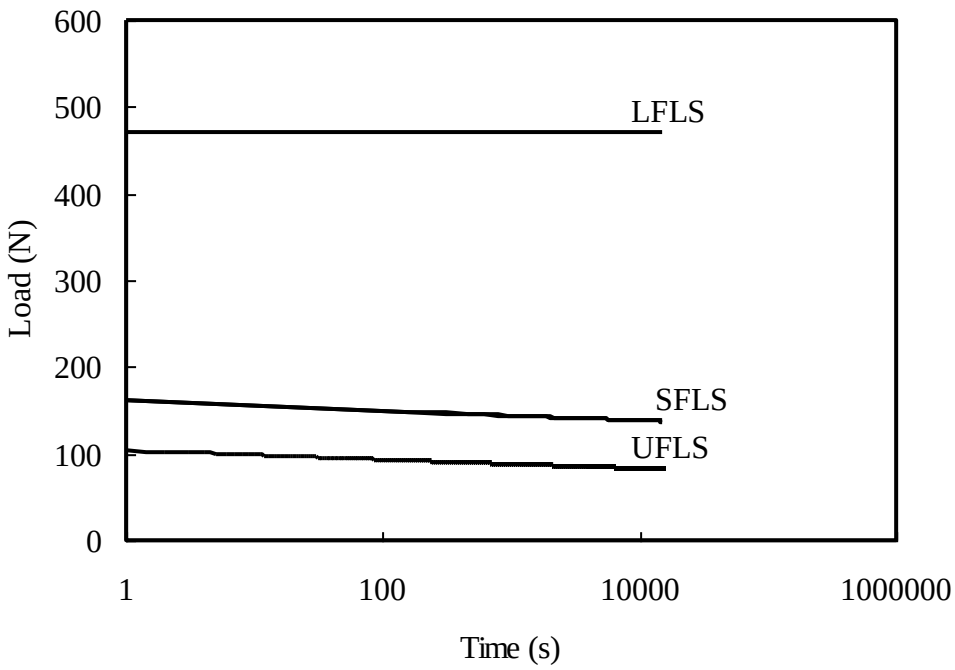

Fig.6.23 Influence of fiber length on load relaxation behavior in thermoplastic leaf springs

6.8 SUMMARY

This chapter discussed the design procedure, development and preliminary performance of the thermoplastic composite leaf spring.

- Various geometric configurations pertaining to SAE standards were considered and the proposed design was evaluated with the aid of finite element analysis after optimization of leaf spring dimension at center.
- Injection molding simulation was carried out to choose best gate location. Presence of fibers in the molded leaf spring found to reduce the volumetric shrinkage.
- Unreinforced, 20 % short glass fiber reinforced and 20 % long glass fiber reinforced polypropylene leaf springs were injection molded and static performance was carried out with the developed fixture in house.
- Spring rate of LFLS was found to be about three times greater than that of SFLS and five times greater than UFLS. Energy storage capability of LFLS was found to be significantly higher that of SFLS and UFLS, which helps to isolate vibrations. Load-deflection behavior of LFLS showed less strain rate sensitiveness than that of SFLS and UFLS.

CHAPTER 7

FATIGUE AND CREEP PERFORMANCE OF THERMOPLASTIC LEAF SPRINGS

7.1 INTRODUCTION

Suspension leaf springs are subjected to fatigue loads when the vehicle periodically passes through surface irregularities on the road. Identification of safe operating regime of the developed thermoplastic composite leaf springs is of practical importance. Apart from identifying the fatigue strength of the component, it is necessary to characterize the damage progression in the component *viz.* hysteresis, damping and stiffness reduction during fatigue test (Orth *et al*., 1993). Processing conditions, fiber length, matrix properties, interfacial properties and testing conditions were identified as the major influencing factors over the fatigue behaviour of the fiber reinforced composites (Sauer and Richardson *et al*., 1980). Increase in fiber loading and length of fibers improved the fatigue crack propagation resistance (Czigany and Karger-Kocsis, 1993). The interfacial strength plays a significant role on the fatigue behaviour of the discontinuous fiber reinforced composites (Bureau and Denault, 2004). Presence of long glass fibers in the polypropylene matrix reduced the energy dissipation characteristics and provides higher fatigue life (Goel *et al*., 2008). Different fatigue failure mechanisms are possible due to the heterogeneous characteristics of the discontinuous fiber reinforced composites and hence understanding the micro mechanisms of product failure helps to design and develop quality components.

Creep performance evaluation is essential due to the requirement of service conditions; leaf springs are subjected to constant stress for long duration as the chassis weight is taken by the suspension system even when the vehicle remains stationary. Besides, leaf springs are also subjected to various stress levels due to the different payload conditions. In the discontinuous fiber reinforced composites, fiber length and temperature influenced the stress transfer which significantly contributes to the creep behavior (Silverman, 1987).

This chapter reported the fatigue and short-term creep performance of discontinuous fiber reinforced thermoplastic leaf springs at various stress levels. Cyclic load-deflection curve of molded leaf springs were utilized as an index to quantify the accumulated leaf spring damage during fatigue testing and safe operating regime was identified. The influence of reinforcement over leaf spring fatigue failure mechanism was also reported in this chapter. In addition, flexural short-term creep performance of leaf springs were investigated and experimental creep performance of 2 h was utilized to predict the creep performance with the aid of empirical model and compared with 24 h experimental creep data.

7.2 FATIGUE PERFORMANCE EVALUATION METHODOLOGY

Unreinforced polypropylene (UFLS), 20 wt % short (SFLS) and 20 wt % long glass fiber reinforced polypropylene (LFLS) leaf springs were used for the fatigue performance evaluation. Details of fixture for the leaf spring testing were reported in section 6.5. Test leaf springs were loaded upto 12 mm deflection (Camber) and released back as per SAE standards (SAE J 1528, 1990). The load taken for this magnitude of deflection of test leaf spring was taken as P_{max}. Since leaf springs are not subjected to completely reversed load in service, tests were performed under

pulsating bending mode with an amplitude ratio, A = -1. Molded test leaf springs were subjected to various levels of alternating loads with respect to P_{max} at a frequency of 0.5 Hz (SAE J 1528, 1990). Tests were conducted under laboratory conditions (32 ± 3°C, RH 57 % ± 5 %). During fatigue test, leaf spring damage was continuously monitored with the help of cyclic load-deflection curve. The cyclic load-deflection plot at $0.8P_{max}$, $0.9P_{max}$ and P_{max} was further utilized to quantify energy dissipation and spring rate drop. Failure of molded leaf springs was considered when the spring rate reduced by 10 % or fracture.

7.3 FATIGUE PERFORMANCE OF THERMOPLASTIC LEAF SPRINGS

7.3.1 Energy Dissipation of Test Leaf Springs

Energy dissipation behavior of a suspension system significantly influences the passengers riding comfort. Although energy dissipation minimizes structural vibration, it significantly reduces the spring rate which is not desirable for suspension application. Schematic representation of cyclic stress-strain loop to evaluate energy dissipation and spring rate under fatigue condition is shown in figure 7.1. The hysteretic characteristic of the polymeric material causes significant energy dissipation under dynamic condition. Energy dissipation ratio (H_c) is the ratio of energy lost/cycle (measured from the area enclosed by the loading-unloading curve) to the strain energy/cycle (area enclosed by the loading curve). Sugimoto and Sasaki (2007) also used energy dissipation ratio parameter as an index for the fatigue performance evaluation. Orth *et al.* (1993) specified energy dissipation ratio as a measure of damping and quantified the instantaneous increase in the damping for valve spring retainer under fatigue conditions.

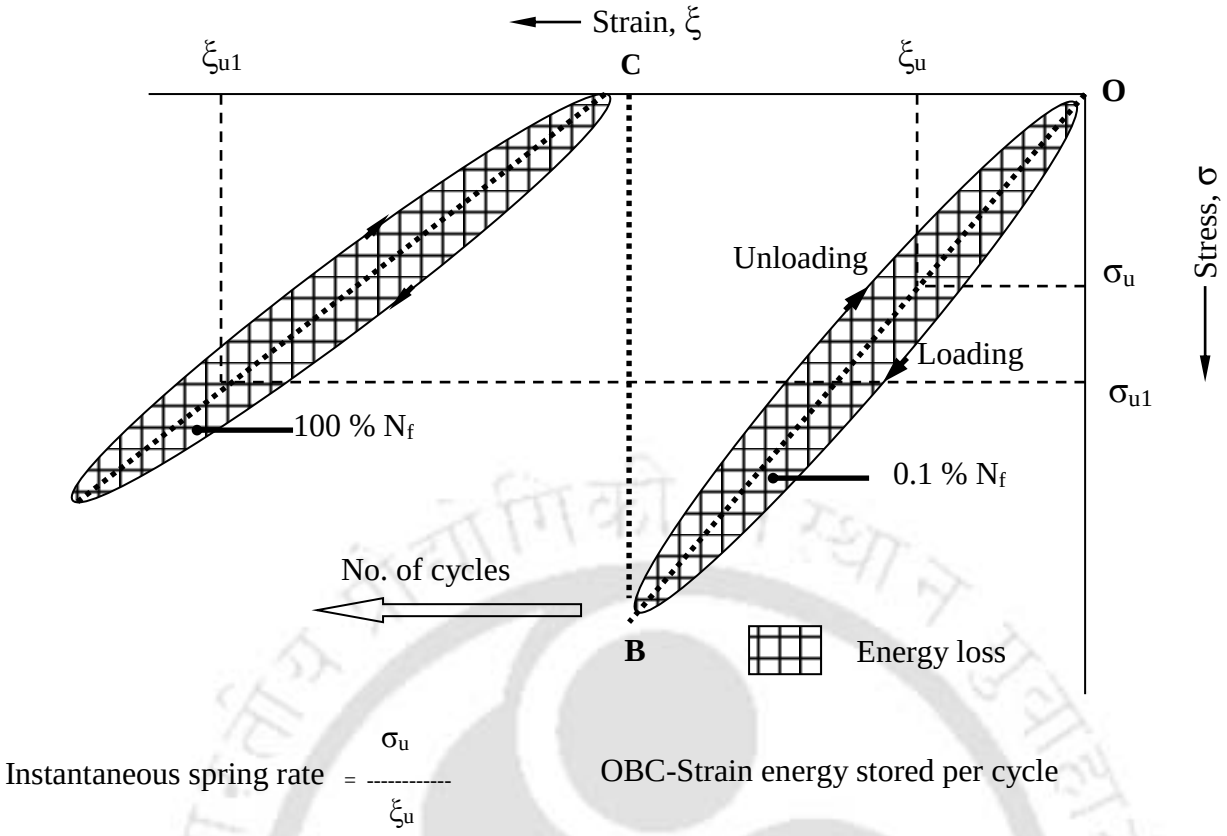

Fig. 7.1 Schematic representation of hysteretic curve obtained from fatigue testing of leaf spring

Fatigue life of LFLS, SFLS and UFLS ranged from 365-2,00,000 cycles, 245-2,00,000 cycles and 195-2,00,000 cycles respectively. Total duration to complete one trail for LFLS, SFLS and UFLS was 227.5, 162 and 175 hours respectively and total number of data (load-deflection) collected per cycle was eight. Total number of load as well as deflection data corresponding to LFLS for one trail is 32,76,080. Similarly total numbers of data corresponding to SFLS and UFLS for one trail are 23,34,128 and 25,32,880 respectively. These load deflection data were utilized for plotting the figures 7.2-7.4 for continuous monitoring of damage induced in test leaf springs. Figures 7.2 (a-c) show the cyclic load deflection curve at various stages of developed composite leaf springs tested at a loading level of P_{max}. Though fatigue performance evaluation is carried out at various loading levels, discussions were illustrated for a loading level of $P_{max.}$ P_{max} for UFLS SFLS and LFLS are 110, 190 and 490 N

respectively which is obtained from the static test. The cyclic load deflection plot is obtained at various stages of fatigue life *viz*. 0.1, 10, 50 and 100 % N_f as shown in figure 7.2, where N_f is the total number of cycles prior to failure.

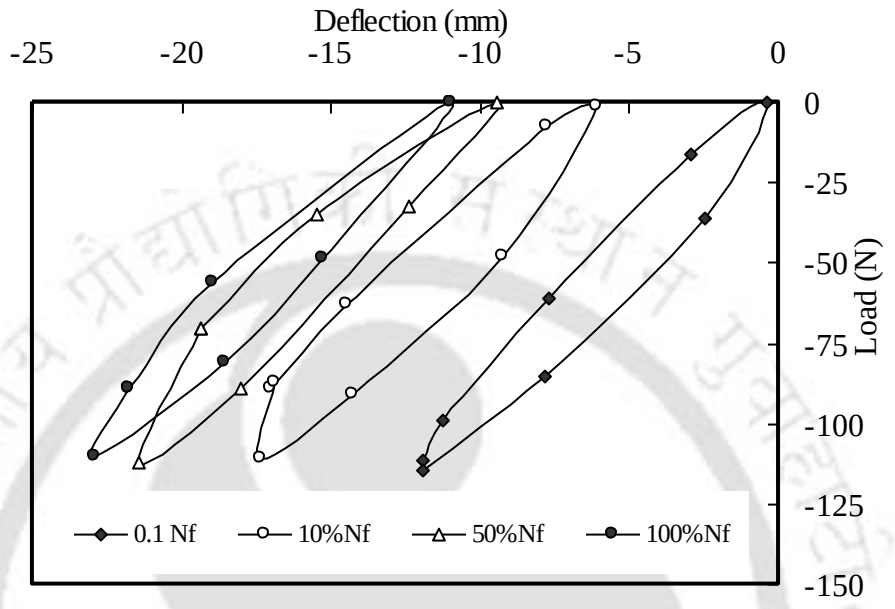

Fig. 7.2a Cyclic load-deflection curve for unreinforced leaf spring at P_{max}

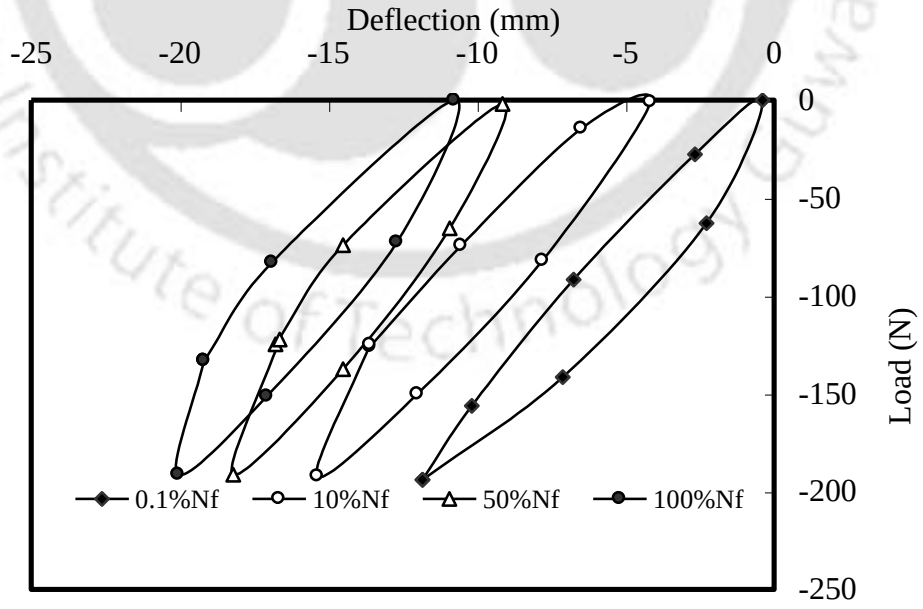

Fig.7.2b Cyclic load-deflection curve for short glass fiber reinforced leaf spring at P_{max}

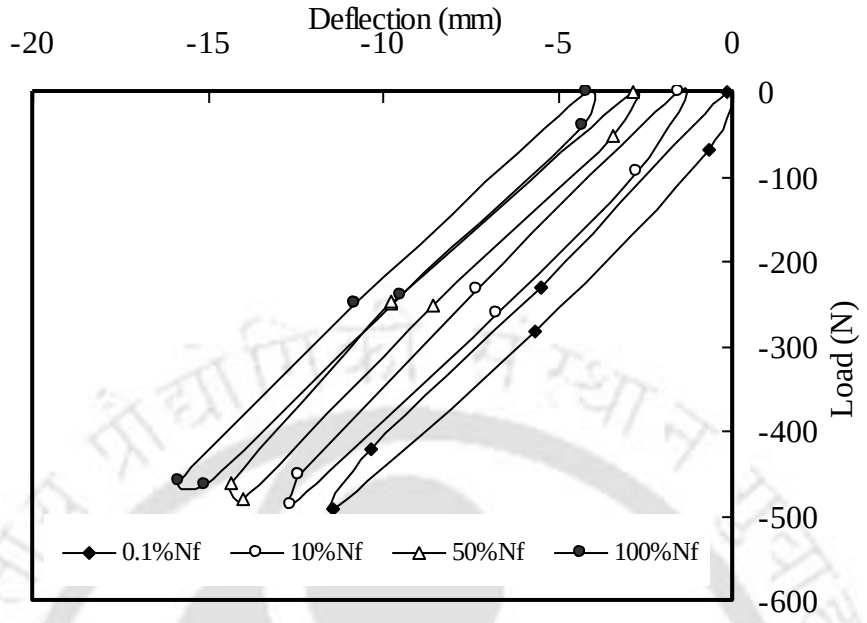

Fig.7.2 c Cyclic load-deflection curve for long glass fiber reinforced leaf spring at P_{max}

(a)

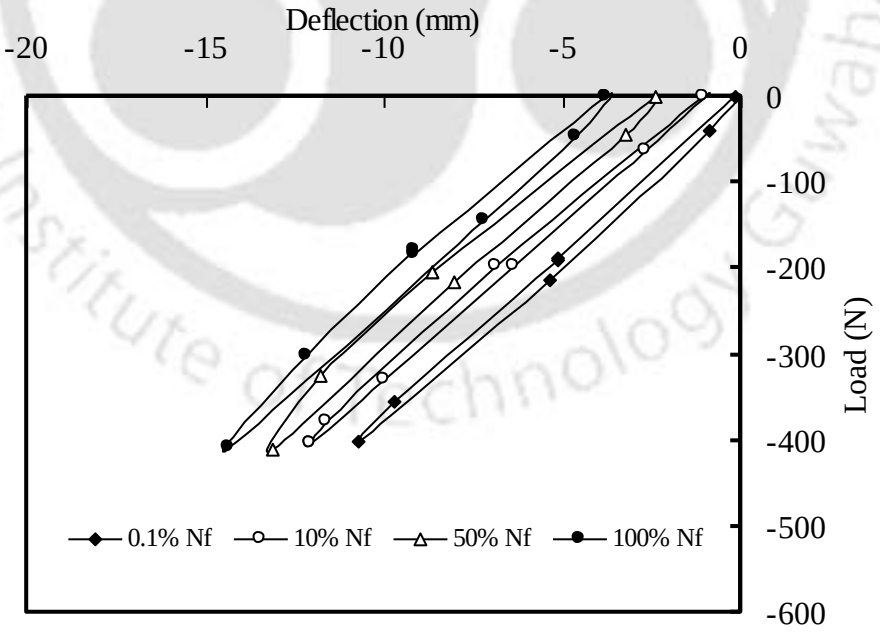

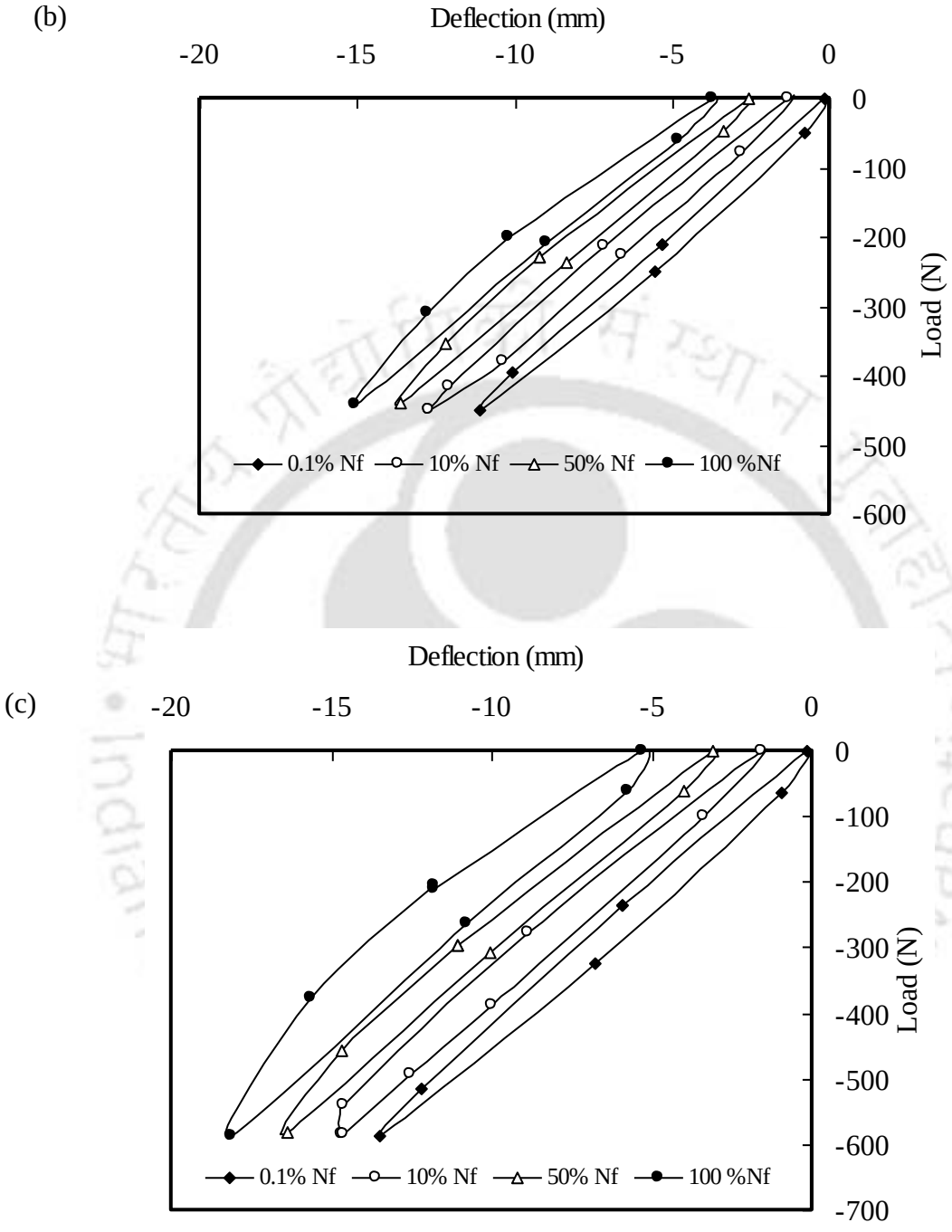

Fig. 7.3 Cyclic load-deflection curve for long glass fiber reinforced leaf spring at (a) 0.8 P_{max} (b) 0.9 P_{max} (c) 1.2P_{max}

Energy dissipation of test leaf spring is evaluated from the cyclic load-deflection plot. To compare the leaf spring performance, the energy dissipation ratio at beginning (10^{th}) and after finite number of cycle (3500^{th}) was computed. The increase in energy dissipation ratio from the beginning to 3500^{th} cycle for UFLS, SFLS and LFLS are found to be 1.40, 1.20 and 1.04 respectively. Earlier investigation (Section 6.7.4) under static condition also confirmed the enhanced energy dissipation behavior of SFLS than that of LFLS. This behavior is due to the presence of more fiber ends in SFLS than that of LFLS. In addition, the presence of high modulus long glass fibers reduces the energy dissipation significantly. Talib *et al*. (2010) also reported the reduced energy dissipation behavior due to the presence of high modulus carbon fiber in the composite springs.

These hysteresis loops move along the deflection axis throughout the life of the component. The shape and size of these loops, depends on the applied stress. Figures 7.3(a-c) show the cyclic load-deflection curve of long fiber reinforced leaf springs subjected to 0.8 P_{max} , 0.9 P_{max} and 1.2 P_{max} at various period of fatigue life (N_f). Cyclic load-deflection plot of test leaf springs exhibited significant increase in deflection with the increase in load during the fatigue loading. Since energy dissipation is associated with the spring rate reduction, further quantification of spring rate is of the practical importance to the suspension application.

7.3.2 Spring Rate of Test Leaf Springs

Spring rate of the vehicle suspension system is decided by the sprung mass (mass of the body and other component supported by the suspension). If the spring rate is very high (excessively rigid springs) than required, then springs do not absorb shock and vibration thereby all the vibrations are transmitted to the vehicle. If the spring rate is

very low (excessively flexible springs) than required, then the springs deflect drastically which contributes to the poor isolation of the vehicle from the road against the vibrations. Hence for the good suspension system, appropriate spring rate is required and to be retained during its service. Fatigue loading of leaf springs causes material damage and reduces spring rate as the cycle progresses. To enumerate the accumulated fatigue damage in the test leaf spring, relative spring rate (ratio of instantaneous spring rate (K) to the initial spring rate (K_o)) was measured and plotted as the performance index. The relative spring rate of test leaf springs at finite number of cycles at various loads were obtained from the cyclic load deflection curve. Figures 7.4 (a-b) show the relative spring rate of test leaf springs at three different loading levels (0.8 P_{max} 0.9 P_{max} and P_{max}). Orth *et al.* (1993) also utilized the stiffness drop for carbon fiber reinforced spring retainer as a damage index under dynamic loading condition. Casado *et al.* (2006) adopted similar methodology for the performance investigation of railway fastening part made of short glass fiber reinforced nylon and reported a continuous stiffness drop and as well as fracture. Leaf spring fatigue failure is taken as spring rate drop/fracture as per SAE standard J 1528. UFLS and SFLS exhibited failure by spring rate drop by 10 % whereas LFLS exhibited fracture failure. Unlike, SFLS and UFLS, LFLS do not exhibit appreciable spring rate drop initially but later significant drop in spring rate was observed, and similar kind of transition was observed for all the chosen loads.

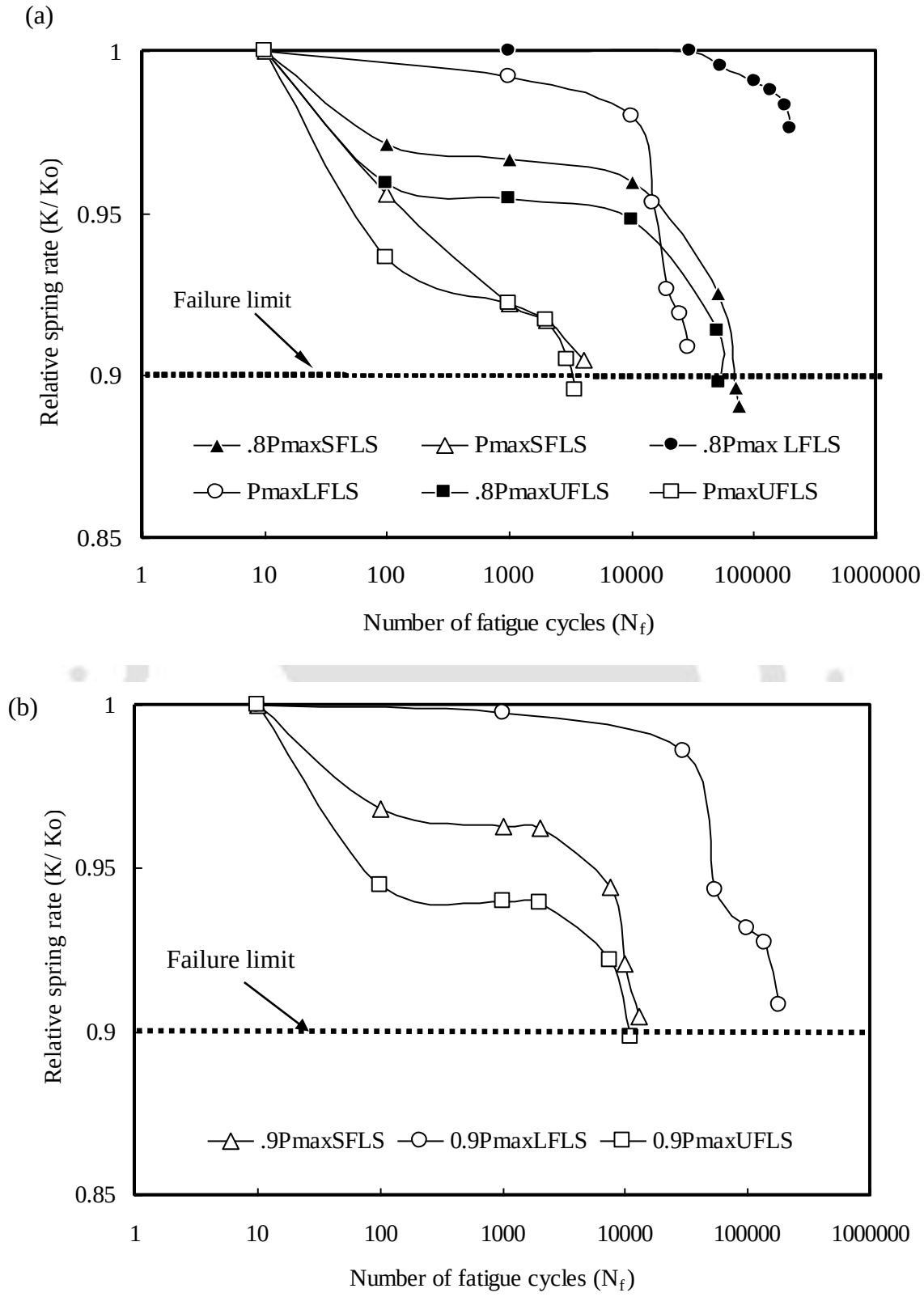

Fig.7.4 Spring rate reduction in reinforced and unreinforced leaf springs for (a) P_{max} and $0.8P_{max}$ (b) $0.9P_{max}$

7.3.3 Fatigue Strength of Molded Leaf Springs

Based on the failure criteria as discussed before, the endurance curve of the thermoplastic leaf spring is shown in figure 7.5 for all the leaf springs. Endurance limit of the tested thermoplastic composite spring is taken as 2 x10^5 cycles (SAE J 1528, 1990) and the run out specimens were indicated by the arrow marks. The induced leaf spring bending stress S_b is computed using relation 7.1. Rajendran and Vijayarangan (2001) made use of the similar equation for designing the mono composite leaf spring for depicting the leaf spring bending stress estimation

$$S_b = \frac{3PL_e}{2b_c t^2} \tag{7.1}$$

where P is the applied load, L_e is effective length of the spring, b_c is the width at the center and t is the beam thickness at center. Test conditions were repeated for three times, and the whole set of data irrespective of load levels were used. A linear interpolation on the semi logarithmic plot (S_{max} - log (N_f)) was performed and the equation for the linear interpolation takes the form

$$S_{max} = S_o - B\ Log\ (N_f) \tag{7.2}$$

This equation is rewritten as

$$S_{max} / S_o = 1 - m\ Log\ (N_f) \tag{7.3}$$

where S_{max} is the maximum bending stress, S_o is the static strength and m is a constant parameter representing the fatigue sensitivity of material. The S-N curve of the test leaf springs shows the parameters of the interpolating line along with correlation index (figure 7.5). The values of correlation index were well within the limits. Linear interpolation was performed using the above equation (7.3) on the semi-logarithmic plot by various authors (Zhou *et al*., 1994; Allah *et al*., 1997). LFLS possessed enhanced fatigue resistance in both the low and high cycle fatigue.

Fatigue performance of leaf springs was found to be improved with the increase in fiber length due to the enhanced load transfer from the fiber to matrix. LFLS showed higher sensitivity towards stress level than that of SFLS and UFLS. Sensitiveness towards stress level is due to reduced ductility of the matrix.

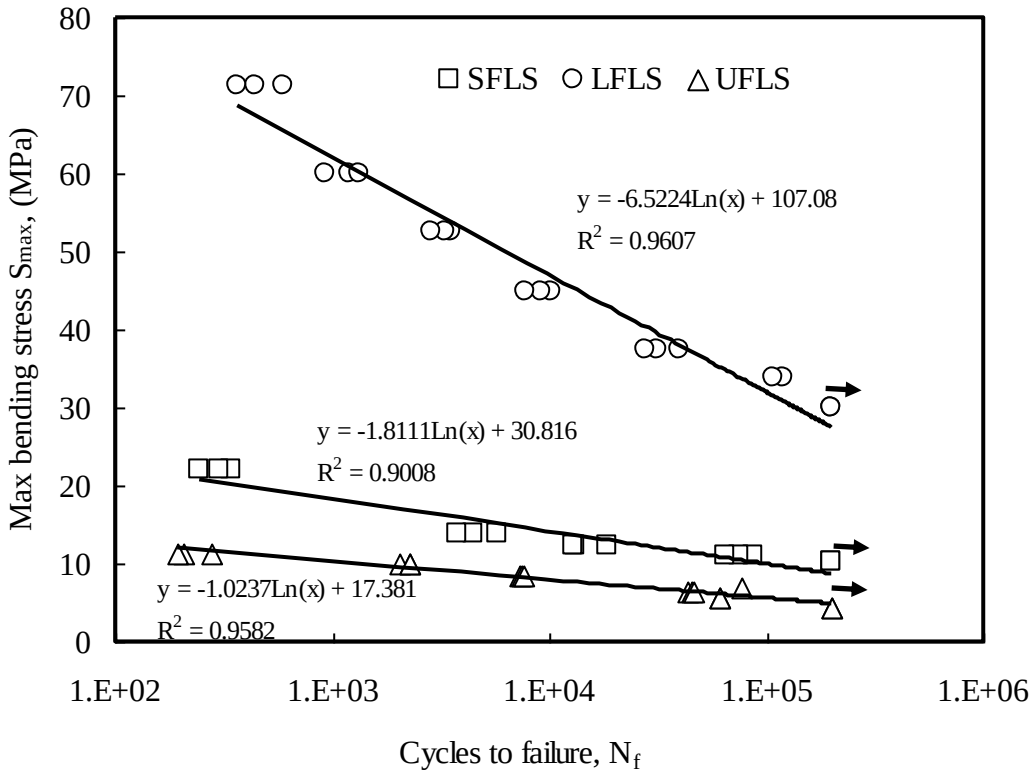

Fig. 7.5 Fatigue stress - life curve of reinforced and unreinforced leaf springs

UFLS and SFLS exhibited drop in spring rate and LFLS exhibited fracture for all the considered loads. Surface morphology of LFLS exhibited cracks on the tensile surface of the leaf spring as shown in figure 7.7. Figure 7.6a shows the schematic position of the cracks on the test leaf spring. Figures 7.6 (b-c) elucidate visible cracks in the transverse direction to leaf spring length and figure 7.6d shows the observed crazes near the cracks on the tensile surface of LFLS.

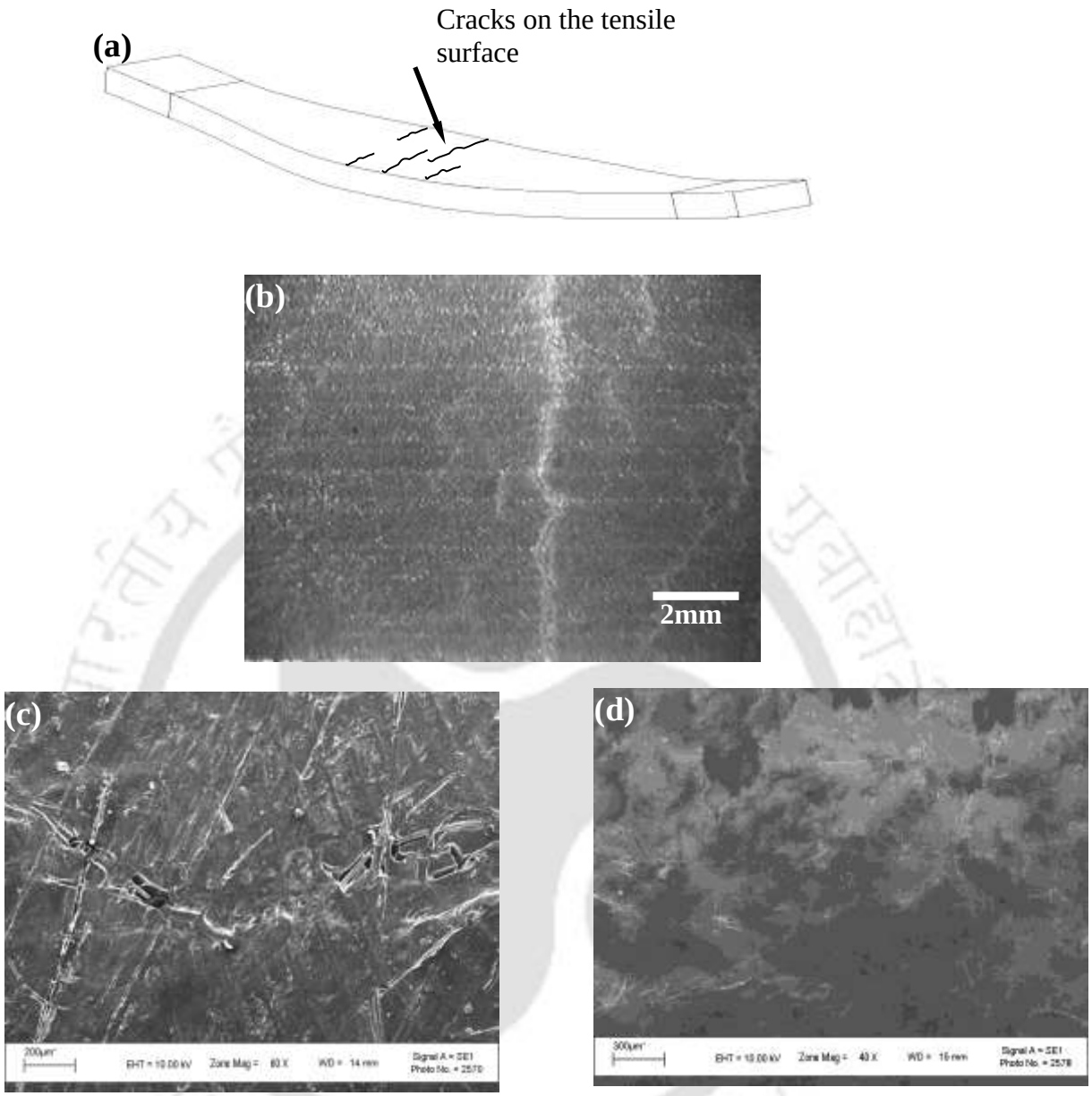

Fig. 7.6 Failure morphology of long fiber reinforced leaf spring (a) schematic cracks on the tensile surface (b) cracks in the direction transverse to the leaf spring length (c) cracks on the leaf spring (d) crazing on the leaf spring.

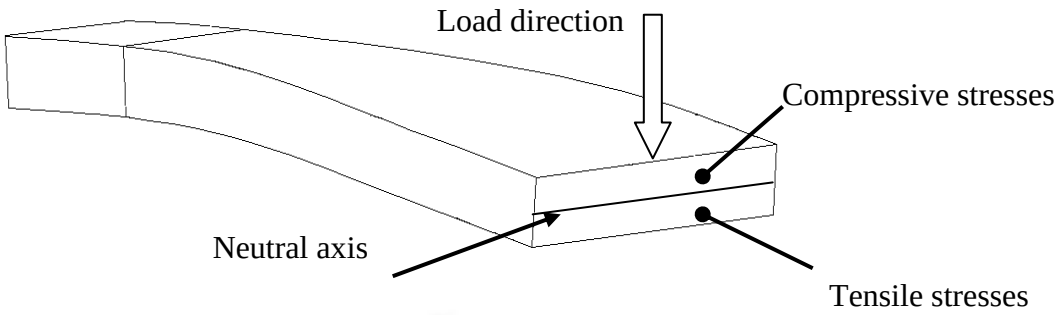

Fig. 7.7 Schematic of the investigated fractured surface of leaf spring

Figure 7.7 shows the schematic cross section of investigated fractured surface of leaf spring, wherein both compressive and tensile stresses exist due to the bending load Figures 7.8 (a-b) show the fractured surface of the LFLS at different loading conditions, wherein two different failure features are observed. The left side of the figure 7.8(a-b) correspond to the leaf spring section which experiences tensile stresses and hence micro ductile/matrix fibrillation was observed. Right side of the figure 7.8 corresponds to the leaf spring section which experiences compressive stresses and hence brittle failure was observed.

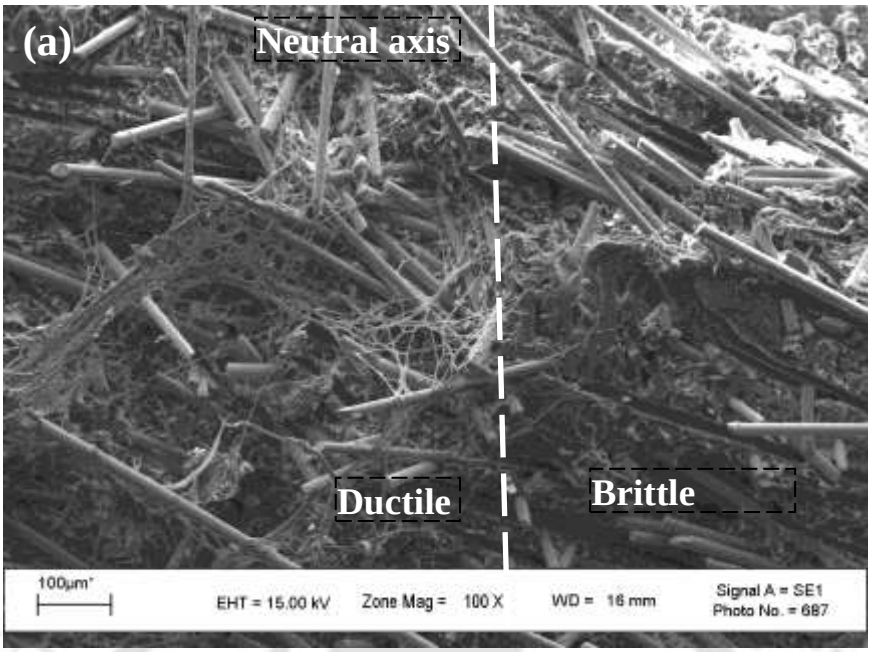

Fig. 7.8a Failure morphology of LFLS at 33.5MPa indicating ductile and brittle failure feature of matrix

t

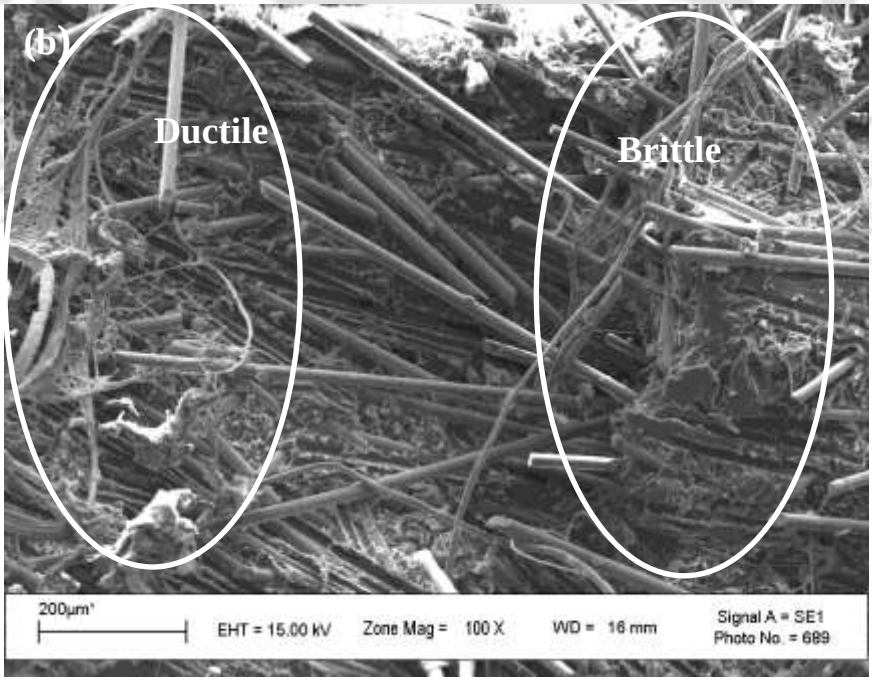

Fig. 7.8b Failure morphology of LFLS at 45 MPa indicating ductile and brittle failure feature of matrix

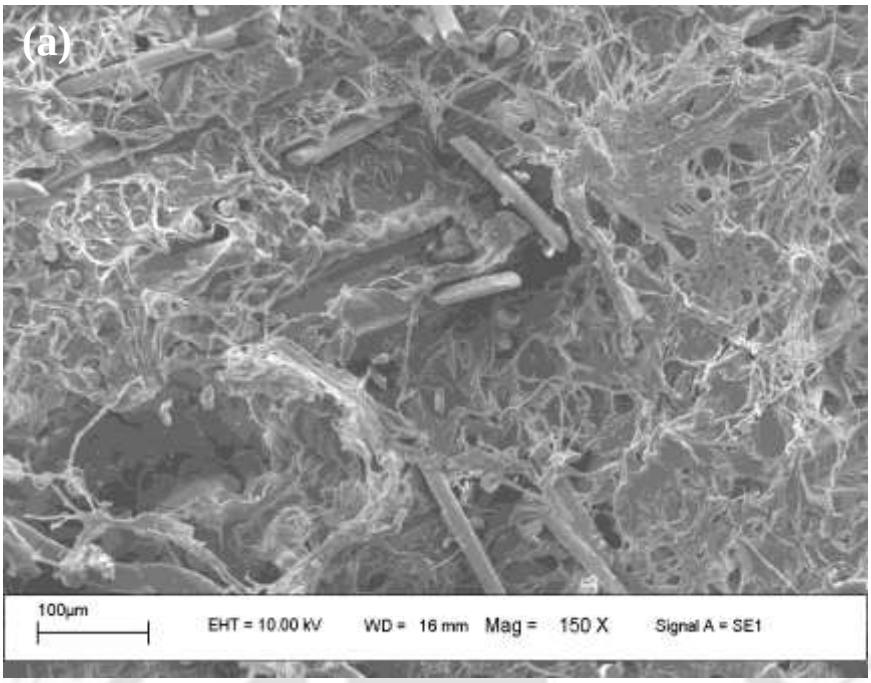

Fig. 7.9a Failure morphology of LFLS at 33.5MPa showing completely ductile failure feature of matrix (*Area corresponding to tensile stress*)

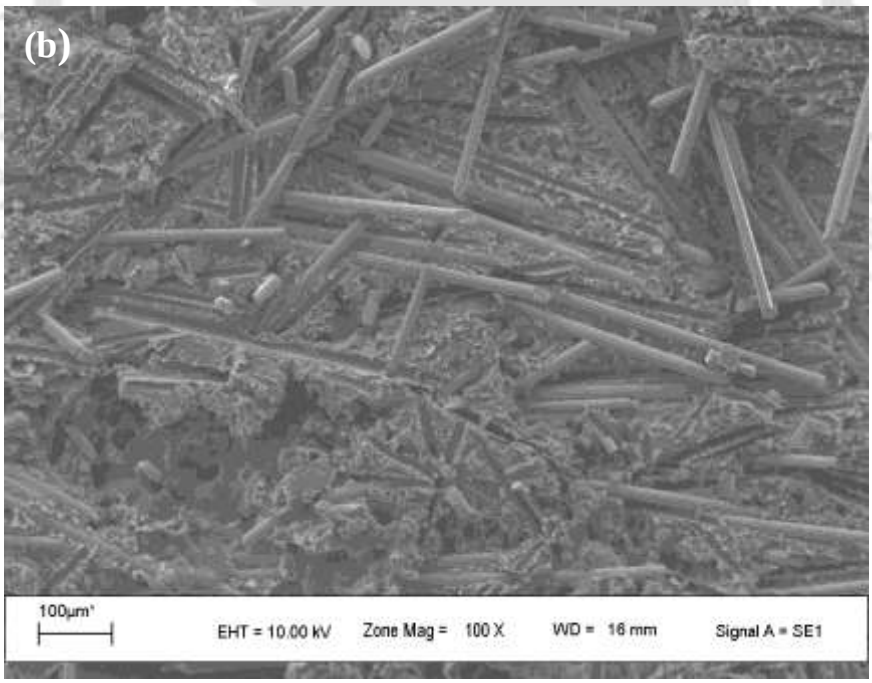

Fig. 7.9b Failure morphology of LFLS at 33.5MPa showing completely brittle failure feature of matrix (*Area corresponding to compressive stress*)

The above failure morphologies (figures 7.8(a-b)) correspond to the region near the neutral axis as indicated in figure 7.7. Fractured surface of LFLS near the edge (*i.e.* away from the neutral axis) was further examined, wherein either tensile or brittle failure feature was observed. Figure 7.9a indicates the micro ductile failure feature which corresponds to the tensile stress region of LFLS leaf spring. Figure 7.9b indicates the brittle failure feature which corresponds to the compressive stress region of LFLS leaf spring. Purslow (1988) investigated the flexural fractured surface of carbon fiber reinforced polyetheretherketone laminates, where compression and tensile failures were observed near the neutral axis. Jeng and Chen (2000) attempted to investigate the flexural fractured surface on injection molded carbon fiber polyetheretherketone near the neutral axis, however, significant difference was not observed on the tensile and compressive side of the fractured surface.

Fatigue strength of discontinuous fiber reinforced part significantly depends on the fiber orientation, which in turn depends mainly on the part shape and gate position in the molding die. Gate position was kept in such a way that the majority of the discontinuous fibers orient along the length of the leaf spring. Figure 7.10 shows the predicted fiber orientation using Mold Flow Plastics Insight® for the molded leaf spring where fibers were oriented along the leaf spring length, which is preferred for load carrying application as load is acting normal to the fiber direction. Figure 7.11 also confirmed that injection molding induced fiber alignment. Investigation to understand failure morphology of LFLS also confirmed this behavior (figures (7.8b,-7.9b)).

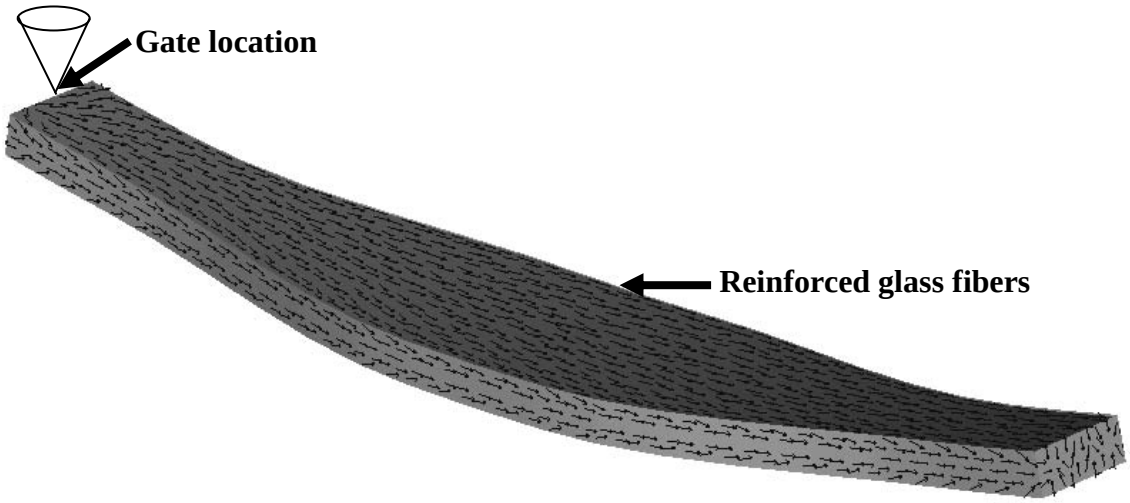

Fig.7.10 Predicted fiber orientation for the molded short glass fiber leaf spring

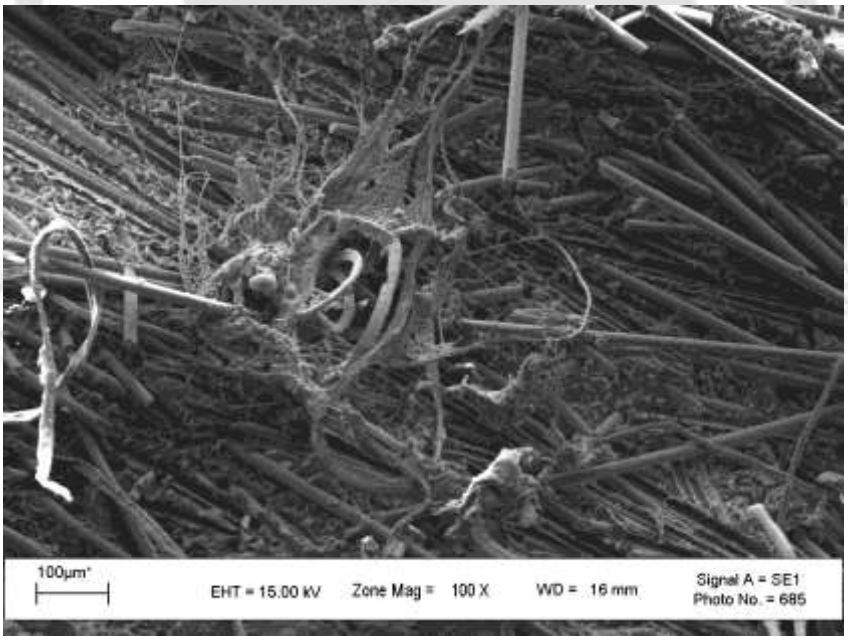

Fig.7.11 SEM of fractured surface of long glass fiber reinforced leaf spring showing fiber alignment

7.4 CREEP PERFORMANCE

The influence of fiber length on the short-term flexural creep performance of thermoplastic composite leaf springs for various stress levels at room temperature condition is discussed in this section. Though leaf spring application demands creep performance evaluation in the range of 1000 h, present experimental work was limited to 24 h and the usefulness of empirical model for the creep performance prediction of molded leaf spring was explored. Since empirical model is used to predict the creep performance of leaf spring, the theoretical background regarding these models is also presented.

7.4.1 BACKGROUND ON CREEP MODELS

7.4.1.1 Findley's Power Law Model

Mechanical behavior of polymeric material under constant stress was developed by Findley and Khosla (1955). The general form of the power law equation was given as

$$\varepsilon(t) = \varepsilon_t^{'} t^n \tag{7.4}$$

where $\varepsilon(t)$ is the time dependent strain , $\varepsilon_t^{'}$ is power law coefficient which is stress and temperature dependent coefficient, n is the power law exponent and t is the time after loading. Park and Balatinecz (1998) used the above equation 7.4 to investigate the flexural creep behavior of wood fiber reinforced polypropylene composites. Power law model is simple in approach and successfully predicted nonlinear viscoelastic creep behavior of thermoplastic composites over large range of stress (Liou *et al.*, 1997; Hadid *et al.*, 2002; Banik *et al.*, 2008) besides this model is also recommended by American Society of Civil Engineers (ASCE, 1986) for structural

plastics design manual in the analysis of composite materials for long term structural behavior.

7.4.1.2 HRZ Model

Findley's power law was unsuccessful in accounting for the stress effect on the mechanical behavior of polymeric material. The two power law parameters in the Findley-Khosla model $\varepsilon_t^{'}$ and n were significantly influenced by the applied stress level. Karian (1999) carried out flexural creep test on polypropylene short fiber composite and observed that creep strain was sensitive to stress level. Hadid *et al*. (2002) modified the Findley's power law to incorporate time and stress dependence in the model where the power law coefficient ($\varepsilon_t^{'}$) and power law exponent (n) were plotted with respect to stress level (σ). The best fitting curve proposed the relation between $\varepsilon_t^{'}$ and σ as

$$\varepsilon_t^{'} = a.(\sigma)^b \tag{7.5}$$

Similarly, the best fitting curve proposed between n and σ value takes the form

$$n = c.exp(e.\sigma) \tag{7.6}$$

Equations (7.5 and 7.6) were used in equation 7.4 and strain at any particular time (t) can be calculated using the following HRZ equation

$$\varepsilon(t) = a.\sigma^b.t^{c.exp(e.\sigma)} \tag{7.7}$$

where a, b ,c and e are the curve fitting parameters obtained from the regression analysis. Chevali *et al*. (2009) used the four parameter HRZ model to fit the experimental data obtained from flexural creep investigation for nylon 6/6, polypropylene and high-density polyethylene based long fiber thermoplastic composites.

7.4.2 CREEP PERFORMANCE EVALUATION METHODOLOGY

Creep performance test were carried out for 24 h for 0.8 P_{max} and P_{max} load levels. In addition, 2 h creep tests were also conducted at 0.6, 1.2 and 1.4 times the P_{max}. The cross-head speed during loading of the leaf spring was adjusted in order to reach the desired load level in a time of 5 s as suggested by ASTM D2990-95 standard (ASTM D-2990, 2005). Constant load was maintained and leaf spring deflection ($\delta(t)$) was continuously measured and recorded. Creep strain at instantaneous time ($\varepsilon(t)$) was computed using the relation 7.8 (ASTM D-2990, 2005).

$$\varepsilon(t) = \frac{6\delta(t).t}{L_e^2} \tag{7.8}$$

where, $\delta(t)$ is the deflection at instantaneous time, t is the thickness and L_e the effective leaf spring length. From the measured creep strain, creep compliance ($J(t)$ in MPa^{-1}) was computed using the relation 7.9 (ASTM D-2990, 2005)

$$J(t) = \frac{4b_c t^3 \delta(t)}{PL_e^3} \tag{7.9}$$

7.5 FLEXURAL CREEP PERFORMANCE OF THERMOPLASTIC COMPOSITE LEAF SPRINGS

7.5.1 Experimental Creep Performance

In the service conditions, suspension leaf springs are subjected to constant stress as the chassis weight is taken by the suspension system even the vehicle remains stationary. Besides, leaf springs are also subjected to various stress levels due to the

different prevailing payload conditions. Thus, creep response investigation of the molded leaf spring under various stress levels is of practical importance.

Creep performance evaluation was carried out at various loading levels corresponding to the value of P_{max}. The induced leaf spring bending stress (S_{max}) was computed using equation 7.1 for the tested load levels. The stress level corresponding to P_{max} for UFLS, SFLS and LFLS were 8.25, 14.25 and 37.75 MPa respectively. It is to be noted that the stress value corresponding to P_{max} is well below the yield stress value of the leaf spring material (Saint Gobain/ Twintex, 2005). Figure 7.12 shows the 24 h creep response of the chosen test leaf springs. A raise in creep compliance was observed with the time period for all the leaf springs. The time-compliance data at 100 s for P_{max} reveals that the LFLS, SFLS and UFLS exhibited creep compliance of 4.0E-04, 8.0E-04 and 1.6E-03 MPa^{-1} respectively. Subsequent to the preliminary rapid increase in creep compliance, the rate of creep compliance decreases. The compliance at the end of 24 h test reveals that LFLS, SFLS and UFLS showed an increase in creep compliance of 20.87, 51.62 and 65.20 % respectively. Three trials were conducted for calculating creep compliance for all the molded leaf springs and deviations for LFLS, SFLS and UFLS were found to be 3.5, 4.2 and 2.5 % respectively. Improved creep resistance behavior of LFLS was due to the improved load transfer from the matrix to the fibers and the matrix constriction to deformation. Chevali *et al*. (2009) also observed a similar behavior with the increase in loading of glass fiber reinforcement in the nylon composites. Since creep compliance increase was associated with the spring rate reduction, quantification of spring rate is of practical importance.

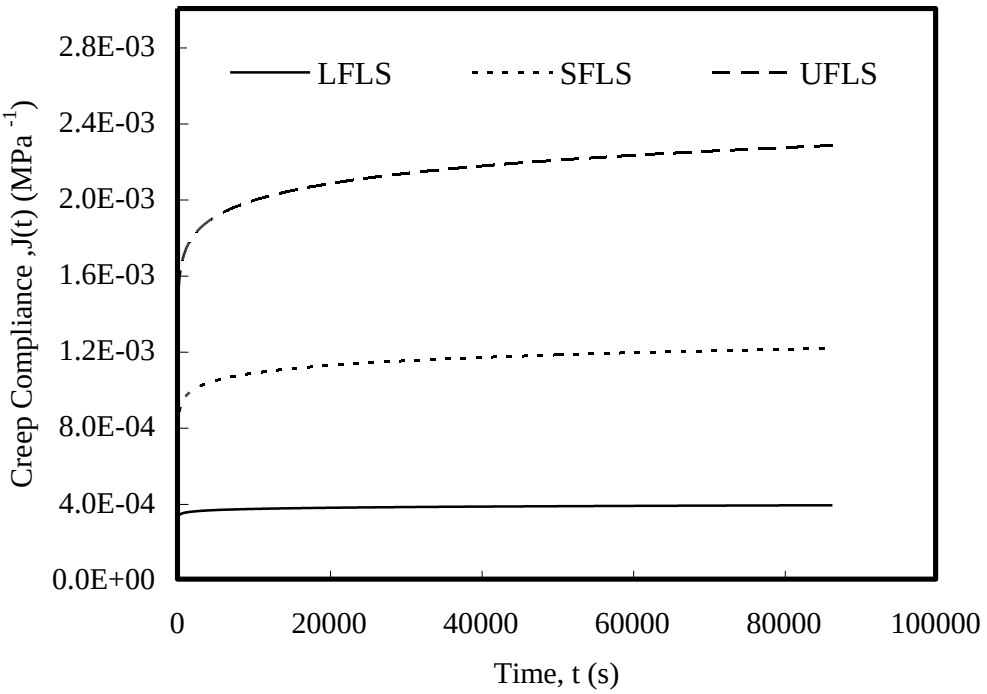

Fig.7.12 Experimental creep performance of molded test leaf springs at P_{max}

7.5.2 Spring Rate of Thermoplastic Composite Leaf Spring

Creep behavior of molded leaf spring results in spring rate reduction with the progression of time. Spring rate (K) was computed using the following relation

$$K = \frac{P}{\delta(t)} \tag{7.10}$$

where P is the constant load and $\delta(t)$ is the deflection at instantaneous time. To investigate the creep damage on the test leaf spring, relative spring rate (ratio of instantaneous spring rate (K) to the initial spring rate (K_o)) was measured and plotted as a performance index. The relative spring rate of test leaf springs at various time intervals were computed and figure 7.13 shows the relative spring rate of test leaf springs at two different loads (0.8 P_{max} and P_{max}) for a time period of 24 h. At the loading level of 0.8$P_{max,}$ initial spring rate (at the end of 30 s) of LFLS, SFLS and

UFLS were 39.8, 15.5 and 9.2 N/mm respectively and after 24 h it dropped to 36.2, 11.9 and 5.9 N/mm.

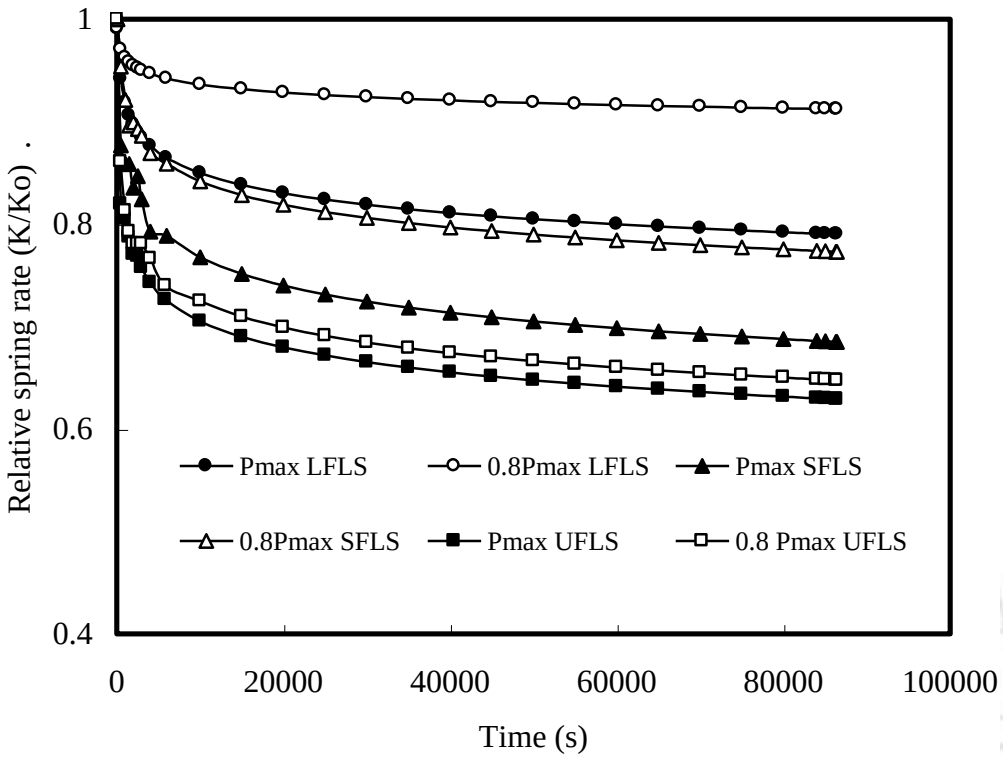

Fig. 7.13 Spring rate performance of molded test leaf springs

Due to the increase in fiber length, spring rate retention was more pronounced in LFLS and better isolation of shocks from the vibration can be achieved. Due to the substantial time requirement for the creep investigation, an empirical model was made use in the subsequent section to predict the leaf spring performance for a specific period of time.

7.5.3 Empirical Model for Predicting Short Term Creep Behavior

The creep performance of molded leaf springs were experimentally investigated for 2h duration in the load range varying from 0.6 P_{max} to 1.4 P_{max} and the test results are shown in figures 7.14 (a-c). Power law function is fitted using equation 7.4 for each and every stress levels thereby power law coefficient (ε_t'), power law exponent (n) and correlation index (R^2) were determined and tabulated in Table 7.1.

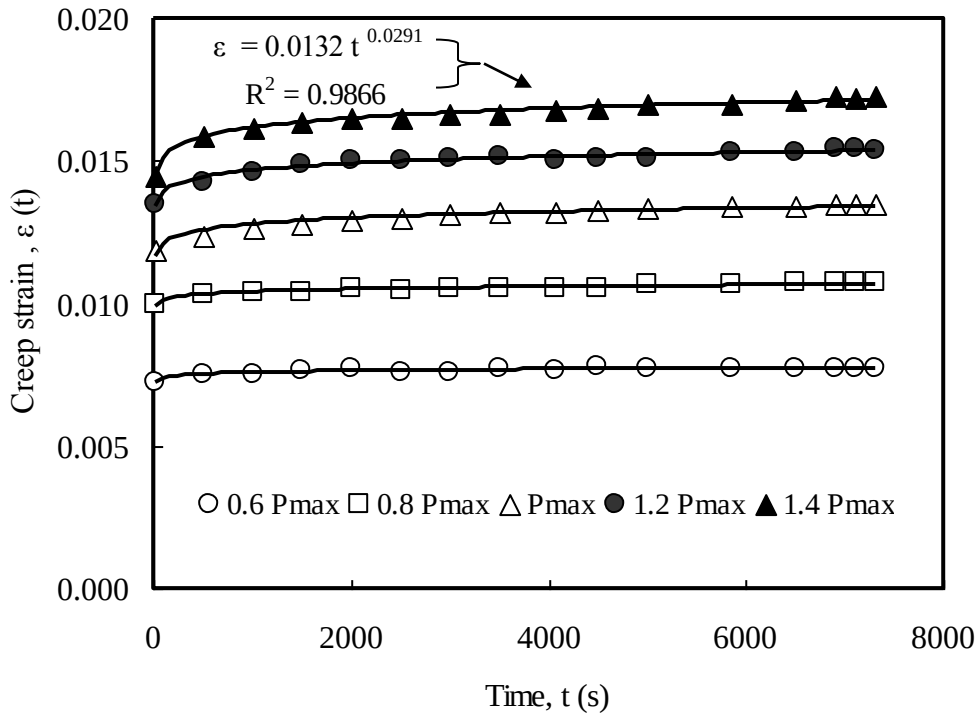

Fig. 7.14a Short-term experimental creep performance of LFLS

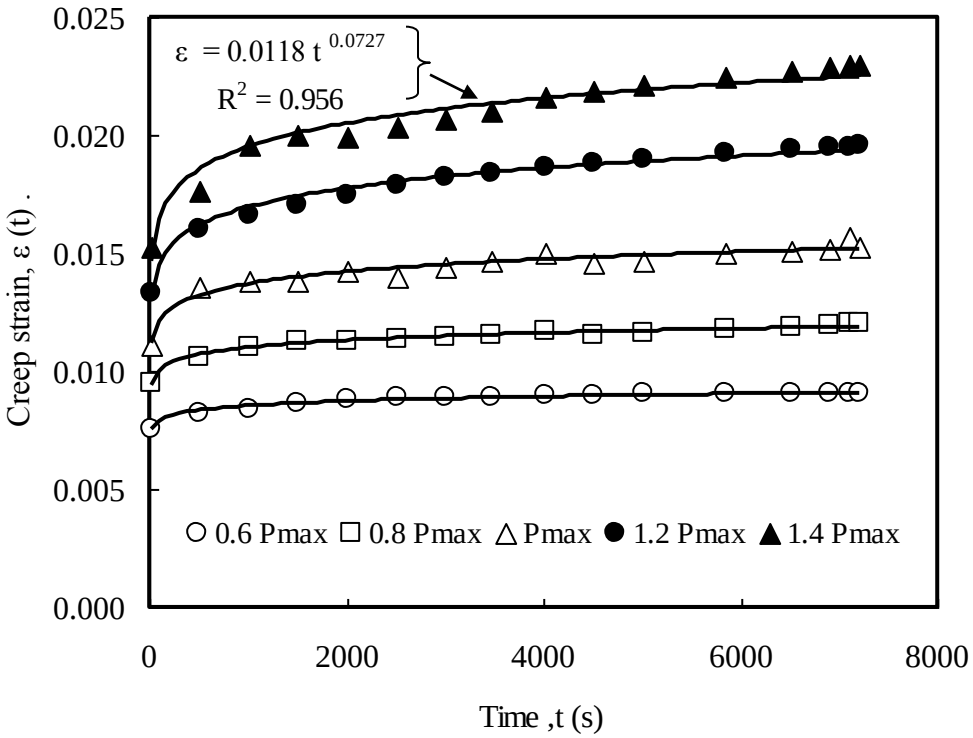

Fig. 7.14b Short-term experimental creep performance of SFLS

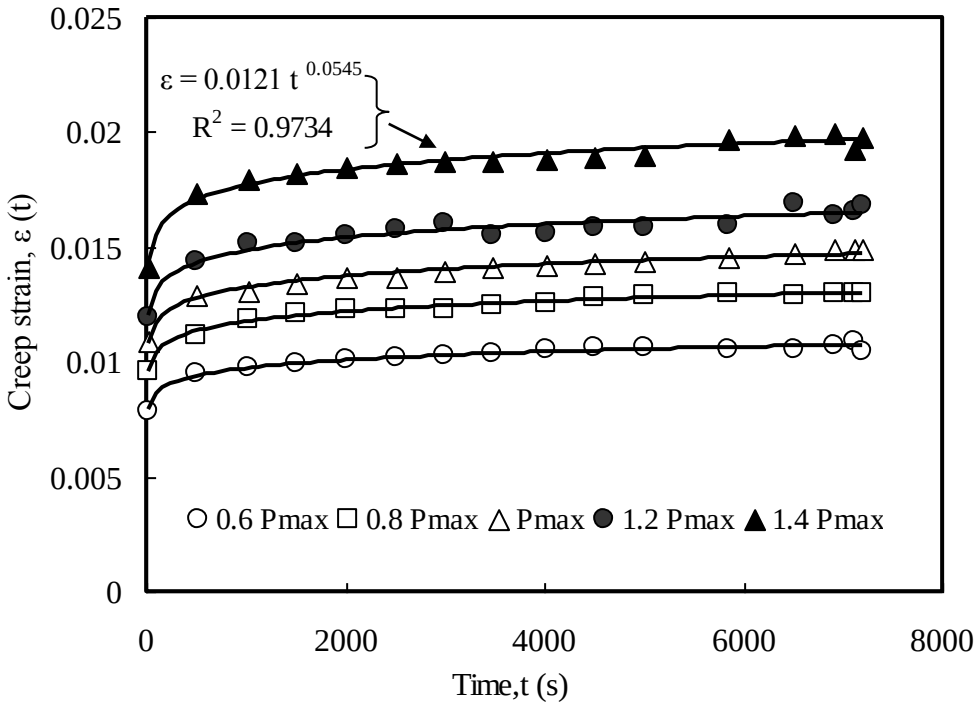

Fig. 7.14c Short-term experimental creep performance of UFLS

Table 7.1 Power law parameters for leaf spring

Material	Constants	Load				
		$0.6P_{max}$	$0.8P_{max}$	P_{max}	$1.2P_{max}$	$1.4P_{max}$
Long glass fiber reinforced leaf springs	Power law coefficient ($\varepsilon_t^{'}$)	0.007	0.009	0.010	0.012	0.013
	Power law exponent (n)	0.011	0.012	0.023	0.023	0.029
	Correlation index (R^2)	0.878	0.921	0.947	0.971	0.986
Short glass fiber reinforced leaf springs	Power law coefficient ($\varepsilon_t^{'}$)	0.006	0.008	0.009	0.010	0.011
	Power law exponent (n)	0.032	0.039	0.052	0.067	0.072
	Correlation index (R^2)	0.974	0.983	0.965	0.985	0.956
Unreinforced leaf springs	Power law coefficient ($\varepsilon_t^{'}$)	0.006	0.008	0.009	0.010	0.012
	Power law exponent (n)	0.051	0.052	0.052	0.053	0.054
	Correlation index (R^2)	0.978	0.989	0.984	0.954	0.973

The correlation index (R^2) indicates that power law function provides a good approximation to the visco-elastic behavior at every stress levels. It is vivid from figures 7.14(a-c) that the power law coefficient ($\varepsilon_t^{'}$) and power law exponent (n) were dependent on the stress level and increases with the increase in stress level. Since the power law coefficient ($\varepsilon_t^{'}$) and power law exponent (n) are sensitive to the stress level, a methodology adopted by Hadid *et al*. (2002) was used to establish the dependence of power law coefficient ($\varepsilon_t^{'}$) (figure 7.15) and power law exponent (n) (figure 7.16) on applied stress level. Figure 7.15 shows the best fitting curve using equation 7.5 and depicts the influence of applied stress (σ) on power law coefficient ($\varepsilon_t^{'}$) for the test leaf springs. The constant curve fitting parameters (a, b from equation 7.5) are also shown in figure 7.15.

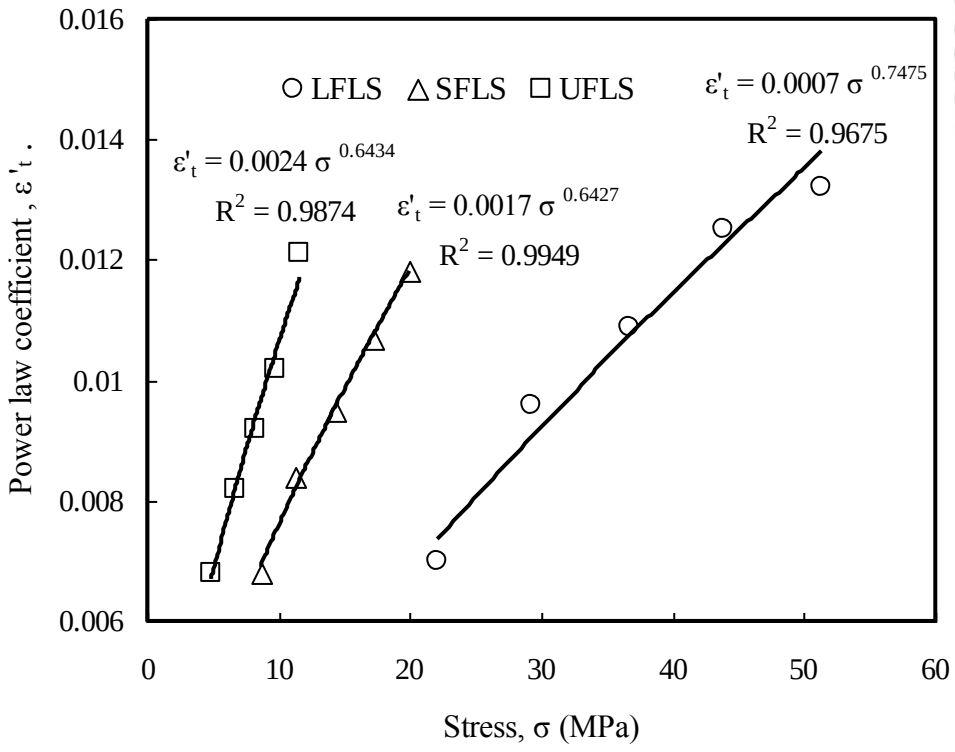

Fig. 7.15 Variation of power law coefficient over leaf spring stress

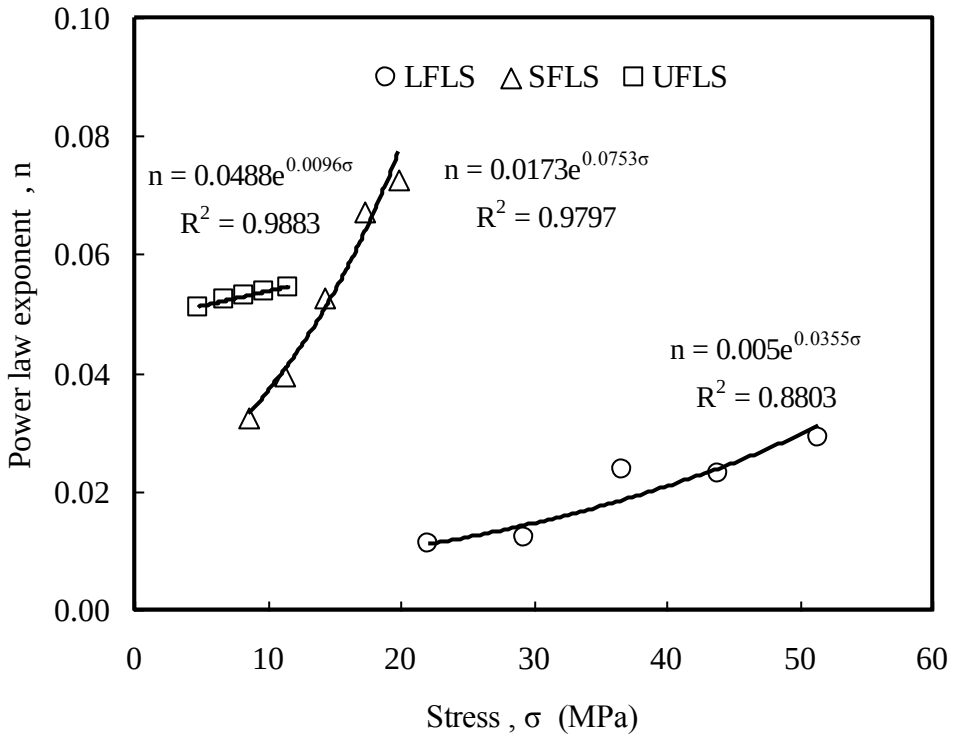

Fig. 7.16 Variation of power law exponent over leaf spring stress

In general, the constant parameters *a* and *b* are dependent on glass transition temperature, degree of crystallinity and fiber orientation in the composite (Chevali *et al*., 2009). These parameters represent the instantaneous strain which is normally visualized during the initial period of load application. Figure 7.16 shows the best fitting curve using equation 7.6 and elucidates the influence of applied stress (σ) on power law exponent (n) for the test leaf springs. The constant curve fitting parameters (c and e from equation 7.6) are also shown in figure 7.17. The constant parameters c and e are dependent on the time period of testing and relaxation mechanisms involved for the composite (Chevali *et al*., 2009). These parameters represent the viscous response visualized during the secondary creep process. Equation 7.7 was used to predict creep performance of molded leaf spring and compared with the 24 h experimental data as shown in figures 7.17(a-c).

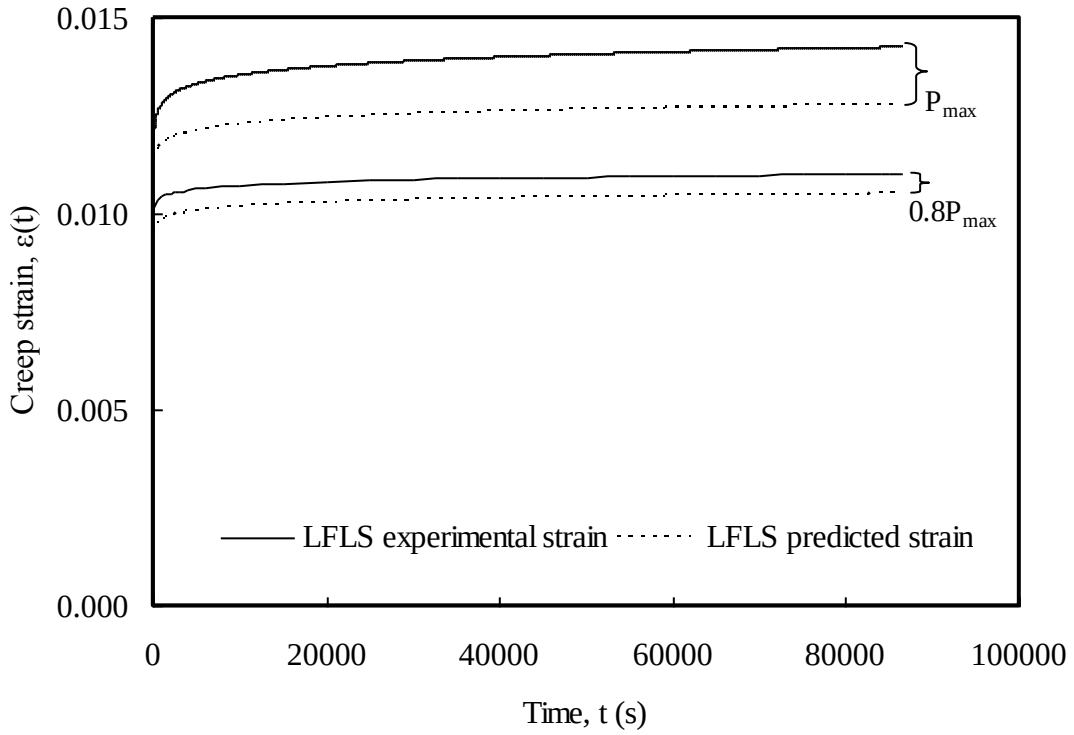

Fig. 7.17a Experimental and predicted creep performance of LFLS

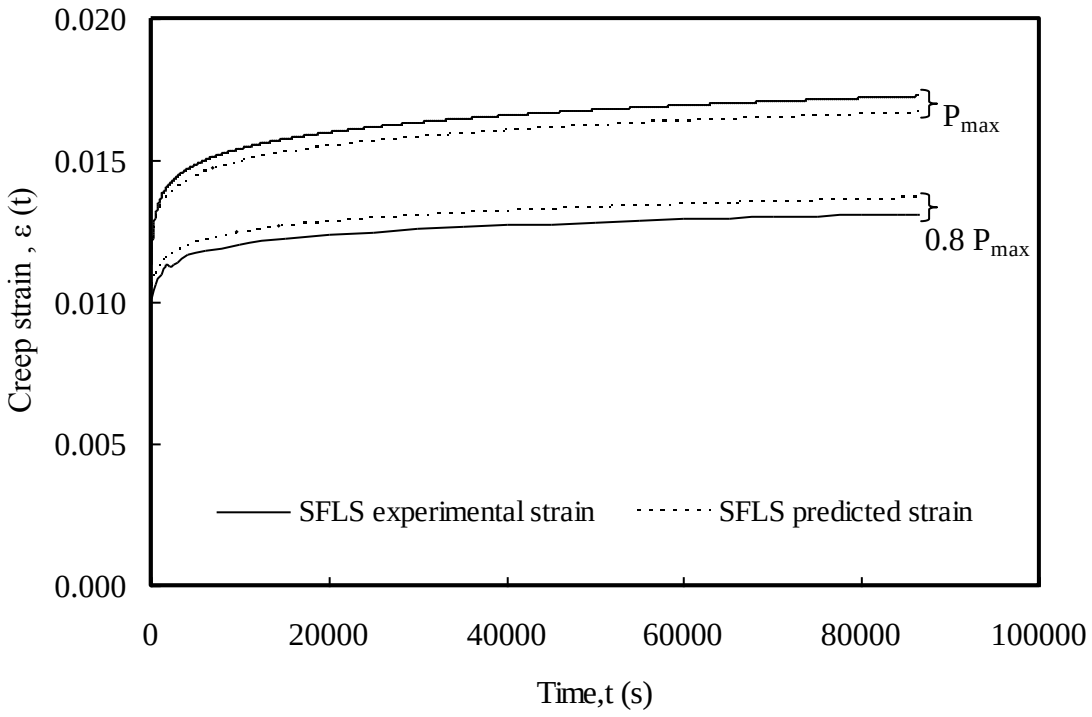

Fig. 7.17b Experimental and predicted creep performance of SFLS

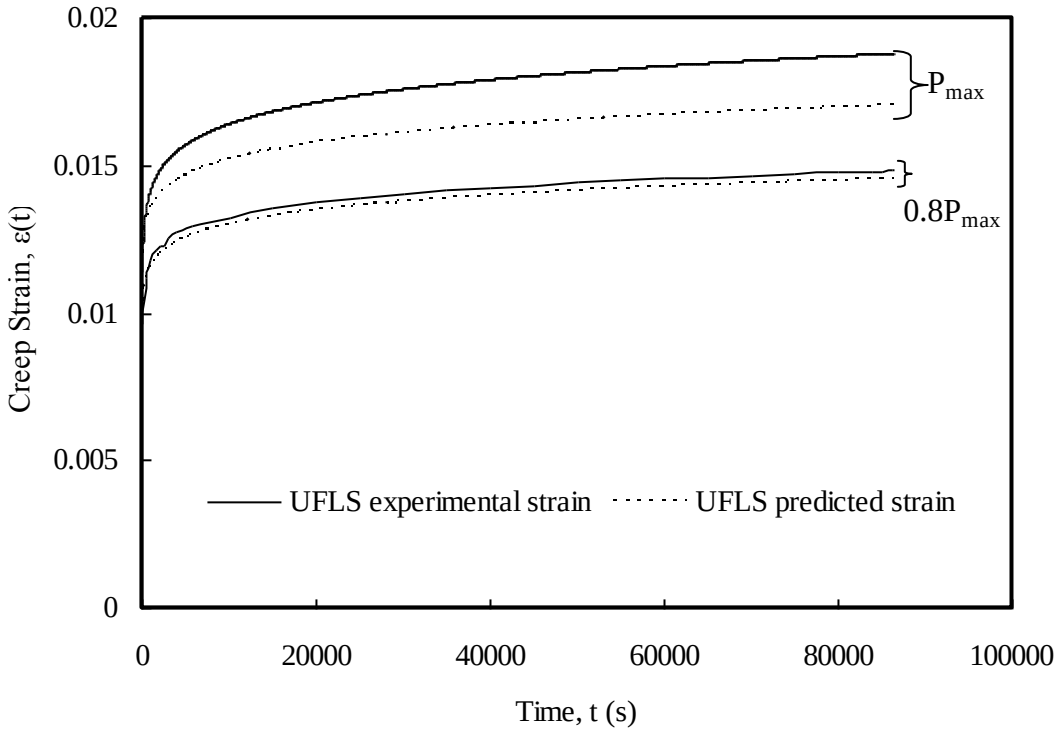

Fig. 7.17c Experimental and predicted creep performance of UFLS

The deviation between the predicted creep strain and experimental creep are shown in Table 7.2. It is found that HRZ model predicted well with the experimental creep performance of the chosen thermoplastic composite leaf springs. Furthermore it was observed that at a loading level of 0.8 $P_{max,}$ the error between experimental and predicted creep strain was less than loading level at P_{max}. Similar observations were visualized by Hadid *et al*. (2002) where the error between experimental and predicted values was high at higher stresses.

Table 7.2 Comparison of HRZ model predicted strain and experimental strain

Material	Loading level	Experimental Creep strain	HRZ predicted Creep strain
Long glass fiber reinforced leaf springs	P_{max}	0.0141	0.0123
	0.8 P_{max}	0.0112	0.0102
Short glass fiber reinforced leaf springs	P_{max}	0.0171	0.0168
	0.8 P_{max}	0.0136	0.0131
Unreinforced leaf springs	P_{max}	0.0188	0.0170
	0.8 P_{max}	0.0148	0.0145

7.5.4 Influence of Material Crystallinity on Power Law Coefficient

Prior investigation with HRZ model for predicting the creep behavior of thermoplastic materials was limited (Hadid *et al*., 2002; Chevali *et al*., 2009). Hadid *et al*. (2002) have not attempted to correlate parameters with any of the material behavior. Chevali *et al.* (2009) reported that the power law coefficient depends on material characteristics which include degree of crystallinity, glass transition temperature and fiber orientation, however, no specific correlations with any behavior was attempted.

In the present investigation, the evaluated power law coefficient ($\varepsilon_t^{'}$) of UFLS, SFLS and LFLS corresponding to 11.55, 19.95 and 22.05 MPa stress were 0.012, 0.011 and 0.007 respectively (Table 7.1). The crystallite size of investigated leaf spring materials; unreinforced, short glass fiber reinforced and long glass fiber reinforced polypropylene were 100.330, 118.615 and 146.784 Å respectively. Detailed methodology and mechanisms were reported in Chapter 4 (Section 4.3.3).

From the crystallite size and power law coefficient, it was confirmed that increase in crystallinity reduced the power law coefficient.

To confirm this correlation further, experimental creep data of Banik *et al.* (2008) was also considered. Banik *et al*. (2008) experimentally evaluated the creep performance of unidirectional polypropylene composites and crossply laminates at various loads and temperatures and compared with an empirical model. In the present investigation, experimental creep response of Banik *et al.* (2008) was extracted and analyzed using data capturing software Windig 2.5, where the creep test was conducted at 30° C for an applied stress of 10 MPa. The extracted creep data results were found to be fit with the power law function. The evaluated power law coefficient of crossply laminates and unidirectional composites were found to be 0.1831 and 0.0729 respectively. Banik *et.al* (2008) measured and reported the crystallinity of crossply laminates and unidirectional composites as 49.5 and 51.0 % respectively. Thus, it was confirmed that increase in material crystallinity reduced the power law coefficient.

7.6 SUMMARY

This chapter discussed the fatigue and short-term flexural creep performance of the mono composite leaf spring.

- Fatigue performance of injection molded thermoplastic composite leaf springs under pulsating compression mode was investigated at various alternating loading levels, wherein performance of leaf spring was found to be improved with the fiber length.
- Increase in deflection and relative spring rate were continuously measured and used as a damage index. Reduction in spring rate was dependent on the applied

stress level for all the leaf springs, and found to be reduced with the increase in fiber length.

- Short fiber reinforced and unreinforced polypropylene leaf springs exhibited 10 % drop in spring rate, whereas long glass fiber reinforced polypropylene leaf spring exhibited fracture failure at tensile surface.
- Creep performance of the molded leaf springs were experimentally evaluated for 2 h and short term creep performance (24 h) was predicted with the aid of HRZ model over wide range of stress. The predicted performance was compared with 24 h experimental results and found to be satisfactory. HRZ model parameters were also utilized to correlate investigated leaf spring material characteristics.

CHAPTER 8

JOINT PERFORMANCE OF THERMOPLASTIC LEAF SPRINGS

8.1 INTRODUCTION

Suspension leaf springs ends are connected to the vehicle chassis and this joint strength must be higher than that of designed leaf spring (Yu and Kim, 1998). Bolted and adhesively bonded joints are commonly utilized for joining the composite structures. Bolted joints are found to be more useful than adhesive bonded joints, due to the superior load transfer, less sensitive to the surface condition and easy to repair (Camanho and Matthews, 1997). Stress concentration plays a significant role in the performance characteristics of the bolted joint strength (Shokrieh and Rezaei, 2003). Tension, shear, bearing, cleavage and pull-through failure modes are the most commonly observed failure modes observed in the bolted joints performance (Thoppul *et al*., 2009). Static and dynamic performances of the composite pinned joints are exceedingly influenced by the joint geometry, environment and testing conditions (Stockdale and Matthews, 1976; Crews, 1981; Lim, 2006; Aktas, 2009). Bearing response of the joint is affected due to the clearance between fastener and hole (McCarthy *et al.*, 2005). Unlike the static mode of failure, fatigue damage should address the progression of damage. Joint damage due to the fatigue can be investigated by measuring the hole elongation with the aid of hysteresis loop (Crews, 1981; Chen, 2001). Composite constituent properties significantly alter the bearing strength performance (Pinnell, 1996).

This chapter presented the parametric investigation of leaf spring joint using finite element analysis. Experimental static and fatigue performance of the chosen composite leaf spring joints were reported in this chapter. Failure morphology of the leaf spring joints was also presented in this chapter to understand the influence of fiber length towards joint performance.

8.2 DESIGN OF JOINT CONFIGURATION

8.2.1 Joint Geometry and Design Methodology

Figure 8.1a shows the detailed geometry of injection molded leaf spring. Flat end portion of the molded leaf spring was considered for the joint strength evaluation. Sectioned geometry from the molded leaf spring is shown in figure 8.1b. Two parallel pin joint with lateral support was chosen for leaf spring application. Based on the bolt design, hole diameter of the joint was chosen as 4 mm. Total length of the plate (L+E) was taken as 30 mm due to the available flat portion of the leaf spring geometry without any curvature as shown in figure 8.1a. Length and width of the chosen specimen are represented as (L+E) and W respectively. Distance between two holes and the distance from the edge are M and K respectively. E is the distance from the free edge to the centre of the hole. Parametric joint strength evaluation was carried out using FEA tool, AnsysR10® and the solution was obtained by varying the value of E from 4 to 7 mm and M from 6 to 18 mm for a fixed width of 25 mm inorder to achieve high bearing strength.

(a)

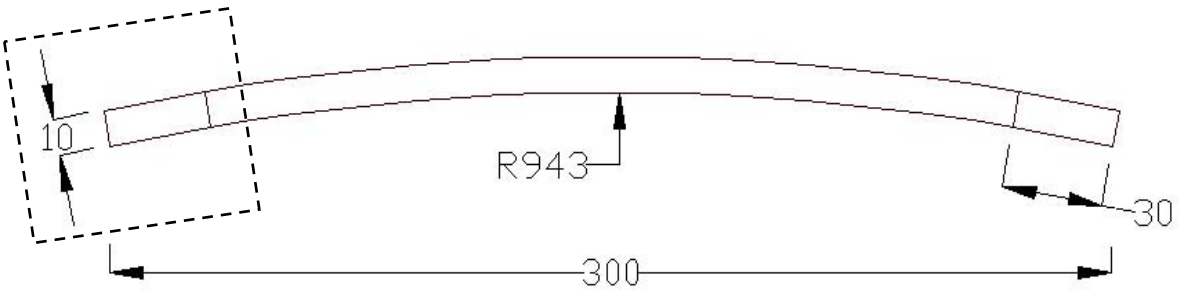

(b)

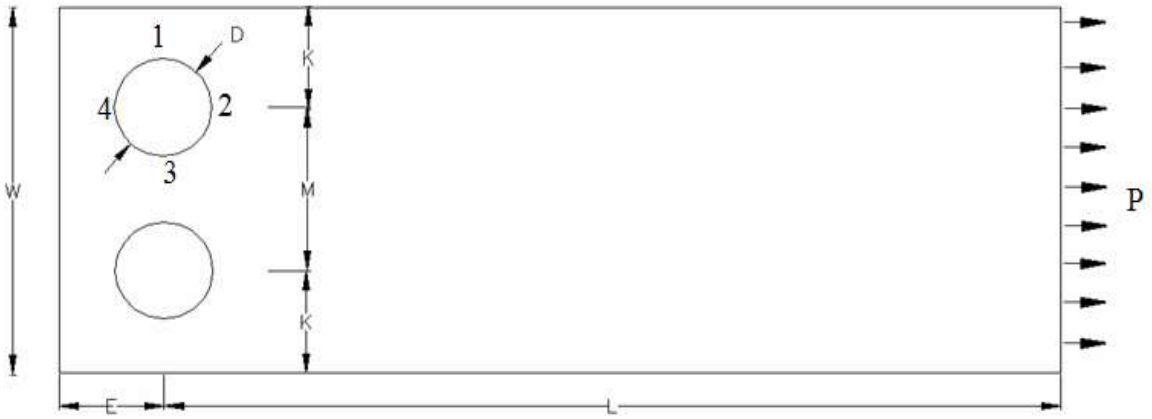

Fig. 8.1 Geometry of molded leaf spring and the proposed joint (a) front view indicating straight portion (marked) (b) sectioned flat portion

8.2.2 Parametric Study using Finite Element Analysis

Quasi-static failure analysis was performed on chosen joint geometry using commercial finite element software, Ansys10®. The composite plate was modeled using SOLID-45 element as a half model due to the symmetry of loading, geometry and material used. This element is defined by eight nodes having three degrees of freedom at each node. The element supports plasticity, large deflection and large strain capabilities.

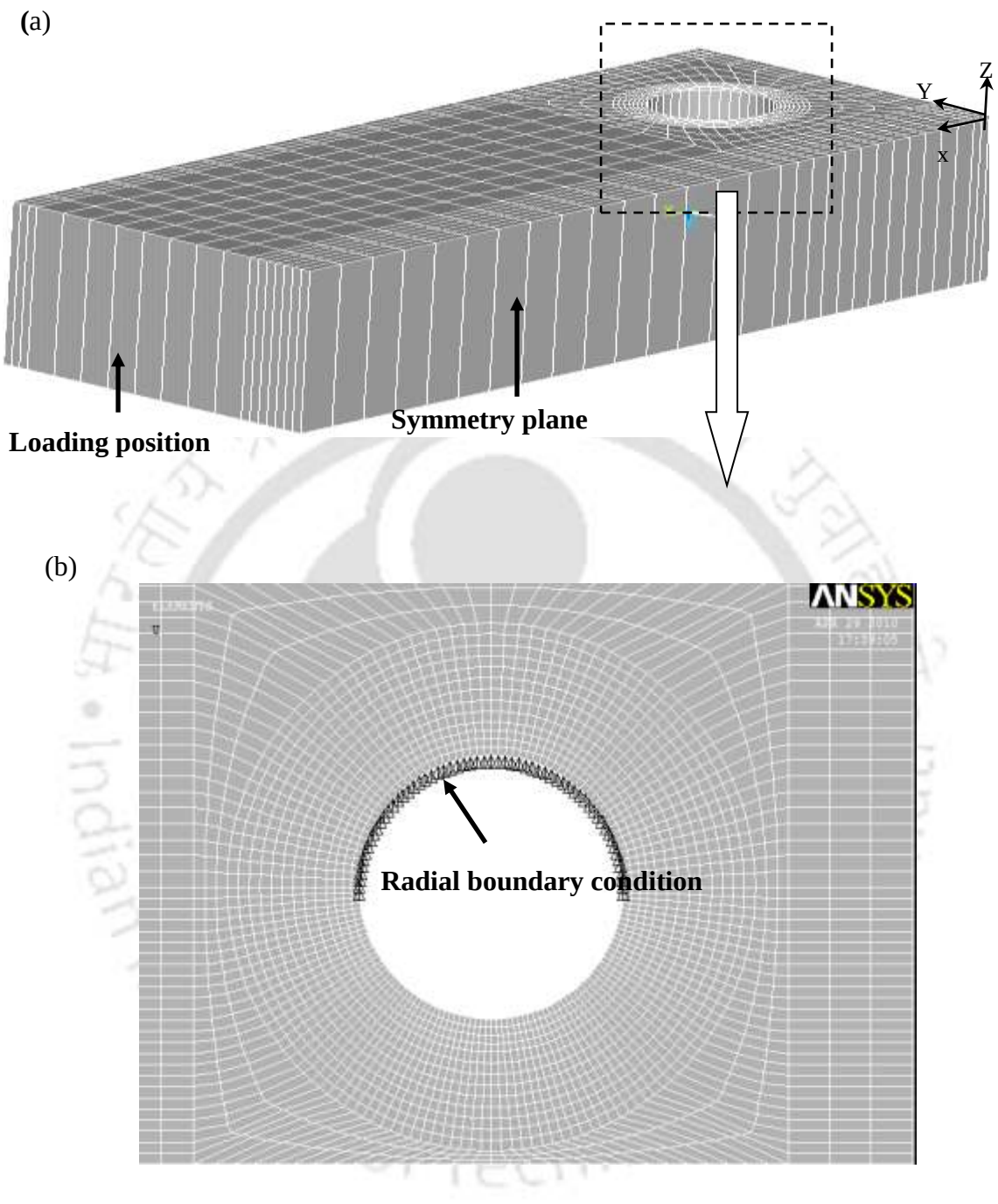

Fig. 8.2 Finite element model of the proposed joint (a) boundary condition and loading position of the composite plate (b) fine radial mesh near the hole

Finite element mesh for the chosen plate is shown in figure 8.2. The meshing of the plate is similar to that of used by Ireman (1993), and mesh density is greater near the

holes as shown in figures 8.2(a-b). To simulate the quasi-static loading pattern, non-linear geometry effects was considered and displacement was applied at the bottom of the plate with small increments (sub steps). The displacement of the symmetry surface was zero in Y direction. To simulate the rigid pin, radial displacement constraints were used on the right hand side of the hole. Von-Mises failure criterion was utilized to estimate the joint strength. Tension, shear, and bearing (figure 8.3) were the most commonly observed failure modes during static and dynamic performance of the bolted joints (Camanho and Matthews, 1997). To illustrate the failure mode for various joint end configurations, circumference of the hole was marked as 1, 2, 3 and 4 and shown in figure 8.1b. Failure at location 1 or 3 is due to the net tension, failure at 4 is due to the cleavage (shear-out) and failure between 1 and 2 or between 1 and 4 is due to the mixed mode (net tension and bearing).

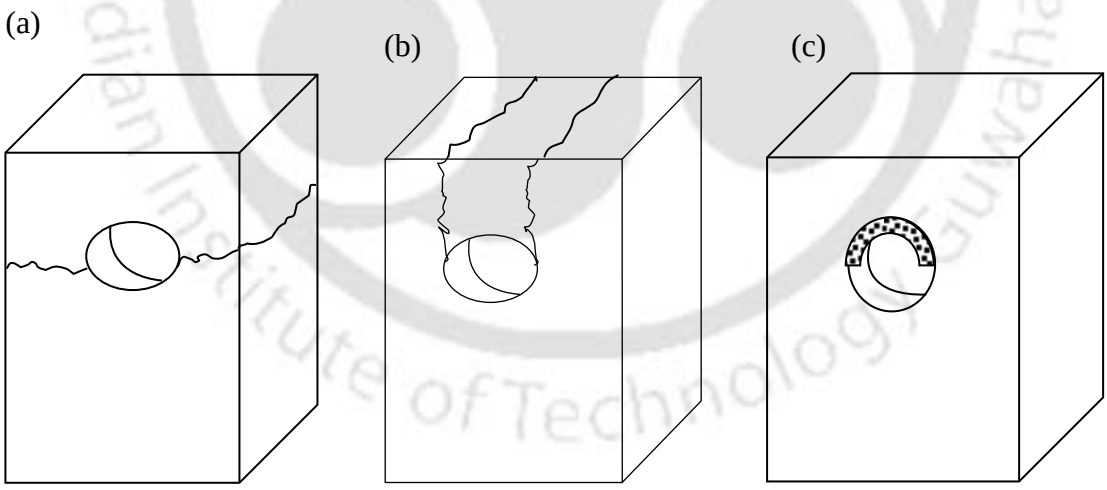

Fig. 8.3 Major types of joint failure (a) net-tension failure (b) shear-out failure (c) bearing failure

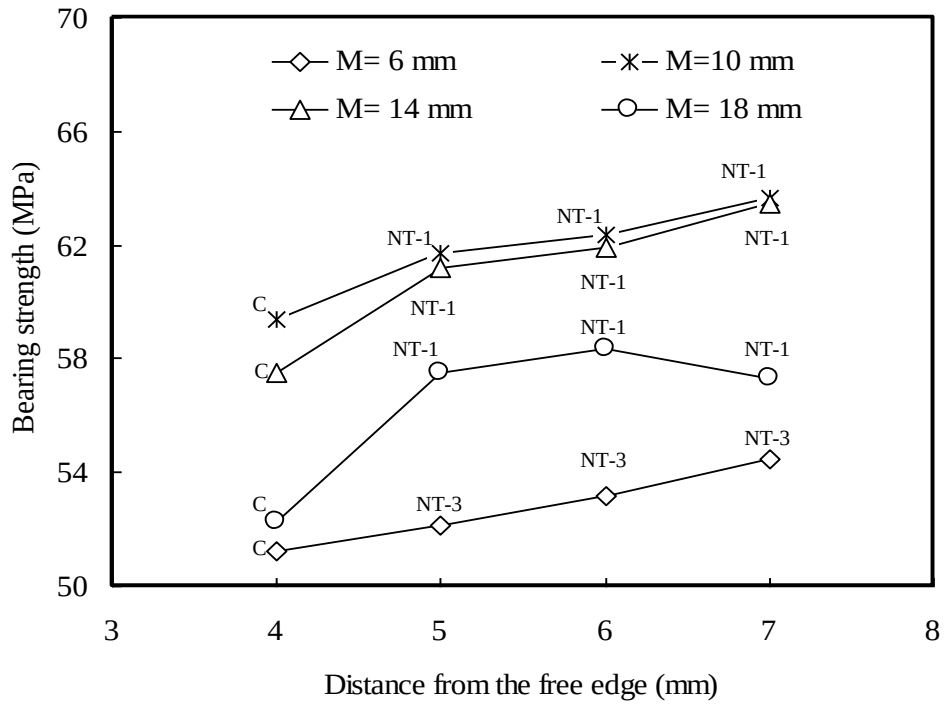

Fig. 8.4 Influence of design parameter over bearing strength and failure modes

Figure 8.4 shows the influence of bearing strength on hole position from the free edge (E) and distance between hole center (M). Failure mode was also marked for the entire joint configurations. C represents cleavage (shear-out), NT-1 represents net tension at site 1 and NT-3 represents net tension at site 3. It was observed from the numerical analysis, joint strength was found to be inferior at E = 4 mm and M = 6 mm and superior at E = 7 mm and M = 10 mm. Maximum bearing strength of 63.7 MPa was obtained for this configuration.

For a constant value of width (W), the load carrying capacity of the joint increases with the increase in free edge distance to the centre of the hole (E). With the increase in hole position from free edge (E), change in failure mode from cleavage (figure 8.5a) at point 4 to net tension at 1 was observed (figure 8.5b). The bearing strength variation for M =10 mm and 14 mm was very less. In both the configurations the maximum stress occurred at same site 1. For M = 6 mm, the failure site is at 3 and net tension failure between the holes is observed resulting in reduced bearing load. For M = 18 mm, maximum stress occurred at point 1 similar to that of M = 10 and M = 14 mm. Since the edge of the plate was closer to the hole, the bearing strength was less for M = 18 mm. FEA results suggest that superior joint strength can be achieved at E = 7 mm and M = 10 mm, however due to the experimental constraint in gripping the free end (to avoid slipping of the pin from the lower gripper), end distance corresponding to E = 5mm was chosen for the experimental investigation. Thus, joint with E = 5 mm and M = 10 mm was chosen for the experimental evaluation.

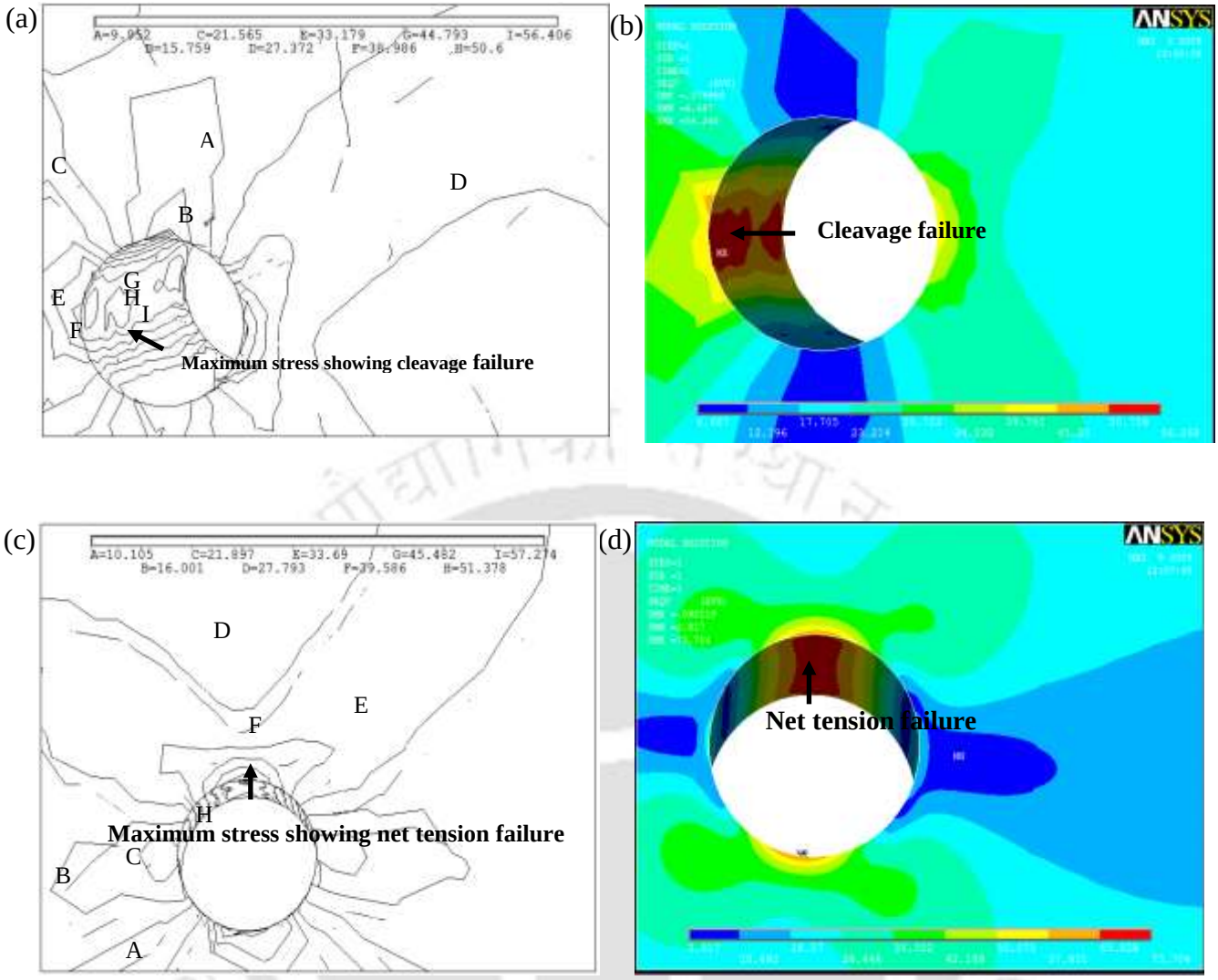

Fig.8. 5 Failure modes on the end joint (a) cleavage failure at E = 4 mm M =10 mm (b) cleavage failure at E = 4 mm M =18 mm (c) net -tension failure at E = 7 mm M =10 mm (d) net -tension failure at E = 7 mm M =18 mm

8.3 JOINT STRENGTH EVALUATION METHODOLOGY

Schematic of considered end section for the joint strength evaluation is shown in figure 8.6. Drilling was cautiously done with the aid of appropriate fixtures to reduce/avoid delamination defects. In addition, discontinuous fibers do not cause any delamination defect unlike continuous fiber composite during drilling. The schematic and experimental arrangement made for the joint performance evaluation is shown in figure 8.8.

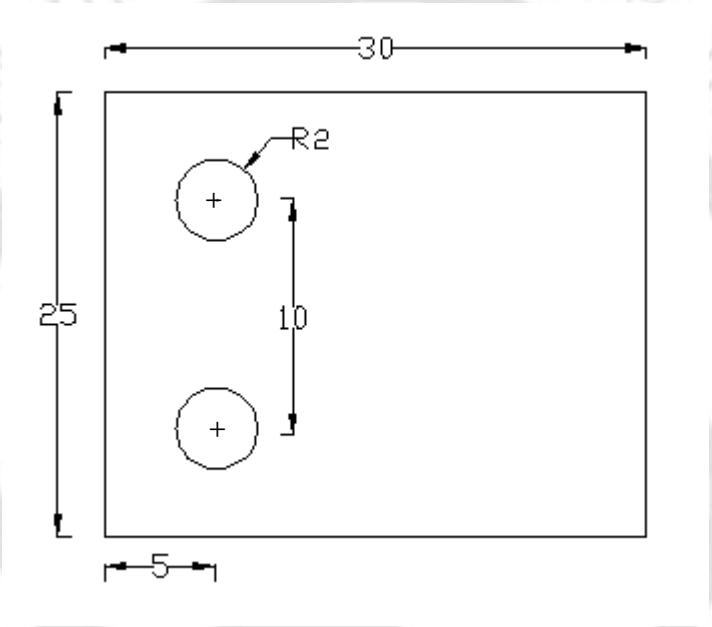

All Dimensions are in mm

Fig.8. 6 Geometry of flat end portion of molded leaf spring for the joint strength evaluation

Servo hydraulic testing facility (Instron 8801) was used for testing joint strength under static and dynamic conditions. Double bolted joint with lateral support was utilized to connect the leaf spring end with steel plate. Bolt diameter of 4 mm was chosen for joining the metal plate with the end of the molded leaf spring. Hydraulic wedge grip of the test facility was utilized for holding the steel plate and sectioned

end part of the molded leaf spring in a plane. Tensile load was applied at the free edge of the composite plate with steel plate fixed on the other side.

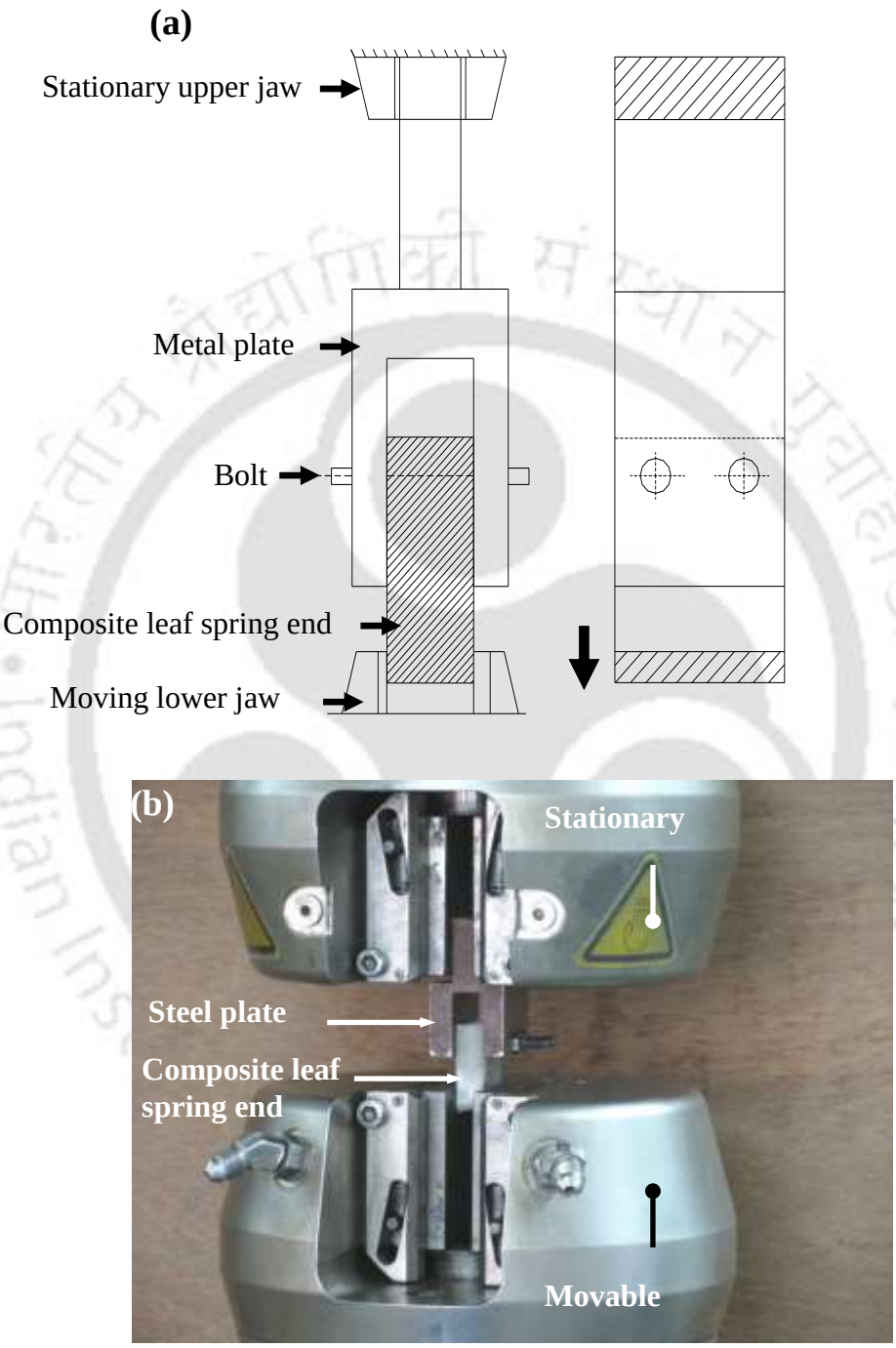

Fig. 8.7 Experimental test setup to evaluate the performance of bolted end joint of leaf spring end (a) schematic figure (b) view of fixture holding leaf spring end and steel plate

Load and cross-head displacements were continuously measured and acquired with the help of the inbuilt data acquisition system of the servo hydraulic testing machine. Joint strength under tensile mode was evaluated under ambient room condition (23°C and 50 % humidity) at constant crosshead speed of 5mm/min. Tests were repeated for at least three times and the deviation was found to be within ± 4 % and the average value is used for further analysis. Maximum load obtained from the load-deflection curve was considered for computing the bearing strength for all the chosen leaf spring.

To understand the influence of bolt-hole clearance on test joint performance, clearance of 200, 400 and 600 µm and interference of 20 µm were considered for the investigation in short fiber reinforced leaf springs. Prior work on the effect of clearance on thermoset composite joint strength investigation (Rowlands *et al*., 1982; Scalea *et al*., 1999) also recommended this range of fit between the bolt and hole. The above desired test clearances were achieved by machining hardened steel pins to a size of 4.02, 3.80, 3.60, and 3.40 mm. Machined steel pin diameters were measured using a micrometer of 1 µm accuracy. Joint strengths were evaluated under tension mode at a constant cross-head speed of 5mm/min.

Fatigue tests for joints were performed with out keeping clearance under completely reversed mode (stress ratio, R = -1). Various alternating load amplitudes were chosen on the basis of the percentage of ultimate bearing strength of the leaf spring joint. Loading frequency of 0.5 Hz was chosen for all the test loads. Joint damage during fatigue was investigated by measuring the hole elongation with the aid of hysteresis loop. Figure 8.8 shows the schematic load-deflection hysteresis loop during the fatigue test. Hole elongation (Δ_N) due to the fatigue can be obtained by subtracting the fastener translation after N_f fatigue cycles (δ_N) and fastener translation

(δ_i) at the initial cycle. Grant and Sawiki (1993) utilized similar technique to measure hole elongation /fastener translation during fatigue.

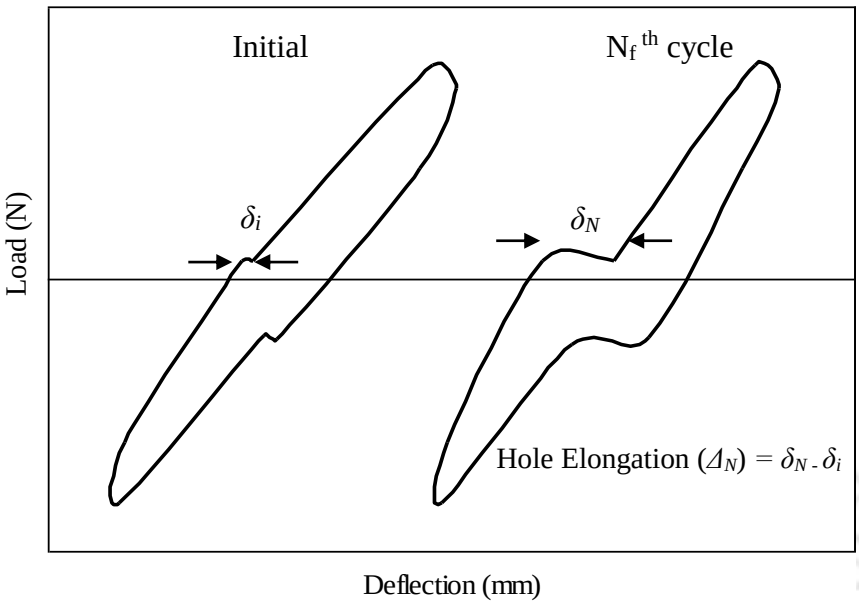

Fig.8.8 Schematic end joint load-deflection hysteresis plot during fatigue

8.4 STATIC JOINT STRENGTH PERFORMANCE

8.4.1 Effect of Fiber Length on Static Joint Strength

Leaf springs in service transmit significant amount of load to the connecting end. These joints are expected to withstand the design load of leaf spring; hence joint strength evaluation is of practical importance. The bearing stress-strain plot of double bolted lap joint of long glass fiber reinforced polypropylene leaf spring (LFLS), short glass reinforced polypropylene leaf spring (SFLS) and unreinforced polypropylene leaf spring (UFLS) is shown in figure 8.9.

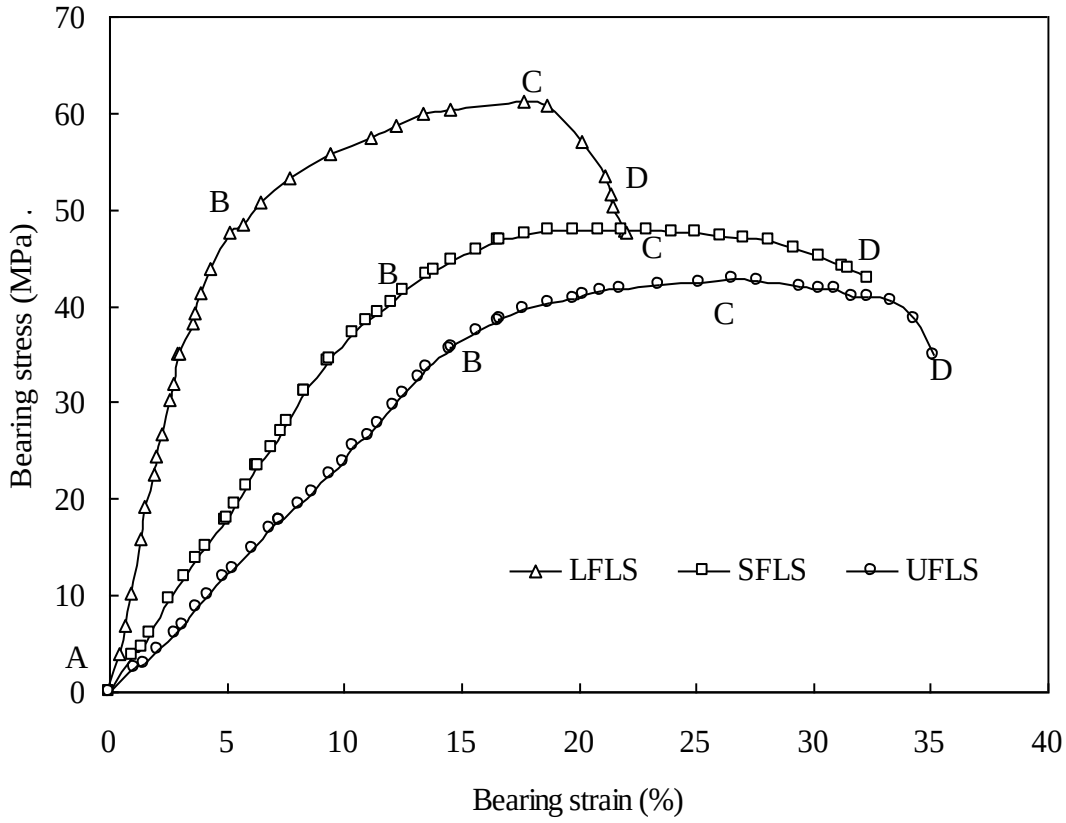

Fig. 8.9 Bearing stress -strain curve of test joints

The bearing stress σ_b was evaluated using following relation

$$\sigma_b = \frac{P}{2dt_p} \tag{8.1}$$

where P is maximum load obtained before failure; d is hole diameter and t_p is thickness of the composite plate. The maximum load reached before failure for LFLS, SFLS and UFLS joints were 4.81, 3.84 and 3.39 kN respectively. Thus, test leaf springs are found to have sufficient end joint strength in view of the estimated design load of 500 N for all the chosen leaf springs. Increase in fiber length results in efficient load transfer from the matrix to the fiber, thereby improving the load carrying capability.

The bearing strain was evaluated using the following relation proposed by McCarthy *et al.* (2005)

$$\xi_b = \frac{\delta_p}{Kd} \tag{8.2}$$

where ξ_b is the bearing strain, δ_p is the fastener/pin displacement, d is the hole diameter and K = 2 for double shear joint with two fasteners. It is observed from figure 8.9 that the stiffness of the bolted joint is improved with increase in fiber length. The joint stiffness computed from the initial linear portion (AB) of the bearing stress-strain curve were 9.94, 3.38, and 2.49 kN/mm for LFLS, SFLS and UFLS joints respectively. Beyond this linear portion, test joints exhibited significant stiffness drop as indicated by the curve BC, until a maximum bearing stress is attained.

The joint failure of LFLS, SFLS and UFLS occurred at a corresponding strain of 20.3, 33.0 and 35.2 % respectively. Thus, reduction in bearing strain prior to the composite failure was confirmed with the increase in fiber length. Failure morphology of all the leaf spring joints under static loading condition exhibited mixed mode failure (tension and bearing failure) as shown in figure 8.10. Hole extension was visualized for all the leaf spring joints and confirmed the bearing damage prior to net-tension failure. Karakazu *et al.* (2008) investigated the influence of geometric parameters over the failure of glass fiber reinforced vinyl-ester plates having similar joint configuration as in the present investigation. Mixed mode of failure was observed (tension and bearing failure), when the ratio of edge distance to the hole diameter (E/d) was between 1 and 5 and the ratio of the distance between two holes to hole diameter (M/d) was 2. It is to be noted in the present investigation that, E/d is 1.25 and M/d is 2.5.

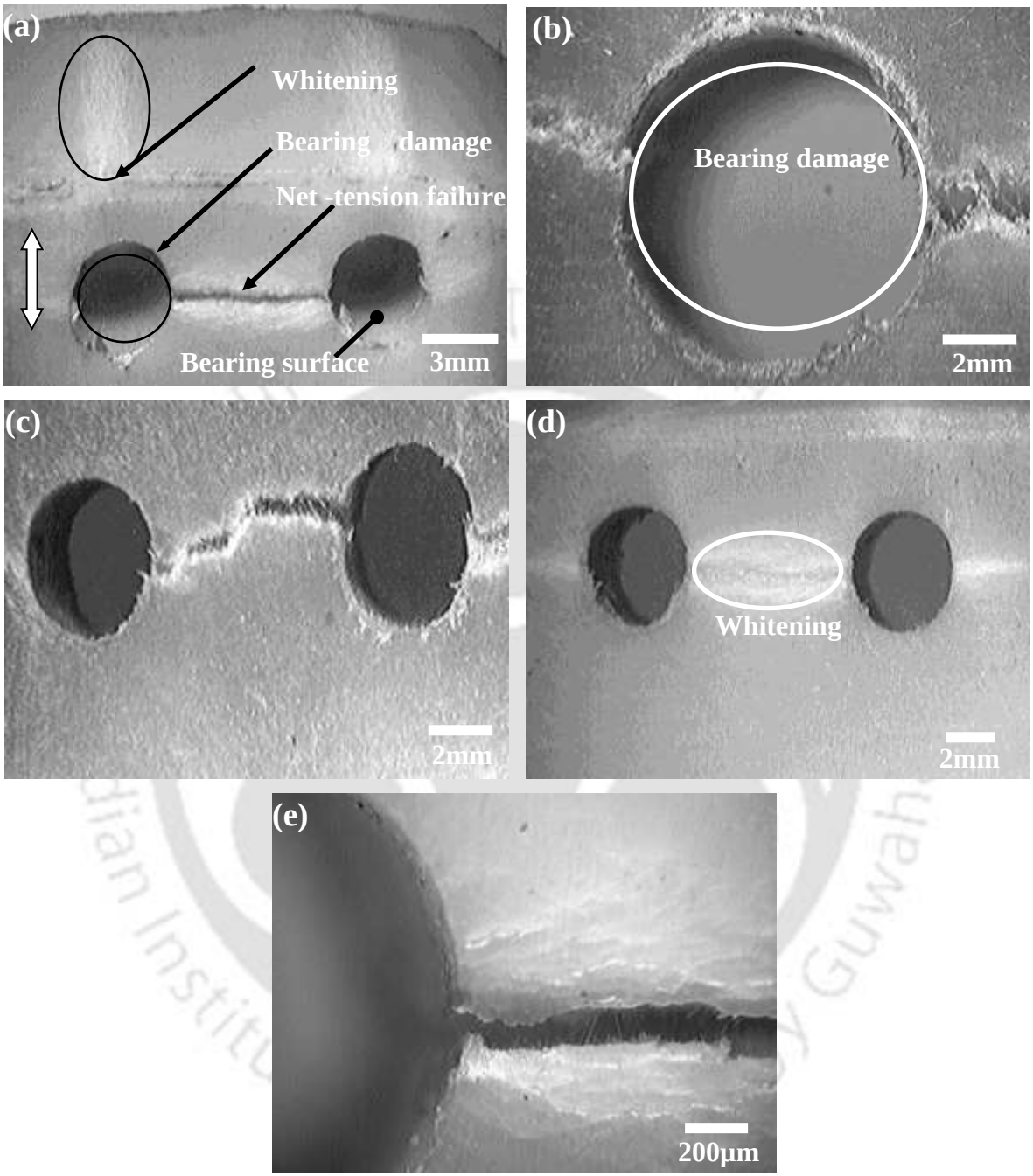

Fig.8.10 Failure morphology of leaf spring joint (a) bearing damage along with net tension failure for SFLS (b) hole extension indicating bearing damage for LFLS (c) net tension failure in LFLS (d) whitening region in UFLS (e) matrix failure along with fiber breakage in SFLS

Figures 8.10 (a and b) show the local damage near the SFLS and LFLS hole with hole elongation. Stiffness drop (BC) in the bearing stress-strain plot (figure 8.9) prior to failure confirmed this behavior. Crack linking between the two holes of the composite plate and perpendicular to the loading direction confirmed the net-tension failure (figures 8.10(a-d)) for all the materials. Stress whitening near the cracked region was visualized in SFLS and UFLS joints (figures (8.10 (a and d)). In general, stress whitening in composites indicates the occurrence of localized yielding with plastic deformation prior to failure (Gong *et al*., 2006). Stress whitening was not visualized in LFLS joint which confirmed the absence of localized yielding near the hole due to the reduced ductility of the composite. The failure site near the hole surface of SFLS depicts the visibility of separated matrix along with the fibers (figure 8.10e). The failure morphology of the bolted composite joints confirmed the bearing failure (stiffness loss) in the early stages followed by the net-tension failure.

Since the chosen leaf spring joints were subjected to bearing damage prior to net tension failure, the failure morphology at the bearing surface was investigated by sectioning the composite leaf spring end as shown in figure 8.11. Though tensile load acted on the joint and net tension failure mode was observed at the joint (figures 8.10(a-e)), the failure morphology of the bearing surface showed severe matrix fibrillation (figures 8.12(a-d)). This fibrillation feature was observed at various locations of the bearing surface. This type of severe matrix deformation and fibrillations are not commonly observed under uniaxial loading condition.

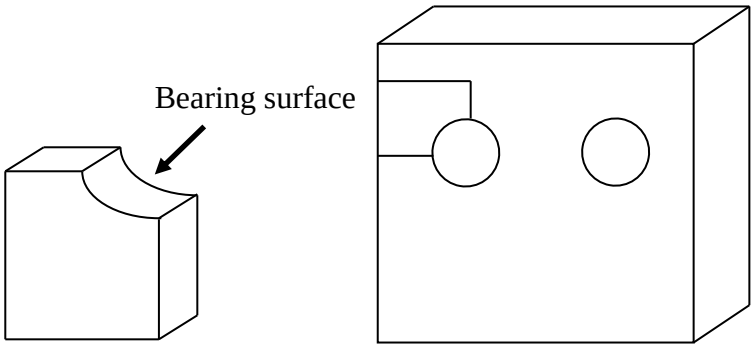

Fig.8. 11 Bearing surface of the leaf spring end

The curved surface of bearing area induced bi-axial stresses in spite of uniaxial load acted at the joint. This bi-axial stress induced severe matrix deformation and matrix fibrillation as observed in figures 8.12(a-d). To substantiate this fact further, flat fractured surface of the SFLS and LFLS tensile specimens were examined. Static tensile test as per ASTM D 638 standard at a strain rate of 5 mm/min was performed on 20 % short and long glass fiber reinforced polypropylene. The flat fractured surface of the tensile test specimen is shown in figures 8.12 (e-f). In this flat fractured surface of the tensile specimen, neither severe matrix deformation nor matrix fibrillations was observed for both the materials.

Bearing surface corresponding to SFLS joint (figures 8.12 (a-b)) shows extensive matrix fibrillation than LFLS joint bearing surface (figures (8.12 (c-d)) due to the pronounced ductility of the composite. Thus, failure morphology confirmed that LFLS joint exhibited less bearing damage than SFLS joint due to the reduced matrix ductility. Since the bearing response of the composite joint is significantly influenced by fastener hole clearance, investigation of clearance towards bearing strength is of practical importance.

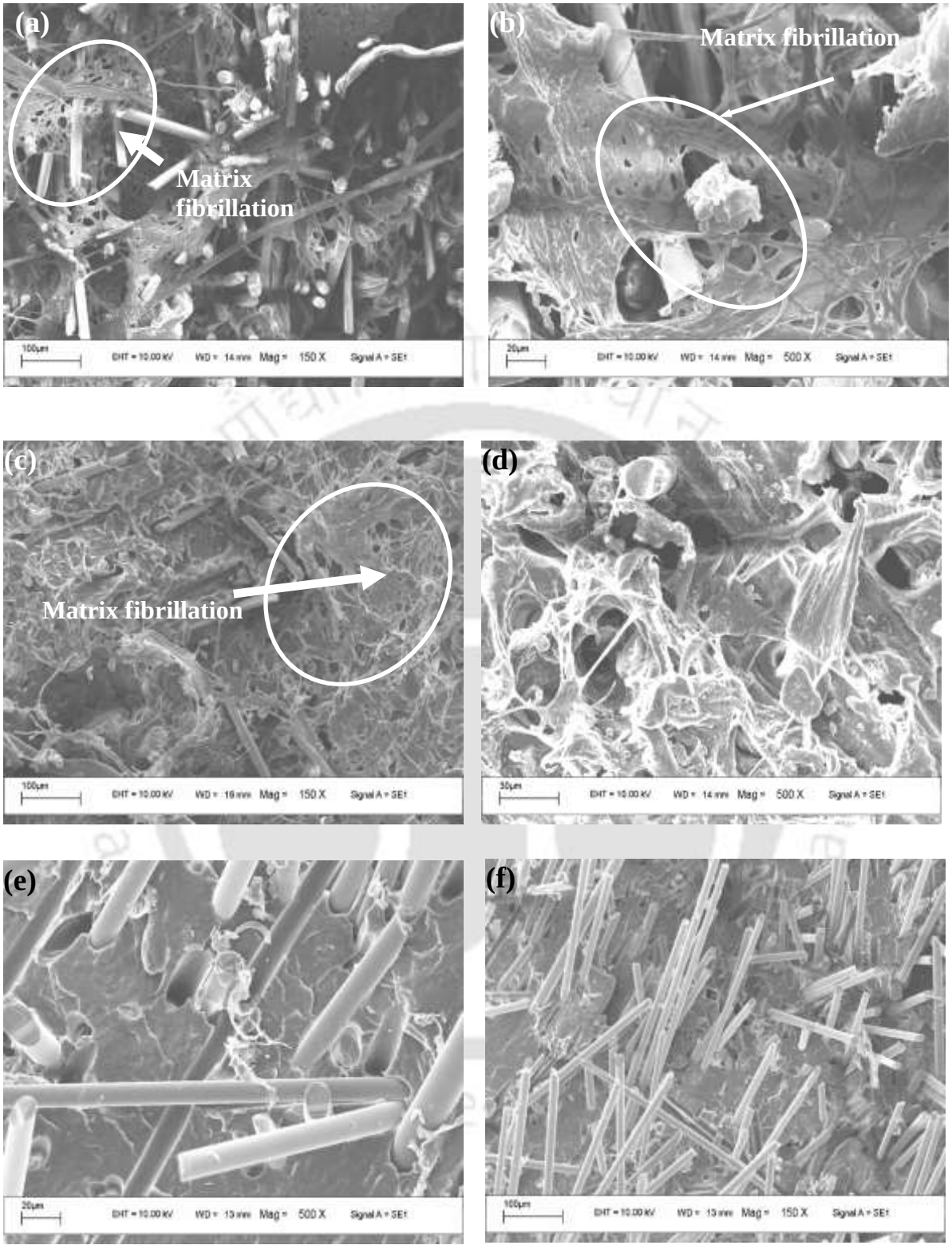

Fig.8.12 Failure morphology of (a-b) fractured bearing surface of SFLS (c-d) fractured bearing surface of LFLS (e) fractured surface of the SFLS tensile specimen (f) flat fractured surface of the LFLS tensile specimen

8.4.2 Effect of Bolt-Hole Clearance on Bearing Strength

Clearance study was carried out on the short fiber reinforced leaf spring joints. Figure 8.13 shows the load-deflection plot of the tested joints with different fits between hole and bolt at a strain rate of 5mm/min. Delay in initial take-up load was markedly visible with the increase in clearance. McCarthy *et al.* (2005) also reported similar behavior in glass fiber epoxy composite with the increase in bolt-hole clearance. The bearing strength was computed using maximum load obtained from the load -displacement plot using equation 8.1. Bearing strength was found to be reduced with increase in clearance as shown in figure 8.14. Besides, figure 8.13 confirmed the decrease in failure strain of the joint with the decrease in clearance between bolt-hole.

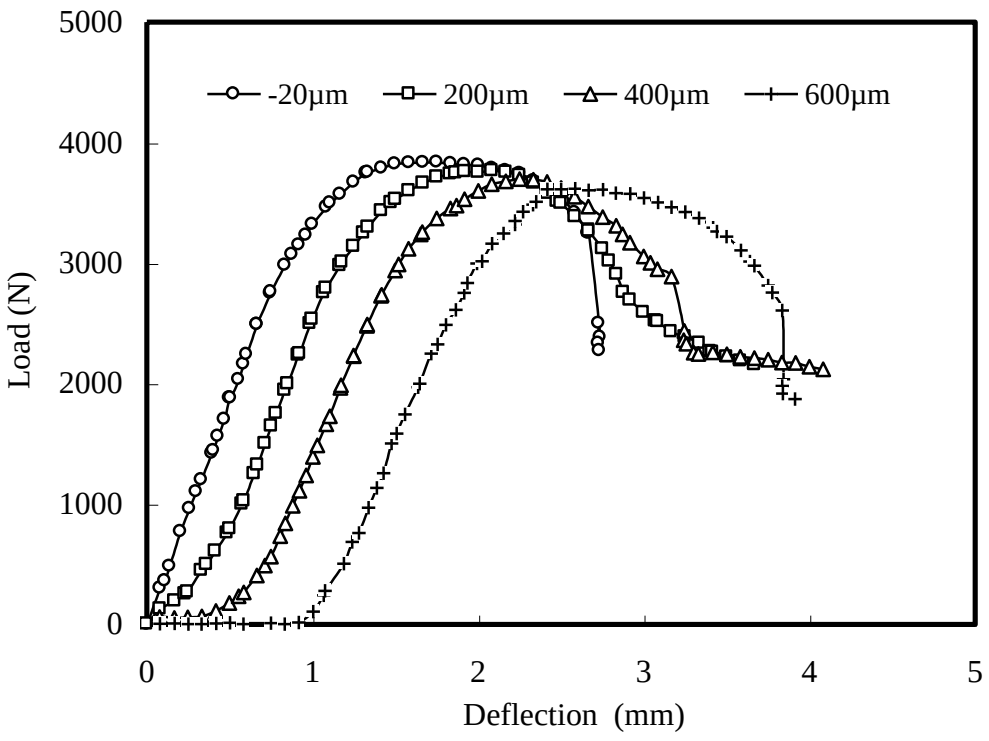

Fig.8.13 Load -deflection curve of tested joint with various fits

Net-tension was observed as the major failure mode for all the investigated joint fits as shown in figures 8.15 (a-d). With the increase in clearance between hole and bolt, the bearing contact area decreases. Chen *et al.* (1995) also reported the influence of bolt-hole clearance on the contact area of bolted joint of the composite plate. Due to the reduced contact area, concentrated load acted on the bearing surface which facilitates the progression of extensive damage. Load-deflection plot of the joint (figure 8.13) also confirmed the increase in bolt displacement for higher clearance between bolt and its hole for a given joint. Since leaf spring fatigue performance depends on the response of end joint characteristics, there is a need to understand the performance of end joint behavior under fatigue loading conditions.

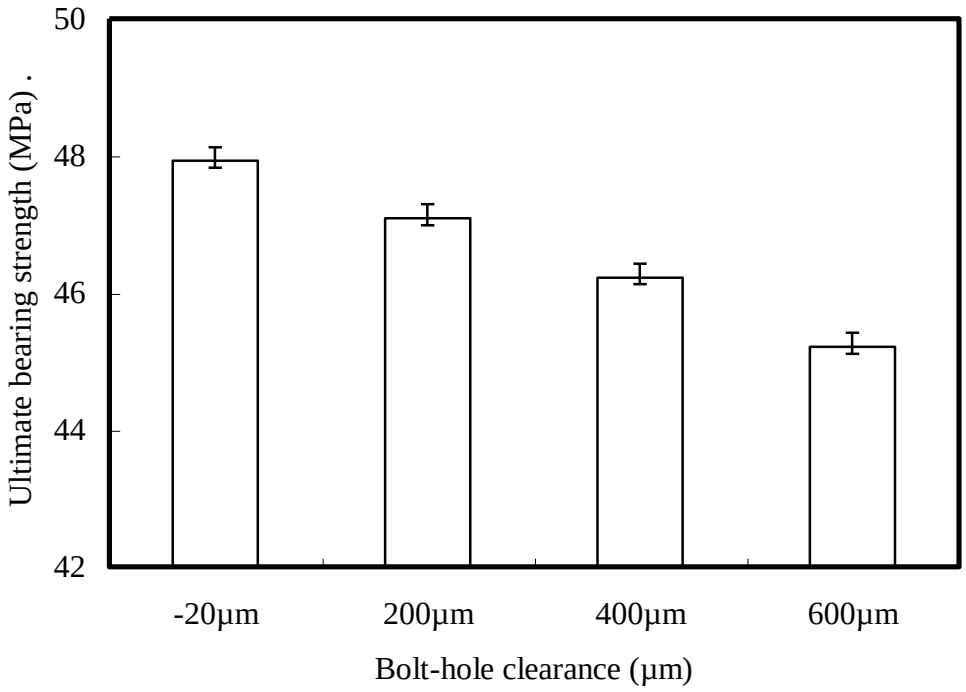

Fig. 8.14 Influence of bolt-hole clearance of the tested joint on bearing strength

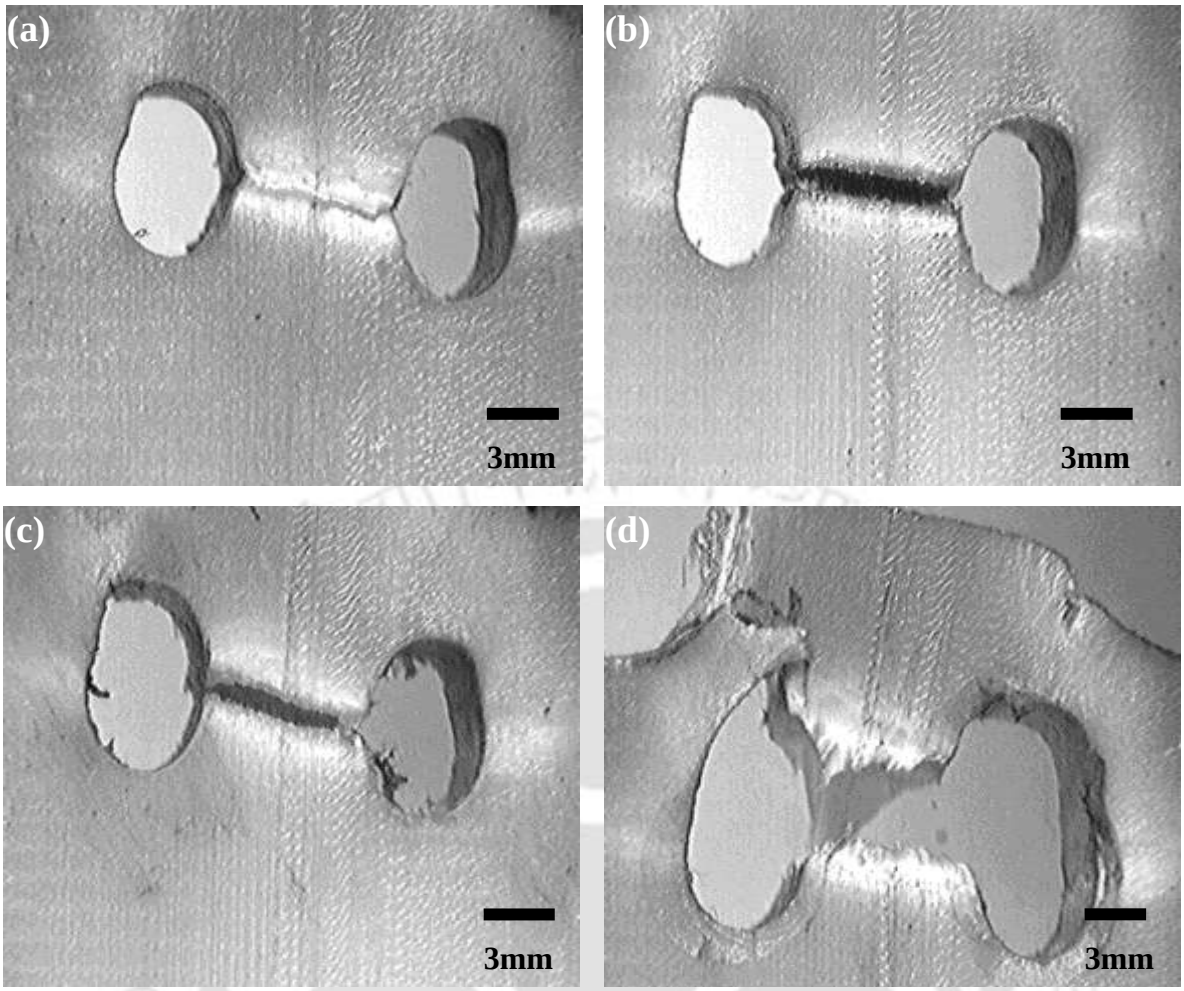

Fig.8.15 Joint failure morphology of bolt-hole fits (a) -20µm (b) 200 µm (c) 400 µm (d) 600 µm

8.5 FATIGUE JOINT STRENGTH PERFORMANCE

8.5.1 Effect of Fiber Length on Fatigue Joint Strength

Fatigue tests were carried out on leaf spring joints with various levels of bearing stress computed from the static tests. As per SAE standards, leaf spring ends were tested for the design load upto 2×10^5 cycles at a frequency of 0.5 Hz (SAE J 1528, 1990). Thus, endurance limit of the tested thermoplastic composite joint was taken as 2×10^5 cycles and fracture of the joint was considered as the failure criteria**.** Figure 8.16 shows the S-N curve of LFLS, SFLS and UFLS joint. From the test results, it was

found that the endurance strength was found to be about 30% of the static joint strength for all the tested materials.

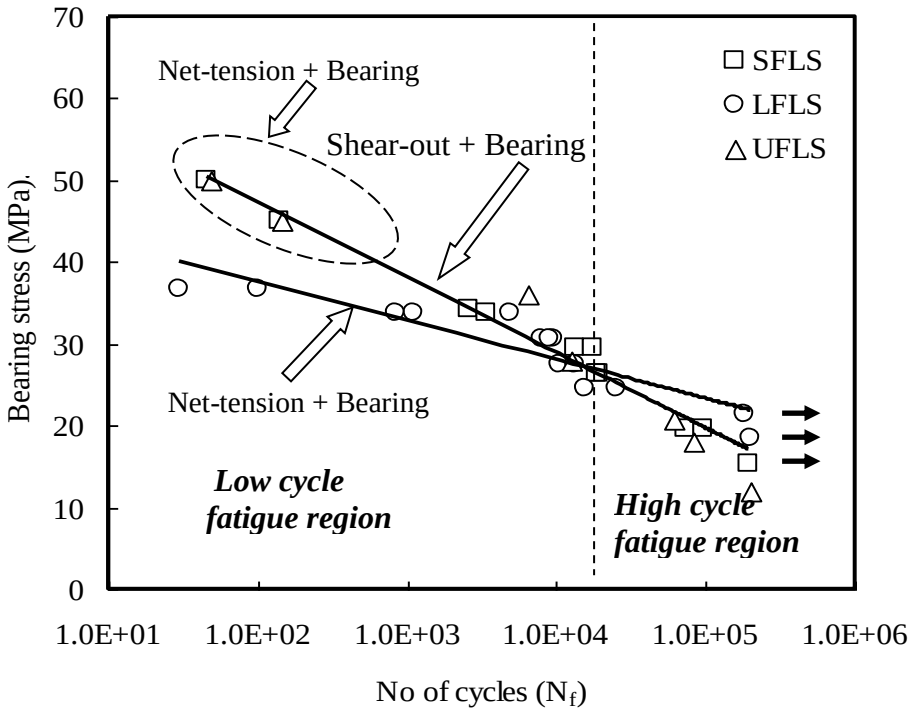

Fig. 8.16 Bearing stress-life curve of test joints for completely reversed loading condition

The alternating load corresponding to the endurance strength of LFLS, SFLS and UFLS joints were 1470, 1050 and 960 N respectively, which is significantly higher than that of the leaf spring design load of 500 N. With the increase in fiber length, the endurance strength of the joint was found to be improved. The S-N curve exhibited two regions of fatigue performance, high and low cycle fatigue as indicated in figure 8.16. In the high cycle fatigue region, LFLS joint showed superior joint performance compared to that of SFLS and UFLS joints. In the low cycle fatigue region, LFLS joint shows inferior performance than that of SFLS and UFLS. Thus, there is a need to investigate the notch sensitive behavior of test material in detail.

To identify the notch sensitive behavior of leaf spring materials, tensile test specimens (as per ASTM D 638) with central hole of 2 mm diameter across the width was considered. Displacement rate of 5mm/min was used for all the chosen leaf spring materials. Figure 8.17 shows the load-deflection curve of notched and unnotched specimens made of LFPP, SFPP and UFPP. For all the test materials, the failure load decreases due to the presence of notch with the reduction in extension. The notch sensitivity factor Q was evaluated by the following relation (Prabhakaran, 2003)

$$Q = (K_s - 1)/(K_t - 1) \quad (8.3)$$

where K_t is the theoretical/elastic stress concentration factor which is equal to 2.6 based on the width to diameter ratio (Peterson, 1951), K_s is the strength reduction factor, and it is given by the ratio between strength of unnotched specimen to the strength of notched specimen.

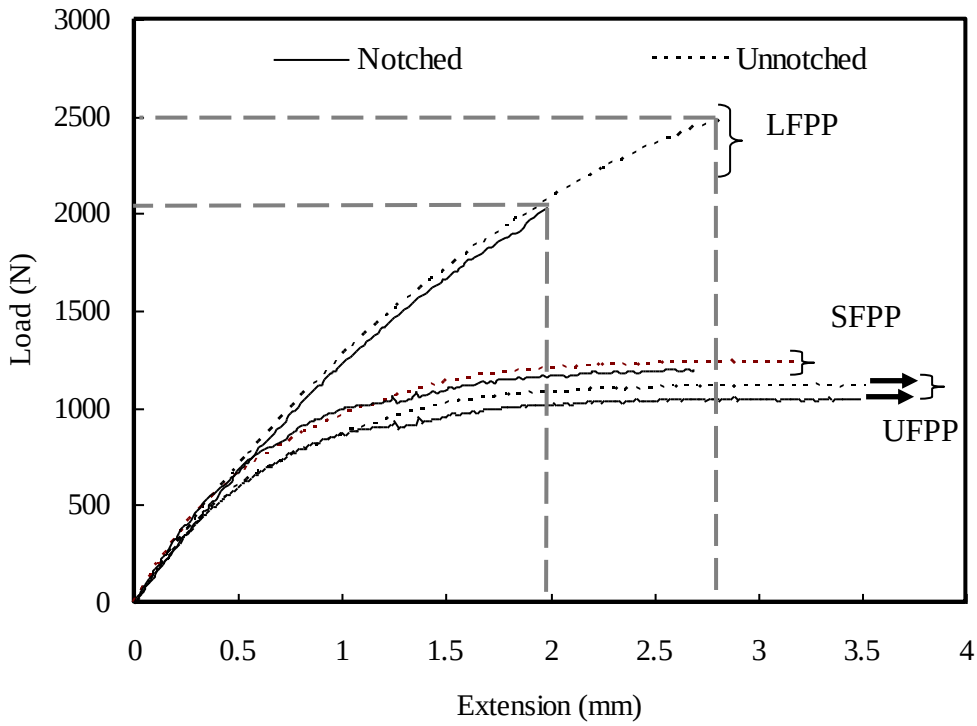

Fig.8.17 Load-deflection curve of notched and unnotched curve for the leaf spring joint materials

From figure 8.17, failure load for unnotched and notched LFPP specimens are 2469 and 2055 N respectively, and hence the strength reduction factor of LFPP was found to be 1.016. Similarly, strength reduction factor of SFPP and UFPP were computed as 0.957 and 0.887 respectively. With the computed strength reduction factor, the notch sensitivity of LFPP, SFPP and UFPP were obtained as + 0.0106, -0.0268 and - 0.0703 respectively using equation 8.3. Thus, it was confirmed that the presence of long fibers in LFPP caused the material more notch sensitive. SFPP and UFPP showed a notch strengthening effect which is observed from the negative value of notch sensitivity factor. Notch strengthening effect implied the material ability to undergo localized yielding near the hole prior to failure (Fouad, 2009). Notch sensitive behavior is generally more visible in the low cycle fatigue condition where the stress level is high. Ferreira *et al*. (1997) investigated the fatigue performance of glass fiber reinforced polypropylene specimens with central and offset holes having different diameters where significant difference between notched and unnotched specimens was observed at low cycle fatigue and very less difference in performance was observed at high cycle condition.

In general, notch sensitivity of the composite material is dependent on matrix and fiber material (Pinnell, 1996). Guynn and Bradley (1989) reported that the ductile matrix exhibited better ability to dissipate stress concentration near the notch than that of brittle material. In the present investigation, LFLS joint exhibited high strength and high modulus associated with lesser bearing strain as indicated in figure 8.9. At low cycle fatigue region where the stress level is higher, the ability of LFLS joint to dissipate the stress concentration near the hole was limited due to the presence of relatively brittle matrix compared to that of SFLS and UFLS joints. This hinders the LFLS joint to withstand at higher stress (absence of local yielding near the hole).

However, at high cycle fatigue where the stress is relatively less, the induced strain near the hole was less and effect of stress concentration was minimum, which leads to superior performance in LFLS joint than that of SFLS and UFLS joints. Thus, it was observed that notch sensitive characteristics of the leaf spring materials played an important role in deciding the low and high cycle fatigue response of the joint. Since the investigated test joint predominantly exhibited bearing failure, an attempt was made to monitor this damage continuously.

Continuous measurement of load-deflection curves of test joint helps to measure the hole elongation in the joint. Completely reversed fatigue load causes the tensile load to act at the ends diametrically opposite to the hole, which causes hole elongation (bearing mode of failure). Figures 8.18-8.20 show the measured hysteresis loop of UFLS, SFLS and LFLS joint at different stages. The increase in hole elongation ($\Delta_N = \delta_N - \delta_i$ as indicated in schematic figure 8.7) during the fatigue loading is shown in figures 8.18(a-d), 8.19(a-d) and 8.20(a-d). Presence of discontinuous fibers in the composite leaf spring alters the hole elongation, and this is reflected from the change in shape of the load-deflection plots. As the cycle progresses, the shape of the load-deflection hysteresis plot of the joint varied due to the change in surface condition of the bearing area and stiffness of the bolted joint.

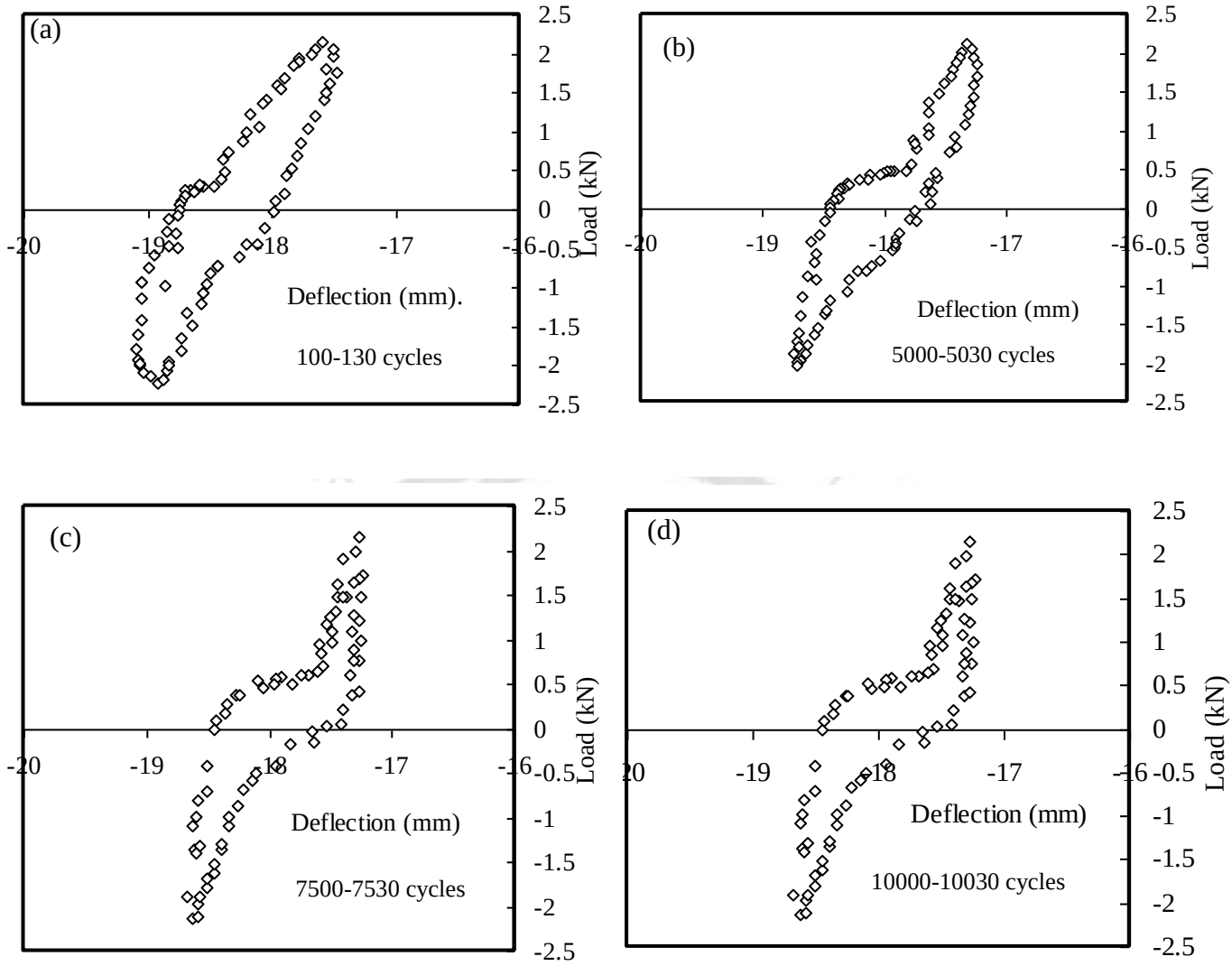

Fig. 8.18 (a-d) Load-deflection hysteresis loop of UFLS joint at an alternating stress of 28 MPa corresponding to 60% ultimate bearing strength

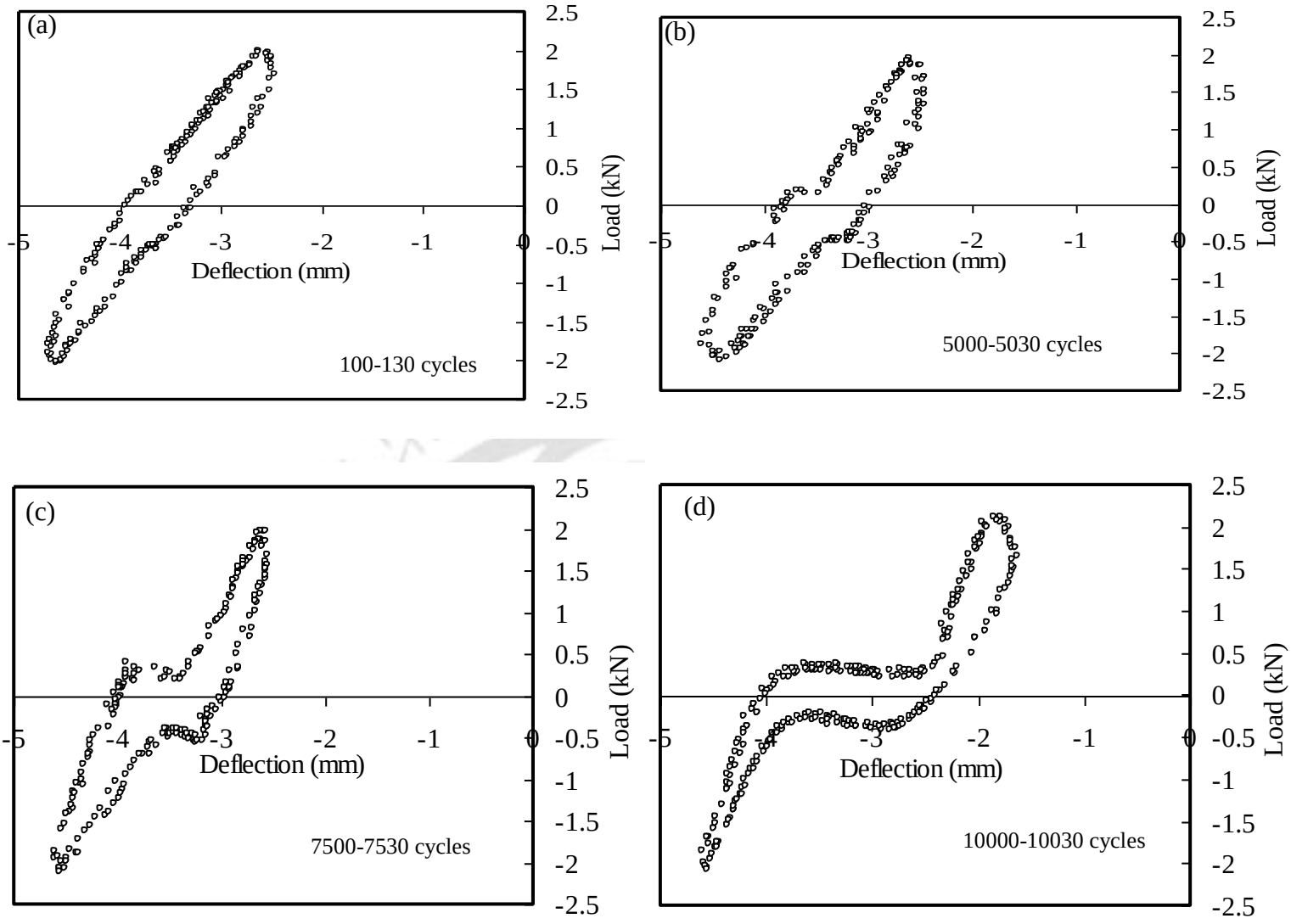

Fig. 8.19 (a-d) Load-deflection hysteresis loop of SFLS joint at an alternating stress of 19.7 MPa corresponding to 45% ultimate bearing strength

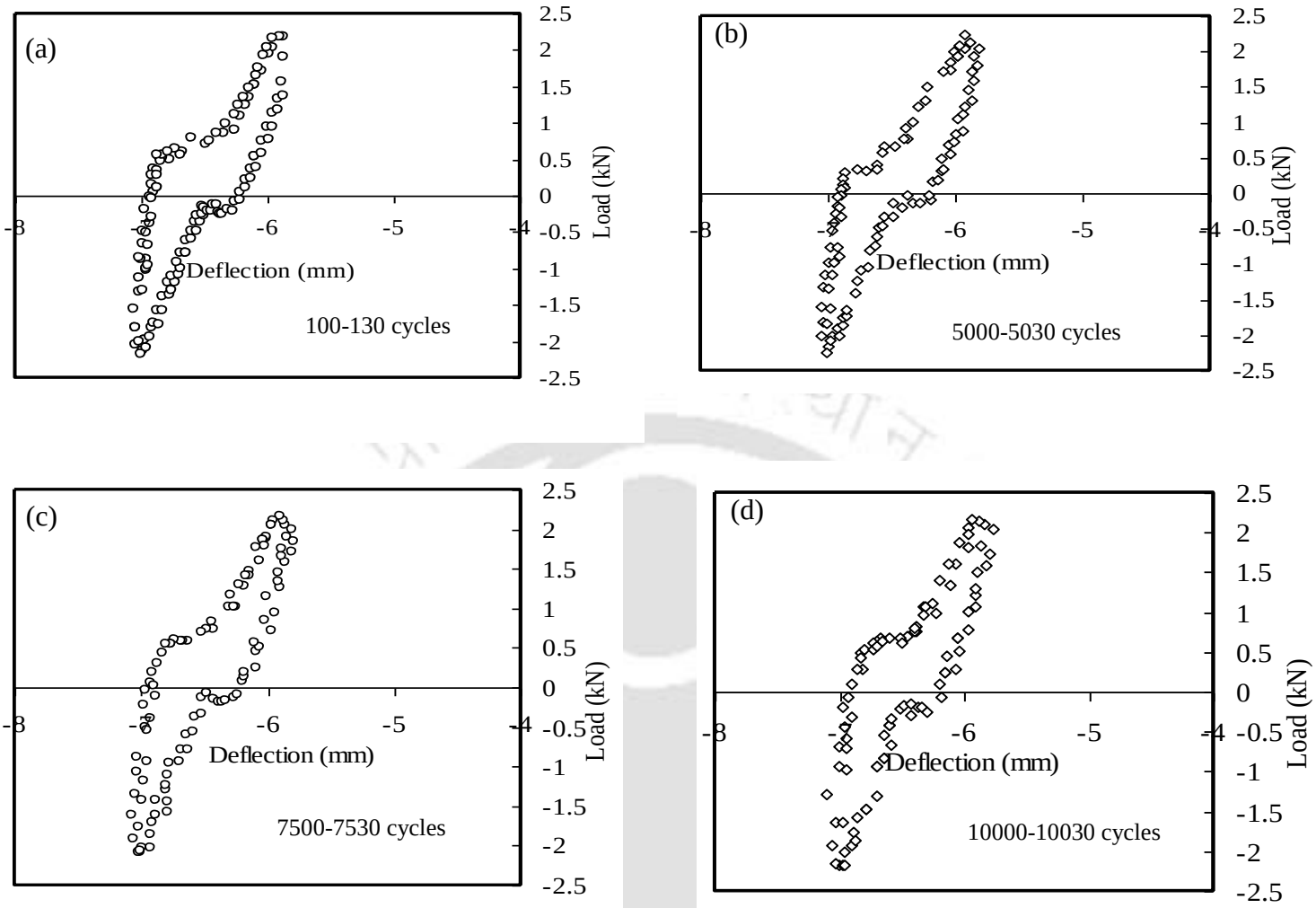

Fig.8.20 (a-d) Load-deflection hysteresis loop of LFLS joint at an alternating stress of 27.5 MPa corresponding to 45% ultimate bearing strength

Figures 8.21 (a-c) show the progressive hole extension when UFLS, SFLS and LFLS joints are subjected to fatigue. With the increase in number of cycles, the hole elongation increases, and it is observed to be more in UFLS joint followed by SFLS and LFLS joint. At an alternating stress of 28 MPa and 1000 cycles, UFLS joint exhibited a hole elongation of 0.22 mm, whereas LFLS joint exhibited only 0.06 mm for an alternating stress of 27.5 MPa. Hole elongation was found to be slow upto 1000 cycles for all the test material joints, and later increased progressively until failure occurred. Besides, the rate of hole elongation was found to be significantly influenced by the bearing stress amplitude. Huth (1986) and Saunders *et al.* (1993) also reported the damage progression using load-deflection plot of the composite joint. In addition to the continuous monitoring of bearing damage, morphology of the fractured joints was also investigated to understand the joint failure mechanism.

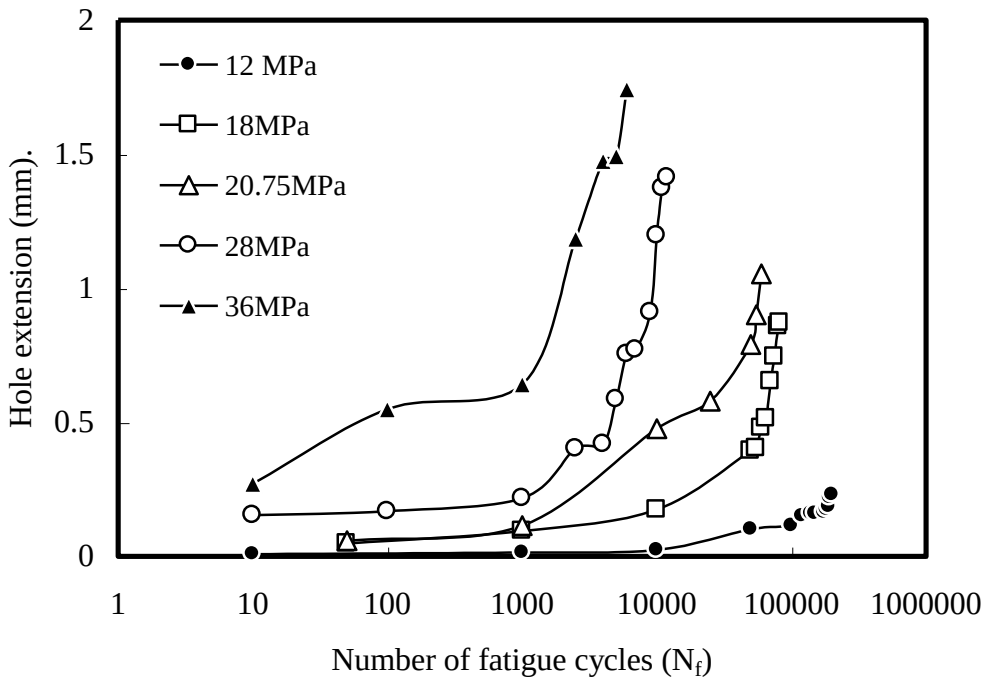

Fig. 8. 21a Hole extension of UFLS joint

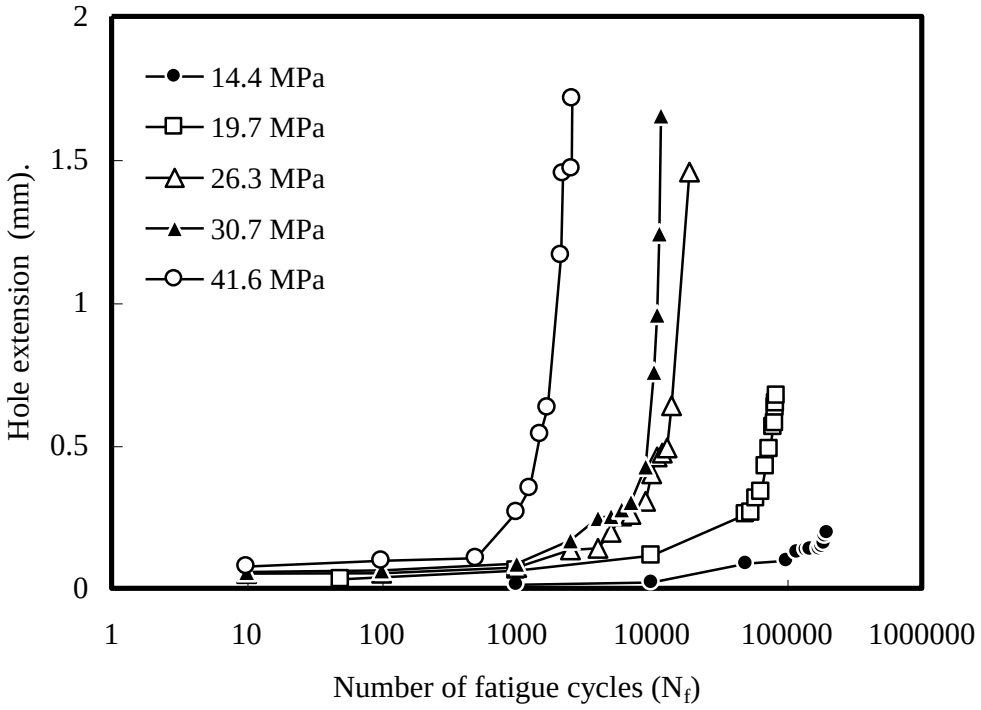

Fig. 8.21b Hole extension of SFLS joint

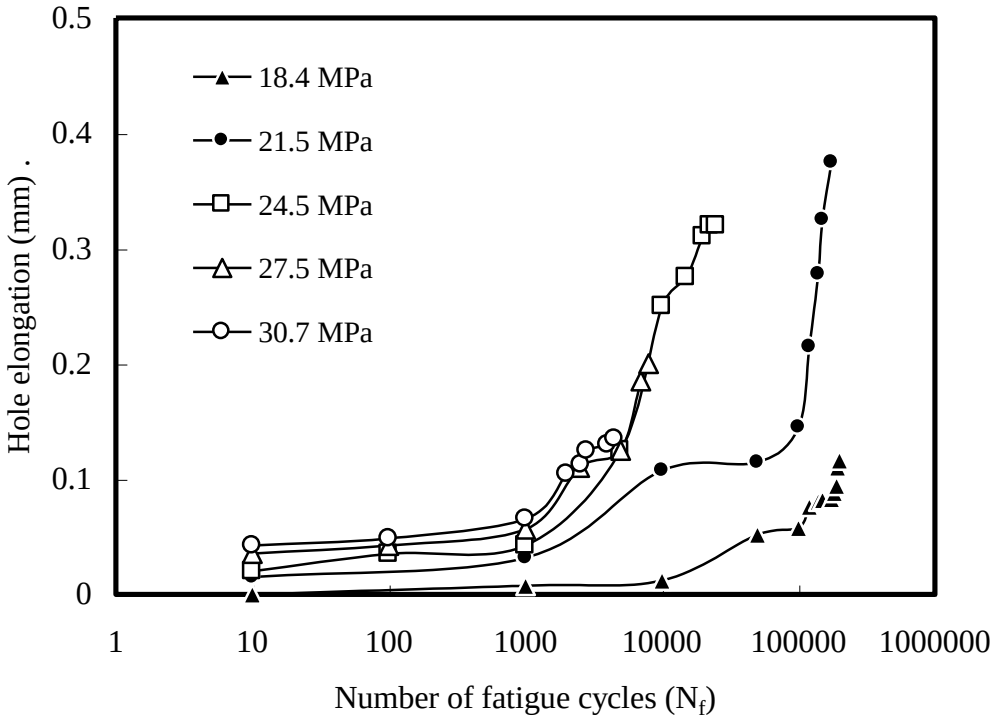

Fig. 8.21c Hole extension of LFLS joint

8.5.2 Effect of Fiber Length on Fatigue Failure Morphology

Failure modes observed in the considered leaf spring joints were found to be dependent on the stress level and leaf spring material. LFLS end joint failed by net-tension (T) + bearing (B) for all the bearing stress levels (figures 8.22(a-b)). SFLS and UFLS joint exhibited net-tension (T) + bearing (B) at higher bearing stress amplitude. Failure mode of SFLS and UFLS joint (figure 8.22c) at higher stress level was similar to that of joint failure observed under static loading condition (figures 8.10a and 8.10d). Starikov and Schon (2001, 2002) investigated static and fatigue performance of carbon fiber epoxy specimens joined with different numbers of bolts and observed a similar observation as reported in the present investigation, where net-tension and bearing failures were observed at static as well as high stress fatigue condition. Observation of whitening in SFLS and UFLS joint confirmed the material yielding (figure 8.22c). Shear out (S) + bearing (B) failure was observed at lower bearing stress amplitude for SFLS and UFLS joint. The progressive damage caused the hole elongation, which leads the bolt motion to cause shear-out failure (figures 8.22(d-e)). The absence of shear out failure in LFLS joint confirmed the lack of hole elongation. This behavior is due to the reduced ductility of the polypropylene matrix in the composite and failure morphology observed at the bearing surface area confirmed this behavior.

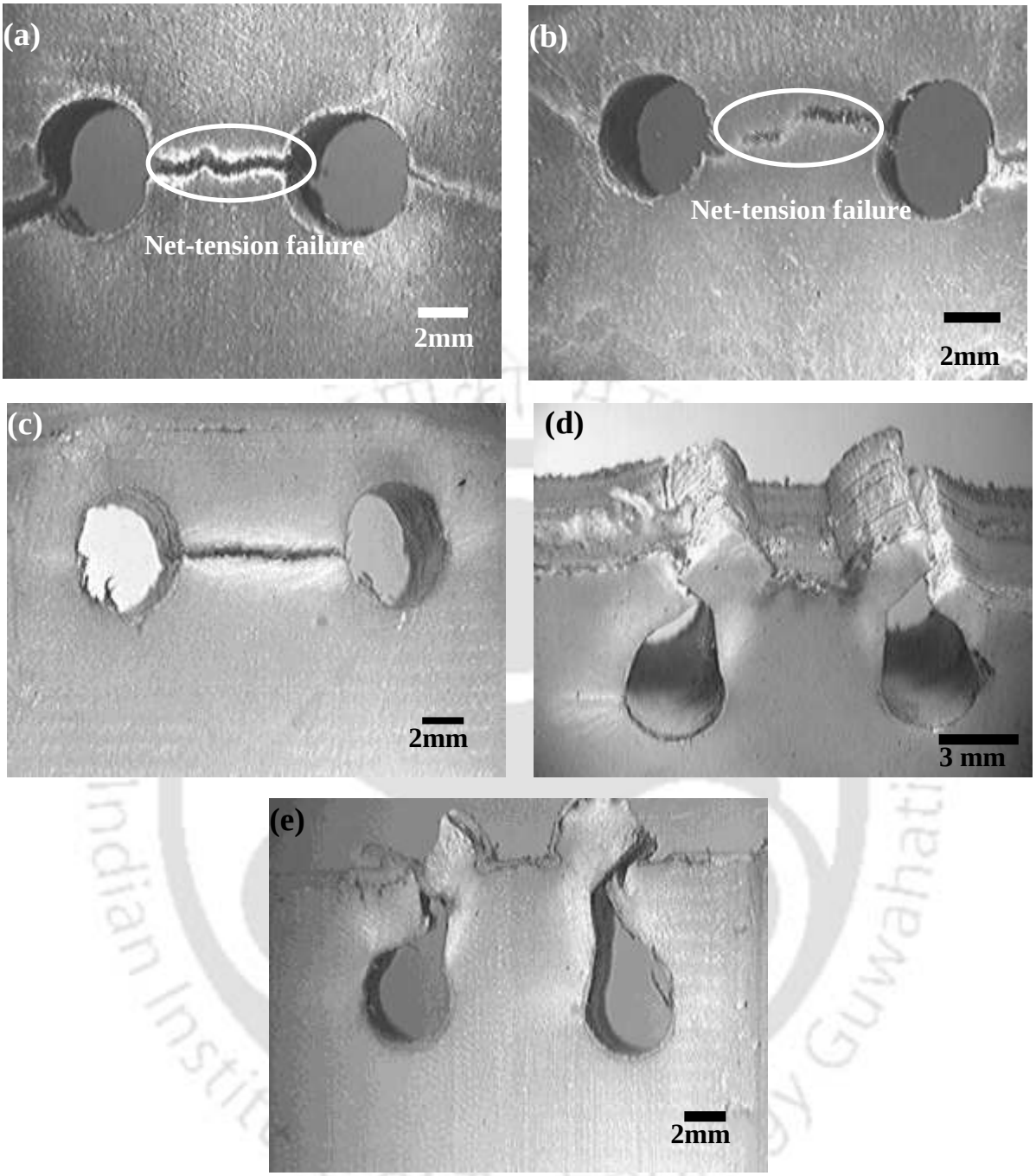

Fig.8.22 Fatigue failure morphology of test joint at various bearing stress (a) net-tension failure in LFLS at 30.7MPa (b) net-tension failure in LFLS at 21.5 MPa (c) net-tension failure of UFLS at 45MPa (d) shear-out failure of UFLS at 28MPa (e) *shear-out failure of SFLS at 30.7 MPa*

Failure morphology (figures 8.23(a-b)) of SFLS joint exhibited matrix fibrillation during fatigue, this behavior is due to considerable hole elongation (bearing damage) prior to the failure. Wear particles were also observed at the bearing surface area due to the sliding friction between bearing hole and bolt shank (figure 8.23a). Figures 8.23 (c-d) show the insignificant matrix stretching due to reduced hole elongation characteristics of LFLS joint. The fibers were well adhered to the matrix and elongation of the matrix was constrained as shown in figure 8.23d. It was confirmed that bearing damage is prominent in SFLS joint than LFLS joint due to reduced ductility of the composite.

Though joint failure morphology under fatigue exhibited shear out/net-tension failure, substantial bearing damage (figures 8.22(a-e)) was also observed at all the investigated stress levels. Despite the fact that uniaxial fatigue load was acted at the investigated joint, bi-axial stress was induced at the bearing surface due to the curved surface of the bearing area as in static condition. This bi-axial stress at the bearing surface severely deformed the matrix as shown in figures 8.23(a-d). To substantiate further, same leaf spring test material; 20 % short fiber reinforced polypropylene was injection molded into tensile test specimen as per ASTM D638 standard and subjected to similar fatigue condition. Loading frequency of 0.5 Hz, alternating loading amplitude of 45 and 60 % UTS was kept for the testing. As expected, the failure morphology of the fractured surface of tensile test specimen was found to be different from the bearing surface of leaf spring end. The morphology of fractured surface of the tensile test specimen subjected to fatigue testing is shown in figures 8.23 (e-f), wherein no severe matrix deformation and fibrillation were found as exhibited at the bearing surfaces.

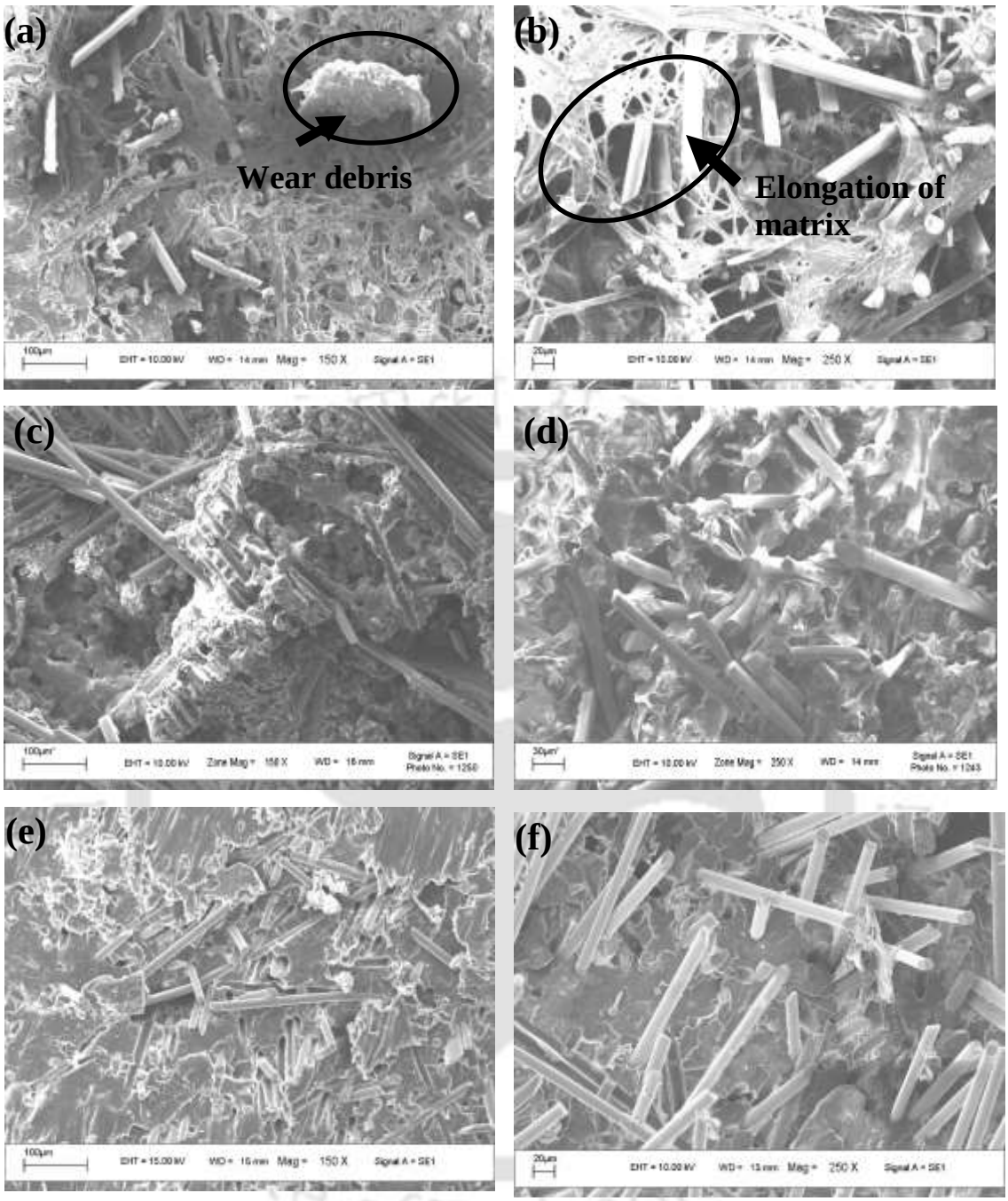

Fig. 8.23 Bearing surface failure morphology of test joint during fatigue (a) matrix fibrillation along with wear debris of SFLS joint at alternating stress of 19.7 MPa (b) excessive matrix fibrillation of SFLS joint at alternating stress of 26.3 MPa (c-d) absence of matrix stretching in LFLS at alternating stress of 24.5 MPa (e) failure surface at 45% UTS of SFLS tensile specimen (f) failure surface at 60% UTS of SFLS tensile specimen

8.6 SUMMARY

This chapter presents the static and fatigue performance of the composite leaf spring end joint behavior.

- Parametric investigation of double pin joint for the molded thermoplastic leaf spring revealed the effect of end distance and distance between the holes in influencing the bearing strength. Load carrying capacity of the joint was found to increase with the increase in free edge distance to hole centre.
- Static and fatigue leaf spring end joint strength evaluation confirmed that the bearing strength increased with the increase in fiber length and sufficient end joint strength was observed for all the material configurations.
- Joint strength was found to be significantly influenced by the fit between fastener and hole under static loading condition. Superior joint strength was exhibited with the decrease in clearance. However for the investigated clearance range, failure mode was found to be same.
- Long fiber reinforced leaf spring joint exhibited superior performance at high cycle fatigue condition than short fiber and unreinforced leaf spring joint. However, notch sensitive characteristics of the material deteriorated the performance of long fiber reinforced leaf spring at low cycle fatigue conditions.
- Hole elongation of long fiber reinforced leaf spring joint was low compared to unreinforced and short fiber reinforced leaf spring joint at all the investigated stress levels.
- Long fiber reinforced leaf spring end joint exhibited net-tension + bearing damage at all the stress levels. Short fiber reinforced and unreinforced leaf spring end joint exhibited net-tension + bearing damage at high stress level and shear-out + bearing at lower stress level.

CHAPTER 9

SUMMARY AND CONCLUSIONS

8.1 SUMMARY

Unreinforced, 20 % short and 20 % long glass fiber reinforced polypropylene materials were considered for injection molding the varying width mono leaf springs. Computer aided injection molding simulation of leaf spring was carried out and then die was manufactured. Desired material properties for the leaf spring applications *viz.*, adhesive wear, abrasive wear and damping performance were examined before manufacturing the leaf spring. Considered materials were injected molded into varying width mono leaf spring. Developed leaf springs were evaluated for static, fatigue and short term flexural creep performance with the aid of servo hydraulic fatigue testing facility. Leaf spring end joint was designed with the aid of finite element analysis and experimentally evaluated for static and fatigue performance. Following major conclusions were drawn based on the investigation.

8.2 CONCLUSIONS

- Adhesive and abrasive wear performance of leaf spring materials confirmed the role of fiber length on the wear performance of leaf spring materials. Improved fiber matrix bonding, hardness and presence of less fiber ends in long fiber reinforced material reduced specific wear rate compared to that of short fiber reinforced and unreinforced material. UFPP exhibited micro ploughing in both adhesive and abrasive modes. Fiber pullout and micro cutting were observed in

SFPP material at adhesive and abrasive mode respectively. LFPP exhibited fiber breakage under adhesive as well as abrasive mode.

- Damping behavior of leaf spring material was significantly affected by the fiber ends and fiber-matrix interface. Short fiber reinforced composite material exhibited superior damping performance to that of long fiber reinforced composite material. Under free vibration, logarithmic decrement and damping factor were found to decrease with the increase in fiber length. Under forced vibration, SFPP exhibited higher phase lag between the excited force and its response than that of LFPP material.

- Long fiber reinforced material exhibited improved crystallinity and thermal stability than that of short fiber reinforced material. Static performance of the molded leaf spring is appreciably influenced with the fiber length. Spring rate of LFLS was found to be about three times greater than that of SFLS and five times greater than UFLS. Energy storage capability of long glass fiber reinforced leaf spring was found to be significantly higher that of SFLS and UFLS, which helps to isolate vibrations. Load-deflection behavior of LFLS showed less strain rate sensitiveness than that of SFLS and UFLS.

- Fatigue performance of the molded leaf spring is significantly altered with the fiber length. Load-deflection of test leaf springs was continuously measured and used as a damage index. Spring rate reduction was dependent on the stress level for all the considered leaf springs and found to decrease with the increase in fiber length. Short fiber reinforced and unreinforced leaf springs exhibited 10 % drop in initial spring rate, whereas long fiber reinforced leaf spring exhibited fracture failure at tensile surface.

- Short-term flexural creep performance of leaf spring was improved with the fiber length due to the improved load transfer from the matrix to the fibers. HRZ model was used to predict the short term creep performance of leaf spring.

- Leaf spring end joint was designed and experimentally evaluated for static and fatigue performance. Static end joint strength evaluation confirmed that the bearing strength increased with the increase in fiber length and decreased with the increase in clearance. LFLS exhibited superior joint performance during high cycle fatigue conditions than that of SFLS and UFLS joints. However notch sensitive characteristics of the long fiber reinforced material associated with reduced composite ductility deteriorated its performance at low cycle fatigue conditions.

In a summary adhesive and abrasive wear resistance was found to be improved with reinforcement; LFPP exhibited superior wear resistance than that of SFPP. Damping performance was found to be deteriorated with the reinforcement; SFPP exhibited superior damping performance than that of LFP. Static, fatigue and creep performance of leaf spring was found to be enhanced due to the reinforcement; LFLS exhibited superior static and dynamic performance than SFLS. Static and high cycle fatigue performance of leaf spring joint was found to be improved due to the reinforcement; LFLS exhibited superior fatigue joint performance than SFLS.

8.3 FUTURE SCOPE

- Current investigation is limited to 20 % weight fraction of fibers, this can be varied and its influence can be studied. With the utilization of high performance base matrix and resins fibers (such as PEEK matrix and carbon fibers) for leaf

spring application, load carrying capability, fatigue life and creep resistance can be significantly enhanced.

- In the current study, varying width and constant thickness leaf springs were molded, further varying thickness as well as varying width leaf spring can be fabricated and its performance can be studied. Leaf spring can be molded to the actual size and fitted in the vehicle to investigate the real time ride characteristics.

REFERENCES

1. **Aberg, J.,** and **Widell, B.** Uniaxial material damping measurements using a fiber optic lattice: A discussion of its performance envelope. *Experimental Mechanics*, 2004, **44**, 33-36.
2. **Acha, B.A., Reboredo, M.M.,** and **Marcovich, N.E.** Creep and dynamic mechanical behavior of PP–jute composites: Effect of the interfacial adhesion. *Composites Part A: Applied Science and Manufacturing*, 2007, **33**, 1507-1516.
3. **Adams, R.D.,** and **Maheri, M.R.** Damping in advanced polymer-matrix composites. *Journal of Alloys and Compounds*, 2003**, 355**, 126-130.
4. **Aggarwal, V.P., Agarwal,** and **Khan, R.A.** A stress approach model for predictions of fatigue life by shot penning of EN45A spring steel. *International Journal of Fatigue*, 2006, **12**, 1845-1853.
5. **Aktas, A., Imrek, H.,** and **Cunedioglu, Y.** Experimental and numerical failure analysis of pinned-joints in composite materials. *Composite Structures*, 2009, **89**, 459-466.
6. **Allah, A., Abdin, E.M., Selmy, A.I.,** and **Khashaba, U.A.** Effect of mean stress on fatigue behavior of GFRP pultruded rod composites. *Composites Part A*, 1997, **28**, 87-91.
7. **Al-Qureshi, H.A.** Automobile leaf springs from composite materials. *Journal of Material Processing Technology*, 2001, **118**, 58-61.
8. **American Society of Civil Engineers.** *Structural Plastic Design Manual*, 1986 (ASCE Publications, Newyork).
9. **Arnold, C., Yang, M., Ayala, E.,** and **Adam Bell.** Effects of filler particles on abrasive wear of elastomer based composites. *Wear*, 1991, **146**, 349-366.
10. **ASM International.** *Engineering Materials Handbook*, 1988 (ASM International, Ohio).
11. **ASTM D-2990.** Standard test methods for tensile, compressive, and flexural creep and creep-rupture of plastics. *ASTM International*: Philadelphia, 2005.

12. **ASTM D5961/D5961M-05E1.** Standard test method for bearing response of polymer-matrix composite laminates. *ASTM International:* West Conshohocken, 2005.
13. **Bahadur, S.** The development of transfer layers and their role in polymer tribology. *Wear*, 2000, **245**, 92-99.
14. **Bahadur, S.,** and **Polineni, V.K.** Tribological studies of glass fabric-reinforced polyamide composites filled with CuO and PTFE. *Wear*, 1996, **200**, 95-104.
15. **Banik, K., Karger-Kocsis, J.,** and **Abraham, T.** Flexural creep of all-polypropylene composites: Model analysis. *Polymer Engineering Science*, 2008, **48**, 941-948.
16. **Barkoula, N.M.,** and **Karger-Kocsis, J.** Effect of fibre content and relative fibre orientation on the solid particle erosion of GF/PP composites. *Wear*, 2002, **252,** 80-87.
17. **Barrett, T.S., Stachowiak, G.W.,** and **Batchelor, A.W.** Effect of roughness and sliding speed on the wear and friction of ultra-high molecular weight polyethylene. *Wear*, 1992, **153**, 331-350.
18. **Bartus, S.D., Vaidya, U.K.,** and **Ulven, C.A.** Design and development of a long fiber thermoplastic bus seat. *Journal of Thermoplastic Materials*, 2006, **19**, 131-154.
19. **Bayer, R.G.** *Mechanical Wear Prediction and Prevention*, 1994 (Marcel Dekker Inc, New York).
20. **Beardmore, P.,** and **Johnson, C.F.** The potential for composites in structural automotive applications. *Composite Science and Technology*, 1986, **26,** 251-281.
21. **Beardmore, P.** Composite structures for automobiles. *Composite Structures*, 1986, **5**, 163-176.
22. **Bekhet, N.E.** Tribological behaviour of drawn polypropylene. *Wear*, 1999, **236**, 55-61.
23. **Bellenger, V., Tcharkhtchi, A.,** and **Castaing, P.** Thermal and mechanical fatigue of a PA66/glass fibers composite material. *International Journal of Fatigue*, 2006, **28**, 1348-1352.

24. **Belogur, V.P., Treshchevskii, A.N.,** and **Yu Konev, S.** Titanium alloys for springs in cutoff fittings. *Chemical and Petroleum Engineering*, 2004, **40**, 696-698.

25. **Bernasconi, A., Davoli, P., Basil, A.,** and **Filippi, A.** Effect of fibre orientation on the fatigue behaviour of a short glass fibre reinforced polyamide-6. *International Journal of Fatigue*, 2007, **29**, 199-208.

26. **Bernasconi, A., Davoli, P., Rossin, D.,** and **Armanni, C.** Effect of reprocessing on the fatigue strength of a fiberglass reinforced polyamide. *Composites Part A*, 2007, **38**, 710-718.

27. **Bijwe, J., Indumathi, J., John Rajesh, J.,** and **Fahim, M.** Friction and wear behaviour of polyetherimide composites in various wear modes. *Wear*, 2001, **249**, 715-726.

28. **Briscoe, B.** Wear of polymers: An essay of fundamental aspects. *Tribology International*, 1981, **14**, 231-243.

29. **Briscoe, B.J.,** and **Evans, P.D.** The influence of asperity deformation conditions on the abrasive wear of γ-irradiated polytetrafluoroethylenes. *Wear*, 1989, **133**, 47-64.

30. **Bundisnki, K.G.** Resistance to particle abrasion of selected plastics. *Wear*, 1997, **203-204**, 302-309.

31. **Bureau, M.N.,** and **Denault, J.** Fatigue resistance of continuous glass fiber/polypropylene composites: consolidation dependence. *Composites Science and Technology*, 2004, **64,** 1785-1794.

32. **Camanho, P.P.,** and **Matthews, F.L.** Stress analysis and strength prediction of mechanically fastened joints in FRP: A review. *Composites Part A*, 1997, **28**, 529-547.

33. **Carlsson, L.A., Aronsson, C.G.,** and **Backlund, J.** Notch sensitivity of thermoset and thermoplastic laminates loaded in tension. *Journal of Material Science*, 1989, **24**, 1670-1682.

34. **Carwalho, W.S.,** and **Rosario Bretas, E.S.** Thermoplastic/carbon fibre composites: Correlation between interphase morphology and dynamic mechanical properties. *European Polymer Journal*, 1990, **26**, 817-821.

35. **Casado, J.A., Carrascal, I., Polanco, J.A.,** and **Gutierrez-Solana, F.** Fatigue failure of short glass fibre reinforced PA 66 structural pieces for railway track fasteners. *Engineering Failure Analysis*, 2006, **13**,182-197.

36. **Cenna, A., Allen, S., Page, N.W.,** and **Dastoor, P.** Modeling the three-body abrasive wear of UHMWPE particle reinforced composites. *Wear*, 2003, **254**, 581-588.

37. **Challa, S.R.,** and **Progelhof, R.C.** A study of creep and creep rupture of polycarbonate. *Polymer Engineering and Science*, 1995, **6**, 546-554.

38. **Chandra, R., Singh, S.P.,** and **Gupta, K.** Damping studies in fiber-reinforced composites – A review. *Composite Structures*, 1999, **46,** 41-51.

39. **Chandradass, J., Ramesh Kumar, M.,** and **Velmurugan, R.** Effect of nanoclay addition on vibration properties of glass fibre reinforced vinyl ester composites. *Materials Letters*, 2007, **61**, 4385-4388.

40. **Chen, H.S.** The static and fatigue strength of bolted joints in composites with hygrothermal cycling. *Composite Structures*, 2001, **52**, 295-306.

41. **Chen, W.H.,** and **Lee, S.S.** Numerical and experimental failure analysis of composite laminates with bolted joints under bending loads. *Journal of Composite Materials*, 1995, **29**, 15-36.

42. **Chen, W.H., Lee, S, S.,** and **Yeh, J.T.** Three-dimensional contact stress analysis of a composite laminate with bolted joint. *Composite Structures*, 1995, **30**, 287-297.

43. **Chevali, V.S., Dean, D, R.,** and **Janowski, G.M.** Flexural creep behavior of discontinuous thermoplastic composites: Non-linear viscoelastic modeling and time–temperature-stress superposition. *Composites: Part A*, 2009, **40**, 870-877.

44. **Cirino, M., Pipes, B.,** and **Friedrich, K.** The abrasive wear behavior of continuous fiber polymer composites. *Journal of Materials Science*, 1987, **22,** 2481-2492.

45. **Clerico, M.,** and **Patierno, V.** Sliding wear of polymeric composites. *Wear*, 1979, **53**, 299-301.

46. **Collings, T.A.** The strength of bolted joints in multi-directional CFRP laminates. *Composites*, 1977, **8**, 46-55.

47. **Corvi, A.** A preliminary approach to composite beam design using FEM analysis. *Composite Structures*, 1990, **16**, 259-275.

48. **Crawford, R.J**. *Plastics Engineering*, 1998 (Butterworth Heinemann, Oxford).

49. **Crema, L.B., Castellani, A.,** and **Serra, A.** Experimental tests for damping measurement on several short glass fiber composites. *Journal of Composite Materials*, 1989, **23**, 978-987.

50. **Crews, J.** Bolt bearing fatigue of a graphite/epoxy laminate. *ASTM STP 749*, 1981, 131-44.

51. **Croce, P., Pietro Orsini,** and **Walter Salvatore.** Vibration isolation and design of automotive test benches. *Engineering Structures*, 2001, **23**, 945-956.

52. **Czigany, T.,** and **Karger-Kocsis, J.** Comparison of the failure mode in short and long glass fiber-reinforced injection-molded polypropylene composites by acoustic emission. *Polymer Bulletin*, 1993, **31**,495-501.

53. **Dally, J.W.,** and **Carrillo, D.H.** Fatigue behavior of glass-fiber fortified thermoplastic. *Polymer Engineering and Science*, 1969, **9**, 434-444.

54. **Daughtery, R.L.** Composite leaf springs in heavy truck applications. In: Proceedings of *Composite Materials, Japan-US Conference,* Tokyo, 1981, pp.529-538.

55. **Deaver, D.,** and **MCllvaine, J.** Use of structural long glass fiber composites to replace steel in automotive running boards. *SAE International*, 2005, Doc No: 1679.

56. **Dwivedi, U.K.,** and **Navin Chand.** Influence of MA-g-PP on abrasive wear behaviour of chopped sisal fibre reinforced polypropylene composites**.** *Journal of Materials Processing Technology*, 2009, **209**, 5371-5375**.**

57. **Eberle, A.P.R., Baird, D.G.,** and **Wapperom**, **P.** Modeling the transient rheology of a polypropylene melt reinforced with long and short glass fibers. In: Proceedings of *AIChE Annual Meeting,* Cincinatti, 2005, pp.1-5.

58. **Ferreira, J.A.M., Costa, J.D.M., Reis, P.N.B.,** and **Richardson, M.O.W.** Analysis of fatigue and damage in glass-fibre-reinforced polypropylene composite materials. *Composites Science and Technology*, 1997, **59**, 1461-1467.

59. **Findley, W.N.,** and **Khosla, G.** Application of the superposition principle and theories of mechanical equation of state, strain, and time hardening to creep of plastics under changing loads. *Journal of Applied Physics*, 1955, **26**, 821–832.

60. **Fouad, H.** Experimental and numerical studies of the notch strengthening behaviour of semi-crystalline ultra-high molecular weight polyethylene. *Materials and Design*, 2009, **31**, 1117-1129.

61. **Fuentes, J.J., Aguilar, H.J., Rodríguez, J.A.,** and **Herrera, E.J.** Premature fracture in automobile leaf springs. *Engineering Fracture Analysis*, 2008, **45**, 3025-3035.

62. **Gamstedt, K.E., Berglund, L.A.,** and **Peijs, T.** Fatigue mechanisms in unidirectional glass-fibre-reinforced polypropylene. *Composites Science and Technology*, 1999, **59**, 759-768.

63. **Gassan, J.,** and **Bledzki, A.K.** Possibilities to improve the properties of natural fiber reinforced plastics by fiber modification-jute polypropylene composites. *Applied Composite Materials*, 2000, **7**, 373-385.

64. **Genta, G.** *Vibration of Structures and Machines*, 1990 (Springer Verlag, Newyork).

65. **Giltrow, J.P.** A relationship between abrasive wear and the cohesive energy of materials. *Wear*, 1969, **15**, 71-79.

66. **Godwin, E.W., Matthews, F.L.,** and **Kilty, P.F.** Strength of multi-bolt joints in GRP. *Composites*, 1982, **13,** 268-272.

67. **Goel, A., Chawla, K.K., Vaidya, U.K., Chawla, N.,** and **Koopman, M.** Characterization of fatigue behavior of long fiber reinforced thermoplastic (LFT) composites. *Materials Characterization*, 2008, **60**, 537-544.

68. **Gong, G., Xie, B.H., Yang, W., Li, Z.M., Lai, S.M.,** and **Yang, M.B.** Plastic deformation behavior of polypropylene / calcium carbonate composites with and without maleic anhydride grafted polypropylene incorporated using the essential work of fracture method. *Polymer Testing*, 2006, **25**, 98-106.

69. **Graham, R.** Strategies for failure analysis. *Advanced Material Process*, 2004, **162**, 45–49.

70. **Grant, P.,** and **Sawicki, A.** Bearing fatigue and hole elongation in composite bolted joints. In: Proceedings of *49th annual forum of the American helicopter society*, St.Louis, 1993, pp.163-170.

71. **Greco, A., Claudio Musardo,** and **Alfonso Maffezzoli.** Flexural creep behaviour of PP matrix woven composite. *Composites Science and Technology*, 2007, **67**, 1148-1158.

72. **Gu, W., Wu, H.F., Kampe, S.L.,** and **Lu, G.Q.** Volume fraction effects on interfacial adhesion strength of glass-fiber-reinforced polymer composites. *Material Science Engineering A*, 2000, **277**, 237-243.

73. **Gupta, B.V.,** and **Lahiri, J.** Non-linear viscoelastic behavior of polypropylene and glass reinforced polypropylene in creep**.** *Journal of Composite Materials*, 1980, **14**, 288-296.

74. **Gupta, V.B., Mittal, R.K.,** and **Malti, G.** Energy absorbing mechanisms in short glass fiber reinforced polypropylene. *Composite Science and Technology*, 1990, **37**, 353-368.

75. **Guynn, E.G.,** and **Bradley, W.L.** Measurements of the stress supported by the crush zone in open hole composite laminates loaded in compression. *Journal of Reinforced Plastics and Composites*, 1989, **8**, 133-149.

76. **Hadi, A.S.,** and **Ashton, J.N.** Measurement and theoretical modeling of the damping properties of a unidirectional glass/epoxy composite. *Composite Structures*, 1996, **34**, 381-385.

77. **Hadid, M., Rechak, S.,** and **Tati, A.** Long-term bending creep behavior prediction of injection molded composite using stress-time correspondence principle. *Materials Science and Engineering A*, 2004, **385,** 54-58.

78. **Hadid, M., Rechak, S.,** and **Zouani, A.** Empirical non-linear viscoelastic model for injection molded thermoplastic composite. *Polymer Composites*, 2002, **23**, 771-778.

79. **Harris, B., Braddel, O., Almond, D., Lefebure, C.,** and **Verbic, J.** Study of carbon fiber surface treatment by dynamic mechanical analysis. *Journal of Material Science*, 1993, **28**, 3353-3366.

80. **Harsha, A.P.,** and **Tewari, U. S.** Tribo performance of polyaryletherketone composites. *Polymer Testing*, 2002, **21,** 697-709.

81. **Harsha, A.P.,** and **Tewari, U.S.** Two-body and three-body abrasive wear behaviour of polyaryletherketone composites. *Polymer Testing*, 2003, **22,** 403-418.

82. **Hashin, Z.** Complex moduli of viscoelastic composites: I. General theory and application to particulate composites. *International Journal of Solids and Structures*, 1970, **6,** 539-552.

83. **Hashmi, S.A.R., Somit, N., Anuradha, P.,** and **Navinchand.** Sliding wear of PP/UHMWPE blends: effect of blend composition. *Wear*, 2001, **247**, 9-14.

84. **Haynes.** *Calculation and Design of Metal Spring*, 3rd edition, 1966 (Chapman and Hall, London).

85. **Helen, C.Y., Cartledge Caroline Baillie,** and **Yiu-Wing Mai.** Friction and wear mechanisms of a thermoplastic composite GF/PA6 subjected to different thermal histories. *Wear*, 1996, **94,** 178-184.

86. **Herrera, E.J., Soria, L.,** and **Gallardo, J.M.** Ingenieria Forense (Diagnosis de fallos), *Anales De Mecánica De La Fractura*, 2004, **21**, 21-27.

87. **Hou, J.P., Cherruault, J.Y., Jeronimidis, G.,** and **Mayer, R.** Design, testing and simulation of fibre composite leaf springs for heavy axle load. *The Journal of Strain Analysis for Engineering Design*, 2005, **40**, 497-504.

88. **Hou, J.P., Cherruault, J.Y., Jeronimidis, G., Mayer, R.,** and **Chvojan. J.** Testing of fibre composite leaf spring for heavy axle loads. *Journal of Thermoplastic Composite Materials*, 2010, DOI: 10.1177/0892705709096552.

89. **Houshyar, S., Shanks, R.A.,** and **Hodzic, A.** Tensile creep behavior of polypropylene fibre reinforced polypropylene composites. *Polymer Testing*, 2005, **24**, 257-264.

90. **Huth, H.** Influence of fastener flexibility on the prediction of load transfer and fatigue life for multiple-row joints, fatigue in mechanically fastened composite and metallic joints. *ASTM STP 927*, Philadelphia, 1986, 221-250.

91. **Imihezri, S.S.S., Sapuan, S.M., Hamdan, M.,** and **Sulaiman, S.** A study on comparison of V and X ribbings for polymeric based composite automotive clutch pedal using mould flow analysis software. *Materials and Design*, 2005, **26**, 157-166.

92. **Ireman, T., Nyman, T.,** and **Hellbom, K.** On design methods for bolted joints in composite aircraft structures. *Composite Structures*, 1993, **25**, 567-578.

93. **Jaydeep Khedkar., Negulescu, I.,** and **Meletis,E.I.** Sliding wear behaviour of PTFE composites.Wear,2002,**253**,361-369.

94. **Jeng, C.C.,** and **Chen, M.** Flexural failure mechanisms in injection - moulded carbon fibre/PEEK composites. *Composites Science and Technology*, 2000, **60**, 1863-1872.

95. **Joseph, P.V., Mathew, G., Joseph, K., Groeninckx, G.,** and **Thomas, S.** Dynamic mechanical properties of short sisal fibre reinforced polypropylene composites. *Composites Part A: Applied Science and Manufacturing*, 2003, **34**, 275-290.

96. **Kanagaraj, S., Mathew, M.T., Fonseca, A., Oliveira, M.S.A., Simoes, J.A.O.,** and **Rocha, L.A.** Tribological characterization of carbon nanotubes/ultrahigh molecular weight polyethylene composites: the effects of sliding distance. *International Journal of Surface Science and Engineering*, 2010, **4**, 305-321.

97. **Karakuzu, R., Taylak, N., Icten, B.M.,** and **Aktas, M.** Effects of geometric parameters on failure behavior in laminated composite plates with two parallel pin-loaded holes. *Composite Structures*, 2008, **85,** 1-9.

98. **Karger-Kocsis, J.,** and **Friedrich, K.** Fatigue crack propagation in short and long fibre-reinforced injection-molded PA6, 6 composites. *Composites*, 1988, **19**, 105-114.

99. **Karger-Kocsis, J., Felhos, D.,** and **Xu, D.** Mechanical and tribological properties of rubber blends composed of HNBR and in situ producedpolyurethane. *Wear*, 2010, **68,** 467-472.

100. **Karian, H.G.** In: Proceedings of the *46th Conference of the SPI*, Newyork, 1999.

101. Kenny, J.M., and **Marchetti, M.** Elasto-plastic behavior of thermoplastic composite laminates under cyclic loading. *Composite Structures*, 1995, **32**, 375-382.

102. Khashaba, U.A., Sallam, H. E.M., Al-Shorbagy, A.E. and **Seif, M.A.** Effect of washer size and tightening torque on the performance of bolted joints in composite structures. *Composite Structures*, 2006, **73**, 310-317.

103. Kim, H.C., Glenn, L.W., Ellis, C.S., and **Miller, D.E.** Selecting long-glass fiber/thermoplastics for creep resistance. *Plastic Engineering*, 1997, **53**, 39-40.

104. Kim, T., Moon, W., and **Kim, S.** Inflence of leaf shapes on performance of progressive multi-leaf springs. *Journal of Vehicle Design*, 2004, **34**, 65-83.

105. Klass, N.V., Mracus, K., and **Kellock, C.** The tribological behaviour of glass filled Polytetrafluoroethylene. *Tribology International*, 2005, **38**, 824-833.

106. Klug, P.H., and **Alexander, L.E.** *X-Ray Diffraction Procedures: For Polycrystalline and Amorphous Materials*, 1974 (Wiley-Interscience, Newyork).

107. Krause, W., Henning, F., Troster, S., Geiger, O., and **Eyerer, P.** LFTD - A process technology for large scale production of fiber reinforced thermoplastic components. *Journal of Thermoplastic Composite Materials*, 2003, **16**, 289-302.

108. Kretsis, G., and **Matthews, F.L.** The strength of bolted joints in glass fiber /epoxy laminates. *Composites*, 1985, **16**, 92-102.

109. Krishnaswamy, R.K. Analysis of ductile and brittle failures from creep rupture testing of high-density polyethylene (HDPE) pipes. *Polymer*, 2005, **28**, 11664 -11672.

110. Kubat, J., Rigdahl, M., and **Welander, M.** Characterization of interfacial interactions in high density polyethylene filled with glass spheres using dynamic mechanical analysis. *Journal of Applied Polymer Science*, 1990, **39**, 1527-1539.

111. Kultural, S.E., and **Eryurek, I.B.** Fatigue behavior of calcium carbonate filled polypropylene under high frequency loading. *Materials and Design*, 2007, **28**, 816-823.

112. Lancaster, J.K. Abrasive wear of polymers. *Wear*, 1969, **14**, 223-239.

113. **Landro, L.D.,** and **Lorenzi, W.** Mechanical properties and dynamic mechanical analysis of thermoplastic-natural fiber/glass reinforced composites. M*acromolecullar Symposia*, 2009, **286**, 145-155.

114. **Lee, I., Kim, B, N.,** and **Koo, K.N.** Dynamic characteristics of thermoplastic composite laminates. *Composites*, 1994, **25**, 281-286.

115. **Leevy, G.,** and **Khoa Cao.** Evaluation of a multi-leaf hybrid springs for automotive suspensions. *SAE Paper series*, 2004, Doc No: 2004-01-0782.

116. **Lhymn, C., Tempelmeyer, K.E.,** and **Davis, P.K.** The abrasive wear of short fibre composites. *Composites*, 1985, **16,** 127-136.

117. **Lim, T.S., Kim, B.C.,** and **Lee, D.G.** Fatigue characteristics of the bolted joints for unidirectional composite laminates. *Composite Structures*, 2006, **72**, 58-68.

118. **Lin, H., Ma, C.C.M.,** and **Tai, N.H.** Long fiber reinforced polyamide polycarbonate composites. I: Fatigue behavior and morphological study. *Journal of Vinyl & Additive Technology*, 1996, **2**, 80-86.

119. **Liou, W.J.,** and **Tseng, C.I.** Creep behavior of nylon-6 thermoplastic composites. *Polymer Composites*, 1997, **18**, 492-499.

120. **Liu, H., Polak, M.A.,** and **Penlidis, A.** A practical approach to modeling time-dependent nonlinear creep behavior of polyethylene for structural applications. *Polymer Engineering Science*, 2008, **48**, 159-167.

121. **Lo, K.H., Mccusker, J.J.,** and **Gottenberg, W.G.** Composite leaf spring for tank trailer suspensions. *Journal of Reinforced Plastics and Composites*, 1987, **6**, 100-112.

122. **Lu, Z.P.,** and **Friedrich, K.** On sliding friction and wear of PEEK and its composites. *Wear*, 1995, **181-183**, 324-631.

123. **Luscher, A.,** and **Houser, D.** An investigation of the geometry and transmission error of injection molded gears. *Journal of Injection Molding Technology*, 2000, **4**, 177-190.

124. **Mallick, P.** *Composites Engineering Handbook*, 1997 (CRC Press, Newyork).

125. **Mandell, J.F.,** and **Chevaillier, J.P.F.** Craze initiation, crack growth, and lifetime trends in fatigue of poly (vinylch1oride). *Polymer Engineering and Science*, 1985, **3**, 170-177.

126. **Mandell, J.F., Huang, D. D.,** and **McGarry, F.J.** Fatigue of glass and carbon fiber reinforced engineering thermoplastics. *Polymer Composites*, 1981, **2**, 137-144.

127. **Manson, J.A., Hertzberg, R.W., Kim, S.L.,** and **Skibi, M.** The β transition and frequency sensitivity in fatigue crack propagation of polymers. *Polymer*, 1975, **16**, 850-851.

128. **Mantena, P.R., Vaughan, J.G., Donti, R.P.,** and **Kowsika, M.V.** Influence of process variables on the dynamic characteristics of pultruded graphite-epoxy composites In: Proceedings of the *Vibro-Acoustic Characterization of Materials and Structures*, ASME , 1992, pp.147-154.

129. **Markarian, J.** Long fibre reinforcement drives automotive market forward. *Plastics, Additives and Compounding*, 2005, **7**, 24-29.

130. **Marshall, D.F.** Long-fibre reinforced thermoplastics. *Materials & Design*, 1987, **8**, 77-81.

131. **Martin, G.C.,** and **Gerberich, W.W.** Temperature effects on fatigue crack growth in polycarbonate. *Journal of Materials Science*, 1976, **11**, 231-238.

132. **Mascarenhas, W.N., Ahreens, C.H.,** and **Ogliari, A.** Design criteria and safety factors for plastic components design. *Materials and Design*, 2004, **25**, 257-261.

133. **Mathew, M.T., Padaki, V., Alagirusamy, R., Deopura, B.L., Fangueiro, R., Rocha, L.A.,** and **Gomes, J.R.** Tribological behaviour of multilayered textile composites: The effect of reciprocating sliding frequency. *Wear*, 2009, **267**, 26-33.

134. **Mathew, M.T., Padaki, V., Rocha, L.A., Gomes, J.R., Alagirusamy, R., Deopura, B.L.,** and **Fangueiro, R.** Tribological properties of the directionally oriented warp knit GFRP composites. *Wear*, 2007, **263**, 930-938.

135. **McCarthy, C.T., McCarthy, M.A.,** and **Lawlor, V.P.** Progressive damage analysis of multi-bolt composite joints with variable bolt-hole clearances. *Composites Part B*, 2005, **36**, 290-305.

136. **Mcgee, A.C., Dharan, C.K.H.,** and **Finnie, I.** Abrasive wear of graphite fiber-reinforced polymer composite materials. *Wear*, 1997, **114**, 97-107.

137. **Menard, K.P.** *Dynamic Mechanical Analysis: A Practical Introduction*, 1999 (CRC Press, Florida).

138. **Mergler, Y.J., Schaake, R.P.,** and **Huis Veld, A.J.** Material transfer of POM in sliding contact. *Wear*, 2004, **256**, 294-301.

139. **Moisa, S., Landsber, G., Rittel, D.,** and **Halary, J.L.** Hysteretic thermal behavior of semi-aromatic polyamides. *Polymer*, 2005, **46**, 11870 -11875.

140. **Morris, C.J.** Composite integrated rear suspension. *Composite Structures*, 1986, **5,** 233-242.

141. **Mukhopadhyay, N.K., Das, S.K., Ravikumar, B., Ranganath, V.R.,** and **Ghosh chowdhury, S.** Premature failure of a leaf spring due to improper material processing. *Engineering Fracture Analysis*, 1997, **4**, 161-170.

142. **Mutoh, Y., Tanaka, K.,** and **Takeda, K.** Fretting fatigue of automotive leaf spring. In: Proceeding of *International Conference on the Fatigue of Engineering Materials and Structures*, Institution of Mechanical Engineers, London, 1986, pp.203-210.

143. **Myshkin, N.K., Petrokovets, M.I.,** and **Kovalev, A.V.** Tribology of polymers: Adhesion, friction, wear, and mass-transfer. *Tribology International*, 2005, **38**, 910-921.

144. **Naik, R.A.,** and **Crews, J.H.** Stress analysis method for a clearance-fit bolt under bearing loads. *AIAA Journal*, 1986, **24,** 1348–1353.

145. **Nelson, D.J.** Dynamic testing of discontinuous fiber reinforced composite materials. *Journal of Sound and Vibration*, 1979, **64,** 403-419.

146. **Nelson, D.J.,** and **Hancock, J.W.** Interfacial slip and damping in fiber-reinforced composites. *Journal of Material Science*, 1978, **13**, 2429-2440.

147. **Ning, H., Uday Vaidya, Janowski, G.M.,** and **George Husman.** Design, manufacture and analysis of a thermoplastic composite frame structure for mass transit. *Composite Structures*, 2007, **80**, 105-116.

148. **Noh, W.J., Choi, M.H.,** and **Chihoon Choi.** Development of a door shield module plate with long-fiber-reinforced thermoplastic polypropylene. *SAE International*, 2006, Doc No: 2006-01-0330.

149. **Okutan, B.** The effects of geometric parameters on the failure strength for pin-loaded multi-directional fiber-glass reinforced epoxy laminate. *Composites Part-B*, 2002, **33**, 567-578.

150. **Orth, F., Hoffmann, L., Zilch-Bremer, H.,** and **Ehrenstein, G.W.** Evaluation of composites under dynamic load. *Composite Structures*, 1993, **24**, 265-272.

151. **Owei, O. S.,** and **Schipper, D.J.** Tribological behaviour of unfilled and composite polyoxymethylene. *Wear*, 1991, **148**, 363-376.

152. **Pakdil, M., Sen, F., Sayman, O.,** and **Benli, S.** The effect of preload on failure response of glass epoxy laminated composite bolted-joints with clearance. *Journal of Reinforced Plastics and Composites*, 2007, **26**, 1239-1252.

153. **Palabiyik, M.,** and **Bahadur, S.** Tribological studies of polyamide 6 and high-density polyethylene blend filled with PTFE and copper oxide and reinforced with glass fibres. *Wear*, 2002, **25**, 369-376.

154. **Park, B.D.,** and **Balatinecz, J.J.** Short term flexural creep behavior of wood fiber/polypropylene composites. *Polymer Composites*, 1998, **19**, 377-382.

155. **Pegoretti, A.,** and **Ricco, T.** Creep crack growth in a short glass fibres reinforced polypropylene composite. *Journal of Material Science*, 2001, **19**, 4637-4641.

156. **Peterson, R.E.** *Design Factors for Stress Concentration*, 1951 (Penton Publication, Belfast).

157. **Pinnell, M.F.** An examination of the effect of composite constituent properties on the notched strength performance of composite materials. *Composites Science and Technology*, 1996, **56**, 1405-1413.

158. **Prabhakaran, E.M., Nair, S.,** and **Sinha, P.K.** Notch sensitivity of polymers. *Journal of Applied Polymer Science*, 2003, **22**, 3011-3020.

159. **Purslow, D.** Fractography of fiber-reinforced thermoplastics, Part3. Tensile, compressive and flexural failures. *Composites*, 1988, **19**, 358-366.

160. **Rabinowicz, E.** *Friction and Wear of Materials*, 1995 (John Wiley & sons, New York).

161. **Rajeesh, K. R., Gnanamoorthy, R.,** and **Velmurugan, R.** Effect of humidity on the indentation hardness and flexural fatigue behavior of polyamide 6 nanocomposite. *Material Science and Engineering A*, 2010, **527**, 2826-2830.

162. **Rajendran, I.,** and **Vijayarangan, S.** Optimal design of a composite leaf spring using genetic algorithms. *International Journal of Computers and Structures*, 2001, **79,** 1121-29.

163. **Ratner, S.B., Ferberova, I., Radyukevich, O.V.,** and **Lure, E.G.** Connection between wear resistance of plastics and other mechanical properties. *Abrasion of Rubber*, 1967, **12**, 7-17.

164. **Rezaei, F., Yunus, R.,** and **Ibrahim, N.A.** Effect of fiber length on thermo mechanical properties of short carbon fiber reinforced polypropylene composites. *Materials and Design*, 2009, **30**, 260-263.

165. **Rittel, D., Eliasha, N.,** and **Halaryb, J.L.** Hysteretic heating of modified poly methylmethacrylate. *Polymer*, 2003, **44**, 2817-2822.

166. **Rosato, D.V., Rosato, D.V.,** and **Rosato, M.G.** *Plastic Design Handbook*, 2000 (Kluwer Academic Publishers, Boston).

167. **Rowlands, R.E., Rahman, M.U., Wilkinson, T.L.,** and **Chiang, Y.I.** Single and multiple bolted joints in orthotropic materials. *Composites*, 1982, **13**, 273-279.

168. **Ruland, W.** Free vibrations of viscoelastic materials with high damping. *Colloid and Polymer Science*, 1984, **262,** 387-396.

169. **SAE HS-78.** *Manual on Design and Application of Leaf Springs*, 1996 (SAE International, PA, USA).

170. **SAE J 1528.** *Fatigue Testing Procedure for Suspension Leaf Springs*, 1990 (SAE International, PA, USA).

171. **Sancaktar, E.,** and **Gratton, M.** Design analysis and optimization of composite leaf springs for light vehicle applications. *Composite Structures*, 1999, **44**, 195-204.

172. **Santika, P., Wiyono, D.,** and **Subagyo, H.** Durability testing of leaf spring and shock absorber. *SAE Paper series*, 1987, Doc No: 871284.

173. **Sato, N., Kurauchi, T.,** and **Kamigaito, O.** Material improvement and quality assurance for composite leaf springs based on micro fracture mechanism. *Journal of Composite Materials*, 1992, **26**, 1240-1253.

174. **Sauer, J.A.,** and **Richardson, G.C.** Fatigue of polymers. *International Journal of Fracture*, 1980, **16**, 499-532.

175. **Saunders, D.S., Galea, S.C.,** and **Diermendjian, G.K.** The development of fatigue damage around fastener holes in thick graphite/epoxy composite laminates. *Composites*, 1993, **24**, 309-321.

176. **Saurez, S.A., Gibson, R.F., Sun, C.T.,** and **Chaturvedi, S.K.** The influence of fiber length and fiber orientation on damping and stiffness of polymer composite materials. *Experimental Mechanics*, 1986, **26**, 175-184.

177. **Scalea, L.D.F., Cappello, F.,** and **Cloud, G.L.** On the elastic behavior of a cross-ply composite pin-joint with clearance fits. *Journal of Thermoplastic Composite Materials*, 1999, **12**, 13-22.

178. **Sefrani, Y.,** and **Jean-Marie Berthelot.** Temperature effect on the damping properties of unidirectional glass fibre composites. *Composites Part-B*, 2006, **37**, 346-355.

179. **Senthilvelan, S.,** and **Gnanamoorthy, R.** Damping characteristics of unreinforced, glass and carbon fiber reinforced nylon 6/6 spur gears. *Polymer Testing*, 2006, **25**, 56-62.

180. **Sepe, M.P**. Use of advanced characterization techniques in evaluating the fitness-for-use of long-glass fiber thermoplastics: San Francisco, 1994, pp.2029-2032.

181. **Seungwon Yoo, Jongchan Park** and **Junghwan Lim.** Fatigue strength evaluation for the leaf spring of commercial vehicle considering u bolt fixing force. *Modeling, Identification and Control*, 2007, Doc No: 2007-01-0853.

182. **Shankar, G. S. S.,** and **Vijayarangan, S.** Mono composite leaf spring for light vehicle-design, end joint analysis and testing. *Material Science*, 2006, **12**, 220-225.

183. **Shokrieh, M.M.,** and **Davood Rezaei.** Analysis and optimization of a composite leaf spring. *Composite Structures*, 2003, **9,** 317-325.

184. **Silverman, E.M**. Effect of glass fiber length on the creep and impact resistance of reinforced thermoplastics. *Polymer Composites*, 1987, **8**, 8-15.

185. **Simoes, J.A.O.** Icarus: the design process of a conceptual vehicle. *Materials and Design*, 2001, **22**, 251-257.

186. **Siswosuwarno, M., Kusalamwardi, H.,** and **Kusuma, G.** Influence of shot-peening on the surface microstructure of leaf spring. *SAE Paper series*, 1985, Doc No: 852227.

187. **Sole, B.M.,** and **Ball, A.** On the abrasive wear behavior of mineral filled polypropylene. *Tribology International*, 1996, **29**, 457-465.

188. **Srinath, G.,** and **Gnanamoorthy, R.** Effect of short fibre reinforcement on the friction and wear behavior of nylon 66. *Applied Composite Materials*, 2005, **12,** 369-383.

189. **Srinath, G.,** and **Gnanamoorthy, R.** Two-body abrasive wear characteristics of nylon clay nanocomposites-effect of grit size, load, and sliding velocity. *Materials Science and Engineering A*, 2006, **435**, 181-186.

190. **Srivastava, V.K.,** and **Pathak, J.P.** Friction and wear properties of bushing bearing of graphite filled short glass composites in dry sliding. *Wear*, 1996, **197**, 145-150.

191. **Stachowaik, G.W.,** and **Batchelor, A.W.** *Engineering Tribology*, 2001, (Butterworth-Heinemann, Boston).

192. **Stockdale, J.H.,** and **Matthews, F.L.** The effect of clamping pressure on bolt bearing loads in glass fiber reinforced plastics. *Composites*, 1976, **7**, 34-38.

193. **Straikov, R.,** and **Schon, J.** Experimental study on fatigue resistance of composite joints with protruding - head bolts. *Composite Structures*, 2002, **55**, 1-11.

194. **Straikov, R.,** and **Schon, J.** Quasi-static behaviour of composite joints with protruding-head bolts. *Composite Structures*, 2001, **51**, 411-425.

195. **Sugimoto, T.,** and **Sasaki, Y.** Fatigue of structural plywood under cyclic shear through thickness III: Energy dissipation performance. *Journal of Wood Science*, 2007, **54**, 169-173.

196. **Sugiyama, H., Ahmed, A., Shabana Mohamed, Omar, A.,** and **Wei-Yi Loh.** Development of nonlinear elastic leaf spring model for multibody vehicle systems. *Computer Methods in Applied Mechanics and Engineering*, 2005, **195**, 6925-6941.

197. **Sun, H.T., Chang, F.K.,** and **Qing, X.** The response of composite joints with bolt-clamping loads, part II: Model verification. *Journal of Composite Materials*, 2002, **36**, 69-92.

198. **Suresha, B., Chandramohan, G., Samapthkumaran, P.,** and **Seetharamu, S.** Three-body abrasive wear behaviour of carbon and glass fiber reinforced epoxy composites. *Materials Science and Engineering: A*, 2007, **443,** 285-291.

199. **Swanson, S.R., Cairns, D.S., Guyll, M.E.,** and **Johnson, D.** Compression fatigue response for carbon fiber with conventional and toughened epoxy matrices with damage. *Transaction of ASME Journal of Engineering Material and Technology*, 1993, **115**, 116-121.

200. **Talib, A., Ali, A., Goudah, G., Lah, N.A.C.,** and **Golestaneh, A.F.** Developing a composite based elliptic spring for automotive applications. *Materials and Design*, 2010, **31**, 475-484.

201. **Tanabe, K., Seino, T.,** and **Kajio, Y.** Characteristics of carbon/glass fiber reinforced plastic leaf spring. In: Proceedings of *SAE International Congress and Exposition*, Detroit, 1982, pp.1628-1634.

202. **Tanaka, K., Mutoh, Y., Sakoda, S.,** and **Leadbeater, G.** Fretting fatigue in 0.65C spring steel and 0.45C carbon steel. *Fatigue and Fracture of Engineering Materials and Structures*, 1985, **8,** 129-142.

203. **Thattaiparthasarathy, B.K., Pillay, S., Ning, N.S.,** and **Vaidya, U.K.** Process simulation, design and manufacturing of a long fiber thermoplastic composite for mass transit application. *Composites*, 2008, **39,** 1512-1521.

204. **Theren, K.,** and **Lundin, A.** Advanced composite materials for road vehicles. *Materials & Design*, 1990, **11**, 71-75.

205. **Thomason, J.L.** The influence of fiber length and concentration on the properties of glass fibre reinforced polypropylene: 5. Injection moulded long and short fibre PP. *Composites Part A*, 2002, **33**, 1641-1652.

206. **Thomason, J.L.,** and **Groenewoud, W.M.** The influence of fibre length and concentration on the properties of glass fibre reinforced polypropylene: 2 Thermal properties. *Composites Part A*, 1996, **27**, 555-565.

207. **Thomason, J.L.,** and **Vlug, M.A.** Influence of fibre length and concentration on the properties of glass fibre-reinforced polypropylene: 1.Tensile and flexural modulus. *Composites Part A*, 1995, **27**, 477-484.

208. **Thoppul, S.D., Finegan, J.,** and **Gibson, R.F.** Mechanics of mechanically fastened joints in polymer- matrix composite structures-A review. *Composites Science and Technology*, 2009, **69**, 301-329.

209. Throp, J.M. Friction of some commercial polymer-based bearing material against steel. *Tribology International*, 1982, **15**, 69-74.

210. Todinov, M.T. Residual stresses at the surface of automotive suspension springs. *Journal of Materials Science*, 2000, **35**, 3313-3320.

211. Tong, J., Ma, J., and **Jiang, M.** Effects of the wollastonite fiber modification on the sliding wear behavior of UHMWPE composites. *Wear*, 2003, **255**, 734-741.

212. Twintex Product Data Sheet. *Long fiber thermoplastic pellets*, 2005 (Saint Gobain Vetrotex America Inc, USA).

213. Unal, H., Mimaroglu, A., Kadioglu, U., and **Ekiz, H.** Sliding friction and wear behaviour of polytetrafluoroethylene and its composites under dry conditions. *Materials and Design*, 2004, **25**, 239-245.

214. Vaidya, U.K., Serrano, J. C., Villalobos, A., Sands, J., and **Garner, J.** Design and analysis of a long fiber thermoplastic composite tailcone for a tank gun training round. *Materials & Design*, 2008, **29,** 305-318.

215. Valtorta, D.J., Lefevre, E., and **Mazza.** A new method for measuring damping in flexural vibration of thin fibers. *Experimental Mechanics*, 2005, **45**, 433-439.

216. Vaziri, M., Spurr, R.T., and **Stott, F.H.** An investigation of the wear of polymeric materials. *Wear*, 1988, **122**, 329-342.

217. Voss, H., and **Friedrich, K.** On the wear behaviour of short-fibre-reinforced PEEK composites. *Wear*, 1987, **116,** 1-18.

218. Vu-Khanh, T., Denault, J., Habib, P, and **Low, A.** The effects of injection molding on the mechanical behavior of long–fiber reinforced PBT/PET blends. *Composites Science and Technology*, 1991, **40**, 423-435.

219. Warty, S., Sauer, J.A., and **Charlesby, A.** Effects of radiation and chain end on fatigue behaviour of polystyrene. *European Polymer Journal*, 1979, **15**, 445-452.

220. Wray, S., Ashton, J. N., and **El-Sobky, H.** An investigation of the influence of anisotropy and frequency on damping in short glass fiber reinforced polypropylene. *Composite Structures*, 1990, **15**, 43-60.

221. Wyzgoski, M.G., and **Novak, G.E.** Fatigue fracture of long fiber reinforced nylon 66. *Polymer Composites*, 1995, **16**, 38-51.

222. Yamada, Y. *Materials for Leaf Springs*, 2007 (Springer, Newyork).

223. **Yamaguchi, Y.** *Tribology of Plastic Materials*, 1990 (Elsevier, Amsterdam).

224. **Yavari, V., Rajabi, I., Daneshvar, F.,** and **Kadivar, M. H.** On the stress distribution around the hole in mechanically fastened joints. *Mechanics Research Communications*, 2009, **36,** 373-380.

225. **Yu, W.J.,** and **Kim, H.C.** Double tapered FRP beam for automobile suspension leaf spring. *Composite Structures*, 1988, **9,** 279-300.

226. **Zainudin, E.S., Sapuan, S.M., Sulaiman, S.,** and **Ahmad, M.M.H.M.** Fiber orientation of short fiber reinforced injection molded thermoplastic composites: A review. *Journal of Injection Moulding Technology*, 2002, **6,** 1-10.

227. **Zhang, H., Zhang, Z.,** and **Friedrich, K.** Effect of fibre length on the wear resistance of short carbon fibre reinforced epoxy composites. *Composites Science and Technology*, 2006, **67,** 222-230.

228. **Zhang, Z.,** and **Hartwig, G.** Relation of damping and fatigue damage of unidirectional fibre composites. *International Journal of Fatigue*, 2001, **24,** 713-718.

229. **Zhou, J., D'Amore, A., Yang, Y., He, T., Li, B.,** and **Nicolais, L.** Flexural fatigue of short glass fiber reinforced a blend of polyphenylene ether ketone and polyphenylene sulfide. *Applied Composite Materials*, 1994, **1**, 183-195.

LIST OF PUBLICATIONS BASED ON THE RESEARCH WORK

Refereed Journals

1. **Subramanian, C.,** and **Senthilvelan**, **S.** Effect of fiber length on the friction and wear of discontinuous fiber reinforced polypropylene material. *International Journal of Plastics Technology*, 2008, **12**, 863-875.
2. **Subramanian, C.,** and **Senthilvelan**, **S.** Effect of reinforced fiber length on hysteretic heating of discontinuous fiber reinforced polypropylene. *International Journal of Polymeric Materials,* 2009, **58(7),** 347-354.
3. **Subramanian, C.,** and **Senthilvelan, S.** Development and preliminary performance evaluation of discontinuous fiber reinforced thermoplastic leaf spring. *Journal of Materials: Design and Applications*, Proc. of Ins. Mech. E Part L, 2009, **223(3)**, 131-142.
4. **Subramanian, C.,** and **Senthilvelan, S.** Abrasive behavior of discontinuous fiber reinforced polypropylene material. *Industrial Lubrication and Tribology*, 2010, **62(4)**, 187-196.
5. **Subramanian, C.,** and **Senthilvelan, S.** Effect of reinforced fiber length on the joint performance of thermoplastic leaf spring. *Materials and Design*, 2010, **31**, 3733-3741.
6. **Subramanian, C.,** and **Senthilvelan, S.** Fatigue performance of discontinuous fiber reinforced thermoplastic leaf spring. *Journal of Materials: Design and Applications*, Proc. of Ins. Mech. E Part L, 2010, **224(3)**, 93-100.
7. **Subramanian, C.,** and **Senthilvelan, S.** Joint Performance of glass fiber reinforced polypropylene leaf spring. *Composite Structures,* 2011**, 93(2),** 759-766.
8. **Subramanian, C.,** and **Senthilvelan, S.** Effect of reinforced fiber length on the creep performance of thermoplastic leaf spring. *Journal of Applied Polymer Science*, 2011, **120(6)**, 3679-3686.
9. **Subramanian, C., Sunil Balwant Deshpande** and **Senthilvelan, S.** Effect of reinforced fiber length on damping performance of thermoplastic composites. *Advanced Composite Materials (Accepted for Publication December, 2010).*

Presentations in Conferences

1. **Sunil Balwant Deshpande, Subramanian, C.,** and **Senthilvelan, S.** Vibration characteristics of thermoplastic composites, *1st International and 6th ISAMPE National Conference on Composites (INCCOM),* Indian Institute of Technology Kanpur, December 12-14, 2007, pp. 535-539.
2. **Subramanian, C.,** and **Senthilvelan, S.** Computer aided design of thermoplastic composite leaf spring, *International Conference on Computer Aided Engineering*, Indian Institute of Technology Madras, December 13-15, 2007, pp. 329-336.
3. **Subramanian, C.,** and **Senthilvelan, S.** Friction and wear performance of long and short fiber reinforced polypropylene, *6th International Conference on Industrial Tribology (ICIT),*Indian Oil R & D Centre, New Delhi, November 06-08, 2008, CD Proceedings.
4. **Subramanian, C.,** and **Senthilvelan, S.** Computer aided design of composite leaf spring joint, *National Conference on Industrial Problems in Machines and Mechanisms* (IPRoMM), Indian Institute of Technology Madras, July 10-11, 2009, pp. 149-156.
5. **Subramanian, C.,** and **Senthilvelan, S.** Effect of material stiffness over joint performance of thermoplastic composite leaf spring, *8th ISAMPE National Conference on Composites (INCCOM),* VSSC, Thiruvananthapuram, Dec 04-05, 2009, pp. 25-33.

CURRICULUM VITAE

1. Name: **C.SUBRMANIAN**

2. Date of Birth: 23-08-1978

3. Permanent Address: S/o S. Chithambaram Pillai
Saraswathy Bhawan,
Door no: 71/9A/8D
4th street, Bharathi Nagar,
East Ramanputhoour
Nagercoil-2
Ph: 0-9944897007, 0-9444903847
Email:subfortune@yahoo.com

4. Educational Qualifications:

1995-1999 **Bachelor of Engineering**

Institution: Annamalai University
Chidambaram 608 002, India

Specialization: Mechanical and Production Engineering

1999-2000 **Master of Engineering**

Institution: Hindustan College of Engineering
Chennai, India

Specialization: Computer Aided Design

2006-2010 **Doctor of Philosophy**

Institution: Indian Institute of Technology Guwahati
Guwahati 781039, India

Registration Date: 25-07-2006

Thesis Submission Date: 08-10-2010

DOCTORAL COMMITTEE

Guide: **Dr. S. Senthilvelan**
Associate Professor
Department of Mechanical Engineering

Chairperson: **Prof. Debabrata Chakraborty**
Professor and Head
Department of Mechanical Engineering

Members: **Prof. Sashindra K. Kakoty**
Professor
Department of Mechanical Engineering

Dr. G. Pugazhenthi
Assistant Professor
Department of Chemical Engineering